# THE EFFECT OF GAMMA IRRADIATION ON THE ELECTRICAL PROPERTIES OF THE EPOXY RESINS

by

SA'AD S. GEDEON

Thesis submitted to

THE UNIVERSITY OF STRATHCLYDE

for the degree of

DOCTOR OF PHILOSOPHY

Department of Electronic and Electrical Engineering,
University of Strathclyde, Glasgow.

April 1988.

## Acknowledgements

The author wishes to extend his greateful appreciation to his family for their financial support and encouragement.

He also wishes to express his gratitude to Professors D. J. Tedford and D. Farish for the opportunity to undertake this research in this department.

A special 'thank you' to Dr. R.A. Fouracre for his patience and guidance during the supervision of the research and to Professor S. Wu for his co-operation.

Additional thanks are due to Dr. H.M. Banford for assistance with the irradiation of samples, to Dr. D. Blair and Dr. M. Given for their comments and suggestions during the work, to Mr P McDiarmid for his technical help and support, and to Mrs M Bennett and Mrs E Allan for their patience in photocoping and binding of this thesis.

Grateful acknowledgements to Miss F. Meighan for typing this thesis and Mr G. Leonidopoulos for his friendship and support during the research.

# CONTENTS

# ABSTRACT

This thesis is concerned primarily with the curing of epoxy resin and the effect of gamma- irradiation on the electrical properties of epoxy resin systems. The particular systems examined were a diglycidyl ether of bisphenol A (DGEBA, Ciba Geigy MY750) epoxy resin cured using one of two hardeners. These were a hydroxyalkylated polyamine (Ciba Geigy HY956) and a dodecenyl-succinicanhydride (DDSA) with an accelerator of benzyldimethylamine.

Different methods of examining the curing of the epoxy resin system have been carried out including differential scanning calorimetry (DSC), infrared spectroscopy (I.R.), dielectric measurements, volume resistivity measurements and thermally stimulated discharge current. The results of dielectric relaxation measurements obtained during the curing of the epoxy resin system were interpreted on the basis of a model considering the growing polymer molecules to be in solution, the solvent being the unreacted monomer and hardener.

The investigation of the effect of gamma-irradiation on the electrical properties (conduction mechanism and dielectric behaviour) of the epoxy resin system was achieved by examining the electrical properties of the fully cured epoxy resin system before and after irradiation and the results compared.

To establish the electrical properties of the fully cured epoxy resin system before and after irradiation, a series of experiments which provide information about the conduction mechanism, the dielectric properties, the infrared spectra (I.R.) and the glass transition temperature (Tg) obtained from (DSC) measurements were carried out. For the epoxy resin system MY750/HY956, it was found that the D.C. conductivity, dissipation factor and capacitance values increase, whereas the glass transition temperature (Tg) and the activation energy,E, obtained from D.C. measurements decreased for the irradiated samples. Furthermore, a modification in the I.R. spectrum in the 1600 to 1800 $cm^{-1}$ range due to the formation of carbonyl groups (C = O) in the irradiated sample has been observed. However in the case of epoxy resin system MY750/DDSA, it was found that the dissipation factor and capacitance values decrease, whilst the glass transition temperature (Tg) and the activation energy obtained from dielectric measurements increased for the irradiated samples.

# List of Symbols

| | |
|---|---|
| $T_g$ | Glass transition temperature. |
| E | Applied electric field/ Activation energy in chapter six. |
| $\overline{M_n}$ | The average molecular weight. |
| $\alpha$ | Alpha- relaxation process/ Polarisability of the molecule in chapter four. |
| $\beta$ | Beta- relaxation process. |
| C | Capacitance value of the sample. |
| $C_o$ | Vacuum Capacitance. |
| $\varepsilon$ | Static relative permittivity. |
| *m* | Electric dipole. |
| $E_L$ | Local electric field strength at the molecule. |
| $\alpha_e$ | Electronic polarisation. |
| $\alpha_a$ | Atomic polarisation. |
| $\alpha_m$ | Orientational polarisation. |
| $\alpha_{m/w/s}$ | Maxwell-Wagner-Sillars polarisation. |
| $\alpha_T$ | The overall polarisability of the system. |
| P | Polarisation. |
| $N_A$ | Avogadro's number. |
| $M_w$,M | Molecular weight. |
| $\rho$ | Resistivity/ Density of the material in chapter four. |
| $\varepsilon_o$ | Permittivity of free space. |
| $\overline{m}$ | The mean electric moment. |
| $\alpha_o$ | Deformational polarisability. |

| | |
|---|---|
| $\mu$ | The drift mobility of the carriers/Permanent moment of each dipole in chapter four. |
| k | Boltzman constant. |
| T | Absolute temperature. |
| t | Time. |
| K | The dielectric constant/Rate coefficient in equ. 4.10/An equilibrium constant in section 5.1.1.2. |
| $\tau$ | Dielectric relaxation time. |
| $\delta$ | The loss angle. |
| D | Electric displacement. |
| $\varepsilon'$ | Dielectric constant. |
| $\varepsilon''$ | Dielectric loss factor. |
| tan $\delta$ | Dielectric loss tangent (dissipation factor). |
| $\varepsilon^*$ | Relative permittivity. |
| Z | Impedance. |
| $C_p$ | Capacitance in parallel/ Concentration of the polymer solute in equ. 4.44,4.43,4.46. |
| $R_p$ | Resistance in parallel. |
| $C_s$ | Capacitance in series. |
| $R_s$ | Resistance in series. |
| $I_c$ | The current across the capacitor. |
| $I_R$ | The current across the resistance. |
| w | Angular frequency. |
| $G_p$ | A.C. conductance. |
| $\sigma_{DC}$ | D.C. conductivity. |
| $\sigma_{AC}$ | A.C. conductivity. |
| $\varepsilon_\infty$ | Static dielectric constant. |

| | |
|---|---|
| $\varepsilon_\infty$ | Permittivity at frequencies well above the relaxation. |
| $\eta_s$ | Viscosity of the solution. |
| $\eta_o$ | Viscosity of the solvent. |
| R | Gass constant. |
| $\sigma$ | Conductivity. |
| Q,e | Charge. |
| N | Concentration of charges. |
| $\theta$ | The ratio of free to trapped charge. |
| $n_o$ | The density of thermally generated free carriers. /Concentration of the ionic compound in section 5.1.1.2. |
| $V_{tr}$ | Transition voltage. |
| S | Thickness of the insulator. |
| A | Area of the capacitor plates. |
| f | The fractional degree of dissociation at equilibrium. |
| $K_o$ | The entropy constant. |
| $\Delta G$ | The change in free energy for the reactions. |
| $\Delta W$ | The energy required to separate the ions in a medium of unit dielectric constant/Change in the weight of the sample in chapter six. |
| $\Delta U^*$ | The height of the potential-energy barrier. |
| $\upsilon$ | Frequency. |
| a | The distance between neighbouring potential wells. |
| U | The mean drift velocity. |
| $J_w$ | Induce current. |

# CHAPTER ONE

# INTRODUCTION

## 1.1 General

During the last century plastics were introduced to engineering technology and challenged the older materials both in their well established uses and also in their range of application. Being economical materials they have been increasingly utilised in all branches of industry. They represent a very important and versatile group of engineering materials. Workers have been closely studying polymers in order that the most appropriate use of their properties may be made in the required field.

The electrical properties of polymers is of interest in the present thesis and is a subject which is inherently interdisciplinary in nature, being closely allied with the mechanical properties of polymers on the one hand, and with the semiconductive properties of inorganic substances on the other. Since the early days of plastic technology, when such materials were regarded electrically, as simply good insulators, observation of subtleties in electrical response has shed a great deal of light on the underlying microscopic structure and molecular dynamics of these materials. This has contributed to polymer science in a general way, and has, at the same time, enabled the development of

materials which meet exacting electrical-engineering requirements.

In the early days of the electrical industry, insulation was achieved by the use of materials such as mica, glass, and porcelain, and also by fibres such as cotton and silk when more flexibility was desired for wiring applications. The properties of rubber, a naturally occurring polymer were quickly exploited and this became a standard insulation material, both in its flexible form and, after vulcanisation to ebonite, in a rigid form. Because of the volume occupied by wire covered by rubber or textile yarn, wire enamels based largely on phenolic resins were developed. Enamel-covered wires enabled more turns to be wound per unit volume on, for example, the stator coil of a dynamo. This lead to increased efficiency because of the higher flux densities obtainable coupled with the higher working temperature of the enamel compared to rubber. Equipment such as transformers was and often still is insulated, by coating or embedding the component in asphalt or bitumen. Such a protection also prevents the ingress of water. This procedure, is however, not very satisfactory mechanically, since the bitumens with a high softening temperature are brittle and susceptible to mechanical damage at room temperature. These materials progressively soften as the machine reaches its operating temperature and will then tend to flow.

Paraffin waxes have been in use as insulation for

many years, particularly in small components such as capacitors for radio equipment. These suffer from the limitations of the low softening point of waxes and mechanical weakness. Therefore, waxes and bitumens are not suitable for potting or encapsulation for many electrical applications. Aircraft and rocket-propelled missiles require for example delicate electrical equipment of increasingly complicated design which has to withstand previously unheard of mechanical shocks at a variety of temperatures and pressures. This equipment also needs to be resistant to moisture, corrosive chemicals, and mould growths. Phenolic resins, while often used as mouldings and in laminates, are not very suitable for potting or encapsulation because of high shrinkage on cure and a high power factor which gives rise to undesirable power losses and consequently to overheating. In order to address this problems a series of resins have been developed. Polyester resins, whilst having reasonable electrical properties, suffer from high shrinkage during and after cure. High shrinkage sets up internal stresses which can give rise to cracking and also can affect the electrical characteristics of a circuit by altering the dimensions of components, particularly if coils or capacitors are involved. Silicone resins possess very good insulation and dielectric properties which are well maintained at elevated temperature, but they possess very poor mechanical strengths, need high cure-temperatures for

development of optimum properties; do not adhere very well to many substrates, and are fairly expensive.

Epoxide resins, however, provide a class of materials which although not possessing such good electrical properties as the silicones are nevertheless superior in this respect to phenolics and polyester resins. The wide variety of epoxy resins have a correspondingly wide range of properties. The physical properties which are important in the study of cured epoxy resin system are the thermal stability, the tensile, compressive and flexural strengths, the impact resistance, the hardness, and the flammability. The heat resistance or thermal stability of cured epoxides have become of increasing importance over the last few years, reflecting the growing use of epoxide resins in surface coatings, rockets and high performance aircraft. This has led to numerous workers to investigate and to attempt to identify the mechanism of thermal degradation. It has been found that resins cured with acid anhydride have greater thermal stability than amine-cured resins, and that epoxidised novolaks are more stable than the diglycidyl ethers of DPP (37). Epoxy resins can be reinformed, with fibrous fillers to achieve very high tensile strengths. The physical strengths of resins increases throughout the curing cycle, as more interatomic linkages develop, but tends to level off after an optimum curing time at a given

temperature. Further heating at elevated temperature would lead slowly to degradation, particularly in the presence of oxygen.

Epoxide resins have attracted considerable attention as electrical insulating materials because of their very good electrical properties, good casting properties, are mechanically strong with a low cure-shrinkage, have good adhesion particularly to metals, are resistant to mechanical and thermal shock, and possess high resistance to moisture, chemical attack, and mould growth. All these properties make epoxide resins particularly suitable for many different in and outdoor electrical engineering application (1,2). The electrical properties which are important in the choice of insulating materials are :-

a - volume resistivity,

b - surface resistivity,

c - dielectric strength,

d - dissipation factor, and

e - permittivity (dielectric constant).

These properties are not usually constant, but vary with time, frequency of applied voltage, and temperature of the material.

The extent to which a material can withstand the passage of a current is given by its volume and surface resistivities, which are usually measured in ohm-cm and ohms respectively. Breakdown in cast insulation can be caused by discharges within the insulation if air voids

or stress cracks are present because of incorrect manufacture, and surface tracking. A further way in which insulators can fail is by thermal breakdown. Apart from the usual heating effects caused by a direct current (D.C.) passing through a material, the passage of an alternating current can also cause heat build up by dielectric heating.

Examples of the use of epoxy resins as an insulating material are in electric motor windings, as a casting material for power transmission equipment, especially where high voltages are concerned, for potential and current transformers and for busbar insulation.

During the present decade the application of polymers in the field of nuclear engineering and technology is being continuously broadened. This is due to rapid progress in the development of polymer chemistry and technology, on the onehand, and the growing requirements of nuclear and power engineering, on the other. Moreover, the appearance of numerous sources of radiation such as nuclear reactors, charged particle accelerators and isotope installations makes it possible to carry out important investigations, directed to the evaluation of available polymers and development of new polymer materials for these applications.

Over the past few years, radiation chemistry has received considerable attention in polymer research. High energy radiation, as obtained from electron beams

and X-or beta rays, initiates ionization and radical formation. It may cause either crosslinking or chain scission, depending on the chemical structure of the polymer and dose rate. In the presence of oxygen, peroxides may be formed. When they are trapped, ions, radicals, or peroxides can produce post-irradiation reactions. High energy radiation may also be used to initiate polymerisation or to engraft mono or multi-functional monomers upon polymeric chains. Low energy radiation, such as ultraviolet light is less penetrating and has been restricted to surface treatment.

The investigation of polymers for use in nuclear engineering and technology is being developed in the following directions: coatings for shielding the equipment and premises of radio-chemical industries and nuclear installation, electrical and thermal insulation, polymer parts (including pipe-lines, packing and sealing products) and polymer-containing screens for biological shielding from radiation. Polymer coatings prepared from the most radiation-resistant polymers, such as Epoxy and polyester coatings are most widely used in the very high radiation level in nuclear reactors for electrical insulation and corrosion protection (3,4,5). They are used as coatings, to the driving gear mechanisms of regulating rods, in equipment for discharging nuclear fuel, suction pumps, control and repair equipment and the mechanism for distributing nuclear fuel in water.

Furthermore Polymers are widely used for shielding from neutron and gamma radiation. Gamma radiation fluxes are most effectively reduced with materials of high atomic number and density. However, the shielding capacity of these materials toward moderated neutrons is low. In this case, the greatest effect is achieved with compounds containing elements of low mass number, particularly hydrogen. Polymers characterised by high hydrogen content are ideal materials for secondary shielding from neutrons. Combinations of polymers such as resins, polyolefins and rubbers with heavy fillers provide simultaneous shielding from irradiation, fast and slow neutrons (4-12)

Space technology is one of the areas where polymer materials find a very wide and complex use. For instance, in spaceships, polymer materials are used as: (1) construction materials (2) ablation and shielding coatings, (3) sealing and pressurization materials, (4) electrical and heat insulation, (5) antivibrational and shock-absorber devices.

The use of polymer materials in space vehicles can be subjected to various effects such as high and low temperature, thermal oscillating motions, corrosive media, high vacuum, vibration, collisions with micrometeorites, and radiation. Reinforced plastics based on epoxy, phenol, polyester, thioformaldehyde, melamine, silicone and other resins are widely used in this situation (13).

## 1.2 Present Work

As briefly out lined above polymers are currently used as electrical insulators in radiation environments such as encountered in nuclear engineering (insulation of superconducting magnets proposed for use in fusion reactors (14, 15, 16) and in space technology (in the micro-electronics used in satellites (16) ). This can lead to a deterioration in electrical properties, leading ultimately to breakdown. The presence of free radicals and ions in irradiated polymers has been demonstrated conclusively (3, 17-19). It is conjectured that the presence of these species is responsible for the insulator degradation. In the case of epoxy resin system, Burnay (20, 21) observed the formation of diphenylethyl cations, radicals and the annealing of UV absorption bands in DGEBA -aliphatic and aromatic amine epoxy system. It was not clear how the presence of ions and the changes in structure would affect the electrical properties of an epoxy system. In the present work, an epoxy resin of diglycidyl ether of bisphenol A (DGEBA) produced by Ciba Geigy as resin MY750 together with two different hardeners were used. One of the hardeners was a hydroxyalkylated polyamine (HY956). The other was a dodecenyl-succinicanhydride (DDSA) with an accelerator of benzyldimethylamine (1 phr). In order to study the electrical properties of epoxy resin systems, it is essential that the curing mechanism and the state of

cure are considered. The conversion of epoxide resin from a liquid state into a three dimensional infusible network, held together by covalent bonds by means of crosslinking reactions is called curing or hardening and is achieved by the addition of a curing agent (hardener). In the present work, different methods of examining the curing of the epoxy resin system have been employed, such as differential scanning calorimetry (DSC) infrared spectroscopy (IR), dielectric measurements, volume resistivity measurements and thermally stimulated discharge current (TSDC). For the epoxy resin samples used to study the electrical properties, the materials were cured to a standard state. This state was one in which the value of Tg had attained the maximum value for the system (see chapter four).

The effect of gamma irradiation on the electrical properties of epoxy resin systems has been investigated. It is thus necessary to establish the electrical properties of the fully cured material that has not be irradiated. A series of experiments which provide information about the conduction mechanism, the dielectric properties, the infrared spectra and the glass transition temperature obtained from (DSC) were carried out. Afterwards, similar experiments to those used to establish the behaviour of the unirradiated epoxy resin system were carried out on irradiated samples and the results compared.

# CHAPTER TWO

# EPOXY RESIN CHEMISTRY

## 2.1 Introduction

Before describing the electrical properties of epoxy resins, it is worthwhile to touch briefly on the chemistry of these compounds. Because epoxy resins are polymeric materials in terms of the arrangements of atoms, in this chapter the main features of polymer structure and in particular that of epoxy resins will be discussed.

## 2.2 Polymers in General

Organic polymers are characterised structurally by the fact that they are long chain molecules built up from a repeating radical or unit known as the "**structural unit**". Some of these repeat units are shown in Fig. (2.1). Each molecular chain will contain a thousand or more repeat units with a backbone formed by carbon atoms, sometimes in combination with oxygen and nitrogen.

Polymers can be classified in many ways. In the present work polymers have been classified from the point of view of linearity. A linear polymer chain can either be open, with the terminal valences saturated by univalent groups, or closed, with the terminal valences mutually joined forming a cyclic structure. A polymer

which has been derived from a single compound has identical structural units, however polymers resulting from the reaction of two or more compounds , will have chains made up from two or more different units. These will be called "linear mixed polymers".

Non linear polymers can be formed by the cross-linking of long chains into two or three dimensional structures. An example of this type of material is that of Epoxy resins.

2.2.1 Polymerisation

The process of forming long chains from chemical combination of small molecules, known as monomers, is called polymerisation.

Carothers (22) first systematised the process of polymerisation. He observed that there are three types of compounds capable of self combination. The polymerisation reactions of the three type are illustrated below

1. Unsaturated compounds such as formaldehyde.

$n(CH_2=O) + H_2O \longrightarrow HO-CH_2O-CH_2O-....-CH_2O-CH_2O-H$

Formaldehyde ∝ - Polyoxymethylene

2. Cyclic compounds such as ethylene oxide.

$n/\underline{CH_2CH_2O}/ + H_2O \longrightarrow HO-CH_2CH_2O-....-CH_2CH_2O-H$

Ethylene oxide Polyethylene glycol

3. Polyfunctional compounds such as ethylene glycol.

$n(HO-CH_2CH_2O-H) - (n-1)H_2O \longrightarrow HO-CH_2CH_2O-....-CH_2$

Ethylene glycol $CH_2O-CH_2CH_2O-H$

Polyethylene glycol

The process of polymerisation itself can be divided into two types:

1. Addition polymerisation

The simplest example of addition polymerisation is the conversion of ethylene to polyethylene according to the following equation:

$$n(CH_2=CH_2) \longrightarrow (-CH_2-CH_2-)n$$

From this chemical reaction it is clear that the bonds which join the ethylene molecules together in the polymer were obtained by breaking up the original double bonds. These double bonds are relatively unstable. The addition polymerisation process only involves the rearrangement of bonds.

There are a number of polymers formed from compounds similar to ethylene, for example

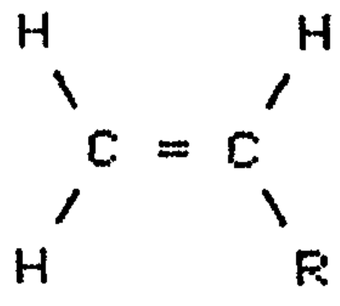

where R may be a chlorine atom, a benzene ring, etc. These are called "vinyl compounds". If R is a chlorine atom for example, the compound is called vinylchloride and the resultant addition polymer is called poly (vinylchloride) or (PVC). Table (2.1) illustrates some vinyl compounds.

The Polyethers, are another example of addition polymer. These have both carbon and oxygen atoms in their backbones. In this case polymerisation occurs

through a ring opening reaction. For example the cyclic compound ethylene oxide forms a polyether as follows

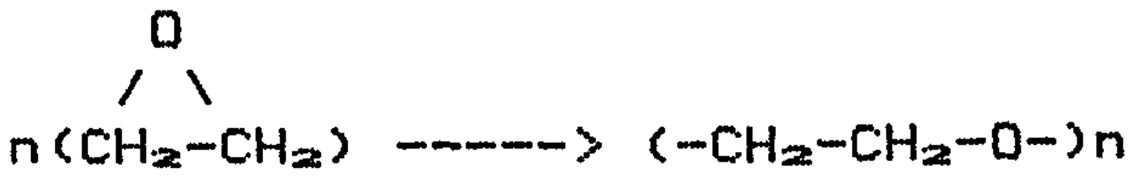

$$n\left(CH_2\text{-}CH_2\right) \longrightarrow (-CH_2\text{-}CH_2\text{-}O-)n$$

## 2. Condensation polymerisation

Polymers can also be formed from monomers which consist of a bivalent radical and reactive end groups which are generally referred to as functional groups. These monomers are known as bifunctional compounds. Reactions can occur between the functional groups of two monomer molecules eliminating a small molecule such as water and binding the two monomers together. This form of reaction is known as condensation polymerisation and produces a linear polymer.

An example of the result of condensation polymerisation is the polyamide Nylon-6. This is derived from ε-amino caproic acid as follows

$$NH_2(CH_2)_5CO\ OH+H\ NH(CH_2)_5COOH \longrightarrow NH_2(CH_2)_5CO.NH(CH_2)_5 COOH + H_2O \text{ etc.}$$

In the example above the bifunctional compound is $NH_2(CH_2)_5COOH$ the functional groups are $NH_2$ and COOH and the bivalent radical (monomer) is $(CH_2)_5$. An example in which two different monomer species, each having similar functional groups combining by a condensation reaction to form Nylon-6,6 is illustrated below. The monomers are adipic acid and hexamethylene diamine. This reaction occurs as follows:

$HOOC(CH_2)_4COOH + NH_2(CH_2)_6NH_2 \longrightarrow HOOC(CH_2)_4CO.NH(CH_2)_6NH_2 + H_2O$ etc.

Another example in which the reaction is exclusively intermolecular and the product is an open chain occurs in the formation of poly(ethylene terephthalate) from ethylene glycol and terephthalic acid:

$nHO(CH_2)_2OH + nHOOC \circledcirc COOH \longrightarrow HO[(CH_2)_2.O.CO \circledcirc CO.O]nH + nH_2O$ .

It should be noted that all of these polymerisation reactions may be terminated by the intervention of monovalent impurities at the active site. This limits the length of the molecular chain.

### 2.2.2 Degree of Polymerisation and Molecular Weight

The degree of polymerisation is the number of mers (structural unit) which have added together to form a polymer. It is directly related to the molecular weight. The degree of polymerisation can determine whether a polymer is a waxy substance or a plastic and it can strongly affect the softening and melting temperature and the degree of its solubility in specific solvents.

To determine the molecular weight of a polymer it is necessary to specify the chemical structure of the monomer units, the chain lengths and the extent to which the chains are interconnected forming branched molecules. The molecular weight of a polymer can only be specified by an average molecular weight, as the

number of monomer units per chain vary from one molecule to another. This is due to the polymerisation reaction which produces different chain-lengths of molecules, distributed according to a probability function which is dependant on the mechanism of the polymerisation and the conditions under which it takes place. The average molecular weight $\bar{M}_n$ is defined by (23)

$$\bar{M}_n = \sum M_x n_x / \sum n_x$$

where $M_x$ and $n_x$ are the molecular weight and relative number, respectively, of the species containing x repeat units.

## 2.3 Epoxy Resins

The name epoxy resin is derived from epoxide, which refers to a three-membered oxide ring, consisting of one oxygen atom and two carbon atoms. The simplest compound in which this ring is found is ethylene oxide. The formulae of a number of substituted ethylene oxides are illustrated in Fig. (2.2). In this context, epoxy resins are defined as compounds which contain more than one epoxide group per molecule. The resins can be classified into five chemical groups, which are illustrated in Fig. (2.3).

The present work is concerned exclusively with the diglycidyl ether of bisphenol A (DGEBA) type epoxies. Examples for different types of glycidyl ethers are shown in Fig. (2.4).

In this group, the epoxides are usually formed by

a condensation reaction between the appropriate diol, dibasic acid, or diamine and epichlorohydrin (ECH) through the elimination of hydrogen chloride. A commonly used epoxide resin is derived by reacting ECH with diphenylolpropane (DPP) also known as bisphenol A. This epoxy resin has good mechanical and chemical properties and reacts with a large number of cross-linking agents. In addition diphenylolpropane can be obtained economically from petroleum based raw materials.

### 2.3.1 Synthesis of Resins

The process of forming epoxide resin based on Dpp and ECH is as follows:-

Dihydric Phenol (DPP)

Dihydric Phenol (DPP) is formed by reacting acetone with an excess of phenol at a temperature of (50°C) in the presence of a strong acid catalyst such as 75% sulphuric acid (see Fig. 2.5).

Epichlorohydrin (ECH)

Epichlorohydrin (ECH) is formed by reacting Propylene with chlorine gas at high temperature and at a moderate pressure. Under these conditions allyl chloride is obtained as well as 1,2 - dichloropropane. The allyl chloride is then treated with dilute hypochlorous acid, forming glycerol dichlorohydrin, which is dehydrochlorinated by using slaked lime or caustic soda. The reactions are illustrated in Fig. (2.6).

Epoxide resin is formed by condensing ECH with DPP in the presence of aqueous caustic soda, the theoretical ratio of ECH to DPP being 2:1. Fig. (2.7) illustrates the reaction in stages. In this reaction, the simplest member of the series of glycidyl ether of DPP, consisting of two terminal epoxide groups and no hydroxyl groups is formed in stage C. There is, however, a competing reaction for DPP (stage D) which leads to higher molecular weight diphenols which can then react further with ECH through stage E. (n) is the number of repeating units, which is essentially dependant on the molar ratio of ECH to DPP used in the resin synthesis.

For example, the value of (n) for the formula in stage C is zero, whereas the value of (n) for the formula in stage E is one. In other words, resins with different degrees of polymerisation (different values of n) can be obtained. Each grade of resin consists of a mixture of molecules having a range of chain lengths and molecular weights. In general resins of a short chain length are viscous liquids, whereas resins of longer chain length (higher molecular weight) are hard and brittle. Table (2.2) illustrates some of the quoted values of n for a range of resins. A pure diglycidyl ether of DPP is a crystalline solid at room temperature, having a melting point of 43°C. The standard types of liquid resin are fluid with crystallisation being

prevented by the presence of higher molecular weight impurities. The tendency of diglycidyl ether of DPP to crystallise increases with the increasing purity of the resin. If the resin is kept under cold storage conditions and crystallisation nuclei such as filler particles are present, this tendency is increased.

## 2.4 Curing agents and Cure Mechanisms:-

Epoxy resins can be transformed from the liquid state to a tough, hard solid. This conversion from a liquid into a cross-linked polymer is called curing or hardening. This hardening is accomplished by the addition of a chemically active reagent known as a curing agent (or hardener or activater). The curing agents can be divided into two broad categories, catalytic and polyfunctional. The cross-linking between the resin molecules is achieved by opening the epoxide ring or by reactions with the hydroxyl groups of the resin. The catalytic curing agents such as lewis bases or acids (eg. tertiary amines or boron trifluoride) act as initiators for resin homopolymerisation, whereas the polyfunctional curing agents function as co-monomers in the polymerisation, leading mainly to the formation of a three-dimensional network composed of resin molecules cross-linked via the curing agents. The epoxide ring can be attacked by a wide range of compounds, for example, phenols, alcohols, thiols, primary and secondary amines and carboxylic acids, all have an active hydrogen atom

which reacts with the epoxy group, or it can be attacked by catalysts such as Lewis bases or acids. The polyfunctional curing agents can be sub-divided into two categories, amines and anhydrides. Amine curing agents can be sub-divided into two types, aliphatic and aromatic.

The curing reaction is exothermic and the rates of reaction increase as the temperature rises. This can cause problems when curing large samples, because it is difficult to dissipate the heat generated during the reaction and leads to an increase in the temperature of the system. This increase in the temperature is dependent on the reactivity of the resin and the curing agent, and also on the temperature of the reactants and their surroundings. The temperature rise can lead to bubbling, degradation of the resin, and void formation. It is important to control the heat of the reaction which can be done by choosing a suitable curing agent. Apart from the curing agent, the environment and electronic influences on the epoxide groups effect the curing process, the first through steric factors (24,25) the second enhance the reactivity of the epoxide groups (24,26,27).

### 2.4.1 Cure Mechanisms

This section gives a brief explanation of the curing agents and cure mechanisms. For more details see Tanak and May (2) and Potter (28). The epoxide ring is

susceptible to attack from a wide variety of substances. Polyfunctional curing agents react by polyaddition to the epoxide. Amines for example react with epoxy resin as shown in Figure (2.8). In this reaction, the primary amine reacts with an epoxy group Fig. (2.8a) to form a secondary amine and a hydroxyl group. This secondary amine can then undergo a reaction with another epoxide group to form a further secondary hydroxyl group and a tertiary amine, Figure (2.8b) Potter (28). It can be seen that amines react with epoxy resin by an addition reaction. Each active hydrogen atom attached to the amine nitrogens reacts with an epoxy group, and therefore a compound with more than two such hydrogen atoms will cross-link adi-epoxide. In addition the present of ether group (C-O-C) in the initial resin chain and each reaction produces a free hydroxyl group, and because of the presence of these highly ionic groups, amine-cured systems show exceptionally good adhesion properties. The polarity of these groups serves to create electromagnetic bonding forces between the epoxy molecule and the adjacent surface. The epoxy groups, like wise, will react to provide chemical bonds with surfaces, such as metals, where active hydrogens may be found (Lee Neville, 29).

When an epoxy resin is hardened with anhydride curing agents, a number of reactions take place. The reactions are illustrated as follows in Figure (2.9). It can be seen that in one of these reactions shown an

epoxy group react with an anhydride group, This is, in fact, not a feasible chemical reaction. To obtain a reaction, it is necessary to use either a resin containing some free hydroxyl, or an anhydride containing free acid. Only a small amount of either is necessary to set off the required chain reaction, free hydroxyl reacting to give an acid group as shown in (Figure 2.9, reaction 1) and free acid giving a hydroxyl as shown in (Figure 2.9 reaction 2). In Figure (2.9) reactions 1 - 3 all lead to the formation of ester linkages while reaction 4 leads to form an ether and no anhydride is involved.

For catalytic curing agents, epoxy groups may be polymerised by the catalysts which may be Lewis bases or inorganic bases or Lewis acids. The terminal epoxy group is opened and homopolymerisation occurs.

Lewis bases, such as tertiary amines, contain an unshared pair of electrons in an outer orbital which are available for bond formation (electron donors). The mechanisms for the polymerisation of epoxide resins by tertiary amines is shown in Fig. (2.10a). Tertiary amine is commonly used as an accelerator for anhydride-cured systems.

In the case of inorganic bases, Alkali metal hydroxides such as sodium or potassium hydroxide also catalyse the polymerisation of epoxide resins (see Fig. 2.10b).

In the case of Lewis acids, such as boron

trifluoride, contain empty electron orbitals in the outer shell of an atom which can be used in forming a bond by another atom donating two electrons to the bond (electron acceptors, see Fig. 2.10c). Boron trifluoride, are the most commonly used catalytic curing agents based on the Lewis acid. This is itself a gas which would react explosively with epoxides. It can be seen that most of the curing reactions are ionic whether the curing agent is an electron donator or an electron acceptor. Newey (30) found that steric factors play a more important part in determining the reaction rate of catalytic cured systems than they do in amine cured systems.

In general, aliphatic amines cure rapidly at room temperature and are strongly exothermic. Aromatic amines however only react with epoxy resin at elevated temperatures (28). Catalytic cured systems tend to be much more brittle because of the high density of cross-linking. They have high heat distortion temperature, show more shrinkage on cure and have poorer adhesion than amine or anhydride cured systems.

It is as equally important to choose the correct curing agent as the resin itself, for both play a part in determining the extent and nature of the intermolecular cross-linking. In the selection of curing agent various factors must be taken into account, such as i- the handling characteristics required in the uncured system (ie viscosity at working temperature, pot

life (the mixture of resin and curing agent has a finite pot life or gel time, beyond which the viscosity of the system has so increased as to render the materials unusable) the degree to which the reaction is exothermic and toxicity. ii- temperature requirements for cure and postcure. iii- the properties (physical, chemical, mechanical and electrical) required of the system. iv- the cost of the curing agent.

## 2.5 Properties of the Cured Resin

A fully cured epoxy resin system consists of a three dimensional network of molecules which has been formed by the cross-linking reactions. Figure (2.11) shows the structure of the network in a plane. The properties of the network are dependant on the basic molecular structure of the polymerised resin, and can be determined by the nature of the resin, the curing agent, the crosslinking segments, and the cure temperature and cure time.

To obtain the most favourable properties in any cured resin system it is important to achieve maximum cross-linking. This condition can often be improved by a post-cure at a temperature above the original cure temperature. Therefore the cure temperature and cure time are very important. The cross-linking density in different systems depends upon the functionality of the reacting species and the distance between their reactive groups. The density of cross-linking is increased by

increasing the functionality of the reacting species and decreasing the distance between the functional groups. This leads to improvements in short term thermal stability, chemical resistance and compressive strengths. The rigidity of the resin or curing agent molecules between these reactive groups, also has a great influence on the physical properties. For more details on the crosslinking processes and the measurement of the degree of crosslinking (see chapter four).

### 2.5.1 Morphology of Cured Resins

Several authors have studied the morphology of epoxy resin systems (31- 36,92). The microscopic studies by Racich and Koutsky (31),Mijovic and Tsay(32),Mijovic and Koutsky(33),and Morgan and O'Neall (34), showed that the inhomogeneous morphology of thermosetting polymers consists of nodular structure which has been attributed to differences in the crosslinking density. It has been postulated that a cured epoxy consists of nodules of a high crosslink density immersed in a low crosslink density matrix. The size of the nodules depends upon the initial cure rate. The properties of the cured resin such as density, the glass transition temperature (Tg)(see section 4.1.1) and hardness are all related to this nodule size.

Studies by Morgan and O'Neall (35) on the relationship between physical structure and mechanical

response show that the mechanical properties are governed by the size and concentration of highly crosslinked regions and the free volume of the material interconnecting such regions. Racich and Koutsky (31), state that bulk fracture occurs between nodules, rather than through them which confirms that the nodules are sites of higher crosslink density. Racich and Koutsky (92) examined the changes in nodule size with respect to curing agent concentration. As the concentration of curing agent increases, the nodule size decreases and at high concentrations the nodules become less defined.

Mijovic and Koutsky(33) studied the correlation between the morphology of epoxy resin systems and their mechanical properties. They suggested that a careful control of cure chemistry can produce a desired morphology, which in turn directly influence the ultimate mechanical properties of the resin. Therefore, the optimization of the mechanical properties of a bulk epoxy resin can be achieved through control of its fundamental morphological structure.

# CHAPTER THREE

# MATERIALS AND SAMPLE PREPARATIONS

## 3.1 Introduction

In this chapter, materials and sample preparation for different measurement applications are described in detail under two main sections.

The materials section outlines the main features of the materials and some of the material tests which were the necessary basis for subsequent explanation and discussion of electrical behaviour. The sample preparation section was concerned with preparing thin films of epoxy resin system. The technical difficulties involved in forming the necessary films are considerable in view of the many variables which may affect their properties. This will be discussed in this section. Difficulties can occur in the preparation of the films because of the close association of the electrical properties of the films and their chemical properties. For example, the films may absorb water vapour, oxygen, or hydrogen etc., when exposed to the atmosphere, or their chemical properties may depend critically on the method of preparation and the conditions during the film preparation. Further problems can also arise in making suitable electrical contacts to the films. These problems make the technological side of thin film work extremely complicated and time consuming.

## 3.2 Materials

The material used in this study was an epoxy resin of diglycidyl ether of bisphenol A (DGEBA) produced by Ciba Geigy as resin (MY750) together with two different hardeners. One of the hardeners was a hydroxyalkylated polyamine produced by Ciba Geigy as hardener (HY 956) mixed in a ratio of 4:1 by weight. The other was a dodecenyl-succinicanhydride (HT964) or (DDSA) with an accelerator of benlyldinethylamine (1 phr), provided by Aldrich chemical co. These materials were mixed in a ratio of 1:1.3:0.01 by weight. The epoxy resin MY750 is in a liquid state because the higher molecular weight impurities prevent the monomer from crystallising. MY750 is a multipurpose liquid resin which may be used with a wide range of hardeners. The choice depends on the combination of specific properties required. The HY956 hardener is a liquid aliphatic amine curing agent. It is a moderately low viscosity, reactive hardener for room temperature casting and laminating. The DDSA is solid anhydride curing agent (see Fig. 3.1a). It is a moisture-sensitive hardener. Benlyldinethylamine is a liquid accelerator (see Fig. 3.1b) used to promote rapid curing of small castings. Accelerators are admixed in small quantities with the less reactive Araldite systems in order to adjust both usable life and curing schedules.

### 3.2.1 Micro analysis and Molecular Weight

Both the epoxy resin MY750 (diglycidyl ether of bisphenol A) and the hardener HY956 (hydroxyalkylated polyamine) were examined by micro-analysis.

In the case of the epoxy resin MY750 the relative proportions of its constituent elements were deduced from the chemical formula given by Crowson and Arridge (38). However this substance was also known to contain small amounts of impurities, and micro-analysis was used to determine their proportion. In the case of the hardener HY956, no such chemical formula was available. Therefore this analysis provided the relative proportions of its constituent elements and the molecular weight may be estimated. The chemical formula can be obtained if the molecular weight is also known. To check the molecular weight estimate, it was also determined by molecular weight osmometry.

#### 3.2.1.1 Carbon, Hydrogen, Nitrogen Method

The method of analysis used was to determined the proportions of carbon, hydrogen, and nitrogen atoms in the compound by gas phase chromatography. From this, the proportion of oxygen atoms was deduced.

The technique is based on the classical PREGL DUMAS METHOD, using a Carlo erba 1106 analyser. Samples were weighed into lightweight tin capsules and dropped at intervals into a vertical quartz tube, maintained at 1030°C and through which a constant flow of helium was

maintained. When the samples were introduced, the helium stream was temporarily enriched with pure oxygen. Flash combustion takes place, primed by the oxidation of the tin capsule. Quantitative analysis was achieved by passing the mixture of gases over $Cr_2O_3$. The mixture of gases was then passed over copper at 650 °C to remove the excess of oxygen and to reduce the oxides of nitrogen to nitrogen. It was then passed through a chromatographic column of PORAPAK QS heated to approximately 100 °C. where the individual components were separated as $N_2$-$CO_2$ -$H_2O$. They were measured by a thermal conductivity detector. The instrument was calibrated by the combustion of standard compounds (Acetanilide).

Molecular weights for both the epoxy resin MY750 and the hardener HY956 were determined. The molecular weight for epoxy resin MY750 was also deduced from the chemical formula given in (38) and from the micro analysis. The impurities content could also be estimated.

### 3.2.1.2 Molecular Weight by Vapour Pressure Osmometry

In the case of the hardener HY956 the molecular weight was also deduced from vapour pressure osmometry measurements. This technique required the material to be dissolved in a solvent. Measurements were made in a constant temperature chamber, filled with a saturated vapour of the appropriate solvent. The chamber contains

two differentially matched thermistors which measure any change in temperature. Two syringes were present, one for the solvent and one for the sample. These were used to apply a drop of sample and solvent onto the thermistor beads. As there is a difference in vapour pressure between the sample and the solvent, the solvent from the saturated atmosphere will condense onto the solution drop causing its temperature to rise and therefore a change in temperature $\Delta T$ will be measured.

As the thermistors were part of a Wheatstone Bridge $\Delta T$ can be measured as the difference in resistance $\Delta R$. It may be shown that the molecular weight is related to $\Delta R$:

$$\text{Molecular Weight} = \frac{\text{Sample weight} \times \text{factor (for solvent)}}{\Delta R}$$

Acetone and chloroform were tried as solvents. It was found that acetone was better because HY956 was more soluble in it. Fig. (3.2a) illustrates the chemical formula for epoxy resin MY750 given in (38). The portion of the molecule in square brackets is a repeating unit (see chapter two), and a typical value of n for this resin is 0.2, so that each molecule has two reactive epoxy end groups, and one molecule in five has an OH group available for reaction. The relative proportions of the constituent elements for the epoxy resin MY750 and the hardener HY956 obtained by micro-analysis method are illustrated in table (3.1). It can be seen that the epoxy resin MY750 contains a small amount of chlorine as

impurity. The molecular weights for the epoxy resin MY750 were calculated from both the relative proportions of the constituent elements obtained by the micro-analysis method and from the chemical formula. These were in very good agreement as shown in table (3.2) (see Appendix 3.1).

The molecular weights for the hardener HY956 were obtained by vapour pressure osmometry method using two different solvents and were also calculated from the relative proportions of the constituent elements obtained by the micro-analysis method (see Appendix 3.1). The results are illustrated in table (3.3). It can be seen that the molecular weight obtained by vapour pressure osmometry using acetone as a solvent was in better agreement with the molecular weight calculated from the micro-analysis method than results made using chloroform as a solvent. The better agreement is attributed to the increased solubility. The chemical formula for the hardener HY956 was deduced from the results obtained from both micro-analysis method and vapour pressure osmometry method as shown in Figure (3.2b).

### 3.2.2 Structure of Epoxy Resin System

Diffraction methods are of considerable importance in the study of the structural analysis of materials. In this section an examination of the epoxy resin system MY750/HY956 by X-ray methods is described.

The X-ray technique in the present work is based on the classical powder method. A detailed description of this method is given in Smallman and Ashbee (39). In the present application a fully cured epoxy resin system was produced, ground into a fine powder and then loaded into a capillary tube. (The cure of epoxy resin systems will be discussed in detail in chapter 4). A standard X-ray powder method camera was used. If the material is crystalline, a series of rings or spots will be produced on the film and if it is amorphous, halos will be produced. If the material is perfectly amorphous, a cloud or fog will be produced on the film. In the present experiment, the diffraction pattern was of a foggy nature, with no indication of halos or preferred scattering at any angle. This indicates that the epoxy resin system MY750/HY956, was fully amorphous as expected.

## 3.3 Sample Preparation

The electrical properties of a material can be determined by using it as a dieletric between the plates of a parallel-plate capacitor. As far as the epoxy resin system is concerned, there are a number of difficulties with constructing a solid thin film capacitor.

I. The materials from which it is formed are mostly liquid (see section 3.2) and the conversion from a liquid into a solid cross-linked polymer makes it hard to produce a sample which is flat, thin and free from

gas bubbles. The change of phase can also produce volume changes.

II. The epoxy resin system is a strongly adhesive material, making it very difficult to manipulate.

In the present work, different sample preparation techniques for epoxy resin systems were tried for different applications.

### 3.3.1 Sample Preparation Techniques for Epoxy Resin System MY750/HY956

#### 3.3.1.1 Sample Preparation Techniques for Conductivity and Dielectric measurements.

In order to study the conductivity and the dielectric properties of the epoxy resin system, two sample preparation methods were tried. These methods were as follows.

##### 3.3.1.1a Microscope Slide Method

In this method, a glass microscope slide was used, which had been cleaned thoroughly by (i) cleaning with tepol (a commercial available detergent), (ii) rinsing thoroughly in running water, (iii) dipping in de-ionised water, (iv) dipping in Methanol and (v) drying in an oven.

The first electrode was then made by evaporating aluminium onto the microscope slide under high vacuum. The epoxy resin system MY750/HY956 was made up in the

indicated ratios by weight (see section 3.2) using a balance measuring to < 0.1 mg. Once the desired ratio was made, it was mixed thoroughly and the mixture was spread uniformly onto the first electrode. By adding 1-3 cm by volume of tolouene ($C_6H_5.CH_3$) as a solvent with the mixture, it was found that the reduction in the viscosity of the mixture, enabled the mixture to be spread more easily onto the first electrode. This meant a thin film produced could be produced more readily. The sample was left in the oven for curing (see chapter four). After the sample was fully cured, the second electrode was then made by evaporating aluminium onto the cured epoxy. For both electrodes, masks were made so that the aluminium only covered a specific area and shape of the sample. The shape was chosen so as to produce as large an area of electrode as possible and which could be made repeatedly and uniformly. It is difficult to make an accurate edge correction, to capacitance measurements because it changes in the presence of the test material.

In order to eliminate the effect of surface conduction round the edges of the specimen, which are particular serious, with hygroscopic materials, the electrodes were kept away from the edge of the specimen and a guard electrode was painted round the top electrode, using silver paint. A fine of copper wire bonded to each electrode by silver loaded epoxy enabled electrical connections to be made to the measuring

circuit. This microscope slide technique for sample preparation was used, in order to study the electrical properties of epoxy resin systems, in particular conductivity, dissipation factor, capacitance and the effect of gamma irradiation on these. However the results produced were poor because of the following reasons:-

1. It was found that the specimens contained voids due to the method of production.

2. It was found difficult to ensure that the specimens were completely flat.

3. It was difficult to make the specimens thinner than 0.3 mm. Specimens of less than 0.1 mm were needed for infra-red spectroscopy and for measuring the ionic jumping distance of the epoxy resin system.

To over come these difficulties the epoxy resin system was found to adhere to the following materials - metal, glass, aluminium, and P.T.F.E. However the epoxy resin system did not adhere completely to mica sheets. In fact it was possible to remove the resin samples from these mica sheets without breaking them provided they were quite small. Unfortunately, tiny pieces of mica remained embedded in these intact samples, as was revealed by examination with a polarisation microscope (40).

The use of a polarisation microscope to identify the tiny pieces of mica which were embedded in the epoxy

resin samples was based on the structure of the epoxy resin system and the mica. The structure of the epoxy resin system is amorphous (see section 3.2.2.), whereas the structure of the mica sheets is crystalline. When plane polarised transmitted light was used, the polarisation microscope produces a bright image for all positions of the rotating stages, both for the epoxy resin system and mica sheets. When crossed polars were used, the polarisation microscope produces a dark image for all positions of the rotating stage with the epoxy resin system as an object. This is because this material is amorphous. Mica sheet, being a crystalline material, rotates the plane of polarised light. This produces images in the polarising microscope which change as the stage is rotated. The image changes alternatively from dark to a greyish blue colour. In the case of tiny pieces of mica embedded in the epoxy resin sample, these appear as regions of either dark or greyish blue when viewed with the polarising microscope. The image changes as the stage is rotated. Since it proved impossible to produce samples of resin free of mica, this method was rejected as a means of producing samples.

3.3.1.1b Polyester Sheet Method

Polyester sheets were tried in place of the mica used in the previous technique. These sheets were much more flexible and easier to manipulate than the mica and in addition, they did not break into small pieces.

Furthermore, it was found that the resin adhered to the polyester sheets only partially and to a less extent than the mica sheets. By very careful manipulation, it was possible to peel the polyester sheets away, even from large samples, leaving them intact. Microscopic examination of the samples showed that there was no trace of polyester sheet left in the epoxy resin system.

In this method, two sheets of polyester were used, each of which had been cleaned thoroughly by (i) cleaning them with Teepol (a commercially available detergent) (ii) rinsing thoroughly in running water, (iii) dipping in de-ionised water (iv) dipping in methanol and (v) drying in an oven. The first polyester sheet was mounted on a piece of glass using sellotape. A rectangular metal frame of dimensions 100mm x 60 mm with a hole in the centre was made. The hole size corresponds to the size of the specimen produced. The edge of the hole was lubricated with silicon grease (general laboratory lubricant, Edwards high vacuum LTD), so that the epoxy resin system only partially adhered to the metal after curing and was thus easy to remove. In the case of dielectric measurements samples, the thickness of the metal frame and the diameter of the hole was 0.2 mm and 35 mm respectively. However in the case of specimens for conductivity measurements, the thickness of the metal frame and the diameter of the hole was 0.5 mm and 20 mm respectively. The epoxy resin system MY750/HY956 was made up in the indicated ratios

by weight (see section 3.2). Once the desired ratio was made, it was placed in a vacuum system which was then evacuated to remove dissolved gas and gas filled voids in the resin. The two compounds were then removed from the vacuum system and mixed thoroughly. The glass on which the polyester with the metal frame was mounted was then placed in the vacuum system. The mixture was poured into the hole in the metal frame through a glass tube, which prevented the mixture penetrating between the metal frame and the polyester sheet. The glass tube was 17 mm in diameter, and fitted into the hole in the metal. The vacuum system was evacuated to remove gas bubbles and air from the mixture. These form during the mixing of the epoxy resin MY750 and the hardener HY956. After mixing the two compounds, the viscosity of the mixture increases with time and this can lead to great difficulty in removing the glass tube from the mixture and prevents the mixture flowing easily to take the shape of the metal frame hole. Consequently only 30 minutes were allowed to elapse before the assembly was removed from the vacuum system and the glass tube very gently removed from the mixture. The second polyester sheet was rolled gently over the metal frame and a heavy weight was then placed over the sheet to produce a second flat surface on the liquid sample. After 10-15 hours at room temperature, during which time partial curing occurs, the assembly was placed in the oven to complete the curing (see chapter four). After curing,the

weight was removed and the two polyester sheets peeled off from the sample. A sharp knife was used to release the solid sample from the edge of the metal frame hole. The fully cured sample was placed in a vacuum system and electrodes made by evaporating aluminium onto each side of the sample under high vacuum. Masks were made so that the aluminium only covered a specific area and shape as in Figure (3.3). Electrode configurations were designed to eliminate both edge and surface conductivity effects. Copper wire was bonded to each electrode by silver loaded epoxy enabled electrical connection to be made to the measuring circuit.

In the present work the polyester sheet technique for sample preparation was used, in order to study the electrical properties of epoxy resin system, in particular conductivity, dissipation factor, capacitance, and the effect of gamma irradiation on these properties. These measurements proved to be satisfactory.

### 3.3.1.2 Sample Preparation Technique for Ionic Jumping Distance Measurements

In the case of ionic jumping distance measurements, when samples of less than 0.1 mm were needed, the sample preparation method was similar to the polyester sheet method, apart from the fact that no metal frame was used. This enabled thinner samples to be made.

### 3.3.1.3 Sample Preparation Techniques for Infra-red Spectroscopy

In the present work, two sample preparation methods for infrared spectroscopy were tried. These methods are as follows.

#### 3.3.1.3a - Potassium Chloride Disc Method

In this method, the epoxy resin system MY750/HY956 was made up in the indicated ratio by weight (see section 3.2). In order to remove the gas bubbles and dissolved air from the two compounds MY750 and HY956 and from the mixture, the pressure over the sample was reduced (see section 3.3.1.1.b). After two hours the mixture was removed from the vacuum system and left for 10-15 hours at room temperature during which time partial curing occurs. An appropriate amount of the partially cured epoxy resin system was weighed out into a 3x 3/8" test tube. Epoxy resin strongly absorbs in the infrared. Therefore it is important that the weight of the material is accurately controlled since it is difficult subsequently to reduce or increase the specimen thickness. In another 3x 3/8" test tube, 200 mg of the potassium chloride was weighted out (the weight of the potassium chloride need not be as accurately controlled as that of the epoxy resin system since it is transparent to IR radiation, and it is permissible to measure out the potassium chloride by volume using a calibrated 3x 3/8" test tube). The epoxy resin system

was in the form of a coarse powder, a micro spatula was used to grind it into a fine powder in the test tube. One third of the potassium chloride was then added to the powdered epoxy. The two substances were mixed together with the micro spatula and the mixture was poured into an agate vibration mill which contains two agate balls, and ground. The amplitude of vibration was changed every 20 minutes during this process. The ground mixture was pressed into a disc using a die and hydraulic ram. The disc was transferred by means of a spatula to one of the special disc holders of the IR - instrument. It was found that the IR-spectrum which was obtained by the potassium chloride disc method was not as well defined as the IR-spectrum which was obtained using a subsequent method (sodium chloride disc method).

3.3.1.3b - Sodium Chloride Disc Method

In this method, the epoxy resin system MY750/HY956 was made up in the indicated ratios by weight (see section 3.2) and degassed as previously indicated. The mixture was allowed to stand under vacuum for 30 minutes. A small drop of the mixture was then smeared over a sodium chloride disc of 25 mm diameter by using a clean polyester sheet. A heavy weight was placed over the polyester sheet to keep the mixture layer thin and flat. After 10 hours at room temperature, after which the epoxy resin was partially cured, the weight was removed and the polyester sheet was peeled off from the

disc. The disc was then transferred to one of the special disc holders of the IR-instrument.

### 3.3.1.4 Sample Preparation Techniques for Conductivity and Dielectric Measurements during the Curing Process

The cure of an epoxy resin systems will be discussed in detail in chapter four. In order to study the changes in conductivity and dielectric properties of the epoxy resin system during curing, two sample preparation methods were tried, these methods are as follows.

#### 3.3.1.4a Cylindrical Method

In this method, the sample was made up as shown in Fig. (3.4). A glass cylinder of diameter 3.5 mm and length of 30 mm was used. The glass tube was cleaned thoroughly and dried in an oven. The epoxy resin system MY750/HY956 was made up in the indicated ratios by weight. Once the desired ratio was made, a vacuum system was used to remove gas bubbles and dissolved air from the two compounds (MY750 and HY956). After this treatment, the compounds were mixed together,the mixture was used to fill the glass tube and metal end caps were mounted on the tube to form the electrodes. Aluminium foil and Sellotape were used to secure the end caps in position. Copper wire was soldered to each electrode for electrical connections. The results which were obtained

by using this method were poor and unsatisfactory compared with the results which were obtained using a subsequent method (sandwich method). The problem leading to the poor results were :

1. It was found that the specimens contained voids due to the method of production.

2. It was difficult to retain the metal end caps in place, at temperatures above 60°C due to the out-gassing of the epoxy resin system.

3. With this type of sample it was very difficult to take any conductivity measurements until 30 minutes after the start of the curing reaction. This was due to the time required to complete the manufacture of the sample. Therefore data on the early stages of curing was unobtainable. This type of sample was rejected for future work.

3.3.1.4b Sandwich Method

In this method, the sample was made up as shown schematically in Fig. (3.5a). Pairs of microscope slides were used. These had been cleaned thoroughly. The contacting electrodes consisted of a thin layer of aluminium which had been evaporated onto each microscope slide under high vacuum. A mask was made so that the metal only covered a specific area and shape of the glass slide (see Fig. 3.5b). The electrode was kept away

from the edge to reduce the effect of surface tracking between electrodes. In order to make electrical contact, a tail was made from the electrode to one end of the microscope slide. A piece of wire was bonded to the aluminium tails by silver loaded epoxy and enabled electrical connections to be made to the measuring circuit. The epoxy resin system MY750/HY956 was made up in the indicated ratios by weight (see section 3.2) and prepared using the procedure described previously. The mixture was sandwiched between the electrodes. When sandwiched, the electrodes were positioned above each other, making sure that they were not skew. The two tails were made to come out at opposite ends of the specimen as shown in Fig. (3.5a). This allowed the substrates to be flat without the connections getting in the way and, also, this meant that the capacitance between the tails would be greatly reduced. Three pieces of polymer wire 1 mm in diameter were used as spacers between the two microscope slides to ensure even thickness of the resin samples Fig. (3.5a). The spacers were held in place by silicon grease.

### 3.3.1.5 Sample Preparation Technique for Differential Scanning Calorimetry

Differential scanning calorimetry (DSC), is one of the methods which were used to study the curing of epoxy resin systems. The curing of epoxy resin systems will be discussed in detail in chapter four.

For DSC sample preparation, the epoxy resin system MY750/HY956 was made up in the indicated ratios by weight (see section 3.2) and prepared using the procedure described in section (3.3.1.3 b), sodium chloride disc method. The mixture was sealed into a small metal pan. An empty sealed pan was prepared also as a reference. Both the sample and the reference pans were transferred by means of a spatula to the DSC instrument. In order to estimate the degree of cure of the epoxy resin system, the sample pan was tested under different curing temperatures.

3.3.1.6 Sample Preparation Technique for Thermally Stimulated Discharge Current (TSDC)

Thermally stimulated discharge current (TSDC), is one of the established methods used for examining the state of curing in the epoxy resin systems. For TSDC sample preparation, the sample was prepared using the same procedure described in the polyester sheet method (section 3.3.1.1.b), except that the metal hole was 36mm in diameter and there was no wire bonded to each electrode for electrical connections.

### 3.3.2 Sample Preparation Techniques For Epoxy Resin System MY750/DDSA

#### 3.3.2.1 Sample Preparation Technique for Dielectric Measurements

The epoxy resin system was made up in the indicated ratios by weight (see section 3.2). Once the desired ratio was made, the epoxy resin MY750 and the hardener DDSA were degassed as previously indicated. The two compounds plus the accelerator were then mixed thoroughly and the mixture degassed again. The mixture was then poured into an aluminium foil dish of 45 mm diameter and 1 mm thick. The specimen was placed in an oven to cure. The fully cured sample was placed in a vacuum system and the top electrode was made by evaporating aluminium on the top side of the sample. A mask was made so that the aluminium only covered a specific area and shape of the sample. The lower electrode consisted of an aluminium foil dish. Wire bonded to the electrodes using silver loaded epoxy resin enabled electrical connections to be made to the measuring circuit.

#### 3.3.2.2 Sample Preparation Technique for Dielectric Measurements During Curing Process

In order to perform dielectric measurements during the curing process a sample was prepared using the same method as described in section (3.3.2.1). Once the

epoxy resin MY750 and hardener DDSA were mixed with the accelerator, the mixture was poured into an aluminium dish and dielectric measurements were performed on the sample while it was still in a liquid state. Therefore the top electrode of the sample consisted of a metal electrode of 38 mm in diameter separated from the sample by a polyethylene film to overcome the influence of ionic conduction (41). Three tiny pieces of 1 mm thick PMMA were placed in the sample to hold and keep the top electrode flat.

### 3.3.2.3 Sample Preparation Technique for Differential Scanning Calorimetry

For DSC sample preparation for the epoxy resin system MY750/DDSA, the sample was prepared using the same method as described in section (3.3.1.5).

The MY750/HY956 and MY750/DDSA samples were kept in a glass jar and $P_2O_5$ was kept in close proximity to the samples in order to keep the samples dry and thus avoid any humidity effects.

# CHAPTER FOUR

# THE STUDY OF THE EPOXY RESIN SYSTEMS DURING CURING

## 4.1 Introduction

This chapter is concerned with the study of the three-dimensional network of the cured resin. The properties of the cured resin and the curing mechanisms were discussed in detail in chapter two. It is clear that their physical, electrical and chemical characteristics, all stem from the basic molecular structure of the polymerised resin. Important factors at the molecular level in determining these properties are:- (i) the extent of cross-linking, ie the degree of cure, (ii) the nature of the resin molecule between cross-links, and (iii) the molecular nature of the curing agent.

To obtain the most favourable properties in any cured resin system, it is important to achieve maximum cross-linking. This condition can often be achieved by a post-cure at a temperature above the original cure temperature (1).

The increased molecular mobility brought about by heating, gives the molecules further opportunities to undergo collision and bond formation leading to a greater degree of cross-linking. Therefore the cure temperature and length of cure time are very important. Molecules present in the resin which do not have one or

more terminal epoxide group and hence do not enter into the curing reaction lead to lower degrees of cure. The cross-link density in different systems depends upon the functionality of the reacting species and upon the distance between their reactive groups. The nature of the resin and curing agent molecule between reactive groups, whether it is rigid or flexible, also has a direct influence on the physical properties. The cross-link density can be increased by decreasing the distance between functional groups and by increasing the functionality of the reacting groups. This leads to improvements in short term thermal stability and chemical resistance. Resin systems with high cross-link densities normally exhibit higher glass transition temperatures (Tg) than those with more widely spaced cross-links.

### 4.1.1 The Glass Transition Temperature (Tg)

As the temperature of a polymer is raised through its glass transition point the nature of the polymer changes from a hard, glassy, and brittle state to a softer and more flexible rubbery one. This is frequently accompanied by quite dramatic changes in properties such as refractive index, thermal conductivity, dielectric loss, mechanical stiffness, heat capacity and the volume expansion coefficient. Tg can be determined by measuring the specific volume of the material as a function of temperature. At the glass

transition the specific volume-temperature curve has an abrupt change in slope. Below Tg, molecular motion is frozen to the extent that there is insufficient thermal energy to allow segments of the molecular chain to move as a whole.

At Tg the thermal energy has sufficiently increased to allow the movement of relatively large molecular segments which jump from one position to another by rotation about carbon-to-carbon bonds (42). Tg is dependent on the chain flexibility and the free volume associated with the chemical structure, as well as the overall crosslink density. The glass transition temperature of a cured epoxide resin will therefore reflect the extent and nature of its cross-linking and can be used as a measure of its thermal stability; it can be determined by various methods such as differential scanning calorimetry (DSC) and thermally stimulated discharge current (TSDC) (see sections 4.2.1 and 4.2.4).

### 4.1.2 Measurement of Degree of Cross-linking

Many different methods have been used to estimate the degree of cure of epoxy resin systems including differential scanning calorimetry (DSC) (43-46), thermally stimulated discharge current (TSDC)(47-53,58), infrared spectroscopy (IR) (64-66,81), dielectric relaxation (45,47,67-77) and electrical volume resistivity (78,83-85). The infrared spectroscopy

methods measure the extent to which the epoxide groups have been consumed and are widely used as a measure of the degree of cure. The other methods are based on the measurement of properties that are directly or indirectly related to the extent and nature of the cross-links.

#### 4.1.2.1 Differential Scanning Calorimetry (DSC)

Commercial differential scanning calorimetry equipment became available during the early 1960's and it provides a convenient and useful method of monitoring the course of exothermic reactions such as those involved in the cure of epoxy resins. Its main advantages are the modest requirements in terms of sample size, of the order of milligrams. It can provide with relative speed quantitative data on overall reaction kinetics. In addition it can measure thermal transitions such as the glass transition temperature (Tg) which are associated with the degree of crosslinking or state of cure of a resin. The method involves measuring the difference in the rate of heat absorption by a sample with respect to an inert reference, as the temperature is increased at a constant rate. In the absence of exothermic or endothermic chemical reactions the measured heat flow output is proportional to the sample heat capacity. A second order transition such as that which occurs at the glass transition temperature (Tg) of a polymer is shown as a

discontinuity in heat capacity. Fava (43) pointed out that Tg increases during cure and is a sensitive index of effective cure. Once Tg reaches the cure temperature, further reactions in the glassy state are extremely limited; hence the importance of curing an epoxy above its Tg for optimum properties. In this chapter, the technique of DSC was used to measure the glass transition temperature Tg associated with the degree of cross-linking.

#### 4.1.2.2 Thermally Stimulated Discharge Current (TSDC)

Thermally stimulated discharge current analysis provides an attractive method for characterising the resin in terms of degree of cure. Furthermore, it allows a precise analysis of the single relaxation process and gives a complete picture of the temperature dependant relaxation. It also allows the relaxation parameters of relaxation time and activation energy, to be determined from a single measurement (frequency equivalence of TSDC is $10^{-2}$ - $10^{-4}$ Hz.). Thermally stimulated discharge current measurements have now become a powerful tool for observing the molecular motion in polymers (50-53). The technique can be used for studying charge motion in solid dielectrics and is based on the thermally activated release of either trapped charges or from localised energy levels. During heating, the release of trapped charge or polarisation from a dielectric produces a current peak analogous to the more widely

known glow curve observed when a thermoluminescent material is heated (54,55). The source of the thermally stimulated current may be, (a) the thermal release of trapped electrons, holes or ions (b) dipole orientation polarisation, or (c) space charge polarisation. If a material contains several traps of different energy and these traps are filled ( polarisation cycle), then a corresponding number of current peaks will be observed during heating (depolarisation) (see Figure 4.4). The procedure for the TSDC technique (56,57), used primarily to study dipole polarisation will now be described. A material containing an electric dipoles is first polarised with a d.c. field, E, for a time, t, at a temperature, T, where dipole orientation can occur. The specimen is then quenched to a suitably low temperature, with the field maintained. At this temperature dipole motion essentially ceases. The field is removed and the specimen temporarily short circuited. During subsequent re-heating, (constant or hyperbolic heating rates are used), the discharge current is measured as a function of temperature. A valuable account of the theory is given by Seanor (49).

Few studies have been performed on epoxy resins. Brittain and co-workers examined the $\beta$ relaxation of (TGDDN/DDS) and found that TSDC can distinguish between different cure conditions and therefore degree of cure (58). The effect of mica flakes incorporated in epoxy composites was investigated by Tanaka and co-workers

(59). It has been found that ionic conduction is the major component of electrical conduction of epoxies in relatively low electric fields (60,61). It is considered, therefore, that conductive ions in the resin matrix play an important role in the interfacial polarisation, namely charge trapping at heterogeneous interfaces. In the present work, the TSDC method has been used in a preliminary examination of the effect of cure on the $\alpha$-transition (Tg).

#### 4.1.2.3 Infrared Spectroscopy (IR)

Infra-red absorption spectra are widely used as a tool to study the characterisation of polymers (63). The most comprehensive published set of infra-red spectra of uncured and cured epoxide resins is given by Lee and Neville (81). The technique is based on the absorption of radiation in the infra-red frequency range due to the molecular vibrations of the functional groups contained in the polymer chain (62). This technique can also be used to determine the epoxide content of a resin system during and after cure (64-66). Infra-red spectroscopy has been used in this study to measure the extent to which the epoxide groups were consumed to determine degree of cure.

#### 4.1.2.4 Electrical Volume Resistivity

The study of electrical volume resistivity as a tool to determined the degree of cross linking is

important since the occurrence of ionic conductivity during the curing of resins has been recognized since the earliest work (80). In epoxies, Fava (79) proposed that sodium and chloride ions are the particular species involved, the origin of the ions being from the reaction used to produce the starting materials. The reaction of epichlorhydrin with Bisphenol A to make the diglycidyl ether of Bisphenol A (DGEBA) produces (HCl) as a by product which is subsequently neutralized with alkali (81) (see chapter two). Even after treatment to remove NaCl, there are residual chloride ions present in commercial DGEBA resins at concentrations typically on the order of tens of pmm (82), with corresponding concentrations of cations. These impurities actually provide a remarkably useful probe of the resin system. Using the change in electrical volume resistivity with time at various temperatures to determine rates of cure and activation energy (78,83), Warfield and Petree (85) suggested that the temperature-dependence of resistivity of the system should be related to the extent of polymerisation. They based this proposal on the observation that uncured resins had but a small temperature-dependence of resistivity, whereas cured resins had a high dependence. Fineman and Puddington (84) pointed out that changes in the resistance during polymerisation are sensitive to changes in the internal molecular arrangement of the polymer and to the rate and extent of cross linking.

In the present work, resistivity was determined continuously throughout the polymerisation process, during which the monomer changes from a low viscosity liquid to a gel and finally to a high crosslinked solid, with an accompanying large increase in the resistivity.

#### 4.1.2.5 Dielectric Analysis

Measurement of the electrical properties of epoxy resin systems, in particular the dissipation factor, are an effective way of investigating curing processes. The theory of the dielectric are discussed in section (4.3.5.1). The change of dissipation factor during curing has been studied by a number of workers (67-73,77). Some investigators (67) have been only concerned with changes in dissipation factor caused by ionic conduction.

However, by studying the dipole behaviour whilst a resin is curing, information can be obtained about the chemical structure of that resin. Most curves of dissipation factor against time, for the curing period exhibit a peak such as the one appearing in Figure (4.21a). Some workers (69,70) consider that such peaks indicate the time at which the resin begins to gel. Others (72,73) disagree with this hypothesis because the time of appearance of the peaks is frequency dependent, which implies that for identical composition and curing temperature gelation is occurring at different times. They suggest that the peak is related to an $\alpha$-relaxation

process caused by the orientation of segments of molecular chains (71,72). The segments responsible for the $\alpha$-peak are able to rotate in the applied field, and will be independent of molecular weight, since the rotation is independent of the motion of the whole molecule. Their point of view also looks very doubtful, since often the peaks occur before there is any real likelihood of long molecular chains being formed.

In the present work, a series of experiments to provide information about the behaviour of both dissipation factor and capacitance during the period of curing and a dielectric relaxation model of the behaviour of epoxy polymer molecules formed in the curing process are described.

## 4.2 Experimental (Instrumentation and Measurements)

In this section the instruments and measuring techniques which were used to investigate the curing process of the epoxy resin systems are outlined. Each technique required its own method for sample preparation. These have been described in section 3.3. Differential scanning calorimetry (DSC) sample preparation was described in sections 3.3.1.5, 3.3.2.3, infrared spectroscopy (IR) sample preparation was described in section 3.3.1.3b, dielectric measurement sample preparation was described in sections 3.3.1.4b, 3.3.2.2, thermally stimulated discharge current (TSDC)

sample preparation was described in section 3.3.1.6 and electrical volume resistivity sample preparation was described in section 3.3.1.4b.

### 4.2.1 Differential Scanning Calorimetry (DSC) Technique

DSC measurements were made on a Du Pont 910 instrument, illustrated in Fig. (4.1). The instrument utilises a silver block chamber with an external heater. The chamber contains a constantan disc with raised platforms for the sample and reference containers. The temperature difference between sample and reference was monitored by area thermocouples formed by the constantan disc and chromel wafers under the platforms. Amplification and electronic compensation of the differential temperature signal provides a linear calorimetric response over a wide temperature range. Cylindrical pans pressed from pure aluminium foil were used as sample containers. The theory of this instruments is discussed by Lee and Levy (86). By using this technique, the degree of cure of the epoxy resin system was determined by measuring the glass transition temperature Tg. During a DSC scan of the epoxy system, the baseline shifts stepwise endothermically, indicating an increase in sample heat capacity. This is the so-called ( $\alpha$- transition). The glass transition temperature was taken as the intersection of extrapolations of the baseline on the low temperature side of the transition and the maximum slope of the

transition as shown in Fig. (4.2). As the cure proceeds, the Tg value increases until a final stable point is reached. The material can then be considered fully cured (43).

### 4.2.2 Infrared Spectroscopy Technique

In the present work, infrared spectroscopy was carried out using a dispersive instrument (Grating infrared spectrophotometer, PERKIN-ELMER 257). This instrument utilises a grating to geometrically disperse the infrared radiation. Using a scanning mechanism, the dispersed radiation was passed over a slit system which isolated the frequency range falling on the detector. In this manner, the spectrum, that is, the energy transmitted through a sample as a function of frequency, was obtained. This infrared method is highly limited in sensitivity because most of the available energy is being thrown away, that is, it does not fall on the open slits. The theory of this instrument is discussed by Miller and Stace (87). The degree of cure of the epoxy resin system was qualitatively observed by noting the changes in the infrared spectra which were taken at various stages during cure.

### 4.2.3 Dielectric Measurement Technique

A capacitance bridge (General Radio type 716-C) was used to measure both dissipation factor and capacitance over a frequency range 200 Hz to 100 kHz.

Measurements at frequencies below 200 Hz were not taken, due to the high ionic conduction and electrode polarisation (67,68). Detail on the capacitance bridge instrument are discussed in chapter five. The temperature during experiments was controlled by an adjustable oven. The temperature was maintained to within 1°C. The frequency was fixed at 10 kHz during the experiments for which frequency effects were not being investigated. Similarly the temperature was 20°C for those experiments for which thermal effects were not being considered.

### 4.2.4 Thermally Stimulated Discharge Current Technique

The apparatus used in this technique is shown schematically in Fig. (4.3). The method is as described by Van Turnout (53). The sample, in disc form, was placed between two electrodes and charged by application of a D.C. field at high temperature. While maintaining the field the sample was cooled to a sufficiently low temperature (usually around room temperature) and short circuited. The discharge current generated as the sample was reheated at a linear rate (3 °C/min.) was measured with a sensitive electrometer, (Keithley 602) and recorded as a function of temperature by an X-Y plotter. The field and temperature cycle during the experiment are shown in Fig. (4.4). The temperature was regulated by a temperature controller and monitored by a Cu/Const thermocouple connected to a digitron thermometer (Model

3750k). The output from the thermometer was coupled directly to the X-Y plotter (Shandon Southern Auto. Graph D). The thermocouple encased in a sealed glass capillary tube, was embedded in one of the electrodes. Sample heating was achieved through two radiant heaters, (tungsten-halogen, rated 300W/110V), placed on either side of the sample. Liquid nitrogen was used in the cooling cycle where the coolant was passed through brass tubing into the vacuum chamber. The electrode assembly was contained in a vacuum system so that moisture can be removed to prevent short circuiting during poling. Gaseous nitrogen was introduced into the chamber after evacuation to provide a cooling medium. A D.C. supply unit,Brandenburg alphas series II (Model No. 2707), with a constant output in the range 0- 15 KV was used to supply the poling voltage.

### 4.2.5 Electrical Volume Resistivity Technique

For resistivity measurement a Keithley 602 electrometer was used in conjunction with a highly stabilised voltage supply (Bradenberg photomultiplier supply type 475R). The temperature during experiments was controlled by an adjustable hot plate (Chemlab SSRH stirrer-hotplate). For more details see chapter five.

## 4.3 Results and Discussion

### 4.3.1 Differential Scanning Calorimetry (DSC)

Figs 4.5(a,b,c) show the results obtained from DSC measurements for the epoxy resin system MY750/HY956, taken at various stages during cure. From these graphs it can be seen that, as the cure proceeds, the glass transition temperature, Tg, increases. It was also found that the fully cured epoxy resin systems MY750/HY956 and MY750/DDSA had Tg values of 108 °C and 25°C respectively as shown in Figures 4.6(a,b). The curing time procedure for both systems is given in table (4.1).

### 4.3.2 Thermally Stimulated Discharge Current (TSDC)

Fig. (4.7) show the result obtained from TSDC measurement for a fully cured epoxy resin system MY750/HY956. This had a Tg value of 107 °C (<- process). From figures (4.6) and (4.7) it can be seen that the Tg value of the fully cured epoxy resin system MY750/HY956 obtained by DSC and TSDC measurements are in very good agreement.

### 4.3.3 Infrared Spectroscopy (IR)

Figs. (4.8), shows the results obtained from infrared spectra for the epoxy resin system HY750/HY956 taken at various stages during cure. From these spectra it can be seen that as the cure proceeds the epoxide

(910 $cm^{-1}$ band) absorption reduces.

### 4.3.4 Electrical Volume Resistivity

Figure (4.9), show graphs of resistivity against curing time at various temperatures for epoxy resin system MY750/HY956. From these graphs it can be seen that the time rate of change of the logarithm of the resistivity was temperature-dependent and could be taken as an index of the rate of polymerisation during the first and second stages of the reaction (85). The first stage is characterised by low viscosity and low conversion to the polymer and the second stage is characterised by the onset of gelation. It is these two stages that are shown by the initial straight segment occurring in the plots shown in Figure (4.9). Transition between the two stages is not apparent as a change in the slope. Kienle and Race (80), have also noted the absence of an abrupt change in the resistance of a thermosetting polymer at the gelation point. The increases in the resistivity during polymerisation is due to the mobility of the ionized impurities (88,89). It is most likely that the number of ions remain constant. As polymerisation proceeds, the mobility of the ions is progressively decreased, with a corresponding increase in the resistivity (84). After polymerisation is complete, the mobility is extremely restricted, hence the high resistivity. The decreasing rates of polymerisation indicated by the non-linear

portions of the curves of Figure (4.9) are due to the fact that the third stage of the reaction has been reached . This stage is characterised by the hard set of the polymer, the small amount of monomer remaining, and the probable control of the reaction by diffusion. Figure (4.10) show an Arrhenius plot of the Ln (maximum slopes) of the resistivity versus 1/T (T: the curing temperature). A linear relationship was obtained having a slope corresponding to an activation energy of 1.26ev.

### 4.3.5 Dielectric Analysis

In order to study and discuss the result of dielectric measurements the main features on the theory of dielectrics are outlined in the section below.

#### 4.3.5.1 Review on The Theory of Dielectric

Dielectric measurements of polymeric materials are one of the techniques which is used to study the dynamics of the molecular behaviour of the polymer at a molecular level.

The phenomenologic study of dielectrics had been formulated by Maxwell (141) as early as the beginning of the nineteenth century. The concept of dipoles in molecules and the microscopic interpretation of dielectric properties are however the work of Debye (142). When an isotropic dielectric material is placed between parallel electrodes, an external applied field interacts with the molecule of the material causing charge separation, positive charges being attracted

towards the negative electrodes and vice versa. This effect is called polarisation of the material. The presence of these polarisation or bound charges means that more charge can be stored on the capacitor electrodes for the same applied voltage and the capacitance of the system is increased with respect to the vacuum response.

The ratio of the increased capacitance, C, to the vacuum capacitance $C_o$, known as the static relative permittivity

$$\varepsilon = \frac{C}{C_o} , \qquad (4.1)$$

varies from material to material and depends on the amount of polarisation occurring in the material. This characteristic ratio is essentially independent of the applied voltage and is therefore also independent of the electric field. It is also known as the dielectric constant of the material.

#### 4.3.5.1.1 Dielectric Polarisation

In the study of polarisation on the molecular level, the effect of the applied electric field is to induce an electric dipole (m) on each individual molecule, the magnitude depending on the local electric field strength $E_L$ at the molecule:

$$m = \alpha E_L , \qquad (4.2)$$

where $\alpha$ is the polarisability of the molecule. Except in certain anisotropic cases, the average direction of

the induced molecular dipoles is in the direction of the applied field, and since the local field $E_L$ (the field acting on an individual polarisable entity like an atom or molecule) is proportional to the overall applied field, thus $m \propto E$.

In the study the polarisation on a molecular or microscopic level in a homogeneous material there are three components of molecular polarisation:

1. Electronic Polarisation ,~e,

An electric field will cause a slight displacement of the electrons of any atom with respect to the positive nucleus. The shift is quite small because the applied electric field is usually quite weak relative to the intra-atomic field at an electron due to the nucleus.

2. Atomic Polarisation ,~a,

This occurs when the applied field causes a displacement of the atomic nuclei relative to each other in a molecule or lattice. The movement of heavy nuclei is more sluggish than electrons so that atomic polarisation cannot occur at such high frequencies as electronic polarisation. It is not observed above infrared frequencies.

3. Orientational Polarisation ,~m,

If the molecules already possess permanent dipole

moments, there is a tendency for these to be aligned by the applied field to give a net polarisation in that direction. The rate of dipolar orientation is highly dependent on molecule-molecule interaction. The orientation of molecular dipoles can make a contribution which is large, but which may be slow to develop, to the total polarisation of a material in an applied field.

In this section so far the specimens are ideal in that they are entirely homogeneous and contact perfectly with the electrodes which apply the electric field.

In practice, a material is always likely to have regions of non-uniformity, and impurities may be present as a second phase. Effects on dielectric properties attributable to material discontinuities are usually called Maxwell-Wagner effects, since Maxwell (143) and Wagner (144) were the first to consider them theoretically.

In heterogeneous materials, additional polarisation is found due to charge build up at interfaces and this additional term is called the interfacial or Maxwell-Wagner-Sillars (MWS) polarisation (M-W-S) (143-145). Complications can also arise at electrodes where contact with the specimen may be incomplete and where entities such as discharged ions may form spurious boundary layers. Electrode polarisation arises because of charge injection which forms a space charge in the polymer close to the

metal/polymer interface. This results in a continual rise in the observed permittivity with decreasing frequency. The overall polarisability of the system $\alpha_T$ is the sum of all the terms :-

$$\alpha_T = \alpha_e + \alpha_a + \alpha_m + \alpha_{m/w/m} + \alpha_E \qquad (4.3)$$

The polarisation is related to the permittivity by the Clausius-Mossotti equation.

$$P = 4/3\ \pi N_A \alpha = \frac{\varepsilon - 1}{\varepsilon + 2}\ \frac{M_w}{\rho} = \frac{N_A}{3\ \varepsilon_o}\ , \qquad (4.4)$$

where P is the polarisation, $N_A$ is Avogadro's number, $M_w$ is the molecular weight, $\rho$ is the density of the material, $\varepsilon_o$ is the permittivity of free space and $\alpha$ is the polarisability of the molecule. The quantity $N_A\alpha/3\ \varepsilon_o$, is called the molar polarisation. It may be as well to remark that P as well as $\alpha$ has the dimensions of volume. In equation (4.4) no account has been taken of the dipole orientation polarisation. In general, the polarisation due to dipolar orientation is directly proportional to the local field strength $E_L$ and inversely proportional to the temperature. The mean electric moment $\bar{m}$ was expressed by Debye (142).

$$\bar{m} = ( \alpha_o + \mu^2 / 3kT )\ E_L\ , \qquad (4.5)$$

where the factor $\alpha_o$ is the normal deformational polarisability, $\mu$ is the permanent moment of each dipole, k is the Boltzmann constant, T is the absolute temperature and the quantity $\mu^2/3kT$ is an orientational polarisability. From the equation above the total effective polarisability $\alpha$ is

$$\alpha = \alpha_o + \mu^2 / 3kT \quad . \tag{4.6}$$

It can be seen from the equation above that the polarisability $\alpha$ is not a constant but depends on temperature, decreasing with increasing temperature. If, therefore, $\alpha$ can be represented as above, the formula for P (molar polarisation) given by Debye (142) will be

$$P = 4/3\ \pi N_A\ (\alpha_o + \mu^2 / 3kT). \tag{4.7}$$

The Debye equation has limitations in that it is only useful for gases and perhaps diluted solutions where, the molecules are sufficiently far apart so that their interaction may be neglected.

The molar polarisation is a purely molecular quantity, giving some information about the electrical properties of the molecule. It should be possible to calculate P by means of the equation

$$P = \frac{\varepsilon - 1}{\varepsilon + 2} \frac{M_w}{\rho}. \tag{4.8}$$

In the case of gases or vapours of low density the difference between $\varepsilon$ and 1 will be very small. A good approximation may then be obtained if the denominator $\varepsilon + 2$ in (4.8) is replaced by 3. In fact this approximation really means that the local field strength $E_L$ is considered to be equal to the applied field, and the mutual interaction of the molecules has been neglected. In this case the calculation of the molar polarisation can be made by the formula

$$p = \frac{\varepsilon - 1}{3} \frac{M_w}{\rho}. \tag{4.9}$$

Actually, materials in general tend to fall into one of two classes. Those in one class show a relatively constant molar polarisation in accord with the simple Clausius-Mosotti relation (see equation 4.4), whilst the members of the other class, which contains materials with relatively high dielectric constants,show a molar polarisation that decreases with increases in temperature. Debye (142) recognized that permanent molecular dipole moments were responsible for the anomalous behaviour. He measured the dielectric constant and the density $\rho$ at different temperatures. P is calculated according to equation (4.9) and plotted as a function of the variable 1/T. Two possibilities were found, illustrated by Fig. (4.11).

(i) P is not dependent on temperature at all. In this case the experiments are represented by a horizontal straight line. The molecule is non-polar, that is, its electric moment $\mu$ is zero.

(ii) P depends on temperature. In this case, the experiments are represented also by a straight line in accordance with the equation (4.7), but this time making a finite angle with the horizontal axis. In this case the molecule is polar, its electric moment having a finite value.

Furthermore, the equation above (4.9) provides a simple method of determining molecular dipole moments from experimental measurements. The slope of the

straight line in Fig. (4.11) is simply related to the square of the dipole moment. The method is most aptly applied to gases, where intermolecular effects may be reasonably neglected. The situation is much more complicated in solids because the inter-molecular effects can no longer be ignored. In the case of polymers there are further complications which arise from the flexibility of the long chains. These effects have been accounted for in various theories by Onsager, Kirkwood, Frohlich and Cole (146).

4.3.5.1.2. Dielectric Relaxation

The relationship between the observed polarisation and the applied field can be considered as the response to either a step function or periodic change in the field. When a step function field is applied to a certain material, it becomes polarised with a value of $P_o$. If the field is then removed, the polarisation decays with time and is known as dielectric relaxation. When the relaxation is ideal, this decay is exponential and its value after a certain time, t, is given by

$$P(t) = P_o \exp(-Kt)$$

$$= P_o \exp(-t/\tau) \qquad (4.10)$$

where K is a rate coefficient and $\tau$ is the characteristic time constant, usually called the dielectric relaxation time (ie the time required for the polarisation to fall to 1/e of its original value). A study of the response of a material to a step function field is only feasible when the time scale of the

process under examination is long. When the response time is not long enough it is more convenient to study the response under the influence of an alternating field.

Considering the application of an alternating electric field E, amplitude $E_o$ and angular frequency w, to a dielectric material, then the field can be represented by

$$E = E_o \cos wt. \qquad (4.11)$$

This will produce polarisation which alternates in direction, and if the frequency is high enough, the orientation of any dipoles which are present will inevitably lag behind the applied field. This can be expressed as a phase lag ( $\delta$ ) in the electric displacement (D)

$$D = D_o \cos (wt - \delta) , \qquad (4.12)$$

which can be written as below:

$$D = D_1 \cos wt + D_2 \sin wt , \qquad (4.13)$$

where $D_1 = D_o \cos\delta$ and $D_2 = D_o \sin\delta$ .

This leads to the definition of two dielectric constants

$$\varepsilon' = D_1 / \varepsilon_o E_o \qquad \varepsilon'' = D_2 / \varepsilon_o E_o, \qquad (4.14)$$

where $\varepsilon'$ is the dielectric constant (a measure of the energy stored in the system per cycle) and $\varepsilon''$ is called the dielectric loss factor (energy dissipated per cycle). The two parameters are related by the equation

$$\text{Tan}\,\delta = \frac{\varepsilon''}{\varepsilon'} \qquad (4.15)$$

where tan $\delta$ is the dielectric loss tangent (dissipation

factor) and $\delta$ is the phase displacement angle or the loss angle. These two quantities $\varepsilon'$, $\varepsilon''$ can be combined into a complex dielectric constant or relative permittivity

$$\varepsilon^* = \varepsilon' - i\varepsilon'' \qquad (4.16)$$

An insulating material with dielectric losses can be represented by either a series or a parallel combination of resistance and capacitance, provided the voltage applied to the material is sinusoidal. Consider the material in a capacitor (capacitance $C_o$ when empty) in a circuit, as shown in Fig. (4.12a). The current I which flows in the external circuit after application of an alternating voltage given by the real part of $V = V_o \exp(iwt)$, may be calculated as follows:

$$\begin{aligned} I &= \varepsilon^* C_o \, dV/dt \\ &= i\, w\, \varepsilon^* C_o\, V \\ &= w\, C_o\, (\varepsilon'' + i\, \varepsilon')\, V. \end{aligned} \qquad (4.17)$$

This implies that the current I passing through the insulation is composed of a capacitance component,

$$I_c = iw\, C_o\, \varepsilon' V\ , \qquad (4.18)$$

which leads the voltage by 90°, and a resistive component,

$$I_R = w\, C_o\, \varepsilon'' V\ , \qquad (4.19)$$

which is in phase with the voltage. The former current $I_c$ depends on the size of the capacitance, whereas the latter $I_R$ represents all capacitor losses depending on the voltage. The losses occur on the surface and in the interior of the dielectric. The loss in the material is normally measured in terms of the loss angle (see Fig.

4.12 b). In the case of the specimen represented by a capacitance $C_p$ in parallel with a resistance $R_p$, as shown in Fig. (4.12c) the total impedance Z will then be given by

$$1/Z = 1/R_p + i\ w\ C_p \ . \qquad (4.20)$$

After the application of the alternating voltage, represented by the real part of $V = V_o \exp(iwt)$, an out-of-phase or capacitive current $I_c$ is produced:

$I_c$ = Imaginary part [V/Z]

$$= i\ w\ C_p\ V \ , \qquad (4.21)$$

and an in-phase or resistive current $I_R$ :

$I_R$ = Real part [V/Z]

$$= V/R_p \ . \qquad (4.22)$$

Comparing equations (4.21) and (4.22) with equations (4.18) and (4.19), respectively,

$$I_c = i\ w\ C_o\ \varepsilon' V = i\ w\ C_p\ V$$

$$\varepsilon' = C_p\ /\ C_o \ , \qquad (4.23)$$

$$I_R = w\ C_o\ \varepsilon'' V = V/R_p$$

$$\varepsilon'' = 1/\ R_p\ C_o\ w \ , \qquad (4.24)$$

and

$$\tan\delta = \varepsilon''/\varepsilon' = 1/\ R_p\ C_p\ w \ . \qquad (4.25)$$

Alternatively, the specimen may be regarded in terms of a series circuit. If the equivalent series components of capacitance and resistance are $C_m$ and $R_m$, respectively (see Fig. 4.12 d), the total impedance will be given by

$$Z = R_m + 1/\ i\ w\ C_m \ . \qquad (4.26)$$

Application of the alternating voltage represented

will produce on out-of-phase or capacitive current $I_C$:

$$I_C = i \frac{V/w\ C_m}{R_m^2 + (1/w\ C_m)^2}, \qquad (4.27)$$

and an in-phase or resistive current $I_R$ :

$$I_R = \frac{V\ R_m}{R_m^2 + (1/w\ C_m)^2}, \qquad (4.28)$$

Comparing equations (4.27) and (4.28) with equation (4.18) and (4.19), respectively,

$$I_c = i\ w\ C_o \varepsilon' V = i \frac{V/\ w\ C_m}{R_m^2 + (\ 1/\ w\ C_m\ )^2}$$

$$\varepsilon' = \frac{1}{R_m^2 + (\ 1/\ w\ C_m\ )^2} \quad \frac{1}{w^2\ C_o\ C_m}, \qquad (4.29)$$

$$I_R = w\ C_o\ \varepsilon'' V = \frac{V\ R_m}{R_m^2 + (\ 1/\ w\ C_m\ )^2}$$

$$\varepsilon'' = \frac{R_m}{R_m^2 + (\ 1/\ w\ C_m\ )^2} \quad \frac{1}{w\ C_o}. \qquad (4.30)$$

and

$$\tan\delta = \varepsilon''/\varepsilon' = R_m\ C_m\ w. \qquad (4.31)$$

The reciprocal of the specimen resistance in the equivalent parallel circuit for a given frequency is sometimes called the AC conductance $G_p$. $G_p$ is an additive combination of DC conductance (the real flow of charge through the sample under the influence of the applied field), and the anomalous conductance due to any time- dependant polarisation processes. The dielectric loss factor at an angular frequency w due to the DC conductivity alone can be calculated for the material in a parallel- plate capacitor as follows given that

$$G_p = \sigma_{DC} + \sigma_{AC}$$

Substituting $G_p$ for resistance in equation (4.24),

$$\varepsilon'' = G_p / C_o w . \qquad (4.32)$$

If the capacitor plates have area A and separation S :

$$G_p = \sigma A / S \quad \text{and} \quad C_o = \varepsilon_o A / S , \qquad (4.33)$$

and hence

$$\varepsilon'' = \sigma / \varepsilon_o w . \qquad (4.34)$$

This shows how DC conductivity causes $\varepsilon''$ to rise rapidly at low frequencies.

By substituting for resistance in equation (4.25),

$$\tan\delta = \varepsilon''/\varepsilon' = G_p / C_p w . \qquad (4.35)$$

$\varepsilon'$ and $\varepsilon''$ are experimentally observable quantities which may be used to characterise the dielectric dispersion over a range of frequencies. For interpreting any such dispersion behaviour, a link between these macroscopic observable quantities and molecular properties is necessary. This can be done by postulating a model which describes the way the molecules respond to the applied field. The frequency dependence of the complex permittivity treatment was first considered by Debye (142). This treatment rests on two essential premises: exponential approach to equilibrium and the applicability of the superposition principle.

Pellat (147) and Debye (142) introduced the familiar equation of the frequency dependence of the complex permittivity as

$$\varepsilon^* = \varepsilon_\infty + \frac{\varepsilon_s - \varepsilon_\infty}{1 + i w \tau} , \qquad (4.36)$$

which is called the Debye dispersion equation. Equating real and imaginary parts of the two sides,

$$\varepsilon'(w) = \varepsilon_\infty + \frac{\varepsilon_s - \varepsilon_\infty}{1 + w^2 \tau^2}, \qquad (4.37)$$

$$\varepsilon''(w) = \frac{\varepsilon_s - \varepsilon_\infty}{1 + w^2 \tau^2} w\tau, \qquad (4.38)$$

$$\tan\delta = \frac{\varepsilon''}{\varepsilon'} = \frac{\varepsilon_s - \varepsilon_\infty}{\varepsilon'} \cdot \frac{w\tau}{1 + w^2 \tau^2} \qquad (4.39)$$

where $\varepsilon_s$ is the static dielectric constant, $\varepsilon_\infty$ is the permittivity at frequencies well above the relaxation (see Fig. 4.13) and $\tau$ is the dielectric relaxation time. The graphs of $\varepsilon'$ and $\varepsilon''$ against frequency, of the applied field, through the dispersion region are shown in Fig. (4.13). The maximum loss value occurs when $w\tau = 1$, corresponding to a critical frequency $w_{max} = 1/\tau$. The location of this peak provides the easiest way of obtaining the relaxation time from experimental results. The dependence of $\varepsilon''$ on $\varepsilon'$ may be used to test the Debye model for each particular system. Elimination of the parameter $w\tau$ between equations (4.37) and (4.38) results in

$$\left(\varepsilon' - \frac{\varepsilon_s + \varepsilon_\infty}{2}\right)^2 + \varepsilon''^2 = \left(\frac{\varepsilon_s - \varepsilon_\infty}{2}\right)^2. \qquad (4.40)$$

This is the equation of a circle, centre $[(\varepsilon_s + \varepsilon_\infty)/2]$, radius $(\varepsilon_s - \varepsilon_\infty)/2$, thus a plot of against should yield a semicircle, as shown in Fig. (4.14). Relaxation observed in polymers, however, show broader dispersion

curves and lower loss maxima than those predicted by the Debye model. This led Cole and Cole (148) to suggest the following semi-empirical equation for symmetric deviations about the mean relaxation time from the Debye model.

$$\varepsilon^* = \varepsilon_\infty + \frac{\varepsilon_o - \varepsilon_\infty}{1 + (i\ w\tau)^{\alpha}} , \qquad (4.41)$$

where $0 < \alpha \leqslant 1$.

This deviation is normally described in terms of a spread of relaxation times. Similarly Cole and Davidson (149) improved the fit with experiment by using a slightly different semi-empirical equation:

$$\varepsilon^* = \varepsilon_\infty + \frac{\varepsilon_s - \varepsilon_\infty}{(1 + i\ w\tau)^{\beta}} , \qquad (4.42)$$

where $0 < \beta \leqslant 1$.

These equations illustrate the contribution from a series of relaxation mechanisms, whose importance depends on the environment of the molecules. The parameters $\alpha$ and $\beta$ describe the breadth and asymmetry of the relaxations respectively. It should be noted however that the equations do not have any particular theoretical foundation apart from the improved agreement with experiment for certain materials.

#### 4.3.5.1.3 Dielectric Relaxation in Solid Polymers

In the solid state polymers normally exhibit several distinct dielectric relaxation processes. This

can be detected by scanning the dielectric loss at constant frequency as a function of temperature and is observable as a dielectric loss peak (see Fig. 4.15).

As the temperature is raised, molecular motion of various types become successively energized and, if dipoles are present in the chains, are then capable of responding to the applied field. The dielectric relaxation processes are designated $\alpha$, $\beta$, $\gamma$,...etc, the labelling beginning at the high temperature loss peak. The high-temperature relaxation process, or the glass transition temperature (Tg) (see section 4.1.1) is associated with micro-Brownian motion of the whole chains. Detailed examination of the relaxations requires isothermal scans of dielectric constant ($\varepsilon'$) and loss ($\varepsilon''$) as a function of frequency f, so that effective dipole movements and activation energies of relaxation times may be obtained. Fig. (4.16) shows a typical pair of plots of $\varepsilon'$ and $\varepsilon''$ values against log f. From a series of such plots the relaxation times can be obtained for the individual relaxation processes as a function of temperature although this presupposes a debye relaxation process. The mechanism of the $\beta$-process may be one of several different types depending on the nature of the dipole group concerned and its position on the polymer chain. Among the most important mechanism are the following:

(a) Rotation of a side group about a C - C bond

which is linked to the main polymer chain (150). It may be a small group, e.g. $-CH_2Cl$ (see Fig. 4.17a), or a more complicated side chain, e.g. $-CO.OC_2H_5$.

(b) Conformational flip of a cyclic unit, such as thus which involves the cyclohexyl side group. The transition from one chair-form to another, alters the orientation of a polar substituent (see Fig. 4.17b).

(c) Local motion of a flexible segment of the main chain. For example, the explanation of the β-process in polyvinylchloride, where the dipolar group is directly attached to the main chain and cannot move independently of the polymer backbone. This kind of movement also arises when there are runs of four or more $CH_2$ units (151) and can be explained as a crankshaft rotation (152) about two collinear C-C bonds (see Fig. 4.17c). The α (Tg) - relaxation peak of an amorphous polymer is typically much narrower than a β-peak, although still considerably broader than that for a simple Debye process. The rate of change of the loss with temperature for the α-process is generally much larger than that of a β-process, signifying the greater thermal activation energy required for the larger scale of motion involved. It has been found that the α-relaxation process near Tg is largely dependent on free volume (150). Molecular structure has a great influence on the glass transition temperatures and their associated dielectric relaxation times. Thus a bulky side group can decrease Tg by preventing the chains from

packing together tightly and vice-versa. Tg can also be reduced by adding a plasticizer. In partially crystalline polymers where crystalline and amorphous phases coexist in the solid, the relaxation spectrum becomes more complicated.

Apart from the orientational processes taking part entirely in the amorphous regions, there are different mechanisms operating inside the crystals and at their boundaries. It is usually possible to decide whether a given loss peak is associated with the amorphous or crystalline phases by varying the degree of crystallinity. Thus reducing the crystallinity, by rapid quenching from the melt, enhances the strength of any relaxation process originating in the amorphous phase. For example on crystallising poly (ethylene terephthalate), from the melt or from the glass (by heating a glass above Tg and slowly cooling) the resultant $\alpha$-process loss peak is much broader than that for the amorphous polymer. It occurs at much lower frequencies, when measured at a given temperature, than that for the amorphous polymer (153,154). For the $\beta$-process, the shape and frequency-temperature location of the process are essentially unaffected by the increase in the degree of crystallinity. Other complications may arise in dielectric relaxation spectra of polymers due to chain branching, which may introduce a distinct relaxation process connected with molecular motion at a branch point and from cross linking which

greatly restricts certain kinds of molecular movement. Relaxation processes in solid polymers are summarised diagrammatically in Fig. (4.18).

4.3.5.1.4 Dielectric Relaxation in Liquids and Solutions

These processes will be significant for dielectric loss processes occurring in a curing resin system. When the material is in the liquid state, especially when it is dissolved in a low -molecular- weight solvent, end-over-end rotation of whole polymer molecules is the more accessible mechanism for orientation of molecular dipoles. In order to study the dielectric behaviour in the liquid state, there are three aspects of polymeric molecules which must be considered:

(i) the type of dipole present on each repeat unit of the polymer, (ii) the equilibrium conformation of the individual molecules, (iii) the flexibility of the molecular chains.

Polar groups in a polymer molecule can be classified according to the relative geometry of their dipole moment with respect to the contour of the polymer backbone into three main types:

(a) Dipoles rigidly attached to the backbone and perpendicular to it (see Fig. 4.19a). In this case the perpendicular dipole units, can orientate individually by segmental motion, provided that rotations about the C-C bonds of the polymer chain are sufficiently free. In liquids and solutions, where there is ample free

volume available, the dipolar relaxation is very rapid and insensitive to the total length of the chain. This is conformed experimentally by North (155).

(b) Dipoles rigidly attached to the backbone and parallel to it (see Fig. 4.19b). In this case the parallel dipole units add vectorially along the length of the polymer chain to give a cumulative moment which is proportional to the end-to-end distance of the molecule (see Fig. 4.19d). This moment can only orient by end-over-end rotation of the whole molecule and remains unaffected by rotation of individual segments about the main chain axis. Thus the associated relaxation process is strongly dependent on the molecular weight, the bigger the molecule the more difficult will it be for it to turn round. This behaviour has been observed by Baur and Stockmayer (156) in liquid poly (propylene oxide).

(c) Dipoles attached to a side chain which can move independently of the main chain (see Fig. 4.19c). A dipole moment of this type in a flexible side chain, imposes a dipole moment which can be resolved into a rigid, perpendicular component and a rotatable component. In practice only one high-frequency relaxation process is observed and one concludes that in solution the side-group rotation and segmental motion in the main chain are combined in a single, fast process (155).

In the liquid phase or in a solution, the

flexible, linear polymers tend to be somewhat coiled-up. In the case of a good solvent, polymer-solvent contacts are preferred energetically to polymer-polymer contacts and so the coils expand and the root-mean-square end-to-end distance, $(\bar{r}^2)^{1/2}$, increases. In contrast, in a poor solvent the polymer will contract and $(\bar{r}^2)^{1/2}$ will decrease leading ultimately to phase separation if the solvent is sufficiently poor. In a general way, the frictional motion of deformable, random-coil molecules in solution has been examined theoretically. There are two basic models: the free-draining model by Rouse (157) which neglects the hydrodynamic interaction between neighbouring parts of the same chain, and the non-free-draining model by Zimm (158) in which viscous drag between different segments assumes a dominant role. The latter model gives a better account of what happens inside the coils of a long molecule, and it gives good agreement with experimental viscosity data for dilute solutions of high polymers. The Rouse model gives better agreement at higher concentrations, however, where the polymer molecules might be expected to intermingle.

On the basis of the above models, the relaxation time $\tau$ for orientation of the total dipole moment of a chain, substantially by end-over-end rotation, may be related to the viscosity of the solvent $\eta_0$ and solution $\eta$, as shown in the two equations below

$$\tau(\text{free-draining}) = 1.21 \frac{(\eta - \eta_0)\, M}{C_p\, R\, T}, \qquad (4.43)$$

$$\tau(\text{non-free-draining}) = 0.85\,\frac{(\eta_s - \eta_o)\,M}{C_p\,R\,T} \qquad (4.44)$$

where $C_p$ is the concentration of the polymer solute (mol per unit volume) and M is the molecular weight of the Polymer. Bates, Ivin and Williams (159) have observed that the backbones of some polymer molecules are of intermediate stiffness. They adopt a coil-like configuration in a solution, but their segmental mobility is so low that dipolar orientation is faster by whole molecule rotation rather than by twisting of individual dipole units. Some polymer molecules have a tendency to form rigid rods in solution and the dependence of the relaxation time of a rigid rod as a function of the molecular weight has been observed for dilute solutions of poly (n-butyl isocyanate) by Bur and Roberts (160). In principle, all polymers will be rod-like at very low molecular weights and progress via stiff coils to flexible coils as the molecular weight is increased. This is reflected in the dependence of dielectric relaxation time on molecular weight as shown schematically in Fig. (4.20).

4.3.5.2 Results

Figure (4.21a) shows the results obtained for the dissipation factor from a series of three experiments conducted at 10kHz and at room temperature. The first readings for each of the three experiments were taken immediately after forming the sample. This

was defined as time zero. From the three curves it can be seen that the peaks were reached at virtually the same time in all three experiments. The same is true of the troughs which proceed the peaks. The small variation in the trough and peak values of tan$\delta$ were a result of the differing amounts of air bubbles contained in the samples and which were produced during their preparation. The samples were otherwise identical.

Figure (4.21b) shows the results of capacitance against time measurements obtained during the three experiments.

Figure (4.22a-e) shows graphs of dissipation factor against curing time for various frequencies and temperatures. From these graphs it can be seen that the higher the frequency the sooner the dissipation factor peaks. It is noteworthy that the time of occurrence of the 100 kHz peak was only about half of that for the 1 kHz peak. Also the peak positions moved to shorter times as the curing temperature was increased.

Figure (4.23) shows the results obtained for dissipation factor against temperature for cured samples at different frequency. There were no peaks. At high temperatures conductance effects became apparent. The samples used in obtaining Figures (4.21-4.25) were epoxy MY750/HY956. The glass transition temperature, Tg, of these cured samples was 108 $^{o}$C as measured using differential scanning calorimetry (44). The gel time at room temperature was 110 minutes. This was determined

approximately by testing the viscosity of the material using a glass rod dipped into the curing resin. There was a significant change in the apparent viscosity at the gel point, as indicated by the formation of filaments of resin attached to the glass rod when it was withdraw from the curing epoxy. The peak at 100 kHz appeared before gelation and the peak at 0.2 kHz appeared after gelation .

Figure (4.24) shows graphs of dissipation factor against curing time for various concentrations of hardener at room temperature . From these graphs it can be seen that the higher the concentration of hardener the dissipation factor peak occurs after a short time and the greater is its magnitude.

Figure (4.26a) shows the results of dissipation factor versus temperature at different frequencies for the fully cured epoxy MY750/DDSA samples. The Tg of the cured samples was 25 °C as measured using differential scanning calorimetry. Figure (4.26b) shows the results of dissipation factor measurements as a function of curing time at different frequencies. The curing temperature was 90°C.

Consider the 1 kHz graph in Figure (4.22) It reflects the behaviour of the dissipation factor during curing. The initial decreases is caused by a large reduction in ion mobility resulting in a reduction in conductivity G (67). The two equations which link ion

mobility to the dissipation factor are (5.1) and (4.35) given in sections 5.1.1 and 4.3.5.1.2 respectively.

From equation (5.1), it is assumed that N ( the ionic concentration) is constant (67), the conductivity effect is more pronounced at lower frequencies (70) . The second equation (4.35), in the absence of any relaxation peaks , gives the value of dissipation factor. From these two equations it can be seen that a reduction in the mobility of the ions decreases the ionic conductivity and this in turn can cause a decreases in tan $\delta$ . During the cure the viscosity increases and hence the ionic mobility decreases with a consequent decrease in tan$\delta$. An increase in measurement frequency decreases the tan $\delta$ value in the initial portion of the curve, as is seen in Figure (4.22) .

What is the actual mechanism causing the peak to appear during the curing of an epoxy resin? As was mentioned earlier (see section 4.1.2.5), it is difficult to consider the peak appearance as a gelation point (68,72,73). From Figures 4.26a and 4.26b it can be seen that the nature of the tan $\delta$ peaks are different. Peaks appearing in a cured resin (Fig. 4.26a) are associated with an $\alpha$-relaxation process due to orientation of long segments of molecular chains and occur above and close to the Tg. If the peaks in figure 4.26b are an $\alpha$ peak then the magnitude is far too large. The cure temperature in Figure (4.26b) is 90°C. In the case of

the resin cured with HY956 hardener, measurements were made below Tg, and no peak was observed for the cured resin at room temperature, Fig. (4.23). However, there is a peak appearing during the curing process, Figure (4.21,4.22). Consequently for both types of resin systems the peaks observed during curing are not likely to be due to an $\alpha$ process. A different explanation of the transitory loss peaks is thus needed.

## 4.4 MODEL OF DIELECTRIC PROCESSES DURING CURING

From the results out lined above a model that can describe the curing behaviour of the epoxy resin system is developed.

In the epoxy system a large number of dipoles are rigidly attached to the backbone of the molecule and are parallel to the polymer chain (23). A schematic diagram of a polymer molecule of epoxy/amine before gelation is shown in Figure (4.27). Also shown are the polar chemical bonds which produce a resultant dipole moment for the whole molecule. This is proportional to the molecular length. The dipole moment of the whole molecule may be orientated with the field by an "end over end" rotation. Blythe (23) has pointed out that such a rotation of the whole polymer molecule is a plausible mechanism for orientation of molecular dipoles when the material is in the liquid state , especially if it is dissolved in a low molecular weight solvent .

The onset of the curing process will now be considered. Molecules of epoxy resin and hardener are dispersed at random forming a uniform liquid phase. Growth of an epoxy/amine molecule occurs when it reacts with an epoxy molecule and a polymer molecule is formed. This system is similar to a solution of polymer molecules dissolved in a low molecular weight solvent namely the remaining unreacted epoxy resin and hardener. Even a fully cured epoxy resin has been shown to be two phases system containing roughly spherical floccules in a low-density liquid medium resembling the uncured starting materials (90) and produced by microgelation prior to the formation of macrogel (74) . The dielectric relaxation measured during the curing process is similar to that occurring in liquids consisting of a dilute solution of dipole molecules except that in this case there is also molecular growth .

This suggests that in the epoxy cure the classical Debye model would be applicable. The model predicts that the value of the dissipation factor is given in equation (4.39) (see section 4.3.5.1.2). From equation (4.39), the dissipation factor has a maximum value when :

$$w\tau = 1 \ , \qquad (4.45)$$

where w is the angular frequency and $\tau$ is the relaxation time.

For random-coiled molecules similar to the growing

epoxy polymer molecules, the relaxation time $\tau$ for orientation of the whole molecule in solution (see section 4.3.5.1.4) is:

$$\tau = \frac{a(\eta_s - \eta_o)\ M}{C_p\ R\ T} \qquad (4.46)$$

where "a" is a constant , $C_p$ is the concentration of the polymer solute (mol per unit volume) , M is the molecular weight and $\eta_o$ and $\eta_s$ are the viscosities of the solvent and solution respectively.

In fact the relationship between the relaxation time and the molecular weight is complicated by changes in molecular shape. Nevertheless, equation (4.46) indicates that both the viscosity and the molecular weight affect the relaxation time. Thus a change in molecular weight would cause a change in relaxation time and dissipation factor.

The experimental results shown in Figure (4.21) may be explained qualitatively on the above basis. In these results the frequency was fixed and the relaxation time varies. At time zero $\tau$ will be small because the molecular weight of the curing polymer will also be small, equation (4.46). As the cure proceeds the molecular weight increases and consequently so does $\tau$ .

If it is assumed that at any instance in time the Debye model is a valid description of the dielectric response then at that instant there will be a maximum in the value of tan $\delta$ for some measurement frequency. The

position of the peak is dependent on $\tau$ through equation (4.45). With increasing time the molecular growth ensures that the peak of tan $\delta$ will occur at progressively lower frequencies. Thus in the measurements at a fixed frequency there will be a given molecular size for which that frequency corresponds to a maximum in tan $\delta$ and the curve of tan $\delta$ versus time will pass through a peak as is observed in Figure (4.21). If the measurements are conducted at a higher frequency,corresponding to a smaller molecular size, the maximum in tan $\delta$ will occur at an earlier time. as depicted in Figure (4.22). Choosing a frequency selects a molecular size and the peak position measures in effect the time taken to reach that size.

Raising the temperature of the cure has two effects. The first is that the curing reaction proceeds more rapidly and hence the molecular weight will also increase faster. The second is that the viscosity of the solvent normally decreases. This counteracts the increasing viscosity due to the increasing molecular weight. The latter will dominate. As a consequence the tan$\delta$ versus time peaks will, for a given frequency, occur at earlier times. The effect of increasing hardener content is also to enhance the speed of the reaction and will have a similar effect to that of raising the temperature. These effects are seen in the results illustrated by Figures (4.22), (4.26b) and (4.24).

Delmonte (69) using three different resins has shown experimentally that a relationship exists between the starting molecular weights and the time taken to reach the peak in tan $\delta$ measured at a fixed frequency. The resins used had nominally similar chemical structures but differing molecular weights and were cured using identical hardeners. The preposed model explains directly the results of Delmonte. The time taken to reach a fixed molecular weight would be less for the initially high molecular weight material than for the initially low molecular weight material.

The model may be extended so that an activation energy for the curing process can be obtained from the results of the present work. In fact, the relationship between ln $\tau$ and t, the time of the appearance of the peak, is a straight line and hence d ln $\tau$ / dt is a constant, Figure (4.25). According to the equation (4.46) and because

$$\ln ( \eta_s - \eta_\infty ) = \beta \ln M$$

where $\beta$ is a constant (75), the following equations can be obtained :

$$\ln \tau = \ln (a / C_p R T ) + (1+\beta) \ln M \qquad (4.47)$$

and

$$d \ln \tau / dt = ( 1 + \beta) d \ln M / dt \qquad (4.48)$$

dM / dt is a rate of increase in molecular weight, and d (ln M )/ dt = 1 / M * dM / dt is a relative rate of increase in molecular weight. The fact that d ln $\tau$/ dt

is a constant implies that d ln M / dt is a constant. If this constant changes with temperature and conforms to an Arrhenius relationship, then the activation energy can be obtained, Figure (4.28). The activation energy derived in such a fashion was 41 KJ/mol (0.42 ev). The same technique may be used to interpret the result of Haran et al (73). Table (4.2) compares activation energies obtained by various authors. As can be seen the value obtained using the analysis described above compares favourably with those obtained using different techniques.

It should also be noted that the model proposed for the pre-cured epoxy resin bears a relationship with the concept of nodular morphology (32,91), agglomerates of colloidal particles (93) and floccules in a low molecular weight interstitial fluid (90) and regions of heterogeneous crosslink density (94) applicable to cured epoxy resin.

## 4.5 Conclusion

Different methods have been used to study the curing and to estimate the degree of cure of epoxy resin systems including infrared spectroscopy (IR), differential scanning calorimetry (DSC), thermally stimulated discharge current (TSDC), electrical volume resistivity and dielectric analysis.

The glass transition temperature, Tg, was obtained

from DSC measurements for a fully cured epoxy resin systems. It is 108°C for MY750/HY956 and 25°C for MY750/DDSA. The Tg's value of the fully cured epoxy resin system MY750/HY956 obtained by DSC and TSDC measurements are in very good agreement.

From infrared spectroscopy spectra a direct relationship between the extent to which the epoxide group has been consumed and the degree of cure was obtained

From electrical resistivity measurements, a relationship between the volume resistivity of the epoxy resin system MY750/HY956 with curing time and temperature was obtained. The temperature-dependence of resistivity of the epoxy resin system MY750/HY956 could be related to the extent of polymerisation. An activation energy for the curing process was obtained (1.26 ev).

For dielectric analysis a comprehensive model of dielectric properties during a thermoset cure which includes correct chemical kinetics and the relationship between state of cure, temperature, and the various dielectric parameters has not yet been developed (77). The proposed whole molecule rotation model in the present work is an initial attempt at this. The results of dielectric relaxation measurements obtained during the curing of the epoxy resin are explicable in terms of chemical reactions in solutions. The loss-peak is associated with the dipole moment of the whole molecule

present on growing polymer molecules which can rotate in the applied field and may be regarded in terms of the Debye model. The relaxation time relate directly to the size or molecular weight of the macromolecule M. The available evidence indicates that the peak in dissipation factor as a function of time is not due to a gelation process nor to an $\alpha$-peak process, but is a consequence of rotation of the complete molecule and that macromolecules are growing uniformly in size. The larger the molecule of epoxy resin, the higher in concentration of hardener and in temperature,the quicker the macromolecules grow in size. Finally, it was possible to establish an activation energy for the curing process. The value of 41 KJ/mol (0.42 ev) compares favourable with that obtained by others for various epoxy systems.

# CHAPTER FIVE

# CONDUCTIVITY AND DIELECTRIC MEASUREMENTS OF CURED EPOXY RESIN SYSTEMS

## 5.1 Introduction

The study of the conductivity and dielectric analysis of polymers is very important because of the information it provides on a diverse range of molecular phenomena. By comparison with metals, where the electrical response is almost totally due to electronic conduction, polymers display a much less dramatic response and a whole set of more subtle electrical effects can be observed. For instance, polarisation arising from distortion and alignment of molecules under the influence of the applied electric field becomes apparent. Examination of such polarisation not only gives valuable insight into the nature of the electrical response, but also provides a means of probing the molecular dynamics and results in an understanding of the behaviour of the polymer on a molecular level.

This chapter outlines the main features of the theory of conduction mechanisms. The theory of dielectric response has been treated in chapter four. In particular attention is concentrated on the properties of thin insulating films of epoxy resin systems. Furthermore, the conduction mechanism for epoxy resin systems MY750/HY956 and the dielectric analysis for

epoxy resin systems MY750/HY956 and MY750/DDSA are discussed in detail.

### 5.1.1 Electrical Conduction

The subject of DC conductivity in polymers has been extensively studied and reviewed (95-97). It is a field in which the complexities of solid state physics and chemistry intermingle. Electrical conduction may occur through the movement of either electrons or ions. In each case, however, a suitable starting point for discussion of the conduction process is the basic equation

$$\sigma = Q N \mu \qquad (5.1)$$

where the conductivity $\sigma$ is resolved into three factors, the charge Q, concentration N and drift mobility $\mu$ of the carriers. The latter parameter characterises the ease with which the charged species will move under the influence of the applied electric field and is expressed as a velocity per unit field ($m^2 v^{-1} s^{-1}$). There may be contributions to the conductivity from several different types of carrier, notably electrons and holes (a hole is an electron vacancy carrying an equivalent positive charge) in electronic conductors, and cation and anion pairs in ionic conductors. Theories of conduction aim to explain quantitatively the processes occurring and how they are influenced by molecular structure as well as by such factors as temperature and applied field.

5.1.1.1 Conduction Mechanisms

In the case of thin insulating films, there would appear to be six possible separate conduction mechanisms. These are:-

i- Space-charge-limited conduction; ii- Tunnelling and internal field emission; iii- Schottky emission and iv- the Poole-Frenkel; v- impurity conduction; and vi- ionic conduction. The general characteristics of these six mechanisms are outlined below.

A- Space-charge-limited flow

Space charge limited conduction is a result of contact between the insulator and the electrodes. This can results in a space charge region in the insulator close to the electrode. This space charge acts as a reservoir of charge which strongly influences the conduction process.

Consider the type of contact which occurs when the electrode has a smaller work function (hence higher Fermi level) than that of the insulator. On contact, electrons are injected from the electrodes into the conduction band of the insulator, giving rise to a space charge region, and hence a space-charge induced field in the insulator. The presence of this field causes the bottom of the conduction band to curve upwards away from the interface (see Fig. 5.1). The application of an external field causes a change in magnitude and a re-distribution of this space charge in both the

insulator and the electrodes. This is illustrated in Fig. (5.2). The positive induced charge on the cathode is just equal to the negative space charge existing in the cathode region ie. the region between the cathode-insulator interface and the virtual cathode. Similarly, the positive charge on the anode equals the space charge in the anode region. The free component of the space-charge existing in the insulator conducts the current. This current is thus termed **"space charge limited current"**

The character and magnitude of space-charge limited currents are determined largely by the presence of localised states which can trap and store charge in equilibrium with the free charge. The study of space-charge-limited currents can therefore yield information about the traps, such as their density, their location in the energy band structure, and their capture cross-section.

There are, in fact, several possible variants of space-charge-limited flow depending on whether the current is due to electrons only or electrons and holes and whether traps and recombination centres are present. Single carrier injected currents can produce either space-charge-limited currents or Schottky currents (see section 5.1.1.1.C). In the case where a space charge is formed and with a perfect trap-free insulator, where all the injected carriers remain free then all the charge contributes to the space-charge and the current flow is

analogous to that in a vacuum diode. The presence of traps generally reduces the current by capturing most of the injected carriers, although as the injection level (applied voltage) is raised all the traps will eventually become filled and the current will rise sharply back to the trap-free value.

The current density- voltage relationship for one carrier space charge limited currents is (99) :

$$J = (9/8)\ \theta\ K\ \mu\ (V^2/S^3) \qquad (5.2)$$

where $\theta$ is a constant ( the ratio of free to trapped charge), K is the dielectric constant, $\mu$ is the mobility and S is the thickness of the insulator.

In the case where thermally generated free carriers with density, ($n_o$) are included, then at low voltages where the injected carrier density is less than $n_o$ Ohm's law will be obeyed.

$$J = e\ n_o\ \mu\ (V/S) \qquad (5.3)$$

The transition from Ohm's law, equation (5.3), to the Mott and Gurney law equation (5.2), takes place at the so-called transition voltage, $V_{tr}$ (99). This occurs when the Ohmic and space charge limited currents are equal ie.

$$e\ n_o\ \mu\ (V_{tr}/S) = (9/8)\ K\ \mu\ \theta\ (V_{tr}^{\ 2}/S^3)$$

$$\text{giving} \quad V_{tr} = (8\ e\ n_o\ S^2\ /\ 9\ K\ \theta\ ) \qquad (5.4)$$

This can be expressed as

$$T_{tr} = \tau$$

where $T_{tr} = S^2\ /\ \mu\ V_{tr}$ (carrier transit time between electrodes at voltage $V_{tr}$)

$\tau = K / e n_o \mu$ ( dielectric relaxation time )

For a single set of "shallow traps" Lampert (100) has calculated the complete current-voltage curve and shown it to consist of four discrete regions as can be seen in Fig. (5.3). At low voltages the injected carrier density is less than the free carrier density and Ohm's law is obeyed, ie. region 1. When the injected carrier density is greater than the free carrier density then the current becomes space-charge-limited, but is modified by the traps in the insulator ie. region 2. At the voltage $V_{TFL}$ (trap-filled-limit-voltage) all the traps are full and the current rises sharply in region 3 until it reaches the trap free space-charge-limited value shown in region 4.

Under double injection ie. with electrons injected from the cathode and holes injected from the anode, space-charge-limited conditions are at least partially overcome and for intermediate injection levels charge neutrality can be assumed through the insulator. However, at high and low injection levels the space-charge again becomes important. As in the one-carrier case, the presence of defect states in the insulator will have a considerable influence on the current. This will be principally due to the fact that the electron and hole lifetimes will differ greatly, and will also vary with injection level if traps and recombination centres are present.

B- Tunnelling and Internal Field Emission

Figure (5.4), which shows the energy band structure of a metal-insulator metal sandwich with an applied voltage, indicates the basic tunnelling and internal field emission processes that have been postulated in insulators and semiconductors. The various electron transitions are:

(i) From the valence to the conduction band - leading to Zener breakdown; (ii) to the conduction band from localised impurity levels (field ionization); (iii) electron tunnelling from the cathode into the insulator in a similar manner to field emission into vacuum; and (iv) from the valence bond to the anode.

The main problem in all these mechanisms is to calculate the transmission probability of an electron through a potential barrier by wave mechanics. The difference between various cases arise due to the different electron supply functions and barrier shapes etc. The internal field emission and tunnelling theories (101) lead to a current density-field expression of the form

$$J = A E^{n} \exp [- B/E ] \qquad (5.5)$$

where A and B are constants and n lies between 1 and 3. The actual values of A,B and n depend on the particular case of tunnelling and are not strongly temperature dependent.

Figure (5.5) gives the current-voltage characteristic for tunnelling into the conduction band of the insulator

for a Ta-$Ta_2O_5$-Au film (102). It can be seen that the experimental results shown by the circles, agree with the theoretical curve (the solid line).

C- Schottky Emission and the Poole-Frenkel Effect

These two processes are similar and will now be discussed.

As a result of the high fields obtainable across thin insulating films Schottky emission of electrons may occur from the metal contact at negative potential into the conduction band of the insulator. This mechanism corresponds to thermal activation of electrons over the metal-insulator interface barrier with the added effect that the applied field reduces the height of this barrier. It is identical with Schottky emission into vacuum (see Fig. 5.4).

Tunnelling currents and Schottky emission currents are likely to have the same order of magnitude and are thus difficult to separate. Figures (5.6) and (5.7) show the current voltage characteristic for a Pb-$AL_2O_3$-Pb structure of approximately 300$A^o$ thick, the current with exp (voltage)$^{1/2}$ dependence is clearly indicated (103). The main tool for distinguishing between Schottky and tunnel currents is the strong temperature dependence of the Schottky currents. Fig. (5.8) shows the variation of the current with the temperature at constant voltage in a Pb-$AL_2O_3$-Pb film (103). The observed current shows strong temperature

dependence down to approximately 200°K. Below 200°K the current is essentially independent of temperature. This suggests that above 200 °K Schottky emission is the dominant electron transfer mechanism while below this temperature tunnel currents become important.

The Poole-Frenkel effect involves a mechanism which is very similar to the previously described Schottky effect, except that it is applied to the thermal excitation of electrons from traps into the conduction band of the insulator (104). Fig. (5.9) show the current- voltage characteristic for a Ta-$Ta_2O_5$-Al film (105). The current with exp (voltage)$^{1/2}$ dependence is also very clear.

D- Impurity Conduction

An electron occupying an isolated donor level in an impure insulator or semi-conductor has a wave function, localised about the impurity and an energy slightly below the conduction band minimum. Because there is a small but finite overlap of the wave function of an electron of one donor with neighbouring donors, a conduction process is possible in which the electron moves between centres without activation into the conduction band. This is known as impurity conduction. The necessary conditions for impurity conduction are the presence of both donor and acceptor centres. The acceptors remove a number of the electrons from the donors, thus allowing the movement of electrons from an

occupied donor to an unoccupied one. Without the presence of the acceptors impurity conduction is not possible until the interaction between centres is very large (high concentration of impurities).

For lower concentrations, two possible mechanism have been proposed for the actual electron transfer. These are:-

1- that the electrons tunnel through the potential barrier from the occupied impurity centre to the unoccupied one (106).

2- that the electrons jump (hopping) over the potential barrier from the occupied to unoccupied sites (107). Mead (105), suggested that "hopping" might be dominant at low applied voltages and high temperatures where the current-voltage relation he obtained was Ohmic and the current, at a constant low voltage, was exponentially dependent on the temperature.

On the other hand the existence of ions as impurities in the material has also a great influence on the conductivity process. For example, in the case of the epoxy resin diglycidyl ether of bisphenol A (DGEBA), sodium and chloride ions are present as impurities and originate from the reaction used to produce the starting materials (see section 4.1.2.4). These impurities can play an important part in the conductivity process, which probably leads to an ionic process.

E- Ionic conduction

In bulk material, ionic conduction occurs due to the drift of defects under the influence of an applied electric field. The large number of defects which are known to exist in amorphous films suggests that this mechanism might be important in these materials. Ionic conduction can also occur due to the presence of moisture absorbed into the bulk of the material and as a surface effect (absorbed layer). The theory of ionic conductivity will be discussed in detail in the section below.

5.1.1.2 The Theory of Ionic Conductivity and Ionic Jumping Distance

The Concept of ionic conduction due to lattice defects is based on the rate of drift of the defects in an applied electric field (108-110). The actual mechanism of this drift consists of ions jumping over a potential barrier from one defect site to the next.

By considering the ionic dissociation reaction:

$$\underset{(1-f)\,n_o}{AB} \longleftrightarrow \underset{fn_o}{A^+} + \underset{fn_o}{B^-} \qquad (5.6)$$

where $n_o$ is the original concentration of the ionic compound and f is the fractional degree of dissociation at equilibrium and the law of Mass Action, an equilibrium constant K can be defined in terms of the concentrations of the reactants and products,as follows:

$$K = \frac{(A^+)\,(B^-)}{(AB)} = \frac{f^2 n_o}{1 - f} \qquad (5.7)$$

The equilibrium will be governed by the change in free energy $\Delta G$ for the reactions, so that

$$K \propto \exp\left(-\frac{\Delta G}{kT}\right) = K_o \exp\left(-\frac{\Delta W}{\varepsilon_o kT}\right) \qquad (5.8)$$

where $\Delta W$ is the energy required to separate the ions in a medium of unit dielectric constant. The entropy terms are taken into the constant $K_o$, k is Boltzmann's constant and T is the temperature. If AB is the only ionizable species present, the conductivity will be given by

$$\sigma = f\, n_o\, e\, (\mu_+ + \mu_-) \qquad (5.9)$$

where $\mu_+$, $\mu_-$ are the mobilities of the positive and negative ions, respectively, and e is the magnitude of the charge on an electron. For a small degree of dissociation, equation (5.7) becomes

$$f = \left(\frac{K}{n_o}\right)^{1/2}, \qquad (5.10)$$

and substitution from equations (5.8) and (5.10) in (5.9) gives:

$$\sigma = (K_o\, n_o)^{1/2}\, e(\mu_+ + \mu_-)\exp\left(-\frac{\Delta W}{2\varepsilon_o kT}\right). \qquad (5.11)$$

The above equation (5.11) shows that:

i- the presence of the dielectric constant in the exponent part of the equation means that it will exert a strong influence on conductivity. Thus the absorption of water, which has a relatively high dielectric constant, generally enhances the conductivity of a polymer greatly;

ii- $K_o$ is temperature dependent. It could be

affected by the applied electric field by increasing the number of ions and this may be the reason for deviation from the straight line when current is plotted against voltage.

iii- $\sigma \propto n_o^{1/2}$ ; and

iv- the apparent activation energy obtained from the slope of the Arrhenius plot of log $\sigma$ against 1/T is $\Delta W/2\ \varepsilon$ .

The square-root dependence of $\sigma$ on $n_o$ and the occurrence of the factor 1/2 in the activation energy both comes from the control of the ionic dissociation equilibrium by the law of Mass Action.

In the case of polymers the ionic conduction mechanism can be explained as an activated ionic diffusion process. In this case the current carrying ions may become temporarily attracted to and trapped by oppositely charged ions which are part of the polymer network. This process can be visualized in terms of "counter-ions" becoming dissociated from fixed ions attached to the polymer network; each counter-ion then diffuses through the polymer network until it is attracted to a second fixed ion. This counter-ion "hopping" can be described by the following model (Mott and Gurney (111)). It is assumed that the polymer consists of a uniform, isotropic material of dielectric constant, $\varepsilon$, and throughout this material there are uniformly distributed $N_o$ ionogenic groups, each of which can give rise to a mobile counter-ion and a fixed

ion. Suppose that the unit motion of an ion in the absence of a field is a jump within the matrix of polymer molecules to a neighbouring position of exactly equal energy, passing over a potential-energy barrier of height $\Delta U^*$. The counter-ion will be in a constant state of vibration (frequency $\nu$) when lodged in a potential well.

By assuming the counter-ions obey Maxwell-Boltzmann statistics, the probability that the counter-ion will pass over the barrier is $\exp(-\Delta U^*/kT)$ in each vibration, or $\nu \exp(-\Delta U^*/kT)$ per second. If, however, a uniform electric field, E, is applied to an array of fixed ion sites in the direction perpendicular to the field the potential energy barrier will be unaffected, but in the direction of the field, and against the field, the barrier heights will be changed by $\mp(1/2)eaE$, respectively. (a) is the distance between neighbouring potential wells or fixed sites (see Fig. 5.10). The probability that the ion will move in the direction of the field will now be $\nu \exp[-(\Delta U^* - (1/2)eaE)/kT]$, and in the opposite direction $\nu \exp[-(\Delta U^* + (1/2)eaE)/kT]$. The mean drift velocity

$$U = [\exp(-\Delta U^*/kT)\ 2 \sinh (eaE / 2kT)]\ a \qquad (5.12)$$

Taking into account that the concentration of ions is proportional to $\exp(-\Delta W/2\ \varepsilon_\infty kT)$ the current density, J, flowing through a specimen across which an electric field, E, is applied will be given by

$$J \propto \exp[-(\Delta W/2\ \varepsilon_\infty + \Delta U^*)/kT] \sinh (eaE/2kT), \qquad (5.13)$$

or, in a simple form, at constant temperature,

$$J \propto \sinh (eaE/2kT). \qquad (5.14)$$

Thus, by re-writing the equation above (5.14) in the form,

$$J = A \sinh BE \qquad (5.15)$$

By fitting the equation to experimental values of J and E, it should be possible to find the values of the constants A and B.

Cherry and Wright (112) examined the changes in the factors A and B with temperature, with the moisture content of the resin and how they are related to the structure of the resin. For ionic conduction a mean jump distance, a, of an ion can be derived from the current-density versus field strength curve.

Fig. (5.11) shows how well the results obtained by Kosaki, Sugiyama and Leda (113) for a sample of PVC fit with the sinh relation (equation 5.15) over a wide range of fields. Furthermore, they found that the estimated ionic jumping distance remains constant (1.2 nm) in the temperature region far below the glass transition temperature (Tg = 87 °C) but starts to increasing in the glass transition region. The value tends to a saturation value (a = 3 nm) in the region just above Tg for unplasticized PVC.

Maurer (114) examined the temperature dependence of the ionic jump distance, of soda lime glass and found that it increases with temperature.

Cherry and Wright (112) investigated the water activity and temperature dependence of the ionic jump distance of epoxy resin systems (DGEBA with different hardeners). They found that the ionic jump distance decreased with decreases in water activity and appears to be independent of temperature.

In the present work, the electrical conduction of epoxy resin system MY750/HY956 was measured over a wide range of fields and below the glass transition temperature (108 °C). Statistical analysis was used to obtain point estimates of A and B from the experimental data. The ionic jumping distance was estimated from the B value.

5.1.1.3 Comparison of Ionic and Electronic Conductivity

Since knowledge of the nature of electrical conduction in insulating materials is incomplete, it is sometimes not clear whether the charge transfer process in a given polymer involves the transportation of ions or electrons. The detection of a steady state current as a function of voltage is one approach which leads to information on the type of charge carrier and the transport mechanism. This which is often linked with the polymeric structure and polymer chain motion (139,115). However, ionic conduction has been proposed, for various polar polymers (116,117). Support for the ionic mechanism can be supplied from: Faraday's law of electrolysis which results in gas evolution when a

voltage is applied to the sample. (118); from the dependence of electrical conductivity on pressure (119), and free volume (120), and the degree of crystallinity (121).

The similarties and differences between ionic conductivity and electronic conductivity are illustrated as follows:-

(A) In both cases (ionic or electronic) the conductivity should increase exponentially with the temperature. The magnitude of the activation energy serves as a basis for a comparison between the two mechanisms. For activation energies Ea, smaller than or equal to 1 ev the conduction is assumed to be electronic and for Ea greater than 1 ev the conduction is assumed ionic, the implication being that ions will find it harder to move through the solid (101). This may be a useful rule for inorganic semi-conductors but its application to insulators is doubtful where the energy involved in freeing an electron will be large ie large band gap. Seanor's results (122) show that the activation energy for proton conduction in the polyamides is 1 ev, while that for electronic conduction is 2 ev.

(B) The mobility of the charge carriers in an electronic conductor as a function of temperature T should vary as $T^{-n}$ where n lies between 1 and 2, while that of an ionic conductor should be of the form

exp(-Em/kT) where Em is the trap depth of the impurity. The variation of mobility as $T^{-n}$ has been found in anthracene by Kepler (123) with very pure single crystals. However, work done on doped anthracene by Hoestery and Letson (124) has shown that as little as 1 ppm of impurity can change the variation of mobility to exp-Em/kT. An activated mobility is also expected from narrow band semiconductors where the charge carrier, instead of moving in a well defined conduction band, behaves as if it were in a trapped state and requires a small activation energy to overcome the potential barrier between the trapped states (125).

The mobility of the charge carriers should be greater in an electronic conductor than in an ionic conductor.

The activation energy for the mobility of the charged species in an ionic conductor should be similar to the activation for diffusion in the lattice (126-128). The conductivity should vary inversely as the viscosity.

(C) Electronic conductivity depends upon the degree of intermolecular orbital overlap, while ionic charge transfer involves the movement of ions in the spaces between the molecules or ions. Thus, factors which increase the intermolecular orbital overlap, such as increased crystallinity or high pressures, should increase the conductivity of electronic semiconductors

while decreasing that of ionic semiconductors. This criterion has been used by the majority of workers such as Amborski (129), Warfield and Petree (130), Sazhin and Podosenova (121) and Fuoss (131). As a criterion for distinguishing the two conduction processes, Amborski (129) and Sazhin and Podosenova (121) investigated the dependence of conductivity and the activation energy with crystallinity. They showed that the effect of crystallinity is to lower the conductivity and also the activation energy. It is assumed that conduction, if by ions, takes place primarily in the amorphous regions and that crystallization reduces the number of carriers or their mobility or possibility both and hence reduces the conductivity. However, the decreasing activation energies would imply that the charge carriers move more readily in the crystalline regions. Warfield and Petree (132) have examined the temperature dependence of the conductiviy of a large number of polymers, and have shown that the activation energy increases on passing from non-crosslinked thermoplastic polymers to rigid highly-crosslinked polymers, i.e. opposite trend from amorphous to crystalline.

(D) Electrode and polarisation effects should be shown by ionic conductors; electronic conductors will probably show space charge effects if trapping take place. The polarisation effects usually show up as a steady decrease in the current with time for a fixed

voltage. Electronic conductors, however, should show steady currents with time eg. the current in the intermediate temperature range of the polyamides is time independent, whereas in the high temperature range, where conduction is ionic, the current is time dependent (122,133). However, the application of a step voltage to most insulating polymers results in long term absorption currents which decay as $t^{-n}$ with $n$ $0.5 < n < 1$. The decay usually occurs over several orders of magnitude in both the current and time, depending upon the voltage and temperature. Polarisation effects can also be expected from electronic conductors should deep trapping take place (134). For example long term currents have been found in anthracene using charge injecting electrodes ( Mark and Helfrich (135) and Adolph (136)) and the very slow decay of the current continued for days or weeks. This was due to traps of extremely small capture cross-section.

(E) Ionic conduction involves mass transfer with either the evolution of gas at the electrodes or the deposition of material upon them. Electronic charge transfer does not involve mass transfer. If the transport is completely ionic, Faraday's transport law should be valid, while deviations should occur if the transport is partly ionic and partly electronic. In the two cases where the tests have been applied ( Murphy (137) and Seanor (138)), only Seanor found deviations

from Faraday's law where he found that the hydrogen evolved accounted for only half the total charge passed. This is probably due to the fact that a fraction of the current is still electronic.

(F) In ionic conduction, many polymers show two well defined regions of conductivity when the temperature dependence of the conductivity was examined over a broad temperature range. This, it has been suggested by Warfield and Petree (130), shows the existence of a glass transition temperature (Tg). Therefore, it is inferred that the change in activation energy is associated with the onset of molecular movement and hence the conduction is ionic.

## 5.2 Experimental

This section outlines the instruments and measuring techniques which were used to study the electrical conductivity and dielectric analysis of the epoxy resin systems. Each technique required its own method for sample preparation. These have been described in section 3.3. The electrical conductivity and dielectric analysis sample preparation for MY750/HY956 epoxy resin system was described in section 3.3.1.1b and dielectric analysis sample preparation for MY750/DDSA epoxy resin system was described in section 3.3.2.1.

### 5.2.1 Instrumentation

#### 5.2.1.1 D.C. Conductivity Measurements

Measurements of D.C. electrical conduction were carried out by a step voltage techniques.

The actual measuring circuit for DC current measurement is shown schematically in Figure (5.12). A sensitive electrometer, (Keithley type 602) was used in conjunction with a highly stabilized voltage supply (Brandenberg photomultiplier supply type 475R), which is able to supply up to 2KV. For plotting the current as a function of time, the output from the electrometer was coupled directly to the X-T plotter ( Farnell, instruments Ltd, type No. PR1). The temperature during experiments was regulated by an adjustable hot plate (Chemlab ss 3 H stirrer hot plate) and monitored by a Ni/Al Cr/Ni thermocouple type K, connected to a digital thermometer (RS components). In general, conduction currents through polymer films are very small, sometimes in the sub-pico amp region. In order to measure these small currents it was necessary to screen the whole apparatus. In the present work the sample was kept in a metal box connected to earth through the electrometer. To avoid induced currents due to earth loops, a single earth point was used and all plug earths were removed.

### 5.2.1.2 Dielectric Measurements

A capacitance bridge (General Radio type 726- C) was used to measure both dissipation factor and capacitance by a direct method over a frequency range of 200 Hz to 100 KHz. The type 716-C Capacitance Bridge is a Schering bridge and it is shown schematically in Fig. (5.13). The bridge was used in conjunction with a signal generator (Transistor decade oscillator type TG 66A, Levell Electronics Ltd.) and detector (Oscilloscope 465, Tektronix Guernsey Ltd.). A schematic diagram is shown in Figure (5.14). The capacitance bridge was combined with a Brookdeal low noise amplifier (type 453, Max. output 3v p.p.). For screening, the sample was kept in a metal box connected to earth. The temperature during experiments was regulated by an adjustable oven (Montford Instruments Ltd.) and monitored by a Cr/Ni Ni/Al thermocouple type K connected to a digital thermometer (RS components type). The measured values for both capacitance and dissipation factor were modified using the correction formulae given in Appendix (5.1).

## 5.3 Results and Discussion

### 5.3.1 Conductivity Measurements

The DC electrical conduction currents of the epoxy resin system MY750/HY956 were measured from low to high electric field strengths and from room temperature to

90°C below the glass transition temperature Tg (108°C, see chapter four). Current (I) versus voltage (V) plots at different temperatures were obtained for several samples of 0.6 *mm* thickness. One of those plots is shown in Figure (5.15a-d). It can be seen that an Ohmic conduction mechanism was operating. When the resultant resistivities were expressed as an Arrhenius plot, a linear relationship was obtained and an activation energy of 0.73 ev. found (see Fig. 5.16).

Fig. (5.17a) shows the current-time relationship obtained at a constant voltage (100 V) and at room temperature. It can be seen that the current decreases monotonically with time and requires a very long time to reach the steady-state current condition (60-120 mins.). Fig. (5.17b) shows the plot of the resistance R as a function of time t obtained from Fig. (5.17a), showing the polarisation effect.

Fig. (5.18 a,b,c,d) show plots of J (current density) against E ( applied field), Log J against E, log J against log V, and ln I against $V^{1/2}$. The data was used from Fig. (5.15a), measurements being made at room temperature.

For ionic jump distance measurements a separate thin specimen was used. Figure (5.19 a,b,c,d,e) show the plots of I against V, J against E, log J against E, log J against log V, and ln I against $V^{1/2}$ at room temperature for thin sample of 0.1 *mm* thickness. From Fig. (5.19b) it can been seen that the plots of measured

data satisfy equation (5.15) for ionic conduction given by Mott and Gurney (111) (see section 5.1.1.2). ie

$$J = A \sinh BE,$$

where A and B are constants. It should be noted that the function deviates from an Ohms law relationship only at high fields.

In the present work, the ionic jumping distance a was derived from the B estimate, and the latter was estimated by statistical analysis (see section 5.3.1.1). It was found that

$B = 0.2793 \times 10^{-6}$ m/v. and this implies that

$a = 14.11$ nm.

The error estimate for the B value $\sigma_B = 3.56 \times 10^{-9}$ m/v.

The measurements were repeated in order to increase the number of data points obtained in the high field region resulting in increased precision of the B estimate. This was achieved by using a thinner sample, which increased the maximum field obtained for the same applied voltage range. The method was prefered to that of increasing the applied volts since the latter caused problems due to corona discharge. Fig. (5.20 a,b,c,d,e) shows the plots of I against V, J against E, log J against E, log J against log V, and ln I against $V^{1/2}$. The measurements were made at room temperature and for the thinner sample (0.08 mm thickness). The ionic jumping distance a and the B estimate (see section 5.3.1.1) for the thinner sample were:

$B = 0.2336 \times 10^{-6}$ m/v. $a = 11.8$ nm.

The error estimate for B value $\sigma_{\hat{B}} = 1.224 \times 10^{-9}$ m/v.

From the two set of measurement above for B and a values it can be seen that increase in the number of data points obtained in the high field region resulting in increased precision of the B estimate which leads to a better value of a (see section 5.3.1.1).

From the study of one carrier space-charge-limited currents (see section 5.1.1.1A), the slope of log current density (J) versus log voltage (V) plot (see equation 5.2) is equal to two, whereas the experimental results show that the slope at low field is equal to 1.0 in Figure (5.18c) and at high field is equal to 1.8 in Figure (5.20d) and is equal to 1.45 in Figure (5.19d). As it can be seen, for high fields the experimental slope in Fig. (5.20d) is close to the theoretical one and this implies that a space charge limited currents may be present. If space charge limited current is present, the discrepancy between the experimental and the theoretical slope may be due to experimental errors.

From the experimental analysis (see section 5.1.1.1A), the density of thermally generated free carriers ($n_o$) at the so called transition voltage ($V_{tr}$ = 300V) was found to be $n_o = 1.458 \times 10^{19}$ $1/m^3$ (assuming no traps occur in the material $\theta = 1$ (see Appendix

5.2a)). From the micro-analysis of the epoxy resin MY750 (see section 3.2.1) the density of the impurities present was found to be 1.2 $\times 10^{26}$ $1/m^3$ (assuming no ion impurities present in the hardener (see Appendix 5.2b)). This means that the maximum number of charges thermally generated ($n_o$) at room temperature is 1 per 1 $\times 10^7$ of the actual charges (n). It can be seen that the two densities are far apart which makes it doubtful if space charge limited currents are present. Furthermore, the above mentioned log J - log V characteristic, despite the reasonable fit to space charge limited currents,also fits the ionic conduction equation (5.15) (see Fig. 5.21c).

In the case of tunnelling and internal field emission, (see section 5.1.1.1B), the current voltage expression is given in equation (5.5), but the experimental results show that the data satisfies equation (5.15) for ionic conduction (111) (see section (5.1.1.2), Fig. (5.15a), (5.19a), (5.20a), (5.21a)). Thus tunnelling and internal field emission mechanism cannot be present.

In the case of Schottky emission and the Poole-Frenkel effect (see section 5.1.1.1C), the logarithm of the current (I) is proportional to (voltage)$^{1/2}$, whereas the experimental ln I against $V^{1/2}$ characteristics (see Fig. (5.18d), (5.19e), (5.20e), (5.21d)) are not a straight line. This implies that these conduction processes cannot be present.

In the case of impurity conduction (see section 5.1.1.1D), the presence of sodium and chloride ions in epoxy resin MY750 (DGEBA) has a great influence on the conductivity process (79). From the present investigation of the conductivity of the epoxy resin system MY750/HY956 described above, it is reasonable to suggest that ionic conduction dominates from the low to the high field regions.

### 5.3.1.1 Statistical Analysis

To obtain point estimates of A and B from the experimental data, two techniques were employed.

The first technique was to employ a least squares method and the second was a form of iterated linear regression analysis. The probability model for the data was as follows:

$$J_i = A \sinh BE_i + \epsilon_i,$$

where $\epsilon_i$ is the error and $J_i$, $E_i$ are the observed values of current density and electric field.

In the least square method the point estimates of A and B were made by minimizing the sum of squares function SS(A,B) using a hill climbing technique

$$SS(A,B) = \sum_i (J_i - A \sinh BE_i)^2$$

Initially the range of current density against field values over which to search were determined by a crude linear regression model. This assumed that the mean current density was proportional to the increase in the electric field. Fig. (5.22) shows a plot of the sum

of squares function in the neighbourhood of the minimum. The diagram reveals that the sum of squares function is shaped like a valley which lies nearly in the direction of constant B value. This indicates that the A estimate could take a wide range of values without effecting the minimum value of the sum of squares function significantly. That is to say, widely differing values for A are entirely consistent with the data which had been obtained. On the other hand, the B value would appear to be lying at the bottom of the valley. Rough estimate for the error for the thinner sample can be obtained as follows:

$$\hat{\sigma}_B^2 = \frac{2\,\sigma^2_{err}}{\partial^2 SS / \partial^2 B} \qquad \hat{\sigma}_B = 1.224 \times 10^{-9}\ m/v.$$

where $\sigma^2_{err}$ is the estimated error-variations obtained by dividing the minimum residual sum of squares by the degrees of freedom. $\partial^2 SS / \partial^2 B$ is obtained directly from SS (A,B). The point estimate of B obtained from this method using the thinner sample was

$B = 0.2336 \times 10^{-6}$ m/v. a = 11.8 nm.

This analysis is based on the description given by Box and Jenkins on estimation from sum of square plots (161).

The iterated regression method relied on first fitting the B value with the A value fixed and then fitting the A value with the B value fixed and so on.

For estimating the B value the linear regression

was performed for $\sinh^{-1} J/A = BE$. The A value regression was performed on $J = A \sinh BE$. This was repeated successively until the B and A estimate converged (see table 5.1). The regression models were fitted using the Glim modelling package (162). The point estimate of B obtained from this method using the thinner sample was

$B = 0.248 \times 10^{-6}$ m/v. $\qquad$ a = 12.53 nm.

The iteration was started again by using the crude regression model which was outlined for the first method.

The Glim model provided the following estimate for the standard error of

$\sigma_{\hat{B}}$

$$\sigma_{\hat{B}} = 5.7 \times 10^{-9} \text{m/v.}$$

This must be treated circumspectly because it is the error estimate for B when A is known using normal error. Nevertheless it does indicate the order of magnitude of the error in fitting the B value.

### 5.3.2 Dielectric Measurements

Dielectric measurements for the epoxy resin system MY750/HY956 were performed from room temperature to just below the glass transition temperature Tg. The Tg of the cured sample was 108 °C as measured using differential scanning calorimetry (see chapter four). Figures (5.23), (5.24), shows the results obtained for the dissipation factor and capacitance respectively as a

function of temperature measured at different frequencies.

From Figure (5.23) it can be seen that the tan $\delta$ values decrease in the temperature range between $\beta$ and $\alpha$ peaks (see section 4.3.5.1.3). Furthermore there are no peaks. Additionally the increase in tan at high temperatures as shown clearly in Figure (4.23) is due to the influence of D.C. conduction processes (equation 4.35).

From Figure (5.24) it can be seen that the capacitance values increase with the temperature and there are no peaks.

In the case of the epoxy resin system MY750/DDSA Figures (5.25), (5.26) shows the result obtained for the dissipation factor and capacitance respectively as a function of temperature measured at different frequencies.

From Figure (5.25) it can be seen that there are peaks. These peaks, can be associated with an $\alpha$ - relaxation process due to the orientation of long segments of molecular chains since they occur above and close to the Tg. (Tg = 25 °C, see chapter four). Furthermore the maximum value of the peak shifts to a higher temperature as the frequency increase.

Fig. (5.27) shows the results obtained for log $\tau$ against 1/T for a series of three samples. $\tau$ is the relaxation time and is equal to $1/2\pi f$. T is the

temperature of occurrence of the peak. It can be seen that there is a good agreement between measurement made in all samples. The small variation in the peak position is due to sample preparation. An activation energy of 2.16 ev. was found.

From Figure (5.26) it can be seen that the capacitance C values increase with the temperature. The slight decrease in capacitance at high temperatures is due to the slight decrease in the density of the sample.

## 5.4 Conclusion

The electrical conduction of epoxy resin system MY750/HY956 was measured from low to high electric field for values below breakdown. The measurements were performed from room temperature to just below the glass transition temperature Tg (Tg = 108 °C).

The mechanism of ionic conduction was found to be the dominant process for all applied electric fields. An activation energy for the conductivity process was found 0.73 ev. The ionic jump distance at room temperature was estimated from the current density versus field strength curve using the equation for ionic conduction given by Mott and Gurney (111) and a statistical analysis was used to estimate the values of the constants A and B in the equation (5.15) (see section 5.1.1.2). The estimated ionic jumping distance was 11.8 nm.

The results of the dielectric loss measurements of

the epoxy resin system MY750/HY956 appears to have no loss peaks, but exhibited d.c. conduction at high temperature, whereas the MY750/DDSA epoxy resin system has a loss peak which is associated with a relaxation process. An activation energy of 2.16 ev. was found from the peak.

# CHAPTER SIX

# THE EFFECT OF GAMMA-IRRADIATION ON THE ELECTRICAL PROPERTIES OF EPOXY RESIN SYSTEM

## 6.1 A Review of Radiation Work on Polymers

In the earliest studies of the radiations emitted by radioactive materials it was found that permanent physical and chemical changes could be produced in a wide variety of materials. Systematic studies of the effect of high energy radiation on organic molecules were carried out in the mid 1920's by Lind (163). The use of radiation to induce polymerisation was investigated by Hopwood and Phillips (164). The use of atomic or high energy radiation to modify polymers was carried out by Charlesby (165). A detailed and systematic study of these radiation effects over a wide range of materials was not, performed until after 1940, when the development of nuclear energy projects made available powerful sources of high energy radiation. This showed the importance of radiation damage to materials.

### 6.1.1 Temporary and Permanent Changes

The effects of high-energy radiation upon the electrical properties of polymeric materials can be separated into two distinct groups. The effects in the first group are temporary and take place only when the

insulation is exposed to a radiation flux. Examples of such temporary phenomena are resistance changes and the photo-electric effect. The second group consists of effects which are cumulative and permanent, such as the physical changes resulting from alteration in the chemical constitution of the molecules of the dielectric. These two types of change are of considerable importance when considering the behaviour of a particular insulating medium designed for continuous operation in a radiation flux, such as would be encountered in nuclear reactor applications as well as in earth satellite and deep space applications.

6.1.1.1 Temporary Radiation Effects :

The effects of radiation upon the conductivity of various organic insulators have been studied extensively by Fowler and Farmer (128,166-174). A small current is induced to flow in an insulator if it is stressed electrically with a D.C. electric field. If this system is exposed to high energy radiation then this static current is augmented by a radiation induced current. It was thought that this current was the result of the production of free electrons and an equal number of positive holes throughout the volume of the dielectric (166). The observed current was thus the sum of two components, the static current and the induced current. Both static current and induced current rose with temperature, although at different rates which indicated

that they were related to different phenomena. Furthermore when the polymer was irradiated, the observed current increased gradually to its final value. Similarly, when the irradiation was discontinued, the current decayed slowly, reaching the static current level after several hours.

The mechanism by which the induced current was carried was to some extent controversial. Mayburg and Lawrence (175) have, postulated that protons, $H^+$ act as charge carriers in polyethylene. The hypothesis that the current was carried by an ionic mechanism was also put forward by Warner, Muller, and Nordlin, (176) and by Feng and Kennedy (177).

Fowler and Farmer (174), assumed that conduction was due to the drift of free electrons in the applied field and that ionic conduction was negligible.

It was found that the induced current ($J_\infty$) for a given applied electric field was a function of the irradiation intensity I and can be expressed as

$$J_\infty \propto I^n, \qquad (6.1)$$

where (n) can have values lying between 0.5 and 1.0 and is a characteristic of the polymer. In an insulator there are charge trapping levels lying between the valence and conduction bands. Electrons which are excited into the conduction band, from these traps, either thermally or by means of the radiation process, can return to these trapping levels with the emission of energy in the form of radiation. Transition from these

traps to the valence band or ground state can only take place by way of the conduction band. Similar arguments apply to holes in the valence band. Fowler (174) has shown that the value of (n) in the expression above can be related to the type of energy distribution of these intermediate traps. The traps are associated with dislocations in the crystal structure or may be introduced by impurities present in the polymer. Where their distribution is uniform, n = 1, whereas with an exponential distribution of traps n = 0.5 (see Fig. 6.1). In the case where n = 1, the conductivity is directly proportional to the number of electrons released from the traps provided that all the free electrons can migrate to the anode without either combining with the positive ions or are permanently trapped after traversing a constant distance (178). The induced conductivity will be nearly independent of the temperature. In the case where n = 0.5, the conducting electrons and ions created by the radiation re-combine rapidly. If the electrons are released from shallow traps by thermal activation, an additional contribution to the current appears, and this will depend on the temperature. The exponent of I may take on values from 0.5- 1.0, depending on the depth and distribution of the traps.

The trap energy distribution is also found to play an important part in the rate of decay of the conductivity after irradiation is discontinued. For n =

1 the decay is approximately hyperbolic and more rapid than in the case where n= 0.5. In the latter case the decay is exactly hyperbolic. It is concluded (169,170), that the electrons released by ionizing radiations may in part combine rapidly with the positive ions, but that a considerable fraction of them move to the anode without recombination. Of this latter fraction, a portion (dependent upon the polymer, the temperature, and the applied voltage) are caught in shallow traps. This occurs at an increasing rate as the temperature is raised. The traps normally present in unirradiated polymer are evidently of this deeper variety (19). After irradiation, the thermal release of electrons from the shallow radiation - formed traps may continue for many days or even months (179).

6.1.1.2 Permanent Radiation Effects :

The chemical and physical changes of a fairly wide range of polymeric materials subject to high-energy ionizing radiation have been studied by many authors (180-185). The presence of free radicals and ions in irradiated polymers has been demonstrated conclusively (3,17-19). These excited entities may react so as to change both the chemical structure of the polymer and the physical properties of the material. These structural modifications effect the mechanical and electrical properties of the polymer.

In the early 1950's, considerable interest was

shown in the potential use of high energy radiation to initiate polymerisation or to modify polymers by such processes as crosslinking and degradation. Irradiated polymers tend to fall into one of two classes;

(i) those in which the irradiation produces increases in cross-linking of the polymer chains, leading first to an increase in molecular weight and, at high enough doses, to the formation of an insoluble three-dimensional network or (ii) those in which radiation induced scission of the molecular chains occurs, resulting in a decrease in average molecular weight. Both processes occur simultaneously in many polymers, and the classification depends upon which is predominant. Table (6.1) shows these two classes, as based on the observation of Lawton (186,187).

The classification in table (6.1) is not entirely rigid, as some polymers may fall on one side or the other according to the conditions employed. For example, the presence of oxygen tends to encourage scission, and certain polymers may show predominant scission or crosslinking, depending on whether oxygen is present or not. The effect of oxygen or air, is to cause oxidation and molecular degradation has been found to take place as the result of the interaction between the oxygen and the free radicals which may be formed during the irradiation process (188). In order to exert a marked effect, the oxygen must of course diffuse into the polymer at a rate comparable to its rate of reaction

with the polymer. If diffusion is very slow compared to radical formation, all the oxygen initially dissolved will be rapidly consumed, and thereafter the reaction within the polymer will proceed normally. Thus, with thick blocks of polymers , the effects of oxygen are confined to the surface (180,189) whereas with thin films, particularly at low dose rates, the effects are observed throughout the samples. Furthermore, in investigations upon the irradiation of long-chain polymers, it has been found that the major reactions involved, cross-linking or degradation, are temperature dependent (184,190,191). The relation between the molecular structure of the polymer and its behaviour on irradiation have been investigated by Miller et al (187). Irradiation of polymers generally results in the evolution of gases such as hydrogen, methane, and the lower hydrocarbons. These result from side-chain fracture. Analysis of the gases evolved from polyethylene, for example shows that at least 85 - 95 per cent of the gas evolved is hydrogen, the remainder being condensable hydrocarbons, depending on the side-chains present initially (192).

The permanent effects of ionizing radiations on the electrical properties of high polymeric dielectric materials is also of considerable technical importance when cables and components are used in the nuclear engineering and space technology industries in environments where the dielectric may be exposed to

radiation for a considerable period of time. A number of investigations have been carried out to assess the electrical performance of samples of various dielectric materials after irradiation (193). It was found that on irradiation the conductivity is increased due to the production of electrons/hole pairs and is a function of the radiation intensity. The continuous exposure of a dielectric to ionizing radiation will exert an accelerating effect upon the normal processes of electrical breakdown. The ionization produced in the material itself or in its immediate environment e.g. oxygen in air, will give rise to an increase in leakage current and will also increase the tendency to surface breakdown by contamination. The flash-over and breakdown voltage of the insulator will be decreased. Epoxy resins are currently being used in radiation environments. Burnay observed the formation of diphany lethyl cations, radicals and also the annealing of UV. absorption bands in the DGEBA-aliphatic/aromatic amine epoxy system (20,21). Furthermore the radiation behaviour of cured epoxy resin systems is strongly dependent on the type of hardener used. For example, aromatic amine cured epoxies are more radiation resistant than aliphatic anhydride cured systems (21). Nevertheless it was not clear how the presence of ions and the changes in structure would effect the electrical properties of an epoxy system.

This chapter describes a series of experiments which provide information about the behaviour of the resistivity( $\rho$ ), dissipation factor (tan$\delta$), capacitance (C), differential scanning calorimetry (DSC) and the infrared spectra (IR) of epoxy resin samples before and after gamma-irradiation, at doses in the range of 0.5 to 2.3 MGy, and also after post-irradiation annealing. Furthermore the relationship between the properties and the structure of the epoxy resin system is discussed.

The gamma-irradiation source which was used in this study was Cobalt-60. Gamma-radiation has the highest penetrating power, compared with other types of radiation. The radioactive isotope Co-60 is most often used because of its rather long half-life, sufficiently high radiation energy, relative simplicity of preparation, availability, and cost.

## 6.2 Experimental

### 6.2.1 Material and Sample Preparation

The material which was used to investigate the effect of gamma-irradiation on the epoxy resin systems was described in section (3.2). Each technique which was used in this study required its own method for sample preparation. These have been described in section 3.3. DSC sample preparation was described in section 3.3.1.5, 3.3.2.3 infrared spectroscopy (IR) sample preparation was described in section 3.3.1.3b,

dielectric measurement sample preparation was described in section 3.3.1.1b, 3.3.2.1 and electrical conductivity sample preparation was described in section 3.3.1.1b.

### 6.2.2 Instrumentation

Each technique which was used in this study required its own instrument and measurement procedure. DSC measurements were made on a DuPond 910 instrument (see section 4.2.1), dielectric measurements were made on a capacitance bridge (see section 5.2.2.2), D.C. current measurement (see section 5.2.2.1), IR measurements were made on a Grating infrared spectrophotometer, PERKIN-ELMER 257 instrument (see section 4.2.2). After suitable packaging, samples were exposed to gamma irradiation from a Co-60 source at doses of 0.5, 1, 1.5, 2 and 2.3 MGy. The dose rate was 5 KGy per hour. After irradiation some samples were annealed in a hot air oven (Montford instruments Ltd.) for 3 hours at 95°C. The electrodes of these samples were connected together electrically during the annealing process (short circuited).

## 6.3 Results

In order to study the effect of gamma -irradiation on both chemical structure and electrical properties of epoxy resin systems, test were conducted on samples under different situations (see table 6.2). The results

for both MY750/HY956 and MY750/DDSA epoxy resin systems are as follows

### 6.3.1 MY750/HY956 Epoxy Samples

Figures (6.2 a,b), (6.3 a,b) show the results obtained for the dissipation factor and capacitance as a function of temperature, measured at 200 Hz for samples exposed to 0.5 MGy and 2 MGy. Fig. (6.7 a,b) show the results obtained for log (tan $\delta$ (A.A.)/tan $\delta$ (B.I.)) see table (6.2) against dose at different temperatures and frequencies. Figure (6.8 a,b) show the results of capacitance measurements, C, plotted in the form log (C (A.A.)/C (B.I.)) against dose at different temperatures and frequencies. From Figs. (6.2,6.7,6.8) it can be seen that the dissipation factor first decreases a little and then increases as the gamma-irradiation dose increases.

Figures (6.4 a,b,c) show the results obtained from DSC measurements of a fully cured epoxy resin system. This has a Tg value of 108°C before irradiation (B.I.), 82°C after irradiation (A.I.) to 0.5 MGy and 98°C after annealing (A.A.). The Tg peak for a sample after irradiation was broader than the peaks obtained both before irradiation and after annealing.

Figures (6.5 a,b) show the infrared spectra of a fully cured epoxy resin system before and after irradiation to 2.3 MGy. From these spectra it can be seen that there are marked changes in the IR spectrum on irradiation. In addition to an increase in overall

absorbancy attributed to a colour change in the material of the sample from clear to brown, a modification to the spectrum was noted in the 1600 to 1800 $Cm^{-1}$ range.

Maxwell and Pethrick (197) studied the thermal modification of amine cured epoxy resins. From their ultraviolet spectroscopic studies, they observed a tail in the region 300-450 nm associated with colour generation in the films at temperatures above 473 $^{o}K$. They concluded that this colour development was due to the formation of polyenyl structures with the possible formation of cyclised conjugated nitrogen compounds (see Fig. 6.15a).

Current voltage plots at different temperatures were obtained for several samples exposed to different doses of gamma irradiation. It was found that an Ohmic conduction mechanism was operating. When the resultant resistivities were expressed as an Arrhenius plot, a linear relationship was obtained and the activation energy found (see Figure 6.6) for samples prior to irradiation (B.I.) and after annealing.

Table (6.3) shows the effect of gamma-irradiation on the resistivity, Tg, current transient length and activation energy of the samples. This is summarised schematically in Fig. (6.9). It can be seen that the conductivity, tan $\delta$ and capacitance increase rapidly for irradiated samples which had not been annealed.

### 6.3.2 MY750/DDSA Epoxy Samples

Fig. (6.10 a,b) show the results obtained for dissipation factor and capacitance as a function of temperature. These are measured at different frequencies. The samples were measured both before irradiation and after a post-irradiation anneal, the dose being 1 MGy. It can be seen that the peaks, which are attributed to dipole-relaxation polarisation, shift to a higher temperature and the amplitude of these peaks decreases after annealing (A.A.). Figure (6.11 a,b) shows the results obtained for ln $\tau$ versus 1/T where $\tau$ is the relaxation time ($\tau = 1/2\pi f$) and T is the temperature of occurrence of the peak : (a) for samples exposed to 0.5 MGy, 1.0 MGy and 2.0 MGy and (b) for different concentrations of hardener for samples exposed to 1 MGy.

From Fig. (6.11 a) it can be seen that there is good agreement between measurements made in all samples prior to irradiation. This indicates that any changes which occur after irradiation are attributable to that irradiation and not to the sample preparation.

Fig. (6.12 a,b) shows the results obtained for : i) $\Delta$ Tm, the difference in the peak position before and after annealing measured at 0.2 kHz ; ii) $\Delta$ E , the difference in the activation energy values between pre-irradiated and post-irradiated and annealed samples; and iii) the Tg values. Graph (a) shows these properties as a function of dose and graph (b) as a function of concentration of hardener for samples exposed to 1 MGy.

Figure (6.13 a,b) shows the results obtained for the ratio of $\Delta\tan\delta m$ to $\tan\delta m$, and $\Delta Cm$ to Cm. $\Delta\tan\delta m$ is the difference between pre-irradiated and post-irradiation annealed values of $\tan\delta m$; $\tan\delta m$ is the peak value of $\tan\delta$ before irradiation, $\Delta Cm$ is the difference between pre-irradiated and post-irradiation annealed values of Cm; Cm is the peak value of C. Graph (a) shows these properties as a function of dose and graph (b) as a function of concentration of hardener for samples exposed to 1 MGy. Measurement was made at 0.2kHz.

Figure (6.14 a,b) shows the results obtained for $\Delta W/W$ as a function of (a) dose and (b) concentration of hardener for samples exposed to 1 MGy. $\Delta W$ is the change in sample weight between the pre-irradiated and the post-irradiation anneal, W is the sample weight prior to irradiation.

## 6.4 Discussion

### 6.4.1 MY750/HY956 Epoxy Samples

#### 6.4.1.1 The Changes in The Properties After Irradiation

The effect of the gamma-irradiation of a MY750/HY956 epoxy system was shown in both Table (6.3) and Figure (6.9). First of all, the conductivity, $\tan\delta$ and C increased rapidly for the irradiated samples (before annealing). The conductivity value increased more than 1000 times (table 6.3), the $\tan\delta$ value became

greater than 1 (see Figure 6.2 b), the value of capacitance changed by 2 to 5 times (Fig. 6.3 b) at a dose of 2 MGy and Tg decreased by 10 to 20 °C. The Tg value of MY750/HY956 epoxy system for a fully cured sample is 108 °C (44). There is a sharp change in the cross-linking and degradation rates of the polymer at Tg. It has been shown that irradiation at T < Tg, leads to degradation while irradiation at T > Tg leads to crosslinking (3). Thus the main effect of irradiation at room temperature in the MY750/HY956 epoxy system should be degradation. This leads to different kinds of ions and hydrogen being formed. It is likely that the broader valley appearing in the DSC measurement (Fig. 6.4 b) and the ill-defined activation energy (Table 6.3) indicate that a more complicated and/or unstable structure exists in these epoxy systems after irradiation. Furthermore the modification to the IR spectrum after irradiation (Figure 6.5) which was noted in the 1600 to 1800 $Cm^{-1}$ range was due to the formation of carbonyl groups (C=O) from pendant (-OH) groups which yield hydrogen (see Figure (6.15 b)) (20,21). The irradiation-produced ions in the MY750/HY956 epoxy system are shown in Figure (6.16) (93).

Hydrogen accumulated in the sample would cause the free volume to increase. This would lead to an increases in the mobility of the ions in the sample (3). It is clear that the Tg decrease can be explained by chain scission and a free volume increase and that the

conductivity increase can be attributed to an increase both in the concentration of ions (3,20,21,194) and an increase in their mobility.

6.4.1.2 The Effect of Annealing

After annealing at 95°C (T<Tg) for 3 hours with the electrodes short circuited, the following changes in properties were found :

(i) The conductivity, tan $\delta$ and C were reduced sharply. The conductivity decreased to about one thousandth of the value of the sample after irradiation (Fig. 6.6 and table 6.3). The tan $\delta$ and C values for low dose at low temperature were less than those before irradiation. The tan $\delta$ and C values measured at high temperature for high doses were higher than before irradiation (Fig. 6.7,6.8).

(ii) Tg returns to a value close to that of a sample measured before irradiation. The peak in the DSC measurement was sharper than that of a sample after irradiation

(iii) The activation energy, E, is larger than the value of the same sample before irradiation (Fig. 6.6 and table 6.3).

Why do the conductivity, tan $\delta$ and C values reduce after annealing ? The effects of crosslinking and also the short circuiting of the sample during annealing should be considered.

A post-irradiation annealing leads to a crosslinking

reaction involving trapped radicals (3). The effect of the process would be to reduce the conductivity, tan $\delta$ and C of an annealed sample. The effect of short circuiting the sample would cause the ions to be discharged at the electrodes thus reducing the concentration of these ions (depolarisation). This process leads directly to a reduction in conductivity and capacitance.

6.4.1.3 The Relationship Between The Electrical properties and The Two Phase Structure of an Epoxy System

The reasons stated above can only explain partially the effects of the irradiation and annealing. For example, why are the conductivity, tan $\delta$ and C values for low dose at T < Tg much less than the original value of a sample before irradiation? The other contradiction is that the tan $\delta$ and C values for high dose samples measured after annealing at T < Tg and low frequency are larger than that of a sample before irradiation, while the conductivity value is less than that of a sample measured before irradiation under the same conditions (Figure 6.6 b).

A fully cured epoxy resin has been shown to be a two phase system (32,90-94,195) containing roughly spherical floccules in a low-density liquid medium. The roughly spherical floccule is formed by crosslinking macromolecules and possesses a high density. The liquid

medium resembles the uncured starting materials and possesses a lower molecular weight. The current, in the form of ions passing through the sample, move preferably through the liquid medium in the sample since most ions will be more mobile in this phase.

The irradiation of polymers is accompanied by ion and radical production. The ions directly affect the electrical properties of polymers. Small, irradiation-produced ions mainly form in the liquid phase, where they will possess a higher mobility and a lower activation energy (shallow trapped charges) than in the floccule. This sharply increases the conductivity of irradiated-samples. Shallow trapped charges in the liquid phase may easily discharge during the post-irradiation annealing and the short circuiting of the electrodes. Larger doses of irradiation produced macromolecular ions and are mainly formed in the floccule. These possess a lower mobility and a higher activation energy than the smaller ions and are deep-trapped charges. Some of the deep-trapped ions are quite stable even at temperatures ,T, slightly higher than Tg. The deep-trapped macromolecular ions in the sample may be effective traps for the opposite polarity active ions. For sample exposed to low radiation doses at $T < Tg$, this is probably the cause for the $\tan\delta$ (A.A.) values being much less than $\tan\delta$ (B.I.). The deep-trapped charge cannot take part in the conduction of the electrical current but can rotate a little in

response to an a.c. field. In the present work, this kind of polarisation is called a relaxation polarisation of a monopole. The intensity of this monopole polarisation, and hence the values of tan $\delta$ (A.A) and C (A.A.), will increase with the temperature and decreases with the frequency of the electric field because of changes in the relaxation times.

### 6.4.1.4 The Effect of The Oxidization and Water Absorption During Annealing

The tan $\delta$ values of samples exposed to different conditions were measured in order to investigate the effect of oxidization and water absorption (Figure 6.2b, 6.9). If the irradiated sample was annealed at a high temperature and for a long period than usual the effect of oxidization should be greater and the value of tan $\delta$ measured in this situation should consequently be higher. This is because of the formation of polar bonds attached to the molecular chains.

From table (6.2) it can be seen that situation A.A. refers to a sample annealed at temperature $T < Tg$ for 3 hours while the situation E refers to the same sample annealed at a temperature $T > Tg$ for a longer period (10 hours).

The results indicate that tan $\delta$ (E) $<<$ tan$\delta$(A.A.) and C (E) $<$ C (A.A). This implies that the effect of oxidization is not an important factor for temperatures $T < Tg$ at the frequency of measurement.

In order to investigate more fully the annealing and water absorption effects, two further situations (D, and F) were considered. In situation D, the A.A. sample was left at room temperature in contact with air for 3 days; whereas in situation F, the sample from test E was left at room temperature in contact with air for 3 days (see table 6.2). From the two situations D and F the difference between $\tan\delta$ (F) and $\tan\delta$ (E) as well as the difference between $\tan\delta$ (D) and $\tan\delta$ (A.A.) can be attributed to water absorption.

Measurement shows that the difference between $\tan\delta$ (D) and $\tan\delta$ (A.A) was larger than the difference between $\tan\delta$ (F) and $\tan\delta$ (E). This indicates that the difference between $\tan\delta$ (D) and $\tan\delta$ (A.A.) is caused by factors other than water absorption (see Fig. 6.2b).

A suggestion can be made that after irradiation the annealed sample (sample A.A.) was not completely annealed compared to sample F, this would imply that in sample (A.A.). there were still deep-trapped ions in the floccule of the epoxy system which may seriously accelerate the absorption of water and other constituents. The trapped ions may be slowly released into the liquid medium to increase the conductivity, tan$\delta$ and C values (see Fig. 6.9). However sample F was completely annealed at T > Tg under short circuiting conditions. Thus the deep-trapped charges would have been discharged, so that the amount of water-absorption is lower, and the effect on electrical properties is

small.

### 6.4.2 MY750/DDSA Epoxy Samples

#### 6.4.2.1 The Effect of The Gamma-Irradiation

From Fig. (6.10) and Fig. (6.11-14a), it can be seen that the effect of the $\gamma$-irradiation may be summarised as follows:-

(i) The peaks in the Tan $\delta$ - T plot (from Fig. 6.10a) and C - T plot (from Fig. 6.10b) shift to a higher temperature with dose I (Fig. 6.12a, Tm -I plot); (ii) the activation energy E derived from the ln $\tau$- 1/T plot in Fig. (6.11a) increases with dose (Fig. 6.12 a, $\blacktriangle$E -I plot); (iii) the glass transition temperature, Tg, also increases with dose I (Fig. 6.12 a, Tg- 1/T); (iv) the value of tan $\delta$ decreases with dose, rapidly at low doses and then at a reduced rate of change for higher doses. On the other hand the capacitance value, C, initially decreases and then increases; (v) the weight of the sample increases with dose I (Fig. 6.14a); (vi) there is little effect of post-irradiation annealing.

The hardener DDSA has a chemical structure shown in Fig. (3.1a). The DDSA is not only a hardener but also a plasticiser, increasing the flexibility of the epoxy system due to the long aliphatic branch with a double bond in the DDSA. The Tg value for MY750/DDSA is close to room temperature (25 °C, DSC measurement ) which implies that the molecular chains in MY750/DDSA are mobile at room temperature. Consequently radicals and

ions produced by the irradiation are mobile and disappear rapidly due either to reaction with the surrounding epoxy resin molecules or with oxygen which has diffused into the sample. Therefore, the properties should not change any further after annealing. Because of the temperature, the main effect in the MY750/DDSA epoxy system should be crosslinking (section 6.4.1.1). This implies that the Tg values, the activation energy, E, and $_{\Delta}$Tm, increase and the tan $\delta$ values decrease with dose I.

It is likely that the increase in weight (Fig. 6.14a) was caused by the oxidizition during the period of the radiation. It is also likely that the increase in C (Fig. 6.13a) is also due to oxidation because of the formation of polar bonds. The weight increase due to oxidizition was greater than the weight loss due to radiolysis.

### 6.4.2.2 The Effect of The Hardener Concentration During The Period of The Radiation

The value of Tg usually decreases if the ratio of epoxy resin to the hardener is not in a stoichiometric mix. The surplus hardener or resin enters into the liquid phase in the two phase system where they will behave as plasticisers, thus reducing the Tg values.

It is likely that the surpluses are sensitive to radiation (196) in that radicals may be produced which can lead to further crosslinking with consequent

increases in the activation energy E.

The increase in tan $\delta$ with the amount of DDSA is probably a result of DDSA being more sensitive to oxidation and radiolysis than epoxy molecules, and is due to the properties of the aliphatic branch with a double bond in DDSA.

### 6.4.3 The Difference of The Effects of $\gamma$-Irradiation on The Two Epoxy Systems

From the study of both systems it can be seen that there are three main differences :

1. On the trapped charge.

The Tg of the sample of MY750/HY956 (108 °C) is much higher than room temperature, thus this sample is in the vitreous state at room temperature. The mobility of the epoxy molecules is at a minimum. Therefore, the irradiation produced radicals and ions can be trapped. The Tg of the sample of MY750/DDSA is close to room temperature. The motion of the epoxy molecular chains is large enough at room temperature to allow movement of the ions and radicals. Thus the irradiation-produced radicals and ions immediately react with the epoxy molecules, other radicals and ions. There are no trapped charges in the sample.

2. On the effect of annealing.

If the temperature rises close to Tg the high reactivity of the trapped radicals or ions is realized and thus produces changes in the structure and the

properties of the epoxy system (post-irradiation annealing). It is clear that there is an effect of annealing for the sample of MY750/HY956 due to the reaction of the trapped charges or radicals during the post-irradiation annealing; whereas there is no effect of annealing for the sample of MY750/DDSA.

3. On the degradation and crosslinking.

During the irradiation of polymer in the vitreous state, the crosslinking reaction is retarded and degradation occurs preferentially. If the irradiation temperature rises above Tg, the crosslinking rate increases sharply. Thus the main effect for the sample of MY750/HY956 is degradation, which leads to decreases in the Tg, resistivity, activation energy, E, and increases in the tan $\delta$ and capacitance C values. In contrast the main effect for samples of MY750/DDSA is crosslinking, which leads to increases in the Tg, the temperature position of the tan $\delta$ peaks, $\Delta$Tm, activation energy E and decreases the tan $\delta$ values with dose I.

## 6.5 Conclusion

The electrical properties, glass transition temperature, Tg, and activation energy, E, of the MY750/HY956 epoxy resin system and the MY750/DDSA epoxy system have been systematically investigated before and after irradiation, after annealing and in other situation (see table 6.2). The following conclusions have been drawn:-

(1) The conductivity, tan$\delta$ and C values of the MY750/HY956 epoxy system after irradiation increase rapidly with dose especially for doses which are greater than 1 MGy. However tan$\delta$ values of the MY750/DDSA epoxy system after irradiation usually decrease even for doses greater than 2 MGy.

(2) The Tg and the activation energy E of the MY750/HY956 epoxy system decrease after irradiation due to degradation at T < Tg, and increase again after the postradiation annealing due to crosslinking. However the Tg and the E value of the MY750/DDSA epoxy system after irradiation usually increase after irradiation or after annealing due to crosslinking at T > Tg.

(3) The radiation produce changes in the chemical structure of the epoxy system MY750/HY956. The formation of carbonyl groups from pendant (-OH) groups after irradiation.

(4) The radiation- produced ions in the liquid phase of the epoxy system have serious effect on the conductivity, tan$\delta$ and capacitance values of the irradiated MY750/HY956 epoxy system before annealing.

(5) The radiation produced macromolecular ions in the flocculeS of the epoxy system seriously effect the tan$\delta$ and capacitance values of the (A.A.) samples of the MY750/HY956 epoxy system under two conditions namely at temperature close to but lower than Tg or at low frequencies. This is due to the relaxation polarisation of the monopole.

(6) The activation energy E and the peak shift ΔTm increase if the ratio of the epoxy resin to the hardener is not in the stoichiometric mix and is probably radio-sensitive.

# CHAPTER SEVEN

# GENERAL CONCLUSION AND FURTHER WORK

## 7.1 General Conclusion

In this study, the curing of epoxy resin and the effects of gamma-irradiation on the electrical properties of epoxy resin systems (MY750/HY956 and MY750/DDSA) has been investigated.

Different methods of establishing the cured state of the epoxy resin system were carried out, including, differential scanning calorimetry (DSC), infrared spectroscopy (I.R), dielectric measurements, volume resistivity measurements and thermally stimulated discharge current (TSDC).

The effect of Gamma- irradiation on the electrical properties of the epoxy resin system was achieved by examining the electrical properties of the fully cured epoxy resin systems before and after irradiation, after annealing and in other situations and the results compared. In this investigation the following facts have been established and these conclusions have been made.

1. During the curing of the epoxy resin system the results of the dielectric measurements were interpreted on the basis of a model considering the growing polymer dipoles to be in solution, the solvent being the

unreacted monomer and hardener. Furthermore, the model proposed for the pre-cured epoxy resin bears a relationship with the concept of nodular morphology (32,91), agglomerates of colloidal particles (93), floccules in a low molecular weight interstitial fluid (90) and regions of heterogeneous crosslink density (94), applicable to cured epoxy resin. In addition, the results of dielectric relaxation measurements obtained during the curing of the epoxy resin are also explicable in terms of chemical reactions in solutions. The loss peak is associated with a dipole present on the growing polymer molecules which can rotate in the applied field and may be regarded in terms of the Debye model. It was also possible to establish an activation energy for the curing process. The value of 41 KJ/mol ( 0.42 ev) compares favourable with that obtained by others for various epoxy systems.

2. For the fully cured epoxy resin system MY750/HY956, the glass transition temperature (Tg) obtained by differential scanning calorimetry (DSC) and Thermally stimulated discharge current (TSDC) are in very good agreement (DSC) (Tg = 108°C).

The mechanisms of ionic conduction were found to be the dominant process for this system over a wide range of electric field and from room temperature to below the glass transition temperature Tg. Furthermore, an activation energy for the D.C. conductivity process was

found (0.73 ev), and the estimated ionic jumping distance was 11.8 nm. Dielectric measurement for this system were also performed from room temperature to below the glass transition temperature of the system and there are no peaks. However, the dielectric measurements for the fully cured MY750/DDSA epoxy resin system show loss peaks present over the same temperature range. An activation energy of (2.16 ev) was found for this loss process.

3. For the fully cured MY750/HY956 epoxy resin system, the D.C. conductivity, tan $\delta$ and capacitance (C) values increase rapidly with dose. These quantities were measured after irradiation.

The Tg and the activation energy E obtained from D.C. measurement, decrease after irradiation due to degradation at T < Tg, and increase again after the post radiation annealing due to crosslinking. In addition, the radiation produced ions in the liquid phase and macromolecular ions in the floccules of the epoxy system, have a serious effect on the conductivity, tan $\delta$ and capacitance values measured before annealing and also on tan $\delta$ and capacitance values after annealing. However, for the fully cured MY750/DDSA epoxy resin system, tan $\delta$ values usually decrease after irradiation. The Tg and the activation energy obtained from dielectric measurements usually increase after irradiation or after annealing due to crosslinking at

T >Tg. Furthermore, the activation energy E and the peak shift Tm increase if the ratio of the epoxy resin to the hardener is not in the stoichiometric mix.

## 7.2 Further Work

From the study of the effect of gamma irradiation on the electrical properties of the epoxy resin systems MY750/HY956 and MY750/DDSA, it was found that for a clearer picture of the subject, the following work should be undertaken.

1. The changes in the electrical, chemical and physical properties of both epoxy resin systems during irradiation should be examined.

2. Dielectric spectroscopy under very low frequency should be examined for both epoxy resin systems before and after irradiation. This , in order to get a clear picture of the morphology of the epoxy resin system and how the morphology can be related to the loss peaks which can be obtained from the TSDC measurements.

3. Thermally stimulated discharge current (TSDC) is a technique which offers an important key to the comprehension of the fundamental mechanisms for charge storage and release in dielectrics and is also considered to be a very sensitive probe of kinetic transitions and molecular relaxation processes in polar

materials. In the present work, this technique was used to examine the state of cure of the epoxy resin system MY750/HY956. Further measurement can be carried out to investigate a number of physico-chemical phenomena such as aggregation and precipitation of ionic dipoles due to annealing or quenching procedures, the effect of moisture, the effect of use different types of electrode materials, the effect of varying the thickness of the insulation and how all these phenomena can be affected after applying gamma-irradiation on both epoxy resin system MY750/HY956 and MY750/DDSA.

4. Surface resistivity should be examined for both epoxy resin systems before and after irradiation. Since surfaces are a dominant factor which can control insulator integrity.

5. The D.C. conductivity measurements of the epoxy resin system MY750/DDSA should be investigated and extended to higher electric fields ( E > 10 Mv/m) for the epoxy resin system MY750/HY956 before and after irradiation.

# APPENDICES

## Appendix (3.1)

The molecular weight for the epoxy resin compound MY750 were deduced from the micro analysis method and from the chemical formula given in (38) respectively as shown below.

From the micro analysis method, the relative proportions of the constituent elements of the epoxy resin MY750 were (see table 3.1):-

Cl = 0.92

C = 73.04

H = 6.52

O = 19.52

By removing the relative proportion of the chlorine element from the epoxy resin compound since it represent the impurty in the compound, and divide every element with its own atomic weight as shown below

C = 73.04 / 12 = 6.08

H = 6.52 / 1 = 6.52

O = 19.52 / 16 = 1.22

Then each value obtained from each element is multiplied by (4) and then multiplied again by its own atomic weight

C = 6.08 x 4 = 24.32 = 24 x 12 = 288

H = 6.52 x 4 = 26.08 = 26 x 1 = 26

O = 1.22 x 4 = 4.88 = 5 x 16 = 80

The molecular weight of the epoxy resin MY750 compound is then equal to

$288 + 26 + 80 = 394\ g\ mol^{-1}$

From the chemical formula given in (38) (see Fig. 3.2a), it can be seen that the number of elements out side the square brackets are shown below

C = 21

H = 24

O = 4

each element is then multiply with its own atomic weight and the result which is obtained from each element is add together

C = 21 x 12 = 252

H = 24 x 1 = 24

O = 4 x 16 = 64

252 + 24 + 64 = 340

By repeating the same procedure above for the elements inside the square brackets

C = 18 x 12 = 216

H = 20 x 1 = 20

O = 3 x 16 = 48

216 + 48 + 20 = 284

The portion of the molecule in square brackets is a repeating unit, and a typical value of (n) for this resin is 0.2. Therefore

$284 \times 0.2 = 56.8$

The molecular weight for the epoxy resin is then equal to

$340 + 56.8 = 396.8 = 397\ g\ mol^{-1}$

In the case of the hardener HY956 compound, the molecular weight were deduced from the micro analysis method as shown below

The relative proportions of the constituent element of the hardener HY956 were (see table 3.1):-

N = 26.65

C = 53.64

H = 11.53

O = 8.18

each value of each element is then divided by its own atomic weight

N = 26.65 / 14 = 1.9

C = 53.64 / 12 = 4.47

H = 11.53 / 1 = 11.53

O = 8.18 / 16 = 0.51

Then each value obtained from each element is multiplied by (2) and then multiplied again by its own atomic weight

N = 1.9 x 2 = 3.8 = 4 x 14 = 56

C = 4.47 x 2 = 8.94 = 9 x 12 = 108

H = 11.53 x 2 = 23.06 = 24 x 1 = 24

O = 0.51 x 2 = 1.02 = 1 x 16 = 16

The molecular weight of the hardener HY956 compound is then equal to

56 + 108 + 24 + 16 = 204 g $mol^{-1}$

## Appendix (5.1)

## General Radio Bridge (Type 716-C)

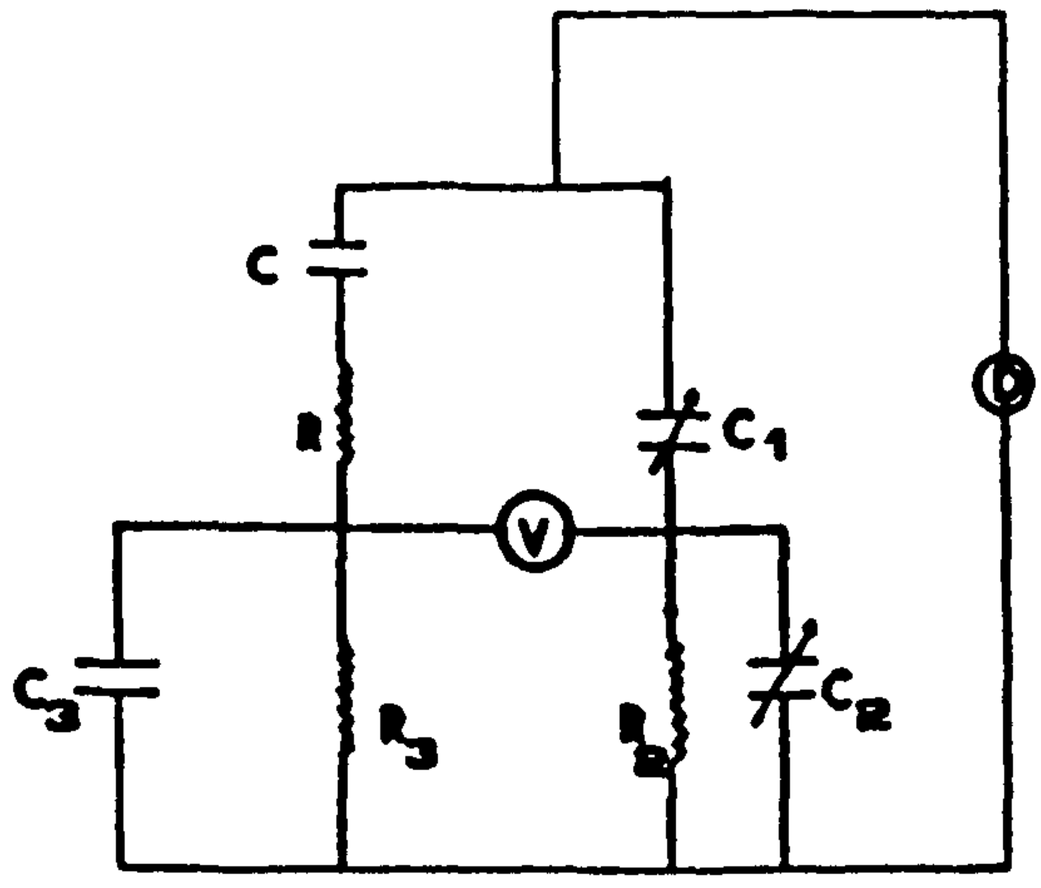


The above circuit is a modified Schering bridge. Balance occurs by varying $C_1$ and $C_2$ (where $C_1$ gives the capacitance reading, $C_2$ the Tan$\delta$ reading.

From the circuit above, balance occurs when

$$\frac{R + 1/JWC}{1/JWC_1} = \frac{R_3}{1 + JWC_2R_2} \cdot \frac{1 + JWC_2R_2}{R_2}$$

$$JWC_1R + \frac{C_1}{C} = \frac{R_3}{R_2} \cdot \frac{1 + JWC_2R_2}{1 + JWC_3R_3}$$

$$JWC_1R + \frac{C_1}{C} = \frac{R_3}{R_2} \cdot \frac{(1 + JWC_2R_2)(1 - JWC_3R_3)}{1 + W^2C_3{}^2R_3{}^2}$$

$$= \frac{R_3}{R_2} \cdot \frac{(1 + W^2C_2R_2C_3R_3) + J(WC_2R_2 - C_3R_3)}{1 + W^2C_3{}^2R_3{}^2}$$

Equating real parts gives

$$C = C_1 \cdot \frac{R_2}{R_3} \cdot \frac{1 + W^2C_3{}^2R_3{}^2}{1 + W^2C_2R_2C_3R_3} \qquad (1)$$

Equating imaginary parts gives

$$R = \frac{1}{C_1} \cdot \frac{R_3}{R_2} \cdot \frac{C_2R_2 - C_3R_3}{1 + WC_3{}^2R_3{}^2} \qquad (2)$$

$$\text{Tan}\,\delta = W\,C\,R$$

$$\text{Tan}\,\delta = \frac{W\,(\,C_2R_2 - C_3R_3\,)}{1 + W^2C_2R_2C_3R_3} \qquad (3)$$

Numerical values (given on data sheet (198))

| | | | | | | | |
|---|---|---|---|---|---|---|---|
| M | 1 | 10 | 100 | 1000 | 1 | 1 | 1 . |
| $f_o$ | 1kHz | 1kHz | 1kHz | 1kHz | 100Hz | 10kHz | 100kHz |
| $R_2$ | 20k | 20k | 20k | 20k | 200k | 2k | 200 |
| $R_3$ | 20k | 2k | 200 | 20 | 200k | 2k | 200 |

From the data sheet, it was noted that

$M = R_2/R_3$ and $R_2.f_o = 2 \times 10^7\ \Omega\text{Hz}$ = constant. (4)

Consider the bridge at balance with an ideal capacitor as unknown, so that Tan $\delta = 0$, and equation (3) gives

$C_2R_2 = C_3R_3$ (for Tan $\delta = 0$).

Equation (1) then becomes $C = C_1.(R_2/R_3)$, ie.

$C = C_1 . M,$

and this indicates that the capacitance reading is the value of $C_1$.

Now, if Tan $\delta \neq 0$ then $C_2R_2 \neq C_3R_3$ at balance, and

$C = C_1.M$

only if $W^2C_3{}^2R_3{}^2 << 1$ (5)

and $W^2C_2R_2C_3R_3 << 1$.

The Tan $\delta$ reading.

The bridge gives accurate readings when

$W^2C_3{}^2R_3{}^2 << 1$

and, $W^2C_2R_2C_3R_3 << 1$, (5a)

from equation (5).

From equation (3), and when equation (5a) holds, then

Tan $\delta = W\,(C_2R_2 - C_3R_3)$.

For $\tan\delta = 0$, $C_2R_2 = C_3R_3$ (whether equation (5a) holds or not.)

ie $C_2 = (R_3/R_2).C_3 = C_3/M$.

When the bridge is balanced with $\tan\delta = 0$, $C_2$ is adjusted to a 'base value' $C_{o\,2} = (C_3/M)$.

When the bridge is balanced with $\tan\delta \neq 0$, $C_2$ is increased by an amount $DC_2 = C_2 - C_{o\,2}$

$= C_2 - (C_3/M)$.

In equation (3), the term $(C_2R_2 - C_3R_3)$ can be written as $R_2(C_2 - C_3(R_3/R_2))$

$=R_2(C_{o\,2} + DC_2 - C_{o\,2})$

$=R_2\,DC_2$

so equation (3) becomes

$$\tan\delta = \frac{W\,R_2\,DC_2}{1 + W^2C_2R_2C_3R_3} \qquad (3a)$$

Presumably the bridge is calibrated for

$W^2C_2R_2C_3R_3 \ll 1$

so that the indicated $\tan\delta$ is

$\tan\delta_1 = WR_2DC_2$

combining this with equation (3a) gives

$$(\tan\delta_1 \,/\, \tan\delta) = 1 + W^2C_2R_2C_3R_3 \qquad (6)$$

Also, $\tan\delta_1 = WR_2DC_2 = 0.01 \times (W/W_o) \times \tan\delta_r$

where $\tan\delta_r$ is the '$\tan\delta$' reading.

$\tan\delta_r = WR_2DC_2 \times 100 \times (W_o/W)$

$= 100\,(R_2\,W_o)\,DC_2$

$= 100 \times 4\pi \times 10^7\,DC_2$

$= 4\pi \times 10^9\,DC_2$

$$DC_2 = \frac{\tan\delta_r}{4\pi \times 10^9}\,F$$

Maximum Tan $\delta_r$ = 55

$$\text{Maximum } DC_2 = \frac{55}{4\pi \times 10^9} F$$

$$= \frac{55 \times 10^{12}}{4\pi \times 10^9} pF$$

$$= \frac{55}{4\pi} \times 10^3 \text{ pF}$$

$$= 4376.7609 \text{ pF.}$$

The maximum $DC_2$ is reached in 11 equal steps, so each

step = $(55/44\pi) \times 10^3$ pF

=397.88736 pF.

## Computation of correction factors

For the values of the bridge components, we have :

$$R_2 = \frac{2 \times 10^7}{f_o}$$ ( where $f_o$ in Hz and $R_2$ in ohm)

and $R_3 = R_2/M$.

If M = 1, $C_3$ = 180 pF

M = 10, $C_3$ = 2064 pF

M = 100, $C_3$ = 20693 pF

M = 1000, $C_3$ = 200,000 pF

as an approximation, let us take $C_3 = M \times 200 \times 10^{-12}$ F

$$C_2 = \frac{C_3}{M} + DC_2 = \frac{C_3}{M} + \frac{\text{Tan } \delta_r}{100 R_2 W_o}$$

$$\text{ie } C_2 = 200 \times 10^{-12} + \frac{\text{Tan } \delta_r}{4\pi \times 10^9} F$$

$$\text{From equation (6), } \frac{\text{Tan } \delta_1}{\text{Tan } \delta} = 1 + W^2 C_2 R_3 C_3 R_3$$

$$= 1 + W^2 \left(\frac{C_a}{M} + \frac{\text{Tan}\,\delta_r}{4\pi \times 10^9}\right) \times \left(\frac{4\pi \times 10^7}{W_o} \cdot C_a \cdot \frac{4\pi \times 10^7}{M\,W_o}\right)$$

$$= 1 + \left(\frac{W}{W_o}\right)^2 \times \frac{C_a}{M} \times \left(\frac{C_a}{M} + \frac{\text{Tan}\,\delta_r}{4\pi \times 10^9}\right) \times (16\pi^2 \times 10^{14}) \qquad \text{------- (7)}$$

Substituting the approximate value for $C_a$,

$$\frac{\text{Tan}\,\delta_i}{\text{Tan}\,\delta} = 1 + \left(\frac{f}{f_o}\right)^2 \left[\, 200\times10^{-12}\left(200\times10^{-12} + \frac{\text{Tan}\,\delta_r}{4\pi \times 10^9}\right) (16\pi^2 \times 10^{14})\right]$$

$$= 1 + \left(\frac{f}{f_o}\right)^2 \left[\, 3200\pi^2 \times 10^2 \frac{1}{4\pi \times 10^9} \left(\text{Tan}\,\delta_r + 800\pi \times 10^{-9}\right)\right]$$

$$= 1 + \left(\frac{f}{f_o}\right)^2 \left[\, 8\pi \times 10^{-8} \left(\text{Tan}\,\delta_r + 0.8\pi\right)\right]$$

$$= 1 + \left(\frac{f}{f_o}\right)^2 \left[\, 2.5 \times 10^{-4} \left(\text{Tan}\,\delta_r + 2.5\right)\right]$$

The correction formula for Tan $\delta$ is

$$\frac{\text{Tan}\,\delta}{\text{Tan}\,\delta_i} = \frac{1}{1 + \left(\frac{f}{f_o}\right)^2 \left[\, 2.5 \times 10^{-4} \left(\text{Tan}\,\delta_r + 2.5\right)\right]}$$

with $f = f_o$ and $M = 1$, the maximum Tan $\delta_r$ is 55, giving

$$\frac{\text{Tan}\,\delta}{\text{Tan}\,\delta_i} = \frac{1}{1 + 2.5 \times 10^{-4}\,(57.5)}$$

$$= \frac{1}{1.014}$$

giving a correction of 1.4 % .

The correction becomes :

larger for $f > f_o$

smaller for $f < f_o$

From equation (1),

$$C = C_i \cdot \frac{R_2}{R_3} \cdot \frac{1 + W^2 C_3^2 R_3^2}{1 + W^2 C_2 R_2 C_3 R_3}$$

$$\text{ie} \quad \frac{C}{C_i} = \frac{1 + W^2 C_3^2 R_3^2}{1 + W^2 C_2 R_2 C_3 R_3} \qquad (8)$$

where $C_i = M C_i$ is the indicated capacitance.

The denominator $1 + W^2 C_2 R_2 C_3 R_3$ is as in equ.(7).

For the numerator, we have

$$1 + W^2 C_3^2 R_3^2 = 1 + W^2 C_3^2 \cdot \frac{(4\pi \times 10^{-7})^2}{W_o^2 M^2}$$

$$= 1 + \left(\frac{f}{f_o}\right)^2 \frac{C_3^2}{M^2} (4\pi \times 10^{-7})^2$$

Substituting the approximate value for $C_3$,

$$1 + \left(\frac{f}{f_o}\right)^2 \frac{C_3^2}{M^2} (4\pi \times 10^{-7})^2$$

$$= 1 + \left(\frac{f}{f_o}\right)^2 (200 \times 10^{-12} \times 4\pi \times 10^{-7})^2$$

$$= 1 + \left(\frac{f}{f_o}\right)^2 (0.64\,\pi^2 \times 10^{-4})$$

$$= 1 + \left(\frac{f}{f_o}\right)^2 (6.4 \times 10^{-4})$$

and eqn (8) becomes (the correction for capacitance)

$$\frac{C}{C_i} = \frac{1 + \left(\frac{f}{f_o}\right)^2 (6.4 \times 10^{-4})}{1 + \left(\frac{f}{f_o}\right)^2 [2.5 \times 10^{-4} (\text{Tan } \delta_v + 2.5)]}$$

with $f = f_o$, $M = 1$ and $\text{Tan}\,\delta_r = 55$,

$$\frac{C}{C_t} = \frac{1.00044}{1.014}$$

again giving a correction of = 1.4 % .

To a fair approximation, the correction for capacitance will be the same as the correction for Tan $\delta$ .

Both capacitance and Tan $\delta$ will be lower than the indicated values, and the error will disappear in both cases for $\text{Tan}\,\delta_r = 0$.

In the analysis above the capacitance value is the series value, because the sample is taken as

Conversion from series R-C to parallel R-C

$$\text{Let } \frac{1}{W C_s} = X_s \; ; \quad \frac{1}{W C_p} = X_p$$

Equivalence requires

$$R_s - J X_s = \frac{R_p\,(-J X_p)}{R_p - J X_p}$$

$$\frac{R_p - J X_p}{-J R_p X_p} = \frac{1}{R_s - J X_s}$$

$$\frac{1}{R_p} + J \frac{1}{X_p} = \frac{R_s + J X_s}{R_s^2 + X_s^2}$$

$$R_p = \frac{R_s^2 + X_s^2}{R_s}$$

$$X_p = \frac{R_s^2 + X_s^2}{X_s}$$

It should be noted that

1- If the impedance is alomst purely capacitive, then

$X_s >> R_s$ and

$$R_p = \frac{X_s^2}{R_s} \quad \text{and} \quad X_p = X_s$$

If the impedance is almost purely resistive, then

$$R_p = R_s \quad \text{and} \quad X_p = \frac{R_s^2}{X_s}$$

2- $$\text{Tan}\,\delta = \frac{1}{W\,C_p\,R_p}$$

$$= \frac{X_p}{R_p} = \frac{R_s^2 + X_s^2}{X_s} \cdot \frac{R_s}{R_s^2 + X_s^2}$$

$$= \frac{R_s}{X_s}$$

$$= W\,C_s\,R_s$$

# Appendix (5.2)

A-

$V_{sr} = 8\ e\ n_o\ S^2 / 9\ K$

where $K = \epsilon \epsilon_r = 5 \times 8.85 \times 10^{-12}$

$e$ (electron charge) $= 1.6 \times 10^{-9}$ c

S(thickness)$= 8 \times 10^{-5}$ m  $V_{sr}$(transition voltage)$= 300$v

$$n_o = \frac{V_{sr}\ 9\ K}{8\ e\ S^2} = \frac{300 \times 9 \times 5 \times 8.85 \times 10^{-12}}{8 \times 1.6 \times 10^{-19} \times 6.4 \times 10^{-9}}$$

$n_o = 1.458 \times 10^{19}$ $1/m^3$

$n_o = 1.458 \times 10^{12}$ for $\theta = 10^{-7}$

$J = 8.27 \times 10^{-8}$

$J = e\ n_o\ \mu\ (\ V_{sr} / S\ )$

$$\mu = \frac{S\ J}{e\ n_o\ V_{sr}} = \frac{8.27 \times 10^{-8} \times 8 \times 10^{-5}}{1.6 \times 10^{-19} \times 1.458 \times 10^{19} \times 300}$$

$$= 9.445 \times 10^{-15}$$

$$T_{sr} = \frac{S^2}{\mu\ V_{sr}} = \frac{6.4 \times 10^{-9}}{2.83 \times 10^{-12}} = 2258.69 \text{ sec}$$

$T_{sr}$ (carrier transit time between electrodes at $V_{sr}$)

$$= K / e\ n_o\ \mu = \frac{4.425 \times 10^{-11}}{1.6 \times 10^{-19} \times 1.458 \times 10^{19} \times 9.44 \times 10^{-15}}$$

$= 2011.363$ sec

where $\tau$ ( dielectric relaxation time).

B-

Density of the mixture $= 967500 \times 4/5 \times 0.92/100$

$= 967500 \times 0.8 \times 0.0092$

$= 7120.8$ g/m$^3$

$$N = \frac{7120.8 \times 6.02 \times 10^{23}}{35.5}$$

$N = 1.20 \times 10^{26}$ number of molecules of Cl of impurties per 1 volume cubic.

# REFERENCES

## References


1. Dakin,T.W.; IEEE Transactions on Electrical Insulation, Vol. EI - 9, No. 4, pp 121 - 128, December (1974).

2. May, C.A. and Tanaka, Y. (Ed.); 'Epoxy Resins: Chemistry and Technology'. Marcel Dekker, N.Y. (1973).

3. Makhils, F.A.; 'Radiation Physics and Chemistry of Polymers'(Translated from Russian), Halsted Press, (1975).

4. Dominighaus, H.; Br. Plast., Vol. 38, part 11, pp. 676, Nov. (1965).

5. Puig, J.R. ; Bull. Inform. Scient et Techn. Commissariat Energie Atom., No. 98, pp. 53, (1965). (in French)

6. Nuclear Sci. Abstr., Vol. 18, No. 3, pp. 563, (1964).

7. Weinberger, J.V.; US Patent KL. 25 - 180, No. 3239669. Application in 25 Nov. 1960. Issued 8 March (1966).

8. Bliss, J.F. et al; US Patent KL. 252 - 478, No. 3247131. Application in 1963. Issued 19 April, (1966).

9. Elbel, K.; Chimie 19, No. 6, pp. 367-381, (1965). (in German)

10. Nuclear News, Vol. 9, No. 8, pp. 48, (1966).

11. Delmonte, J. ; Proc. 20th Anniversary Techn. Conf. SPI. Reinforced Plast. Div. Chicago, 1965. New York Soc. Plast. Ind., Soc. 6D, pp. 1-4, (1965).

12. It.Kava Vatasu.; Japanese Patent. KL. 25 Do. No. 10919. Application in 6 August 1960, Issued 13 August 1962. Referat Zh. "Khimiya" Vol. 22, 5525p, (1965). (in Japanese)

13. Mauri, R.E.; J. Envir. Sci. Y., Vol. 7, No. 4, pp. 18-24, (1964).

14. Siew, W.H., Banford, H.M. and Tedford, D.J.; 4th Int. Conf., 'dielectric materials measurements applications', pp. 38, Lancaster (1984).

15. Banford, H.M., Frame, R.I., Stew, W.H. and Tedford D.J.; Conf. 'Radiation effects in

insulators 3', pp. 69, Guild Ford 15-19 Jul (1985).

16. Banford, H.M.; Advance in Nuclear Science and Technology. Vol. 16, J. Lewins and Becker, M. (Ed.), Plenum Press, New York (1984).

17. Osawa, Z., Nakano, H., and Mitsui, E.; J. Polym. Sci., Vol. 17, pp. 139-145, (1979).

18. Blackburn, R., and Charlesby, A.; Nature, Lond., Vol. 210, pp. 1036, (1966).

19. Bovey, F.A.; Effects of Ionizing Radiation on Natural and Synthetic High Polymers. Interscience, New York, (1958).

20. Barnay, S.G.; Radiation - Induced Changes in the Structure on Epoxy Resin, Radiat. Phys. Chem., Vol. 16, pp. 389 - 397, (1980).

21. Burnay, S.G.; Radiation - Induced Structure Changes in an Epoxide Resin System - 2, Radiat. Phys. Chem., Vol. 19, No. 2, pp. 93-99 (1982).

22. Carothers, W.H.; Chem. Rev., Vol. 8, pp. 353-359, (1931).

23. Blythe, A.R.; 'Electrical Properties of Polymers', Elec. Prop. of Polym., Cambridge University Press, Cambridge (1979).

24. Shechter, L. and Wynstra, J.; Ind. Engng. Chem., Vol. 48, pp. 86-97, (1956).

25. Smith, I.T.; Polymer, Vol. 2, pp. 95-108, (1961).

26. Parker, R.E. and Isaacs, N.S.; Chem. Rev., Vol. 59, pp. 737-799, (1959).

27. Chapman, N.B., Parker, R.E. and Isaacs, N.S.; J. Chem. Soc., Vol. 2, pp. 1925-1934, (1959).

28. Potter, W.G.; 'Epoxide Resins,' I. Liffe Books, London (1970).

29. Lee, H.N.;'Epoxy Resins, their Applications and Technology', (1957).

30. Newey, H.A.; Gordon Research Conf on Polymers, New London, U.S.A. (1955),

31. Racich, J.L. and Koutsky, J.A.; J. Appl. Polym. Sci., Vol. 20, pp. 2111-2129, (1976).

32. Mijovic, J. and Tsay, L.; 'Correlations between

Dynamic Mechanical Properties and Nodular Morphology of Cured Epoxy Resin', Polymer, Vol. 22,2, pp. 902-906, (1981).

33. Mijovic, J. and Koutsky, J.A.;'Correlation between Nodular Morphology and Fracture Properties of Cured Epoxy Resins, Polymer, Vol. 20,2, pp. 1095-1107, (1979).

34. Morgan, R.J. and O'Neall, J.E.; J. Macromol. Sci. Phys., Vol. B15, pp. 139-169, (1978).

35. Morgan, R.J. and O'Neall, J.E.; 'Chemistry and Properties of cross Linked Polymers'. S.S. Labana (Ed.), pp. 285. Acad. Press NY. (1977).

36. Cuthrell, R.E.; J. Appl. Polym. Sci., Vol. 11, pp. 949-952, (1967).

37. Lemon, P.H.R.B.; Br. Plast., Vol. 36, No. 6, pp. 336, June (1963).

38. Crowson, R.J. and Arridge, R.G.C.; Polymer, Vol. 20,1, pp. 747-754, (1979).

39. Smallman, R.E. and Ashbee, K.H.G.;'Modern Metallography', Pergamon Press, 1st ed., (1966).

40. Kerr, P.F.; 'Optical Mineralogy'. Press. McGraw-Hill, 3rd ed., (1959).

41. Sanjana, Z.N. and Selby, R.L.; 'The use of Dielectric Analysis to Study the Cure of a filled Epoxy Resin', IEEE Vol. EI - 16, pp. 496-501 (1981).

42. Gordon, M.;' High Polymers Structure and Physical Properties', published for the Plastics Institute by I. Liffe, 2nd ed., London (1963).

43. Fava, R.A.; Polymer, Vol. 9, No 3., pp. 137-176, (1968).

44. Gedeon, S., Ren. P. Fouracure, R.A., Frame, R.I. and Banford, H.M.; Gamma Irradiation Effects in an Epoxy Resin, 2nd International Conference on Conduction and Breakdown in Solid Dielectrics, West Germany, July 7 - 10 (1986).

45. Horie, K., Sawada, M., Mita, I. and Kambe, H.; J. Polym. Sci., Part A1, Vol. 8, pp. 1357-1372, (1970).

46. Barton, J.M.; Adv. in Polym. Sci., Vol. 72, Dusek, J. (Ed). Springer- Verlag, pp. 111-154, (1985).

47. Block. H.; Adv. in Polym. Sci., Vol. 33, Springer-Verlag, pp. 93-167, (1979).

48. Nan derschueren, J. and Gasiot, J.; 'Field-induced thermally stimulated Currents', in Braunlich, P. (Ed.) 'Thermally stimulated Relaxation in Solids, Topics in Applied Physics, Vol. 37, Springer -Verlag Berlin, Heidelberg, New York (1979).

49. Seanor, D.J.; 'Electrical Properties of Polymers', Academic Press (1982).

50. Pearlmann, M.M.; J. Appl. Phys., Vol. 42, pp. 531-533, pp. 2645-2652, (1971).

51. Van Turnhout, J.; Polymer J., Vol. 2, No. 2, pp. 173-191, (1971).

52. Takamatsu and Fukuda, E.; Polymer J., Vol. 1, pp. 101-106, (1970).

53. Van Turnhout, J.; 'Thermally Stimulated Discharge of Polymer Electrets'. Elsemer, Amsterdam (1975).

54. Grossweiner, L.I.; J. Appl. Phys., Vol. 24, pp. 1306-1307, (1953).

55. Bube, R.H.; J. Appl. Phys., Vol. 37, pp. 21-31;

(1966).

56. Bucci, C., Fieschi, R and Guidi, G.; Phys. Rev., Vol. 148, pp. 816-823, (1966).

57. Bucci, C and Fieschi, R.; Phys. Rev. Lett., Vol. 12, pp. 16-19, (1964).

58. Su, W.F.A., Carr, S.H. and Brittain, J.O.; J. Appl. Polym. Sci., Vol. 25, pp. 1355-1363, (1980).

59. Tanaka, T., Hayahi, S. and Shibayama, K.; J. Appl. Phys., Vol. 48, pp. 3478-3483, (1977).

60. Takahama, T., Hayashi. O and Sato, F.; Prog in Polym Phys. (Japan), Vol. 22, pp. 407, (1979).

61. Miyamoto, T and Sugano. T.; Polym. J., Vol. 6, pp. 451, (1974).

62. Mertzel, E and Koenig, J.L.; Adv in Polym. Sci., Vol. 75, pp. 73-112, (1985).

63. Thompson, H.W.; Proc. Roy. Soc., Vol. A184, pp. 21, (1945).

64. Dannenberg, H and Harp Jnr., W.R.; Analyt. Chem., Vol. 28, pp. 86-90, (1956).

65. Dannenberg, H.; S.P.E. Trans., Vol. 3, pp. 78-88, (1963).

66. Feltzin, J., Longenecker, D.M., Petker, I.; S.P.E. Trans., pp. 111-116, April, (1965).

67. Bromberg, M.L. Day, D.R. and Snable K.R.; 'Measurement and Application of Dielectric Properties'. IEEE Electrical Insulation Magazine, Vol. 2, pp. 18-23, (1986).

68. Sheppard, N.F., Coln, M and Senturia, S.; 'A Dielectric Study of the Time-Temperature Transformation (TTT) Diagram of DGEBA Epoxy Resins Cured with DDS', Proc 29th SAMPE Symposium, Reno, NV, pp. 1243-1250, (1984).

69. Delmonte, J.; J. Appl. Polym. Sci., Vol. 2, pp. 108-113, (1959).

70. Sanjana, Z.N. and Selby, R.L.; IEEE Vol. EI - 16, pp. 496-501, (1981).

71. Olyphant, M.; Proc of the 6th Elec. Insulation Conf. Supplement, Oct. (1985).

72. Adamec, V.; J. Polym. Sci., Part A1, Vol. 10,

pp. 1277-1295, (1972).

73. Haran, E.N., Gringras, H. and Katz., D.; J. Appl. Polym. Sci., Vol. 9, pp. 3505-3518, (1965).

74. Solomon, D.H., Loft, B.C. and Swift, J.D.; J. Appl. Polym. Sci., Vol. II, pp. 1593-1602, (1967).

75. Cowie, J.M.G.; Polymers: Chemistry and Physics of Modern Materials, Intertext Book (1973).

76. Babayevsky, P.G. and Gillham, J.K.; J. Appl. Polym. Sci., Vol. 17, pp. 2067-2088, (1973).

77. Senturia, S.D. and Sheppard, N.F.; Adv. in Polym. Sci., Vol. 80, Springer-Verlag, pp. 3-47, (1986).

78. Warfield, R.W. and Petree, M.C.; J. Polym. Sci., Vol. 37, pp. 305-308, (1959).

79. Fava, R.A. and Horsfield, A.E.; Brit. J. Appl. Phys. (J. Phys.D.), Vol. 1, pp. 117-120, (1968).

80. Kienle, R.H. and Race, H.H.; The Electrical, Chemical and Physical Properties of Alkyd Resins. Trans. Electrochem-Soc., Vol. 65, pp. 87-107, (1934).

81. Lee, H. and Neville, K.;' Handbook of Epoxy Resins.', New York, McGraw-Hill (1967).

82. Wright, W.W.; Brit. Polym. J., Vol. 15, pp. 224, (1983).

83. Aukward, J.A., Warfield, R.W. and Petree, M.C.T.; J. Polym. Sci., Vol. 27, pp. 199-205, (1958).

84. Fineman, M. and Puddington, I.R.; Ind. Eng. Chem., Vol. 39, pp. 1288, (1947).

85. Warfield, R.W. and Petree, M.C.; S.P.E. Trans., Vol. 1, pp. 3-8, (1961).

86. Lee, J.D. and Levy, P.F.; North American Thermal Anal. Soc. Proc., 11th Conf. (1981).

87. Miller, R.G.J. and Stace, B.C.; 'Laboratory Methods in Infrared Spectroscopy', 2nd ed.,Heyden and Son Ltd., (1972).

88. Fuoss, R.M., in Burk, R.E. and Gummitt, O.; The Chemistry of Large Molecules, Interscience, pp. 192-193, New York (1943).

89. Houwink, R.; Technology of Synthetic Polymers,

pp. 52, Elsevier, New York, (1947).

90. Cuthrell, R.E.;'Epoxy Polymers II,Macrostructure', J. Appl. Polym. Sci., Vol. 12, pp. 1263-1278, (1968).

91. Raach, J.L. and Koutsky, J.A.; 'Boundary Layers in Thermosets', Chemistry and Properties of Crosslinked Polymers, ACS. Symposium on Chemistry and Properties of Crosslinked Polymers, San Francisco (1976).

92. Racich, J.L. and Kontsky, J.A.; pp. 303 in ref 35.

93. Erath, E.H. and Robinson, M.; 'Colloidal Particles in the Thermosatting Resins', J. Polym. Sci., Part C, No. 3, pp. 65-76, (1963).

94. Morgan, R.J. and O'Neall, J.E.; 'A review of the Relation between the Physical Structure and Mechanical Response of Epoxies', ACS Symposium on Chemistry and Properties of Crosslinked Polymers, San Francisco (1976).

95. Rembaum, A.; in: Encyclopaedia of Polymer Science and Technology, Vol. 11 ed., Bikales, N.M. and Courad, J., eds., pp. 318, New York: London-Sidney- Toronto: Interscience (1969).

96. Mann, H.T.;'Electrical properties of thin polymer films.', J. Appl. Phys., Vol. 35, pp. 2173, (1964).

97. Goodings, E.P.; Chem. Soc. Rev., Vol. 5, pp. 95, (1976).

98. LE Blanc, O.H.;'Band structure and transport of holes and electrons in anthracene.', J. Chem. Phys., Vol. 35, pp. 1275, (1961).

99. Mott, N.F. and Gurney, R.W.;'Electronic Processes in Ionic Crystals', O.U.P., New York, (1940).

100. Lampert, M.A.; Phys. Rev., Vol. 103, pp. 1648-1656, (1956).

101. Lamb, D.R.; 'Electrical Conduction Mechanisms in thin Insulating Films', Methuen and Co. Ltd. (1967).

102. Mead, C.A.; J. Appl. Phys., Vol. 32, pp. 646, (1961).

103. Pollack, S.R.; J. Appl. Phys., Vol. 34, pp. 877, (1963).

104. Frenkel, J.; Phys. Rev., Vol. 54, pp. 647-648, (1938).

105. Meas, C.A.; Phys. Rev., Vol. 128, pp. 2088-2093, (1962).

106. Abrahams, E. and Miller, A.; Phys. Rev., Vol. 120, pp. 745-755, (1960).

107. Mycielski, J.; Phys. Rev., Vol. 123, 1, pp. 99, (1961).

108. Frenkel, J.; Z. Physik, Vol. 35, pp. 652, (1926).

109. Wagner, C.Z. and Schottky, W.; Physik. Chem., Vol. B.11, pp. 163-210, (1930). (in German)

110. Wagner, C.Z.; Physik. Chem., Vol. B.22, pp. 181-194, (1933). (in German)

111. Mott, N.F. and Gurney, R.W.; 'Electronic Processes in Ionic Crystals', Oxford University Press, (1948).

112. Cherry, B.W. and Wright, P.H.; 'The Electrical Resistance of Epoxy Resins', A.T.R., Vol. 7, No. 1, (1973).

113. Kosaki, M., Sugiyama, K. and Leda, M.; J. Appl. Phys., Vol. 42, pp. 3388-3392, (1971).

114. Maurer, R.J., J. Chem. Phys.; Vol. 9, pp. 579-584, (1941).

115. Read, R.E.C. and Stow, C,D.; J. Phys. D, Vol. 2, pp. 567-576, (1969).

116. Adamec, V.; Proc. Inst. Elec. Engrs. (London) , Vol. 116, pp. 1119, (1969).

117. Smith, F.S. and Scott, C.; Brit. J. Appl. Phys., Vol. 17, pp. 1149-1154, (1966).

118. Seanor, D.A.; Adv. in Polym. sci., Vol. 4, pp. 317-352, (1965).

119. Saito, S., Sasabe, H., Nakajima, T., and Yada, K.; J. Polym. Sci. A2, Vol. 6, pp. 1297-1315, (1968).

120. Miyamoto, T. and Shibayama, K.; J. Appl. Phys., Vol. 44, pp. 5372-5376, (1973).

121. Sazhin, B.I. and Podesenova N.G.; Sov Phys. - Solid State, Vol. 6, pp. 1755-1757, (1965).

122 Seanor, D.A.; J. Polym. Sci., part C, Polymer

Symposia, No. 17. Elect. Conduction Polymers (Interscience), pp. 195-212, (1967).

123. Kepler, R.G.; Phys. Rev., Vol. 119, pp. 1226-1229, (1960).

124. Hoestery, D.C. and Letson, G.M.; J. Phys. Chem. Solids, Vol. 24, pp. 1609, (1963).

125. Morin, F.J.; Phys. Rev., Vol. 93, pp. 1195-1199, (1954).

126. Baker, W.O., and Yager, W.A.; J. Am. Chem. Soc., Vol. 64, pp. 2171, (1942).

127. Foss, A., and Dannhauser, W.; J. Appl. Polym. Sci., Vol. 7, pp. 1015-1022, (1963).

128. Fowler, J.F., and Farmer, F.T.; Nature, Vol. 174, pp. 800, (1954).

129. Amborski, L.E.; J. Polym. Sci., Vol. 62, pp. 331-346, (1962).

130. Warfield, R.W. and Petree, M.C.; Makromol Chem., Vol. 58, pp. 139, (1962).

131. Fuoss, R.M.; J. Am. Chem. Soc., Vol. 61, pp. 2329,

(1939).

132. Warfield, R.W. and Petree, M.C.; S.P.E. Trans, Vol. 1, part 2, pp. 80-85, (1961).

133. Eley D.D. and Spiney D.I.; trans. Far. Soc., Vol. 57, pp. 2280, (1961).

134. Morrison, D.T.; 'Electrical Conduction in Polyethylene', PhD. Thesis, Strathclyde University, Glasgow (1970).

135. Mark, P. and Helfrich, W.; J. Appl. Phys., Vol. 33, pp. 205-215, (1962).

136. Adolph, J. Baldinger, W., Czaja, W. and Granacher, I.; phys. Letters, Vol. 6, pp. 137-139, (1963).

137. Murphy, E.J.; Canad. J. Phys., Vol. 41, pp. 1022-1035, (1963).

138. Seanor, D.A.; Conf. on Elect. Insul. and Diel. Phenomena, Washington, (1967).

139. Inuishi, Y. and Powers, D.A.; J. Appl. Phys., Vol. 28, pp. 1017-1022, (1957).

140. Lawson W.G.; Brit. J. Appl. Phys., Vol. 16,

pp. 1805, (1965).

141. Maxwell, J.C.; 'Treatise on Electricity', Oxford Univ. Press, London. (1881).

142. Debye, P.; 'Polar Molecules'. Chemical Catalog Co., Reprinted by Dover Publications, (1929).

143. Maxwell, J.C.;'Electricity and Magnetism', Oxford University Press, pp. 452, (1892).

144. Wagner, K.W.; Arch. Elektrotechn., Vol. 2, pp. 371, (1914). (in German)

145. Sillars, R.W.; J. Instn. Electr. Engrs., Vol. 80, pp. 378, (1937).

146. Hill, N.E., Vaughn, W.E., Price, A.H. and Davies, M. (Ed).; 'Dielectric Properties and Molecular Behaviour', Van Nostrand, Rheinhdd, London (1969).

147. Pellat, H.; J. Physique, Vol. 9, pp. 313-325, (1900). (in French)

148. Cole, R.H., and Cole, K.S.; J. Chem. Phys., Vol. 9, pp. 341-351, (1941).

149. Davidson, D.W., and Cole, R.H.; J. Chem. Phys.;

Vol. 18, pp. 1417, (1950).

150. Blythe, A.R., and Jeffs, G.M.; J. Macromol. Sci., Phys., B3, pp. 141-152, Marcel Dekker, Inc., New York, (1969).

151. Willbourn, A. H.; Trans. Faraday Soc., Vol. 54, pp. 717-729, (1958).

152. Schatzki, T.F.; J. Polym. Sci., Vol. 57, pp. 337-356, (1962).

153. Mc Crum, N.G., Read, B.E. and Williams, G.; Anlastic and Dielectric Effects in Polymeric Solids, New York: Wiley, (1987).

154. Ishida, Y.; J. Polym. Sci., Part A2, Vol. 7, pp. 1835-1861, (1969).

155. North, A.M.; Chem. Soc. Rev., Vol. 1, pp. 49, (1972).

156. Baur, M.E. and Stockmayer, W.H.; J. Chem. Phys., Vol. 43, pp. 4319, (1965).

157. Rouse, P.E.; J. Chem. Phys., Vol. 21, pp. 1272, (1953).

158. Zimm, B.H.; J. Chem. Phys., Vol. 24, pp. 269, (1956).

159. Bates, T.W., Ivin, K.J., and Williams, G.; Trans. Faraday Soc., Vol. 63, pp. 1964-1975, (1967).

160. Bur, A.J., and Roberts, D.E.; J. Chem. phys., Vol. 51, pp. 406-420, (1969).

161. Box and Jenkins;'Time series analysis forcasting and control', Sanfrancesco holden day (1974).

162. Glim 3.77 update 0 (copyright) 1985 Royal Statistical Society, London (computer pakage).

163. Lind, S.C., Bardwell, D.C., and Perry, J.H.; J. Amer. Chem. Soc., Vol. 48, pp. 1556-1575, (1926).

164. Hopwood, F.L., and Phillips., J.T.; Proc. Phys. Soc., Vol. 50, pp. 438, (1938).

165. Charlesby, A.; Proc. Phys. Soc., Vol. 57, pp. 496-518, (1945).

166. Fowler, J.F.; Proc. Roy. Soc., Vol. A236, pp. 464-480, (1956).

167. Farmer, F.T.; Nature, Lond., Vol. 150, pp. 521,

(1942).

168 Fowler, J.F. and Farmer, F.T.; Nature, Lond., Vol. 171, pp. 1020-1021, (1953).

169. Fowler, J.F. and Farmer, F.T.; Nature, Lond., Vol. 173, pp. 317-318, (1954).

170 Fowler, J.F. and Farmer, F.T.; Nature, Lond., Vol. 174, pp. 136-137, (1954).

171. Fowler, J.F. and Farmer, F.T.; Nature, Lond., Vol. 175, pp. 516-517, (1955).

172. Fowler, J.F. and Farmer, F.T.; Nature, Lond., Vol. 175, pp. 590-591, (1955).

173. Fowler, J.F. and Farmer, F.T.; Nature, Lond., Vol. 175, pp. 648, (1955).

174. Fowler, J.F. and Farmer, F.T.; Brit. J. Radiol N.S., Vol. 24, pp. 118, (1956).

175. Mayburg, S. and Lawrence, W.L.; J. Appl. Phys., Vol. 23, pp. 1006-1011, (1952).

176. Warner, A.J., Muller, F.A., and Nordlin, H.G.; J. Appl. Phys., Vol. 25, pp. 131, (1954).

177. Feng, P.Y. and Kennedy, J.W.; J. Amer. Chem. Soc., Vol. 77, pp. 847-851, (1955).

178. Mayer, R.A., Bouquet, F.L., and Alger, R.S.; J.Appl. Phys., Vol. 27, pp. 1012-1018, (1956).

179. Ramsey, N.W.; Nature, Lond., Vol. 172, pp. 214, (1953).

180. Charlesby, A.; Proc. Roy. Soc., Vol. A215, pp. 187-214, (1952).

181. Charlesby, A.; Proc. Roy. Soc., Vol. A222, pp. 542-557, (1954).

182. Charlesby, A.; Proc. Roy. Soc., Vol. A224, pp. 120-128, (1954).

183. Baskett, A.C. and Miller, C.W.; Nature, Lond., Vol. 174, pp. 364-365, (1954).

184. Alexander, P., Black, R.M., and Charlesby, A.; Proc. Roy.Soc., Vol. A232, pp. 31-48, (1955).

185. Miller, A.A., Lawton, E.J., and Balwit, J.S.; J. Phys. Chem., Vol. 60, pp. 599-604, (1956).

186. Lawton, E.J., Bueche, A.M., and Balwit, J.S.; Nature, Lond., Vol. 172, pp. 76-77, (1953).

187. Miller, A.A., Lawton, E.J., and Balwit, J.S.; J. Polym. Sci., Vol. 14, pp. 503-304, (1954).

188. Chapiro, A.; J. Chem. Phys., Vol. 52, pp. 246, (1955).

189. Dole, M., Keeling, C.D. and Rose, D.G.; J. Amer. Chem. Soc., Vol. 76, pp. 4304-4311, (1954).

190. Alexander, P., Charlesby, A. and Rose, M.; Proc. Roy. Soc., Vol. A223, pp. 392-404, (1954).

191. Black, R.M.; Nature, Lond., Vol. 178, pp. 305-306, (1956).

192. Lawton, E.J., Zemany, P.D., and Balwit, J.S.; J. Amer. Chem. Soc., Vol. 76, pp. 3437-3439, (1954).

193. Sisman, O. and Bopp, C.D.; ORNL- 928, Nuclear. Sci. Abst., Vol. 8, No. 2792, (1951).

194. Hedving, P.;'Electrical Conductivity of Irradiated Polymers', Chapter 8 of the Radiation Chemistry of Macromolecules (Edited by Malcolm (Dole), Vol. 1, Academic Press (1972).

195. Wu, S. Gedeon, S. and Fouracre, R.A.; A Dielectric Relaxation Model and Measurement of the Whole Molecule Response of an Epoxy Resin During the Curing Process (in Press) IEEE Electrical Insulation (1986).

196. Van de Voorde, M.H.; Radiation Effects on Polymeric Materials and Components, CERN European Organization for Nuclear Research, CERN 70 - 5, 26 Feb. (1970).

197. Maxwell, I.D., and Pethrick, R.A.; J. Polym. Degradation and Stability, Vol. 5, pp. 275-301, (1983).

198. Capacitance Bridge, Operating instructions for type 716-C, General Radio Company, Feb. (1951).

# TABLES

Table 2.1 List of some vinyl compounds

| Vinyl compound name | Monomer formula |
|---|---|
| Ethylene | $CH_2=CH_2$ |
| Propylene | $CH_2=CH$ <br> \| <br> $CH_3$ |
| Vinyl chloride | $CH_2=CH$ <br> \| <br> $Cl$ |
| Styrene | $CH_2=CH$ <br> \| <br> $C_6H_5$ |

Table 2.2 Theoretical values of some epoxide resin properties (Ref. 28)

| Value of (n) | Molar ratio ECH : DPP | Molecular weight (Mn) | Number of epoxide groups |
|---|---|---|---|
| 0 | 2 : 1 | 340 | 2 |
| 1 | 3 : 2 | 624 | 2 |
| 2 | 4 : 3 | 908 | 2 |
| 3 | 5 : 4 | 1192 | 2 |
| 4 | 6 : 5 | 1476 | 2 |
| 5 | 7 : 6 | 1760 | 2 |
| 6 | 8 : 7 | 2044 | 2 |
| 7 | 9 : 8 | 2328 | 2 |

Table 3.1 Microanalysis for MY750/HY956 epoxy system.

| Epoxy Resin MY750 | | Hardener HY956 | |
|---|---|---|---|
| Element | Found % | Element | Found % |
| Cl | 0.92 | N | 26.65 |
| C | 73.04 | C | 53.64 |
| H | 6.52 | H | 11.53 |

Table 3.2 Molecular weight of MY750.

| Epoxy Resin MY750 | |
|---|---|
| Method | Molecular Weight |
| From the Micro analysis | 394 |
| From the formula | 397 |

Table 3.3 Molecular weight of HY956 .

Hardener HY956

| Solvent | Molecular Weight (Mn) |
|---|---|
| Chloroform | 235 |
| Acetone | 214 |
| From the Micro analysis | 204 |

Table (4.1) Curing procedure for MY750/HY956 and MY750/DDSA epoxy systems.

| Epoxy System | | Time (hours) | Temperature °C |
|---|---|---|---|
| <u>MY750/HY956</u> | a | 5-10 | 22 |
| | b | 1 | 40 |
| | c | 2 | 60 |
| | d | 10-15 | 100 |
| <u>MY750/DDSA</u> | a | 5-10 | 22 |
| | b | 1 | 40 |
| | c | 2 | 60 |
| | d | 10 | 90 |

Note. The above procedures are sequential.

TABLE 4.2

Activation Energy Values E

| Diamine | E kJ/mol(eV) T < Tg | E kJ/mol(eV) T > Tg | Reference |
|---|---|---|---|
| m - Phenylenediamine | 46(0.48) | 49(0.51) | (12) |
| 4,4 - Diaminodiphenylmetane | 38(0.39) | 51(0.53) | (12) |
| 4,4 - Diaminodiphenyl Sulfone | 46(0.48) | 49(0.50) | (12) |
| Benzidine | 46(0.48) | 52(0.54) | (12) |
| HY 965 | 41(0.42) | | this |
| Diethylenetriamine (7) | 49(0.50) | | paper |
| Ethylenediamine | 57(0.60) | | (13) |
| Trimethylenediamine | 57(0.60) | | (13) |
| Hexamethylenediamine | 54(0.56) | | (13) |

T - Temperature of the reaction

Table (5.1)

| A_ESTIMATE | B_ESTIMATE |
|---|---|
| 0.04358 | 0.2848 |
| 0.05786 | 0.2718 |
| 0.06632 | 0.2642 |
| 0.07183 | 0.2593 |
| 0.07563 | 0.2560 |
| 0.07830 | 0.2537 |
| 0.08022 | 0.2521 |
| 0.08158 | 0.2510 |
| 0.08253 | 0.2502 |
| 0.08323 | 0.2496 |
| 0.08376 | 0.2491 |
| 0.08420 | 0.2488 |
| 0.08447 | 0.2486 |
| 0.08465 | 0.2484 |
| 0.08483 | 0.2483 |
| 0.08492 | 0.2482 |
| 0.08501 | 0.2481 |
| 0.08510 | 0.2480 |
| 0.08519 | 0.2480 |

Table (6.1) Effect of high energy radiation on polymers (Ref. 186)

| Cross-linking | Chain scission |
|---|---|
| Natural rubber | Polyethylene terephthalate (Terylene) |
| Polyacrylic esters | Polymethylmethacrylate |
| Polyesters | Polyvinylidene chloride |
| Polystyrene | Polytetrafluoroethylene |
| Polyacrylamide (Nylon) | Polychlorotrifluoroethylene (KelF) |
| Polyethylene | Cellulose |
| Polyacrylic acid | Cellulose derivatives |
| Chlorinated polyethylene | Polyisobutylene |
| Chlorsulphonated polyethylene | Casein |
| Polychloroprene (Neoprene) | Urea-formaldehyde |
| Polybutadiene | Melamine-formaldehyde |
| Thioplasts | Polyvinyl formal |
| Styrene–butadiene copolymers | Poly α-methyl styrene |
| Butadiene–acrylonitrile copolymers | Unfilled phenolic resins |
| Styrene–acrylonitrile copolymers | Polyvinyl butyral |
| Polydimethyl siloxanes | |
| Polyvinyl chloride | |
| Polyvinyl carbazole | |
| Polyvinyl alcohol | |
| Polyvinyl pyrrolidone | |
| Polypropylene | |
| Polyvinyl toluene | |

Table (6.2) Sample state.

| Designation | State |
|---|---|
| B.I. | Before irradiation |
| A.I. | After irradiation and before annealing |
| A.A. | After irradiation and after annealing at 95°C for 3 hours in air |
| D | A.A. sample contacting with air, at room temp. |
| E | D sample annealed at 115°C for 10 hours, in air |
| F | E sample contacting with air at room temp. |

Table (6.3) The effect of gamma-irradiation on the properties of a DGEBA epoxy resin cured with HY956.

| MGy | B.I. | A.I. | A.A. | D |
|---|---|---|---|---|
| $\rho$: Resistivity, $\Omega$.m (room temp.) | | | | |
| 0.5 | 1.1 E13 | 4.2 E11 | 3.1 E14 | 6.9 E12 |
| + | (1) | (0.035) | (25.83) | (0.575) |
| 1 | 1.7 E13 | 9.6 E11 | 6.5 E14 | |
| + | (1) | (0.056) | (38.23) | |
| 2 | 1.6 E13 | 2.3 E11 | 2.4 E15 | 3.8 E13 |
| + | (1) | (0.014) | (150) | (2.37) |
| Current transient, hours (room temp.) | | | | |
| 2 | 1-2 | 2-3 | 3-5 | |
| E : Activation energy, kJ/mol, (ev) | | | | $\Delta$E |
| 0.5 | 19.30 | | 27.6 | 8.3 |
| | (0.827) | * | (1.2) | (0.36) |
| 1 | 0.7 | | 27.6 | 6.7 |
| | (0.90) | * | (1.2) | (0.29) |
| 2 | 16.6 | | 29.9 | 12.2 |
| | (0.72) | * | (1.3) | (0.53) |
| Tg : Glass transition temp., $^{o}$C | | | | |
| 0.5 | 108 | 82# | 98 | |
| 1 | 108 | 91# | 105 | |
| 1.5 | 108 | 92# | 102 | |

# Broad peak

* Scattered points

+ Ratio of the resistivity

# FIGURES

**Polyethylene**

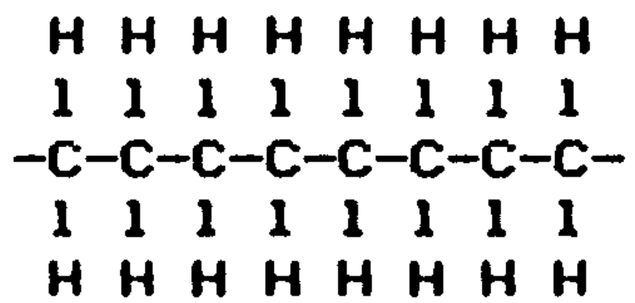

**Polyamides (Nylons)**

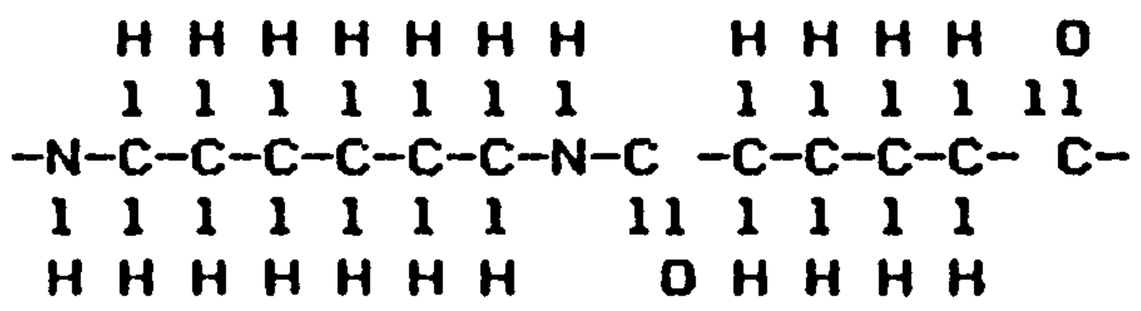

Figure 2.1 Some of the repeat units in polymers

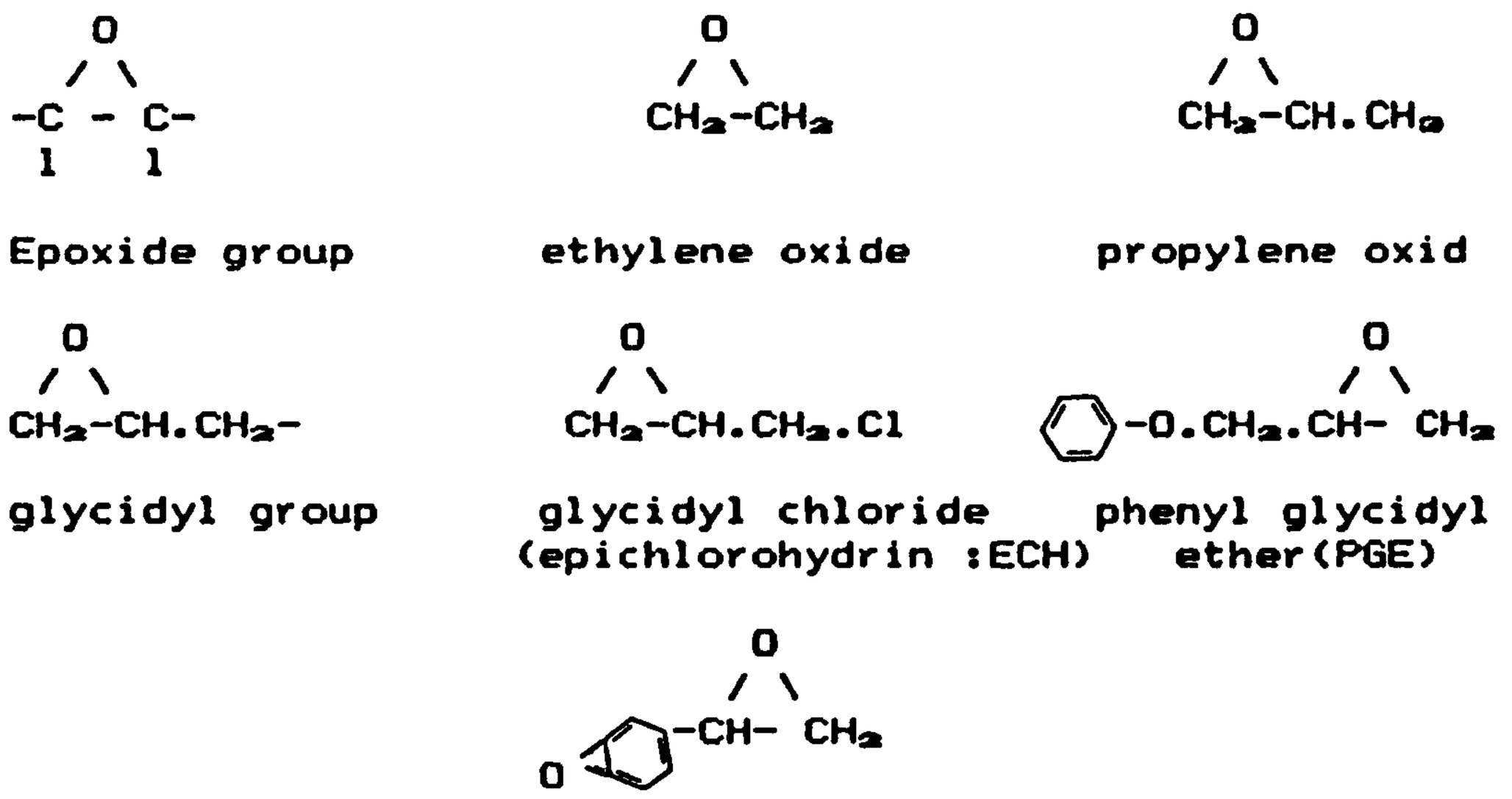


Figure 2.2 The formulae for a number of substituted ethylene oxides

1. Glycidyl ethers

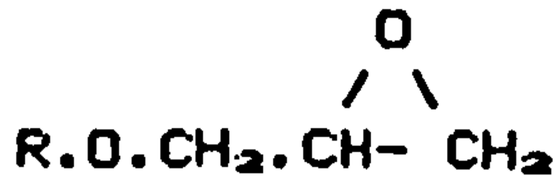

2. Glycidyl esters

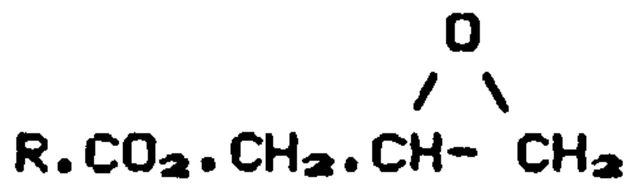

3. Glycidyl amines

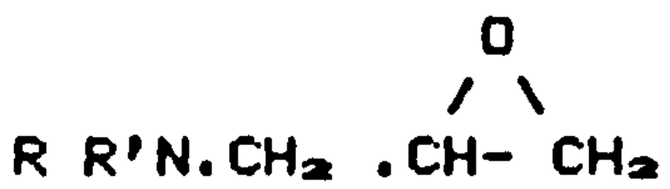

4. Linear aliphatic

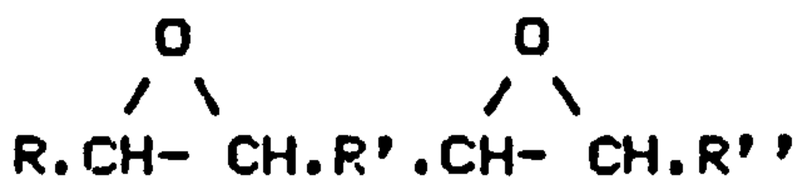

5. Cycloaliphatic

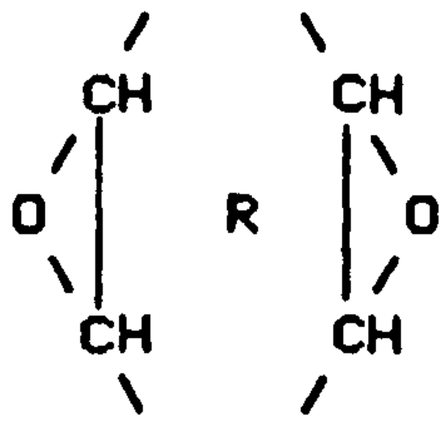

Figure 2.3 The chemical classifcation of the resins

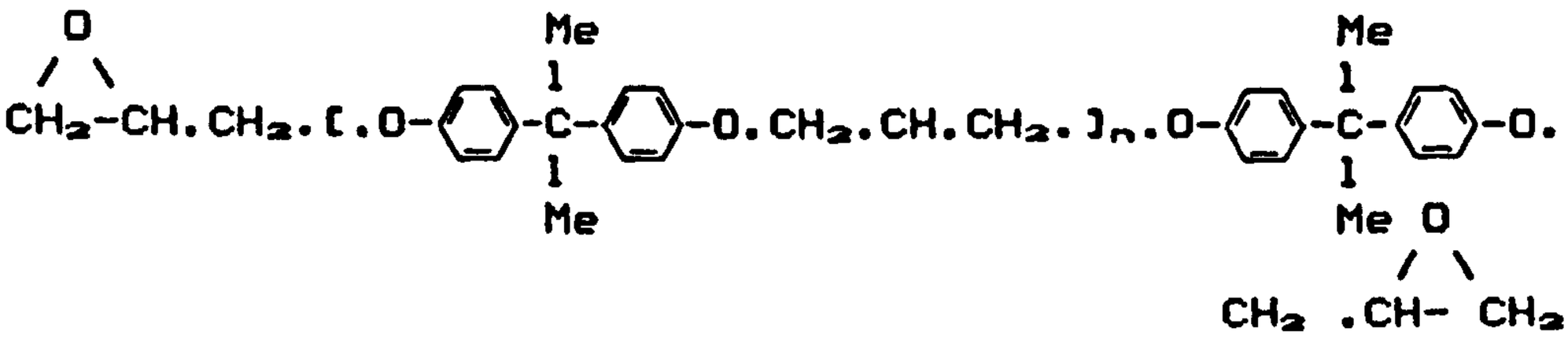

Glycidyl ether of bisphenol A

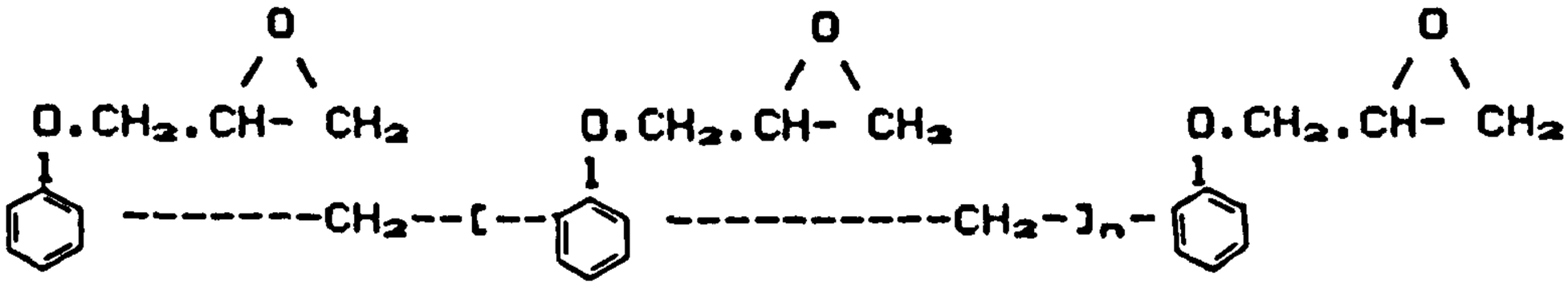

Glycidyl ether of novolak resin

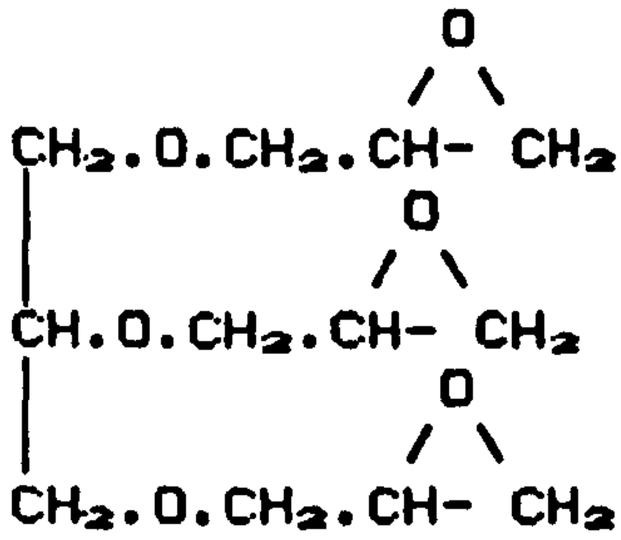

Glycidyl ether of aliphatic polyol

Figure 2.4 Types of glycidyl ether

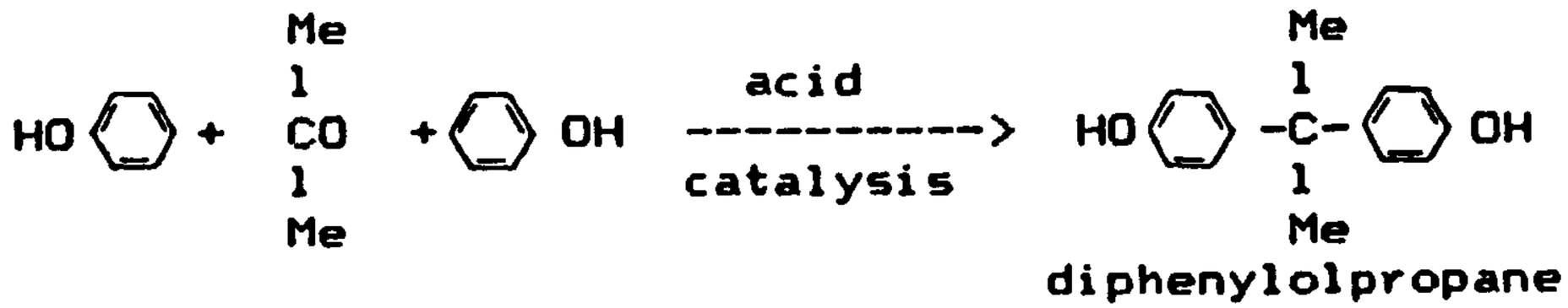


Figure 2.5 Preparation of diphenylolpropane (DPP)

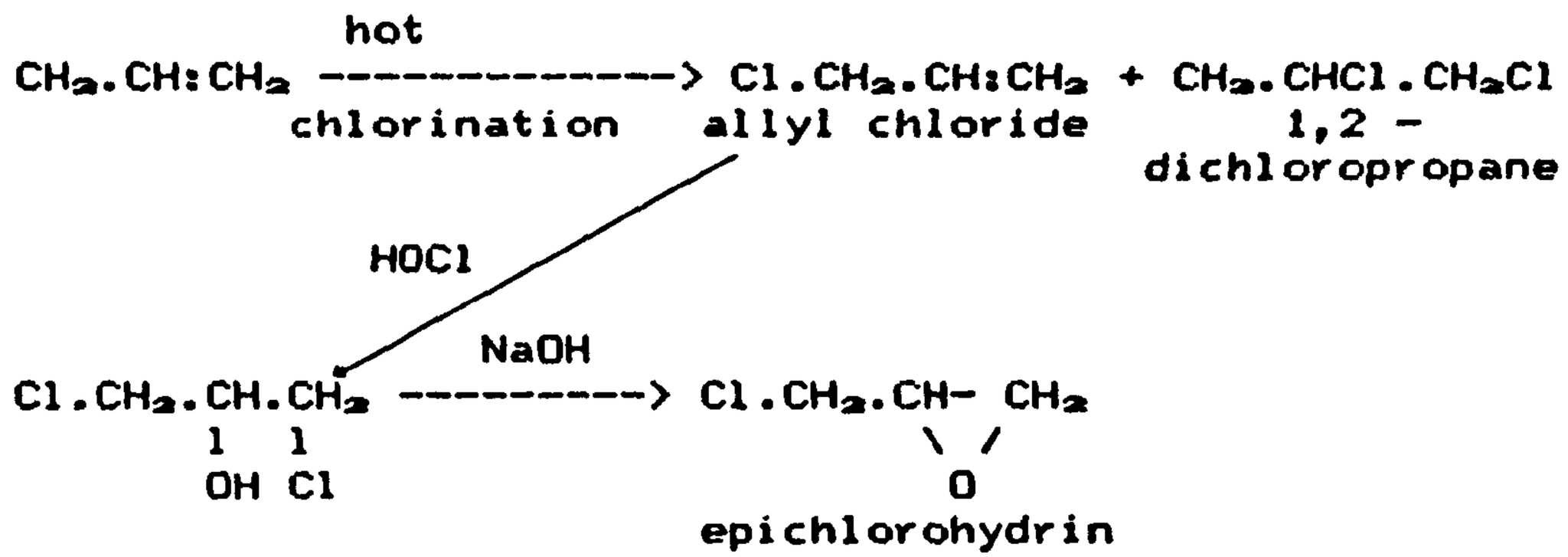


Figure 2.6 Preparation of epichlorohydrin (ECH)

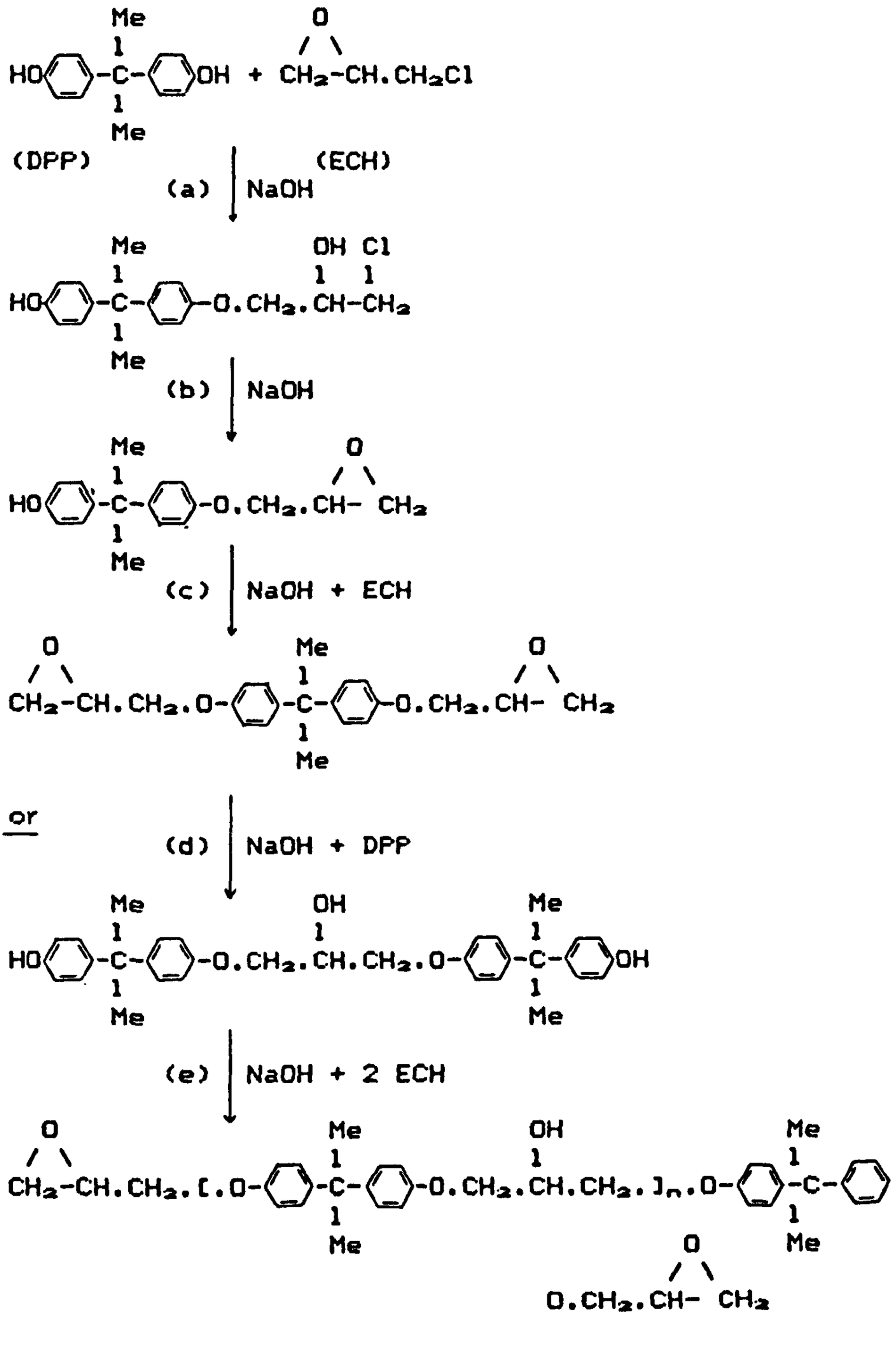


Figure 2.7 Preparation of liquid epoxide resin

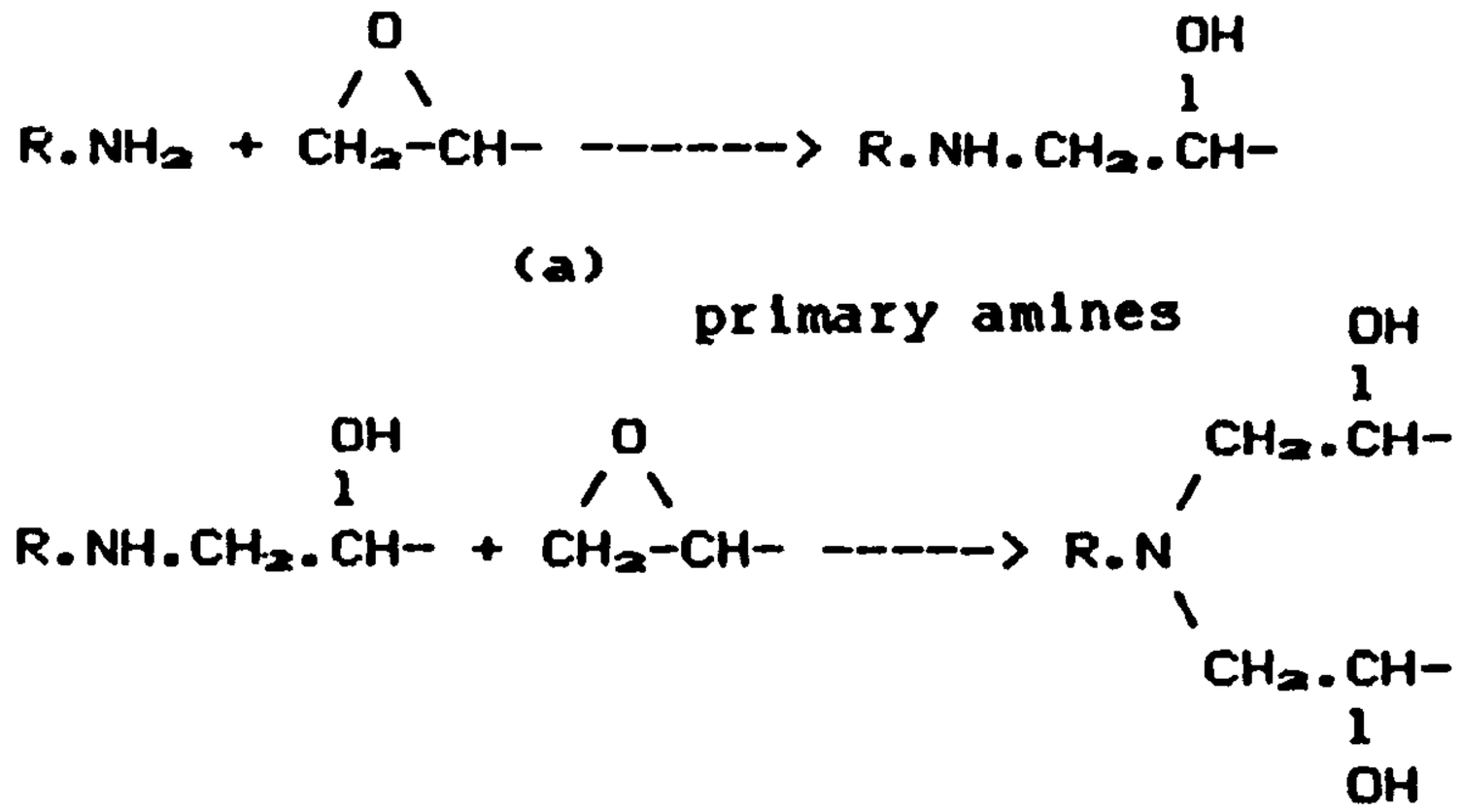


Figure 2.8 Amines-Epoxy cure mechanism

Reaction 1

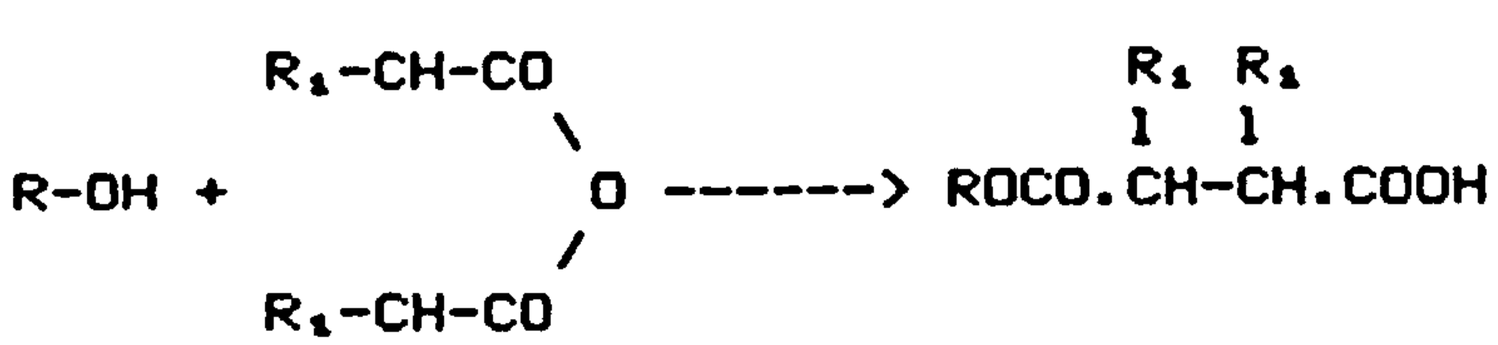


Reaction 2

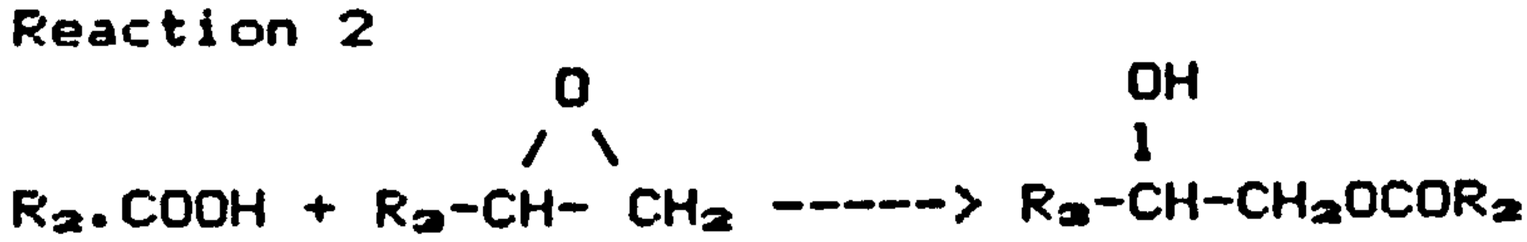


Reaction 3

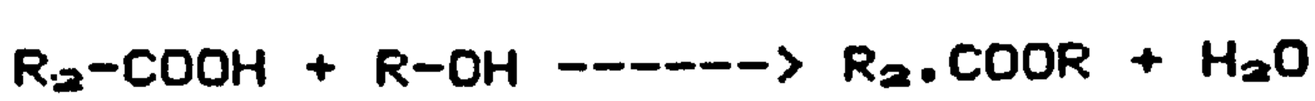


Reaction 4

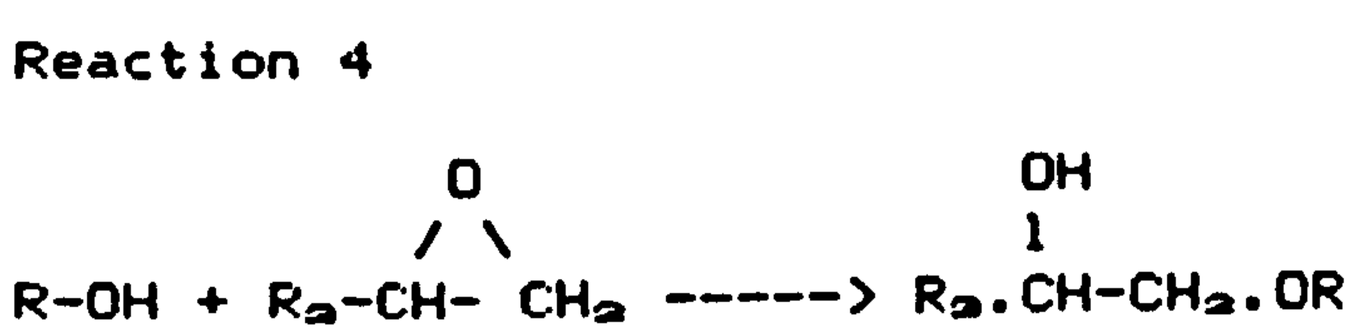


Figure 2.9 Anhydride-Epoxy cure mechanism

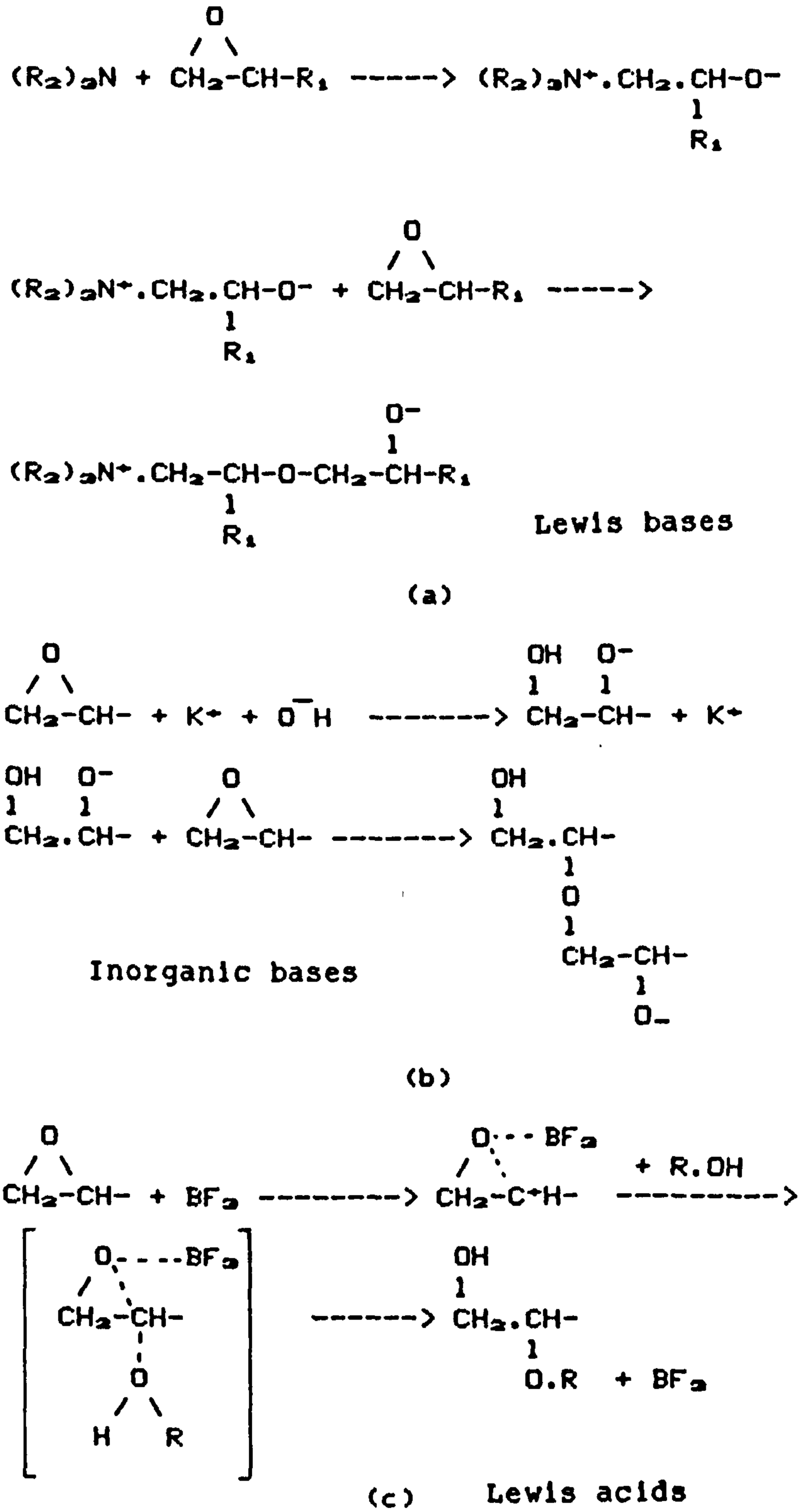


Figure 2.10 Catalytic-Epoxy cure mechanism

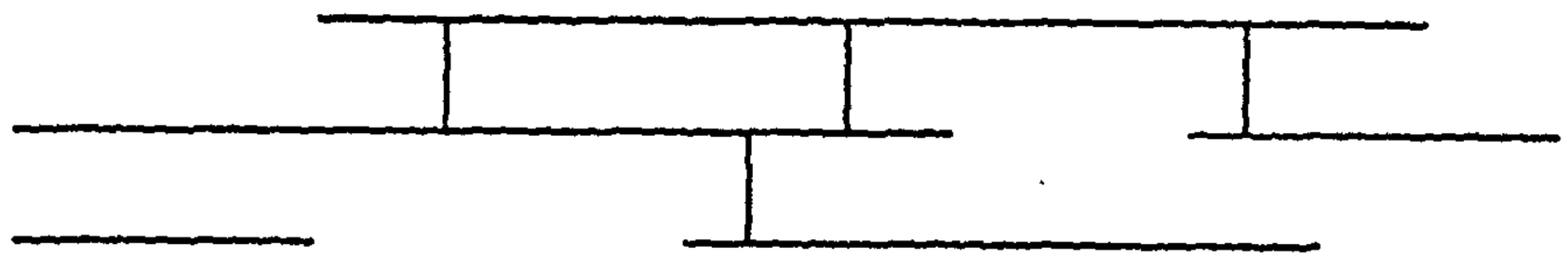

Figure 2.11 Structure of the epoxy resin system

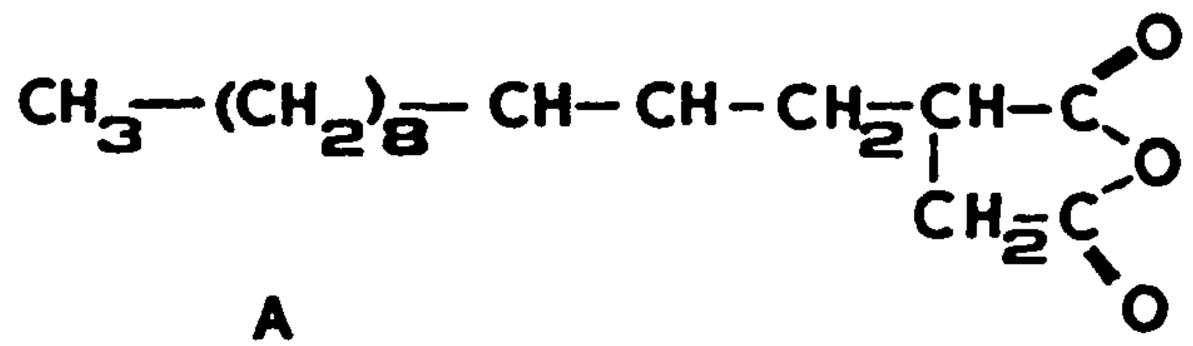

A

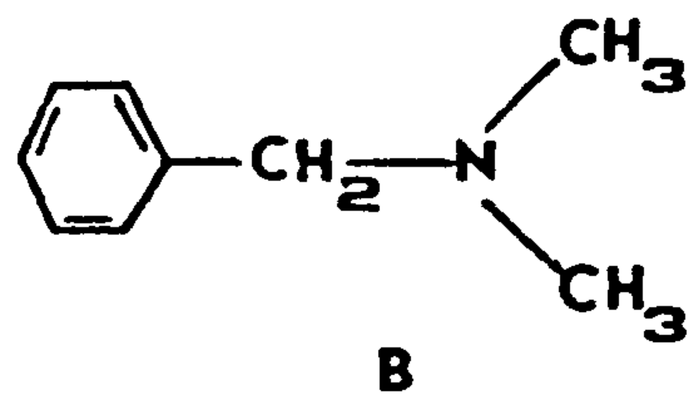

B

Fig. (3.1) Chemical formula for

a- Dodecenyl-succinicanhydride (DDSA)

b- Benzyldimethylamine.

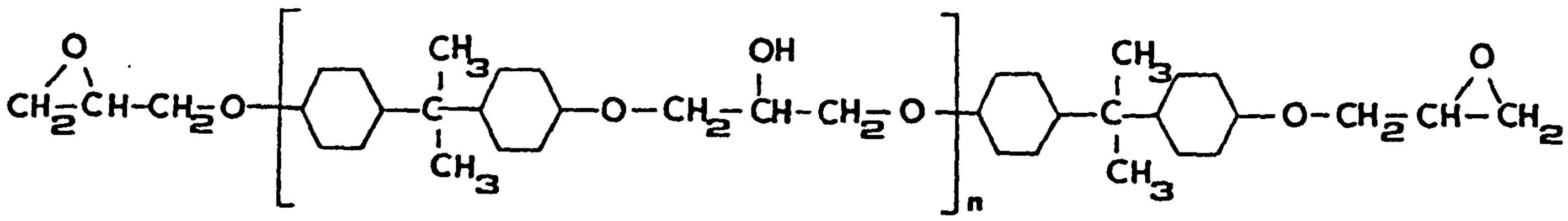

A

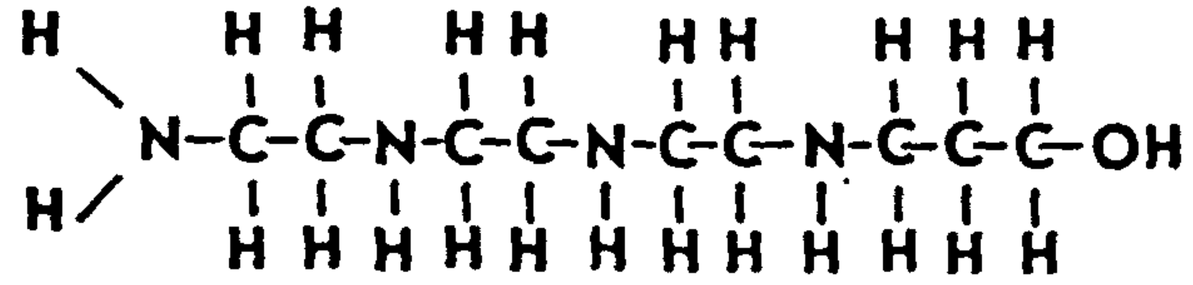

B

Fig. (3.2) Chemical formula for

a- Diglycidyl ether of bisphenol A (DGEBA, MY750)

b- Hydroxyalkylated polyamine (HY956).

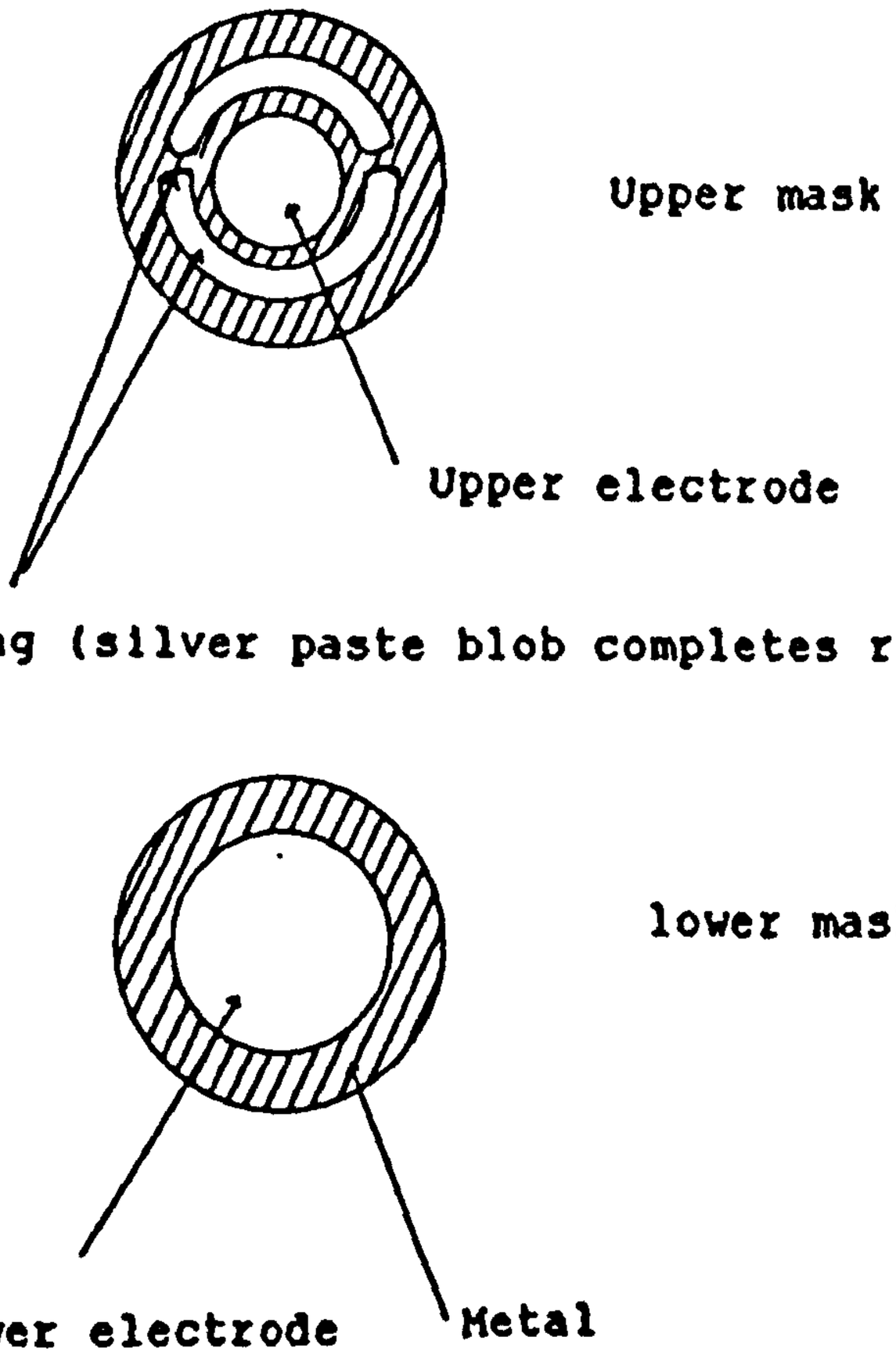


Fig. (3.3) Specimen masks for polyester sheet method.

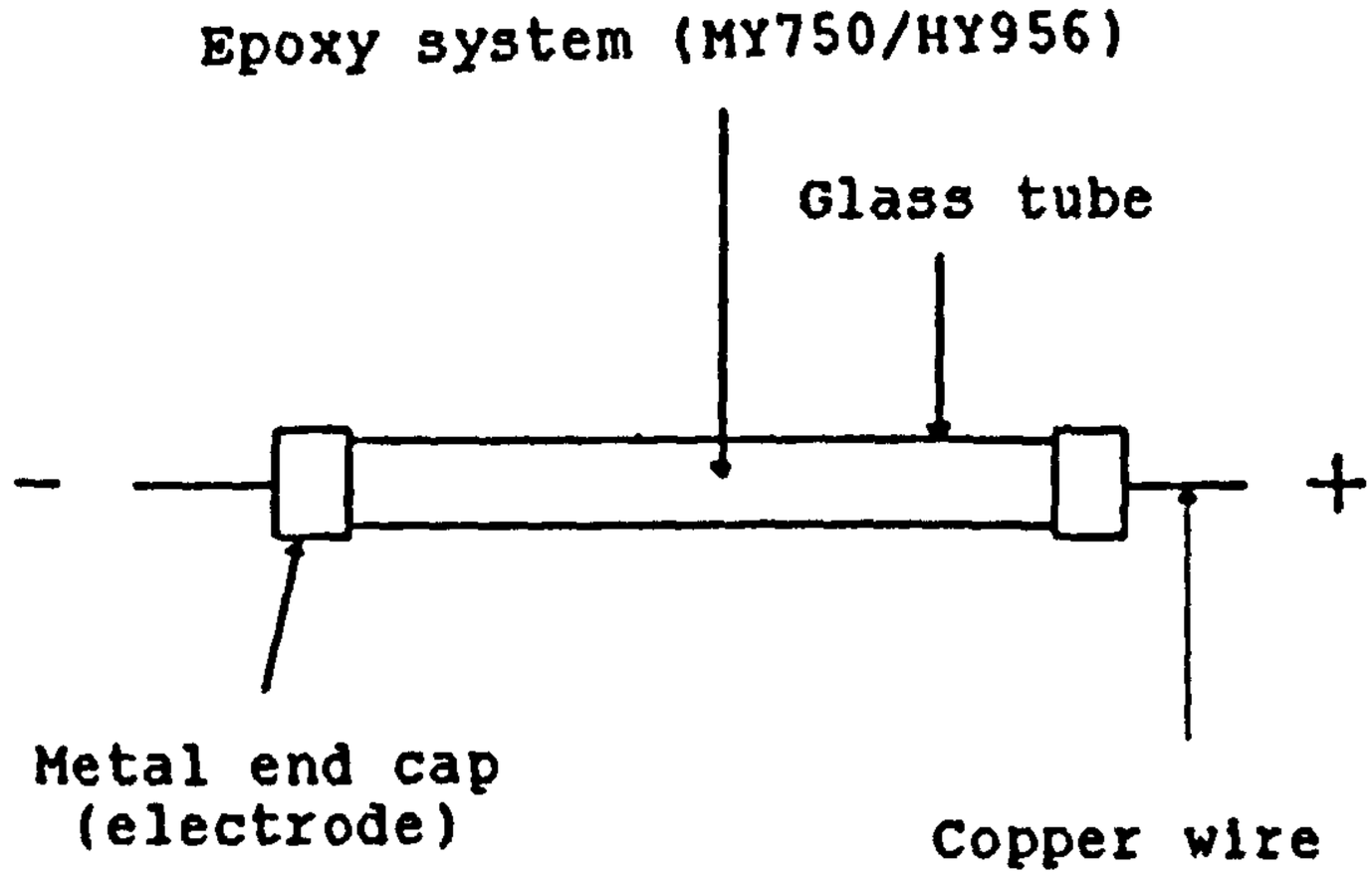


Fig. (3.4) Schematic diagram for cylinderical method.

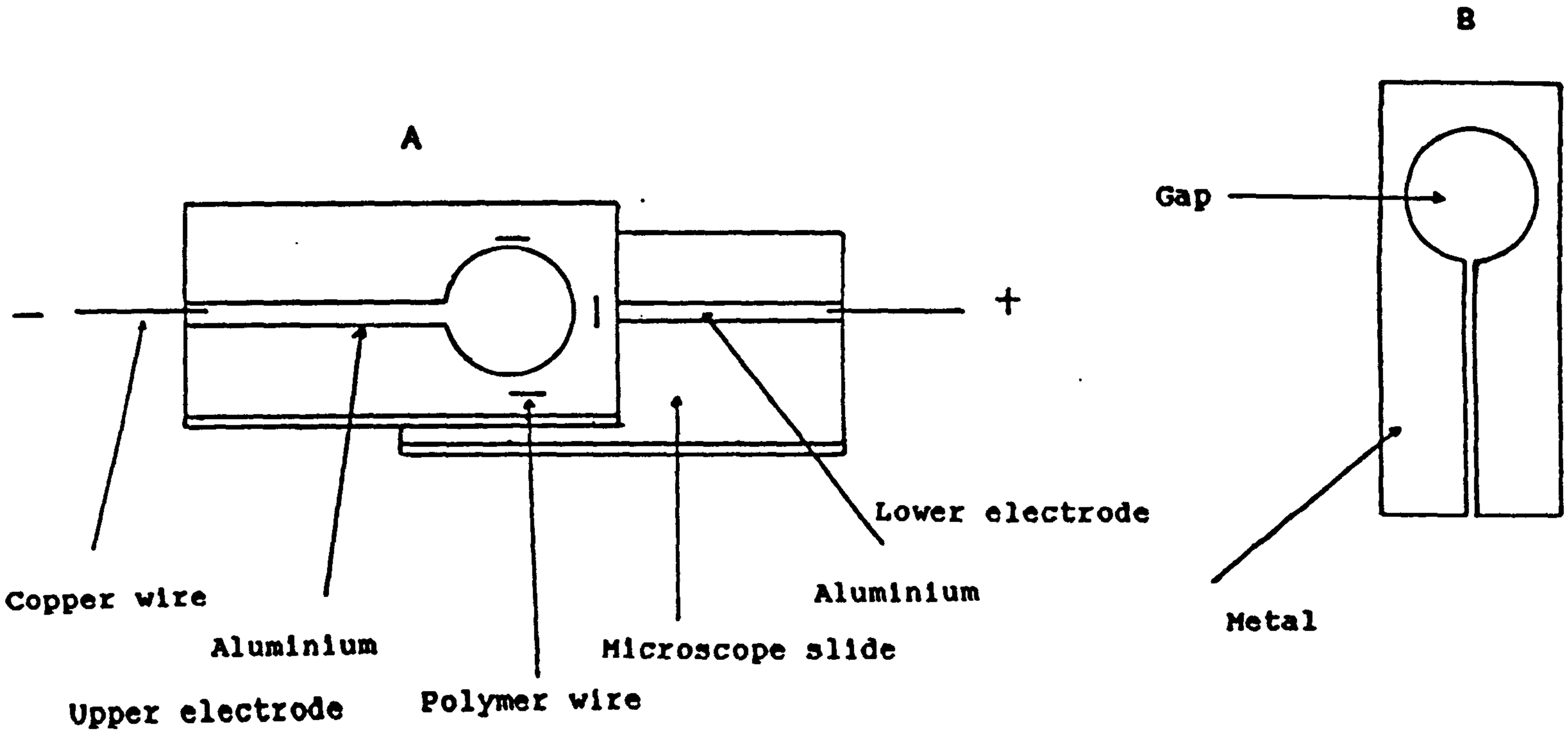


Fig. (3.5) a- Schematic diagram for sandwich method

b- Specimen mask for sandwich method.

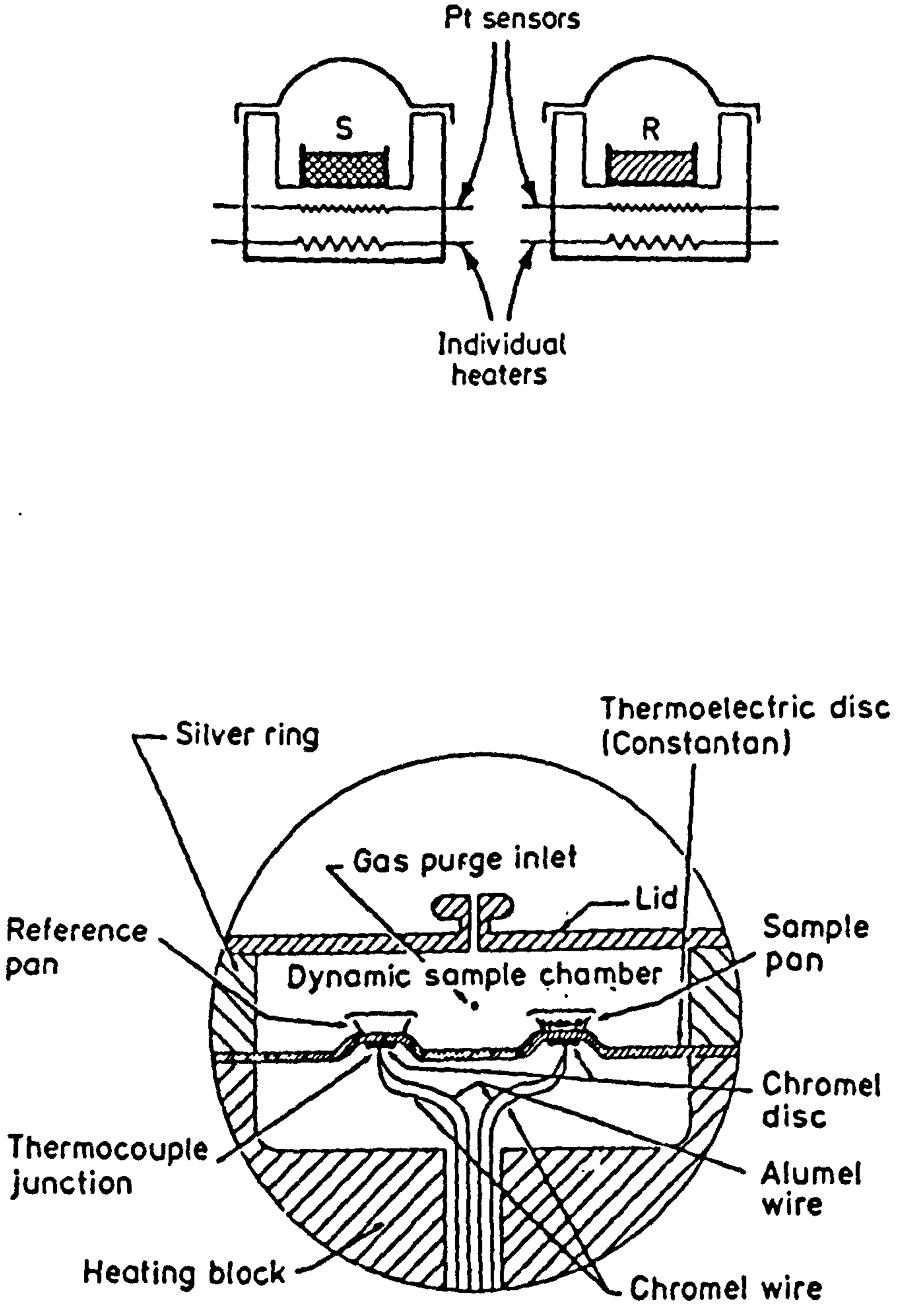


Fig. (4.1) Diagram showing the DSC cell.

(ref. 46)

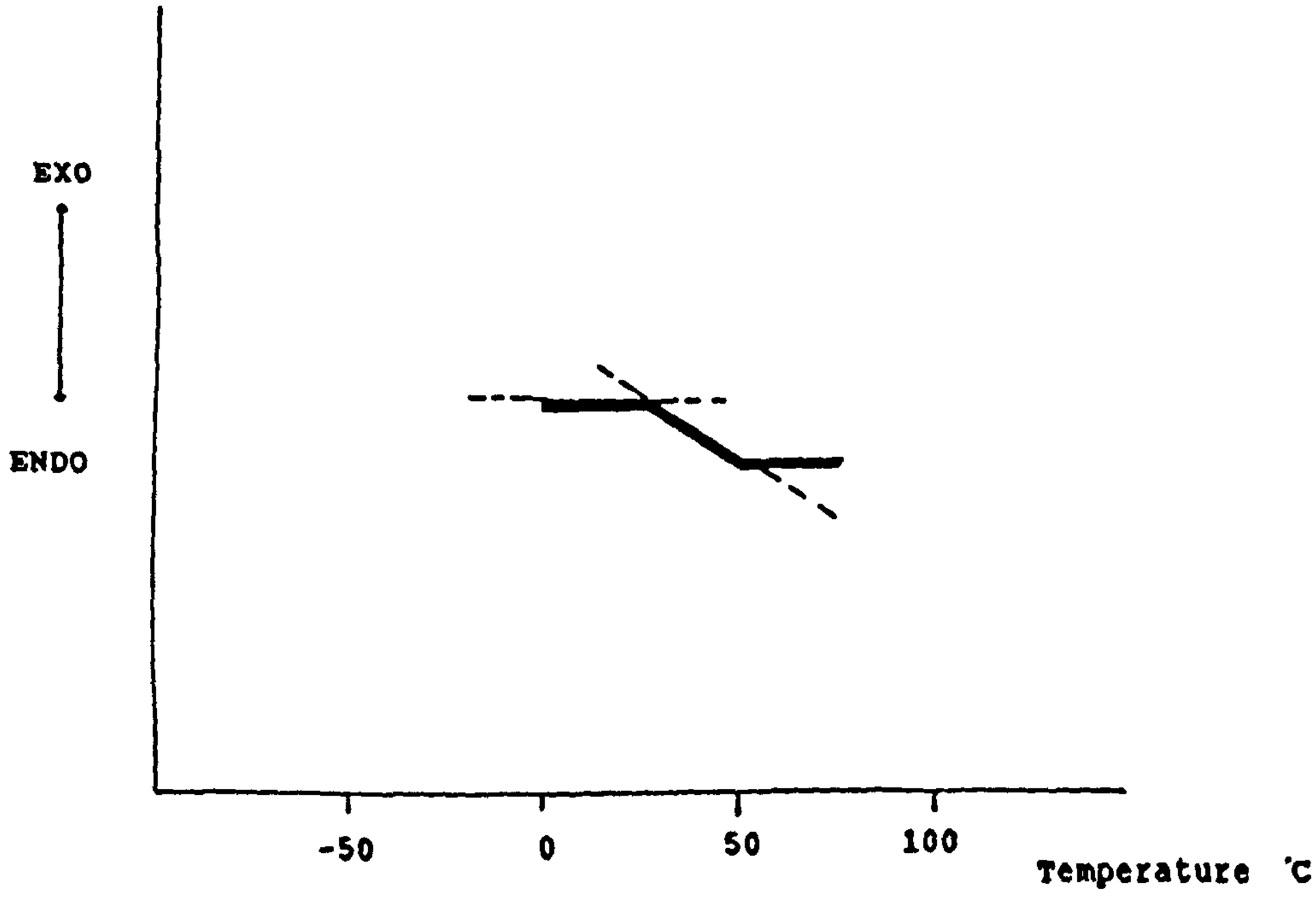


Fig. (4.2) Diagram showing the determination of Tg value.

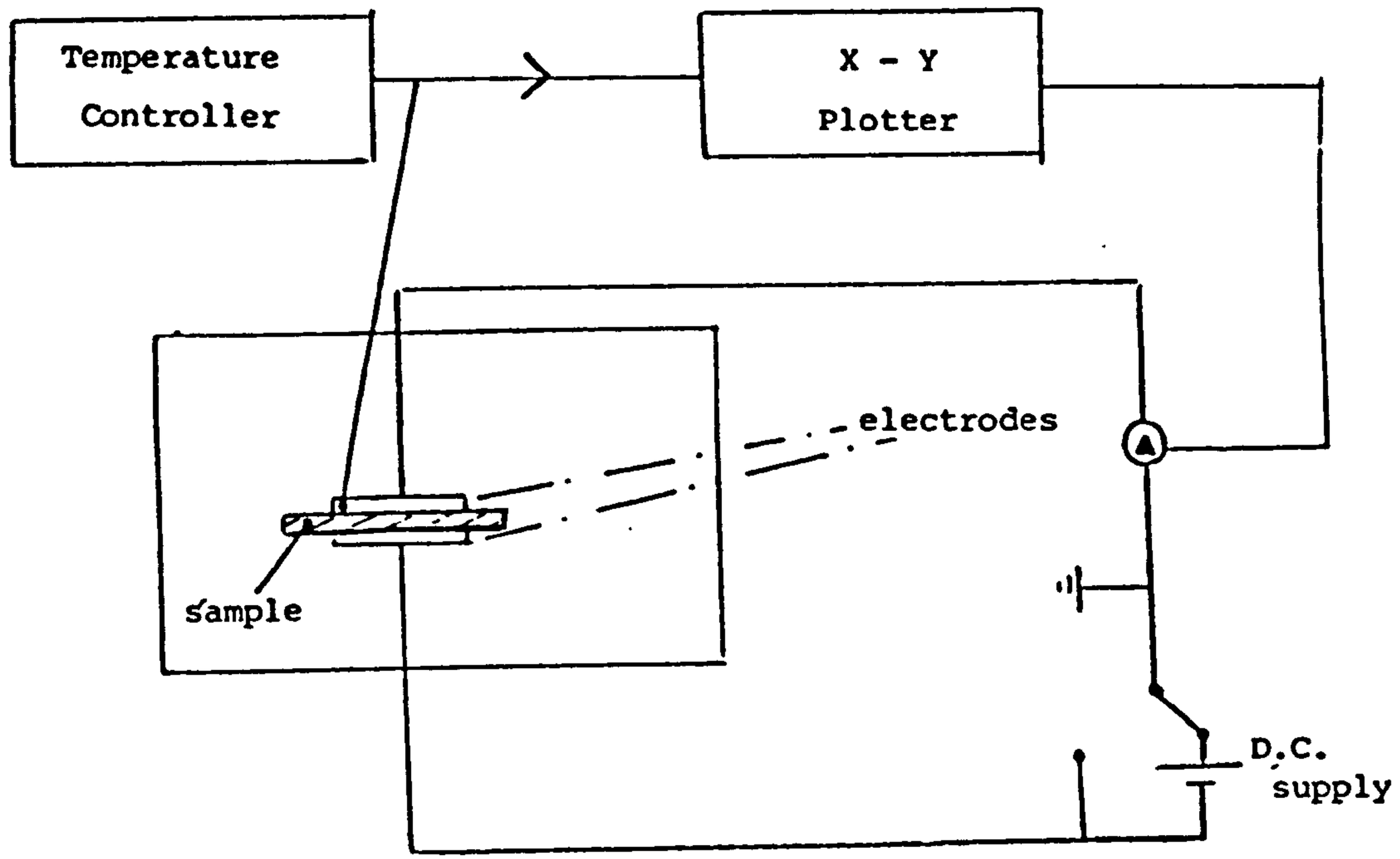


Fig. (4.3) Circuit diagram for TSDC.

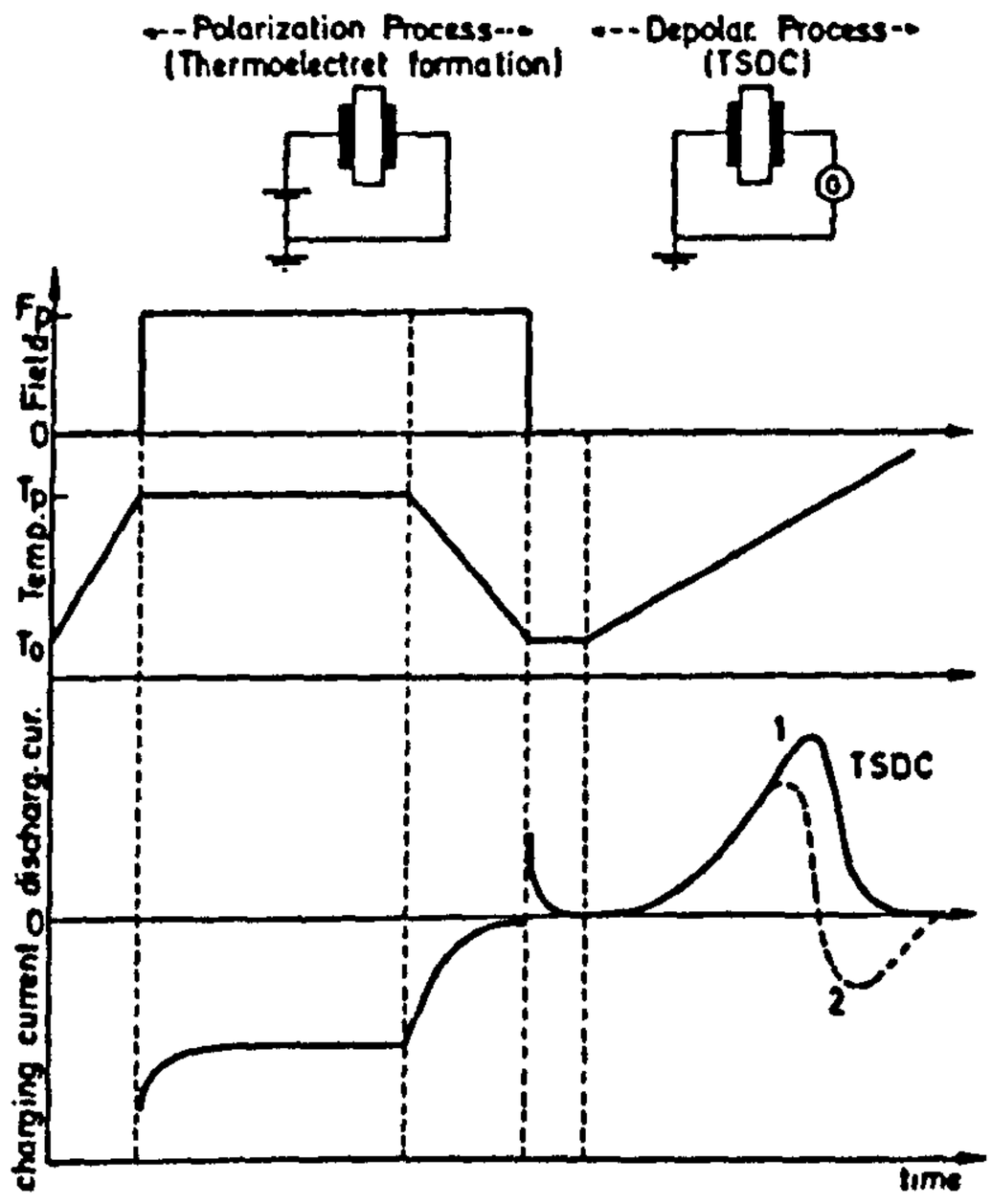


Fig. (4.4) Schematic diagram for TSDC measurements.

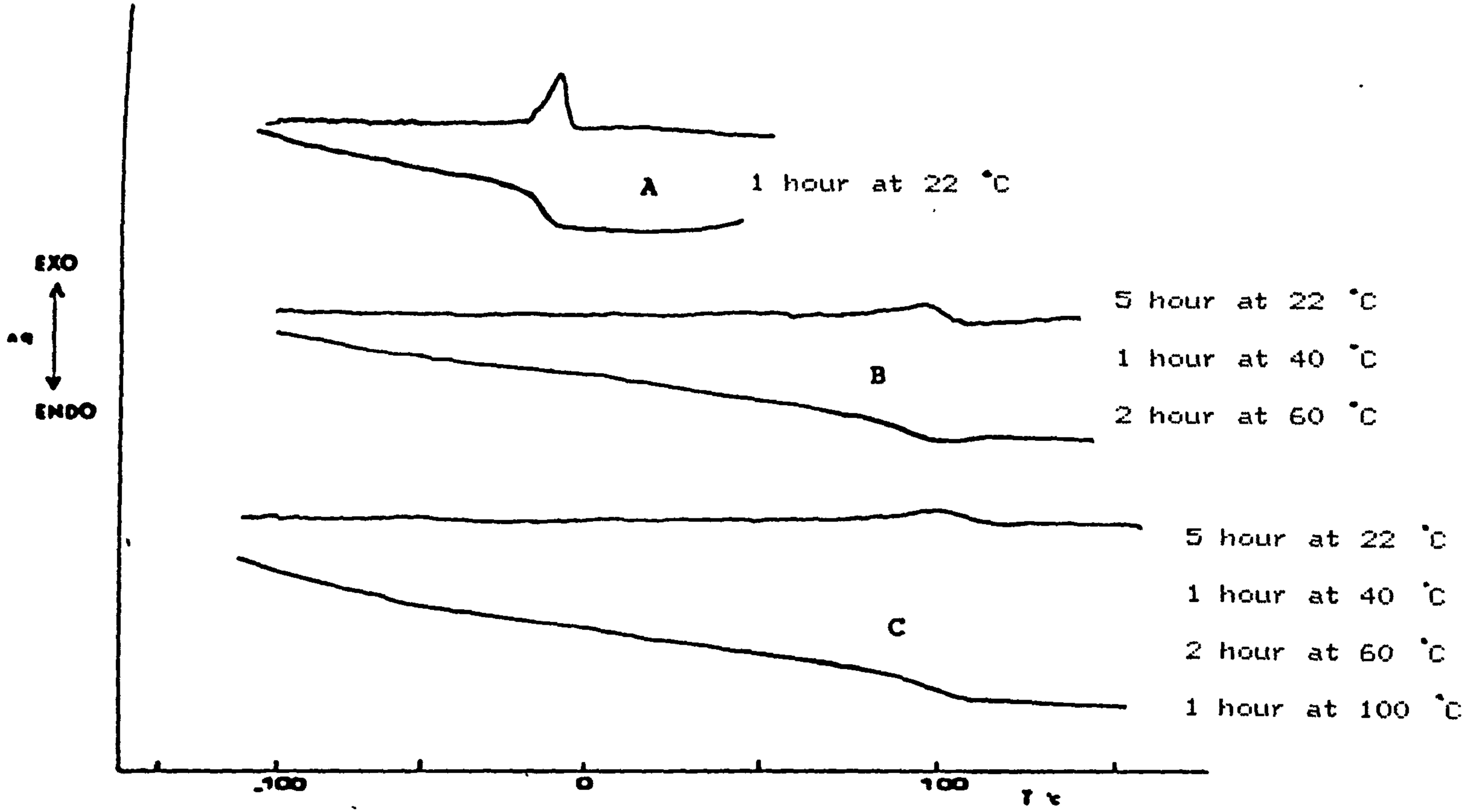


**Fig. (4.5) DSC of MY750/HY956 sample at different stages of cure.**

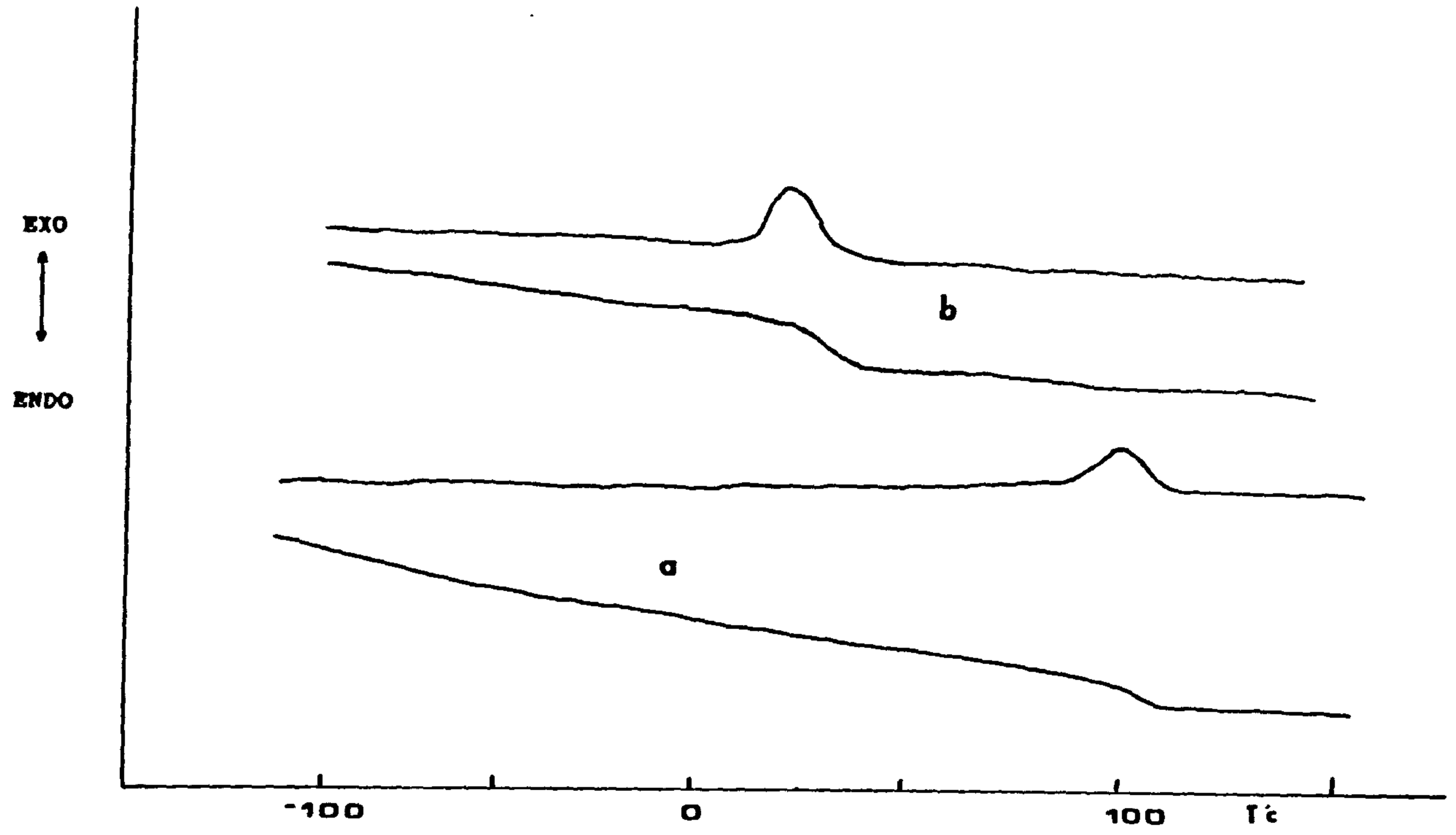


Fig. (4.6) DSC of fully cured epoxy system

a- MY750/HY956  b- MY750/DDSA.

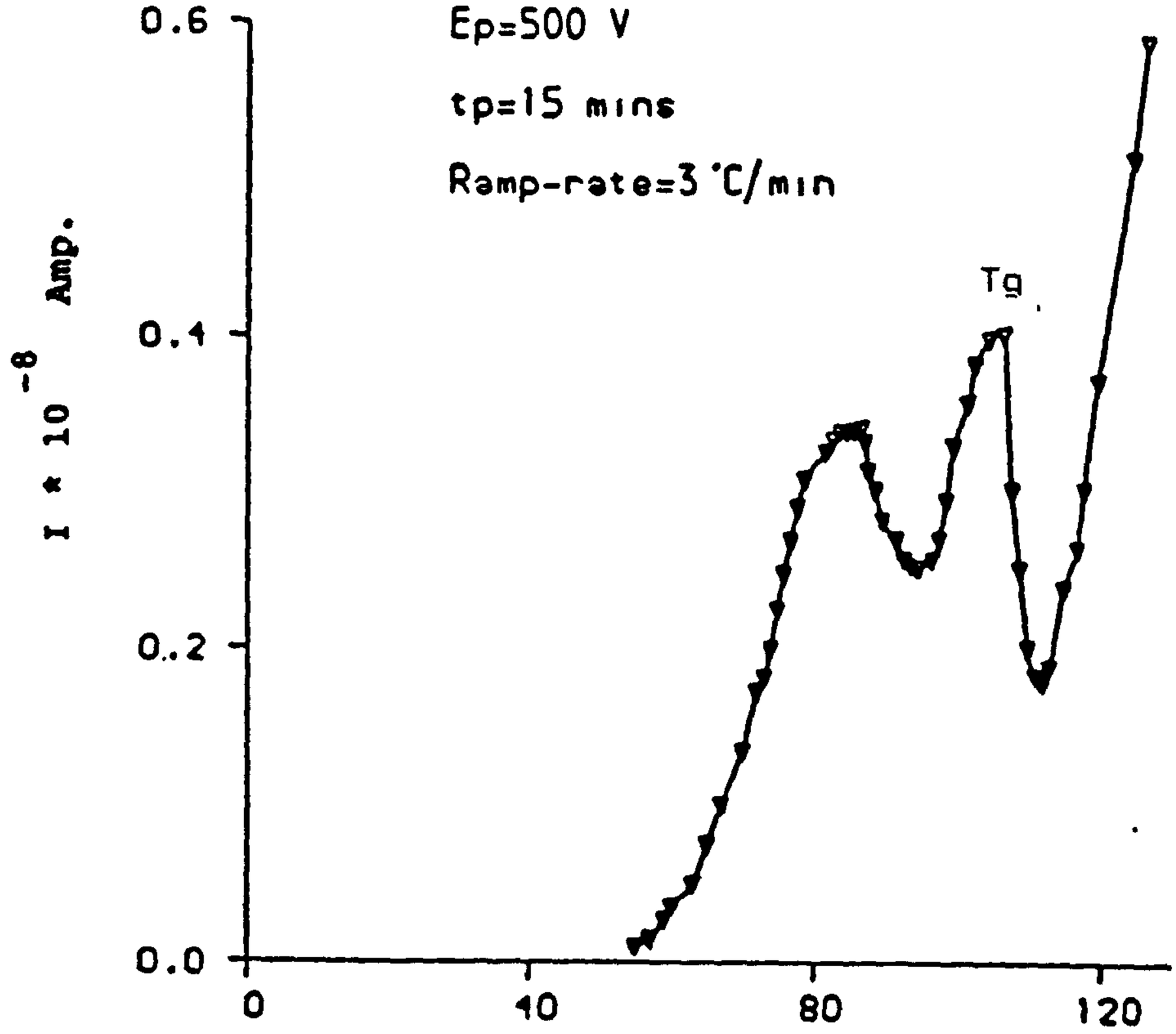


Fig. (4.7) TSDC of fully cured MY750/HY956 epoxy system.

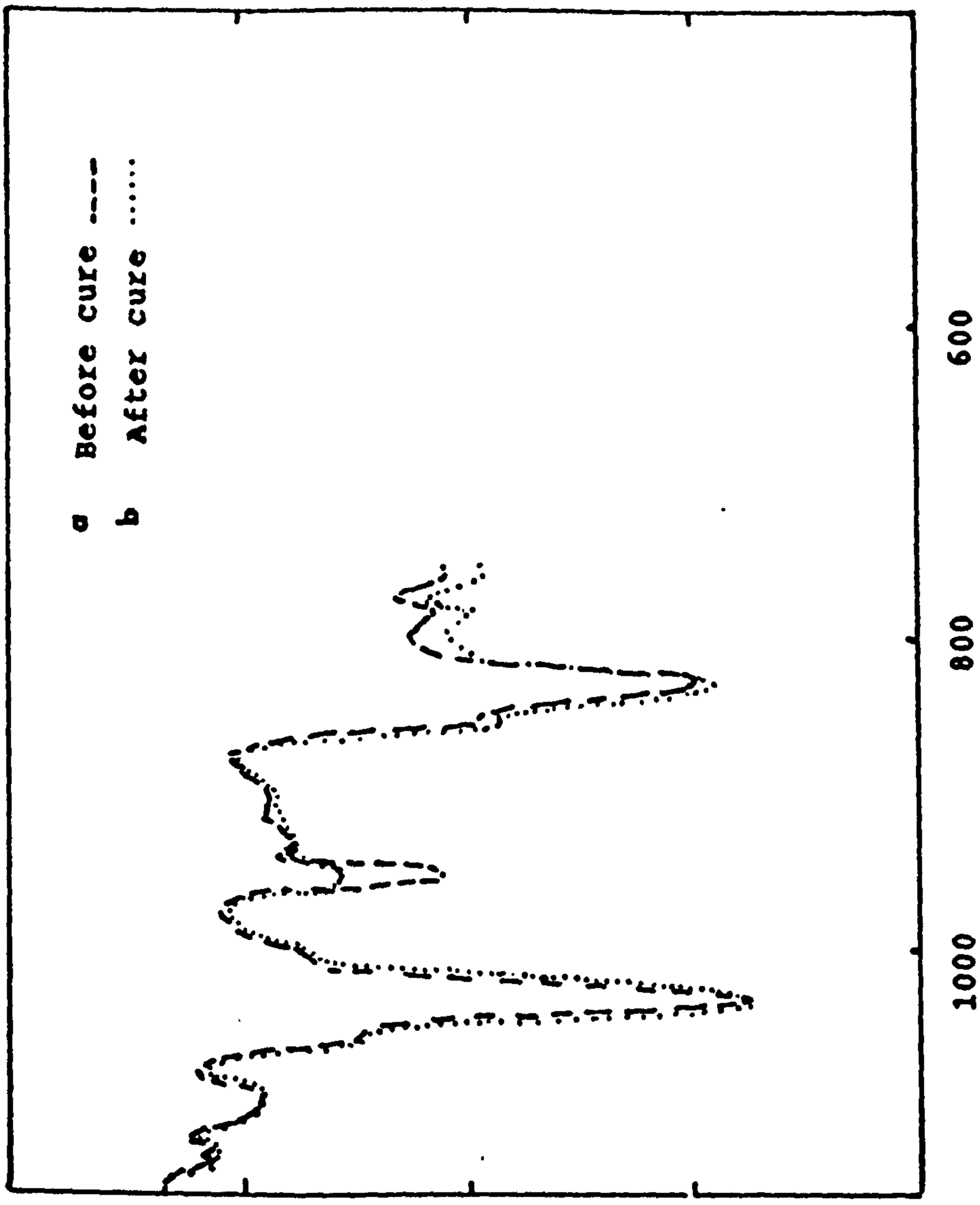


Fig. (4.8) IR of MY750/HY956 sample a- before cure b- after cure.

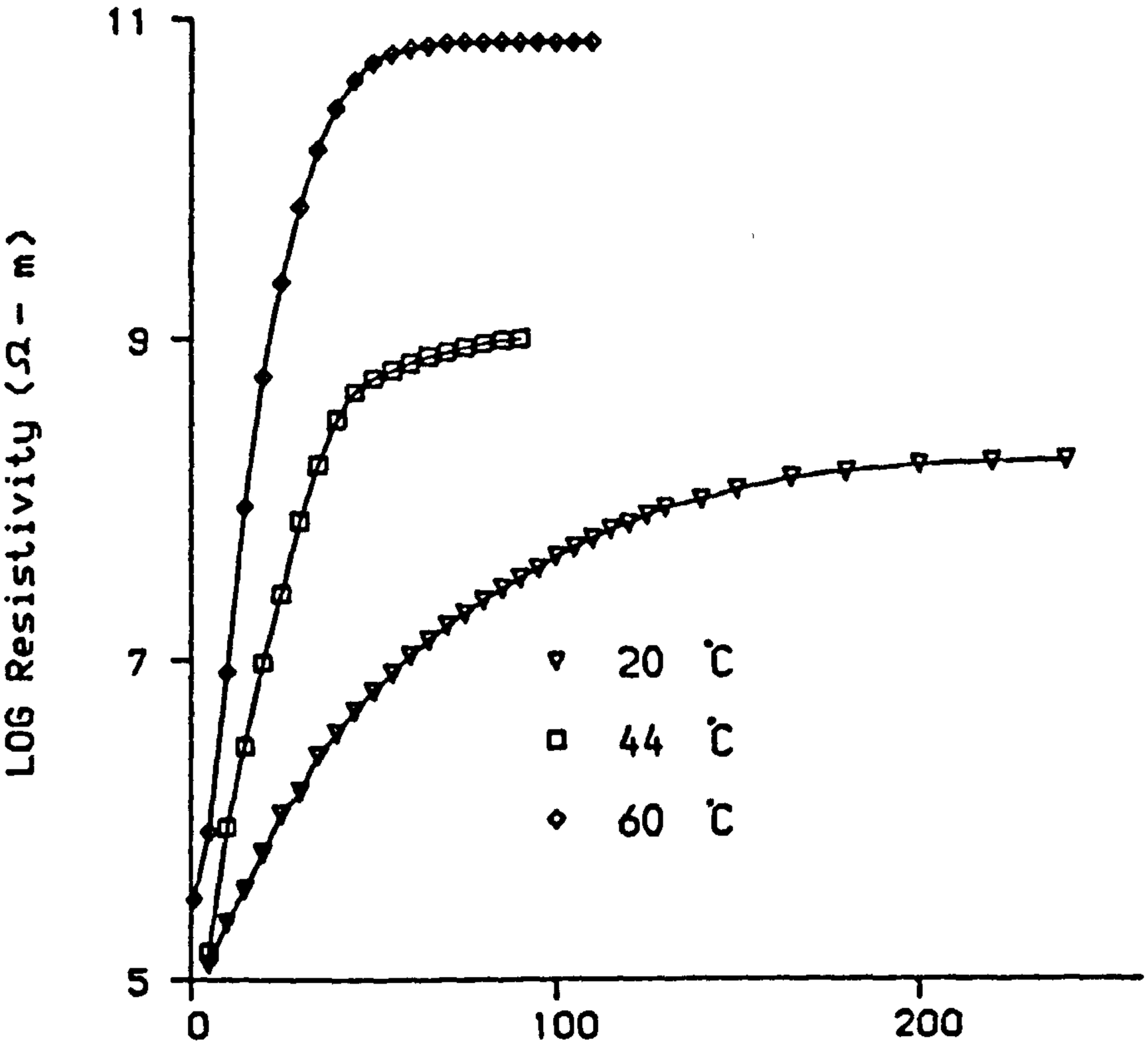


Fig. (4.9) Log resistivity versus reaction time during curing for MY750/HY956 sample at different temperature.

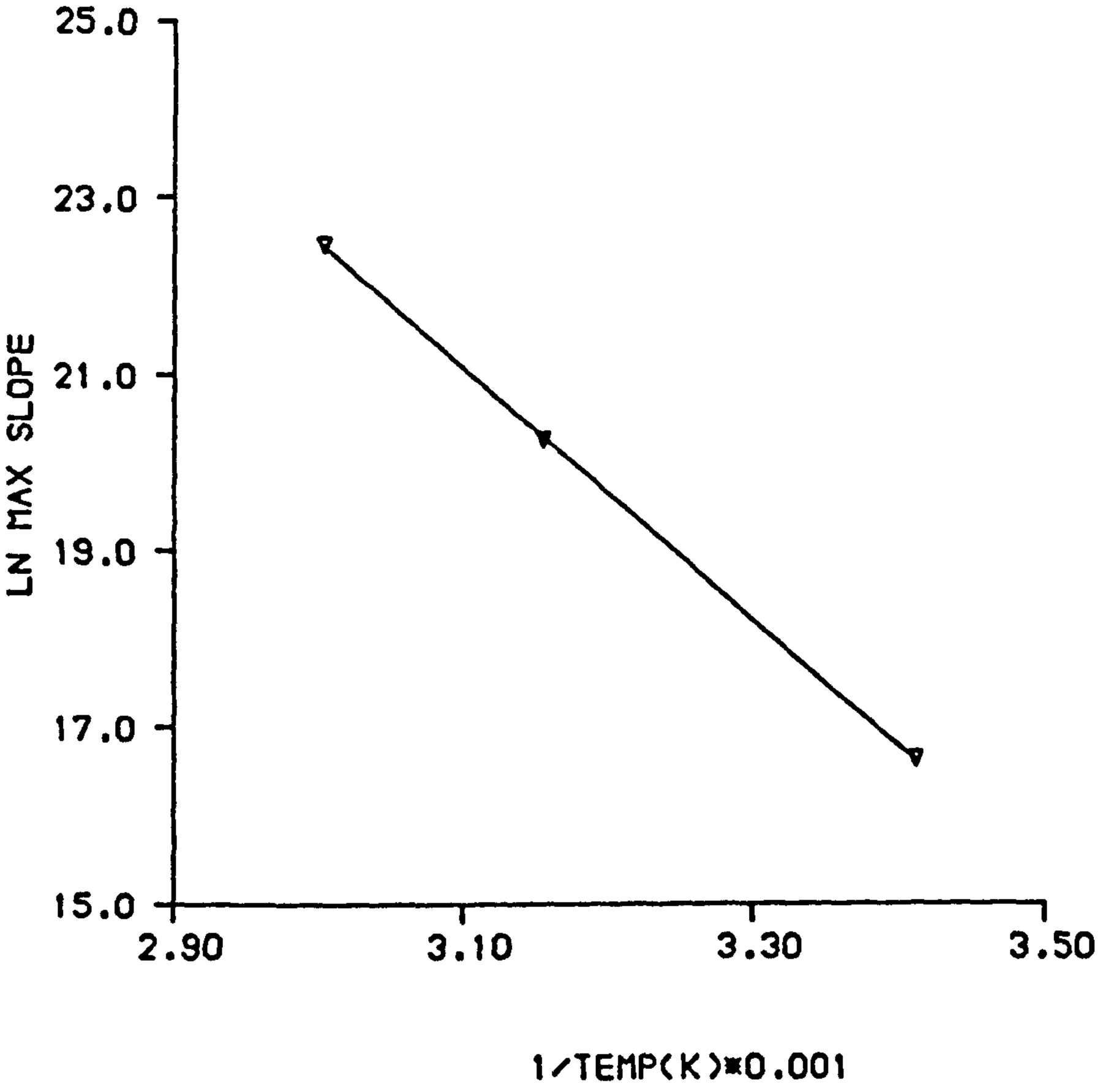


Fig. (4.10) Ln maximum slope of fig. (4.9) versus 1/temperature for MY750/HY956 sample.

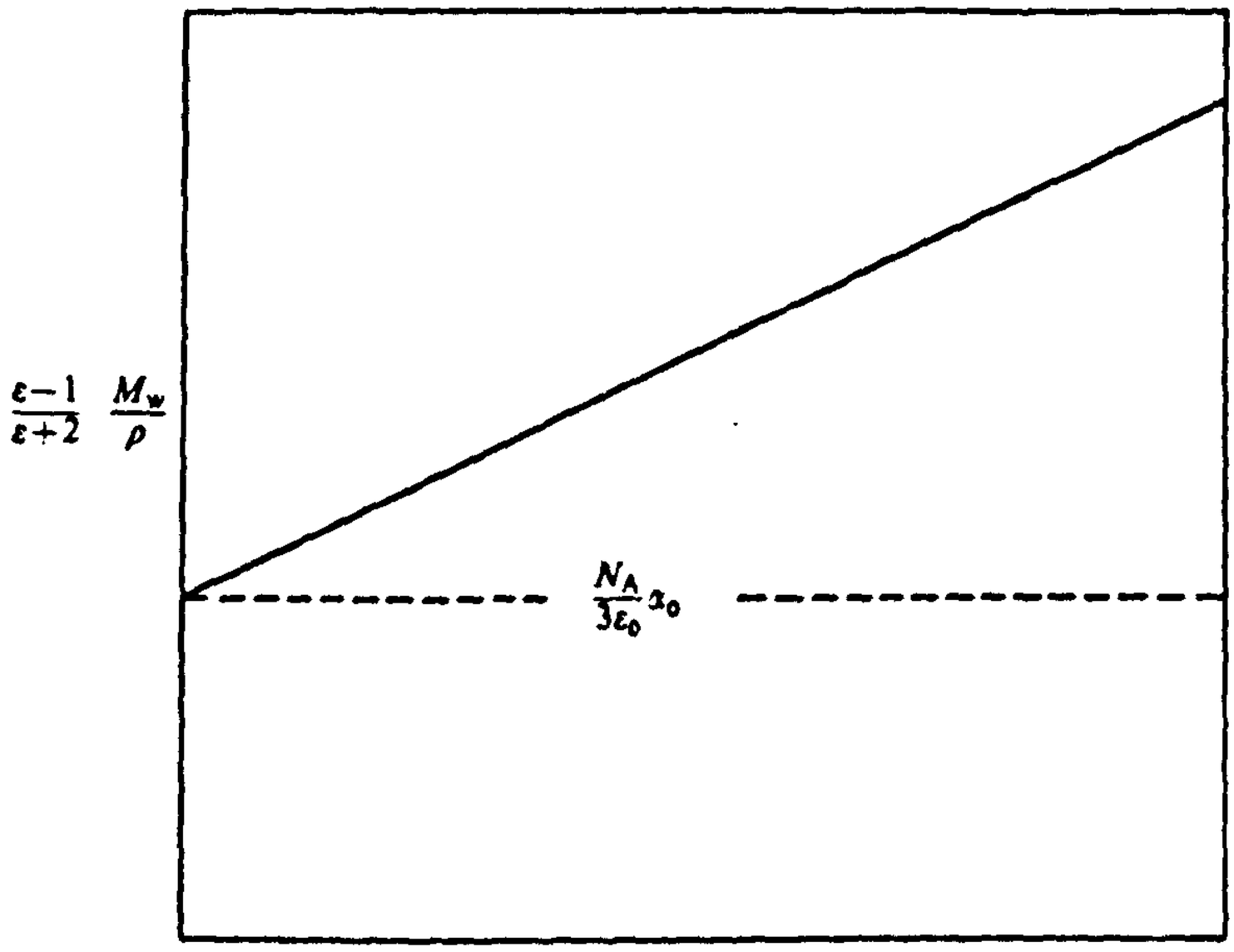


Fig. (4.11) Temperature dependence of molar polarisation. (ref. 23).

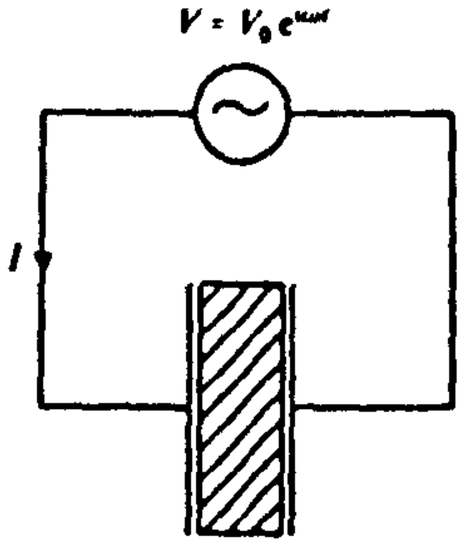


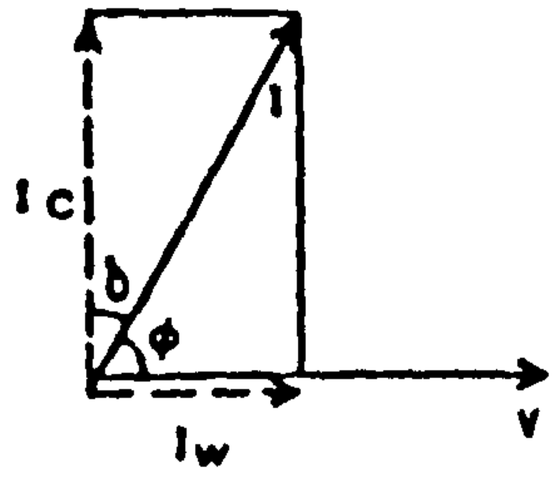


$$\tan\delta = \frac{Iw}{Ic} \quad \text{and} \quad \cos\Phi = \frac{Iw}{I}$$

A B

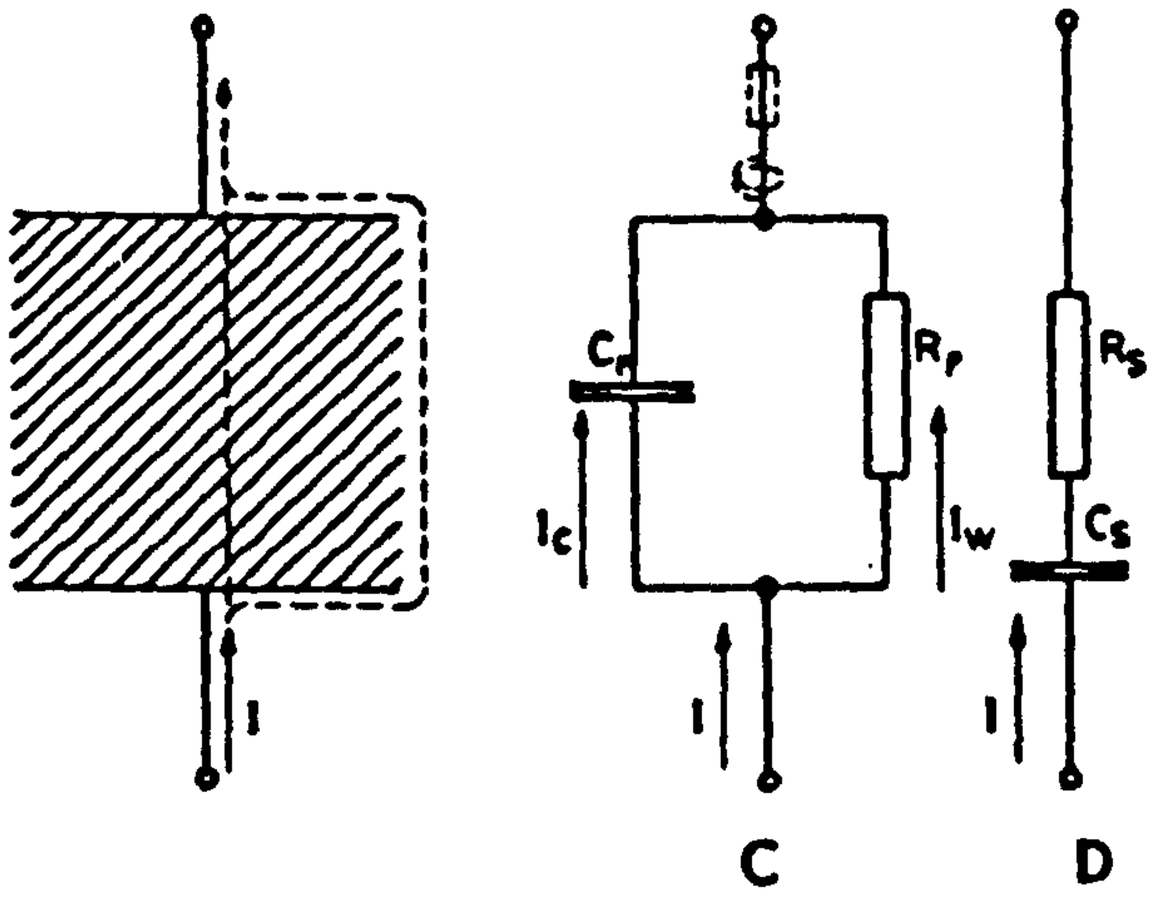


Fig. (4.12) a- Circuit diagram for A.C. losses in a dielectric, b- the loss angle, Equivalent circuits of a dielectric with loss c- parallel, d- series.

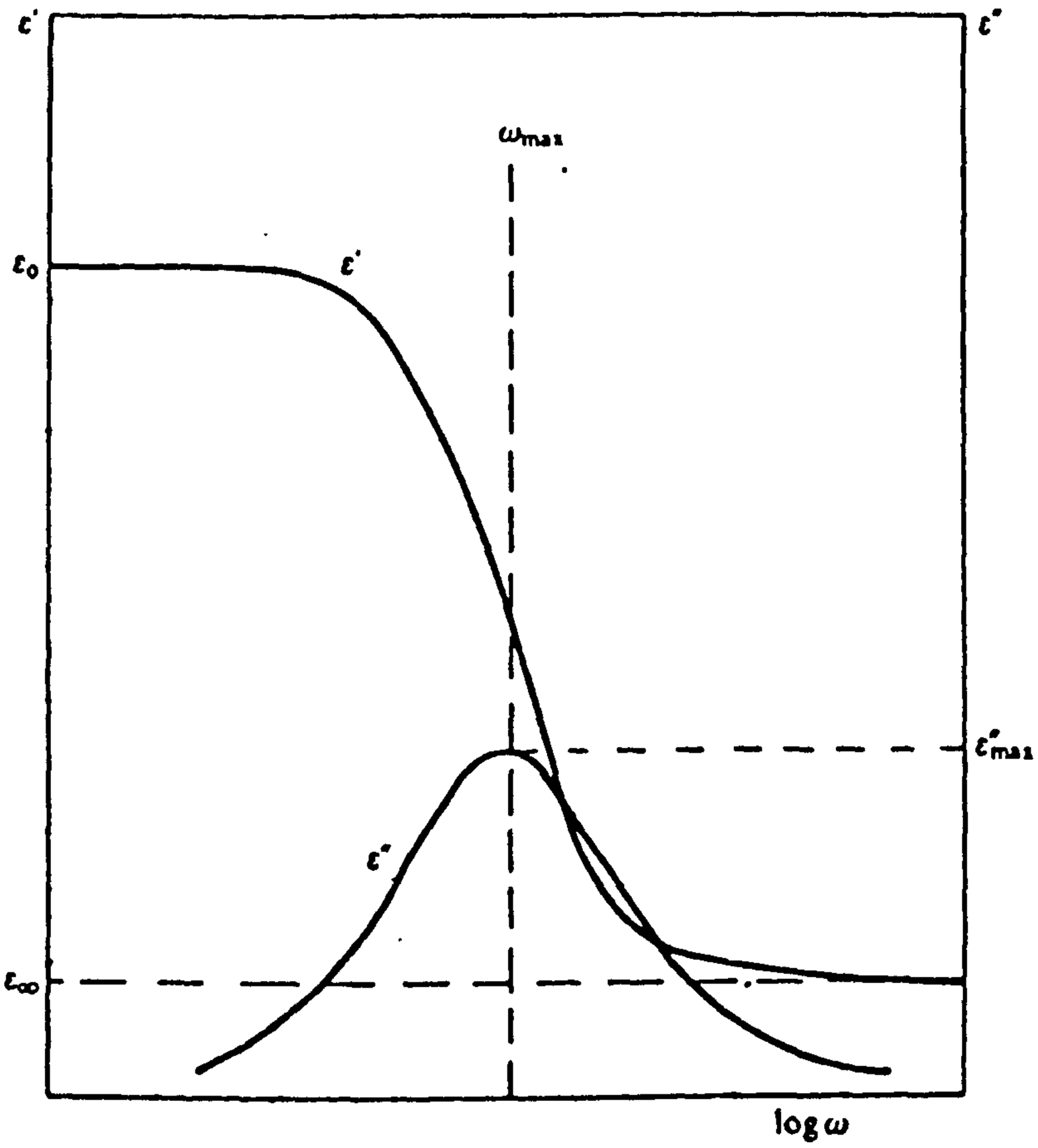


Fig. (4.13) Debye dielectric dispersion curves.
(ref. 23)

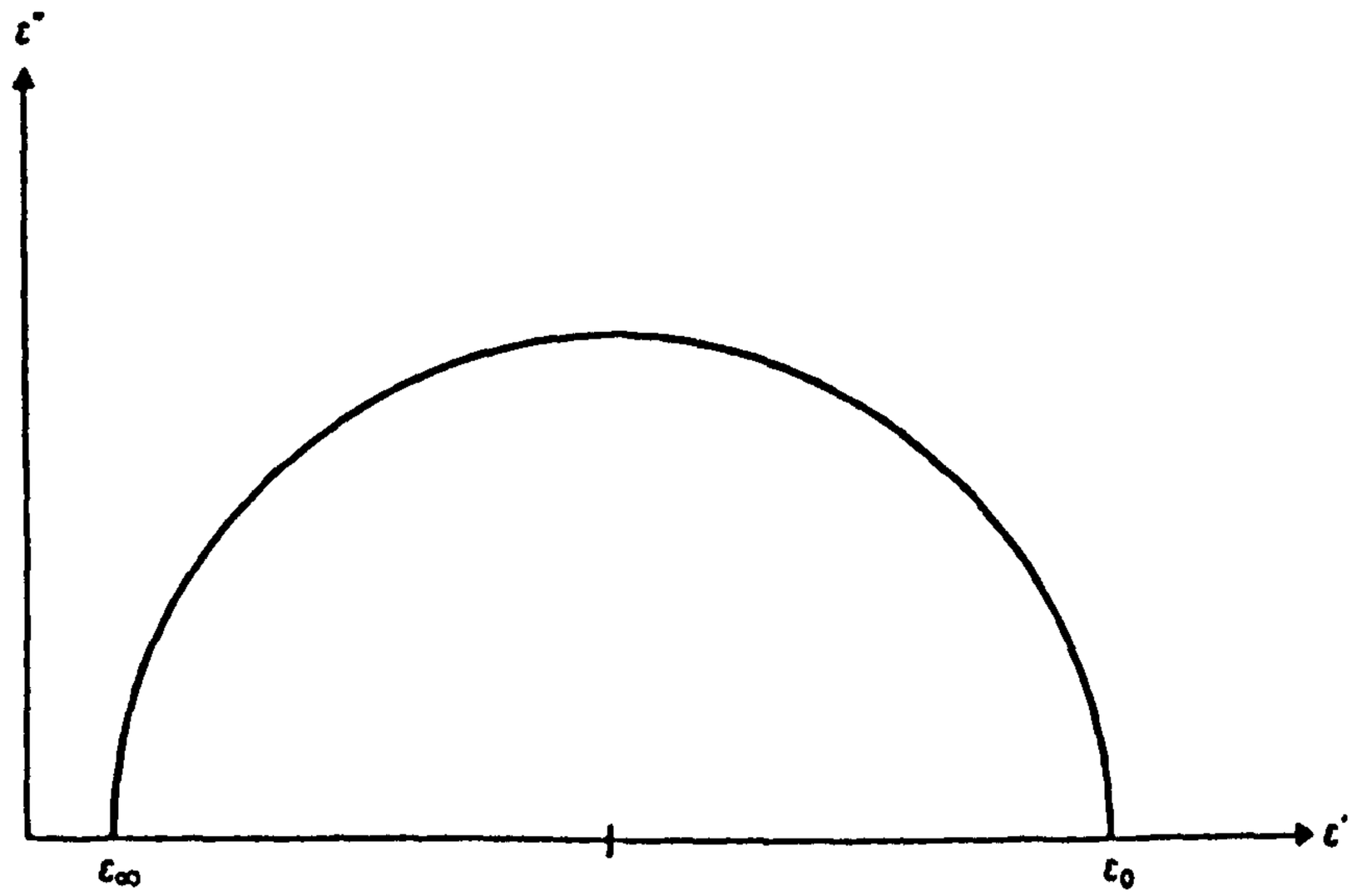


Fig. (4.14) Semicircular Cole-Cole plot.(ref. 23)

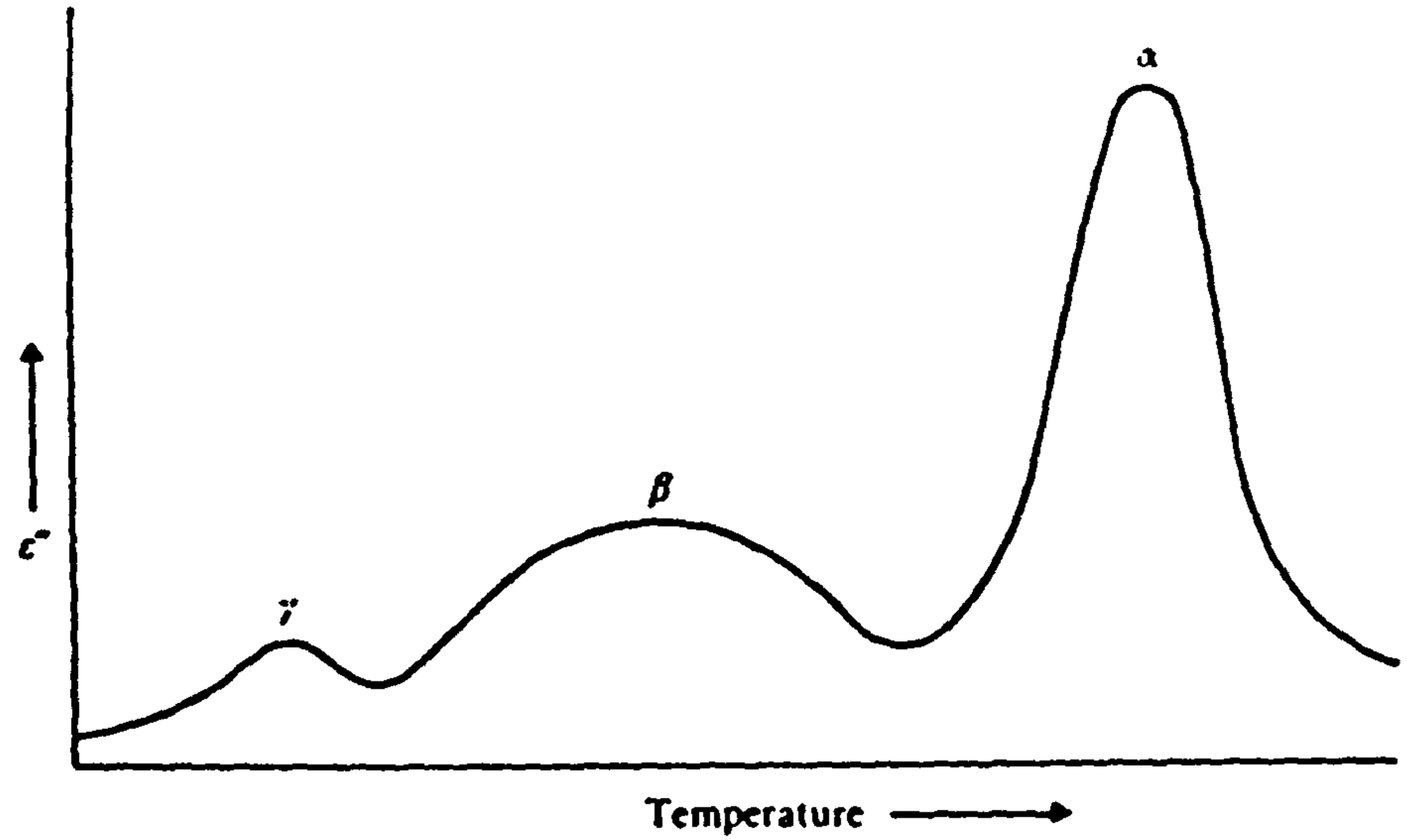


Fig. (4.15) A schematic dielectric loss curve.(ref. 23)

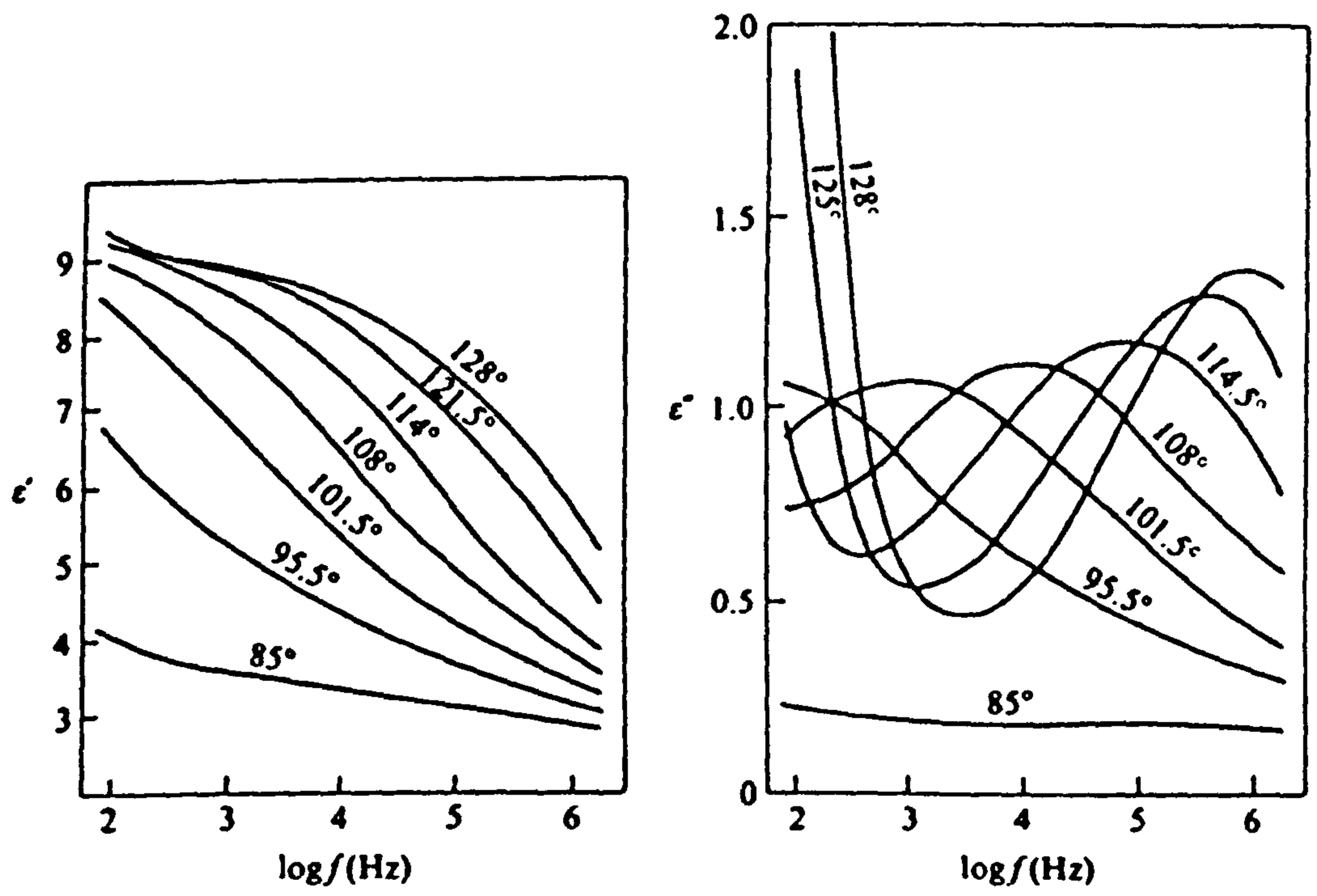


Fig. (4.16) Dielectric relaxation curves for poly(vinyl chloride) in the ∝-relaxation region.(ref. 23)

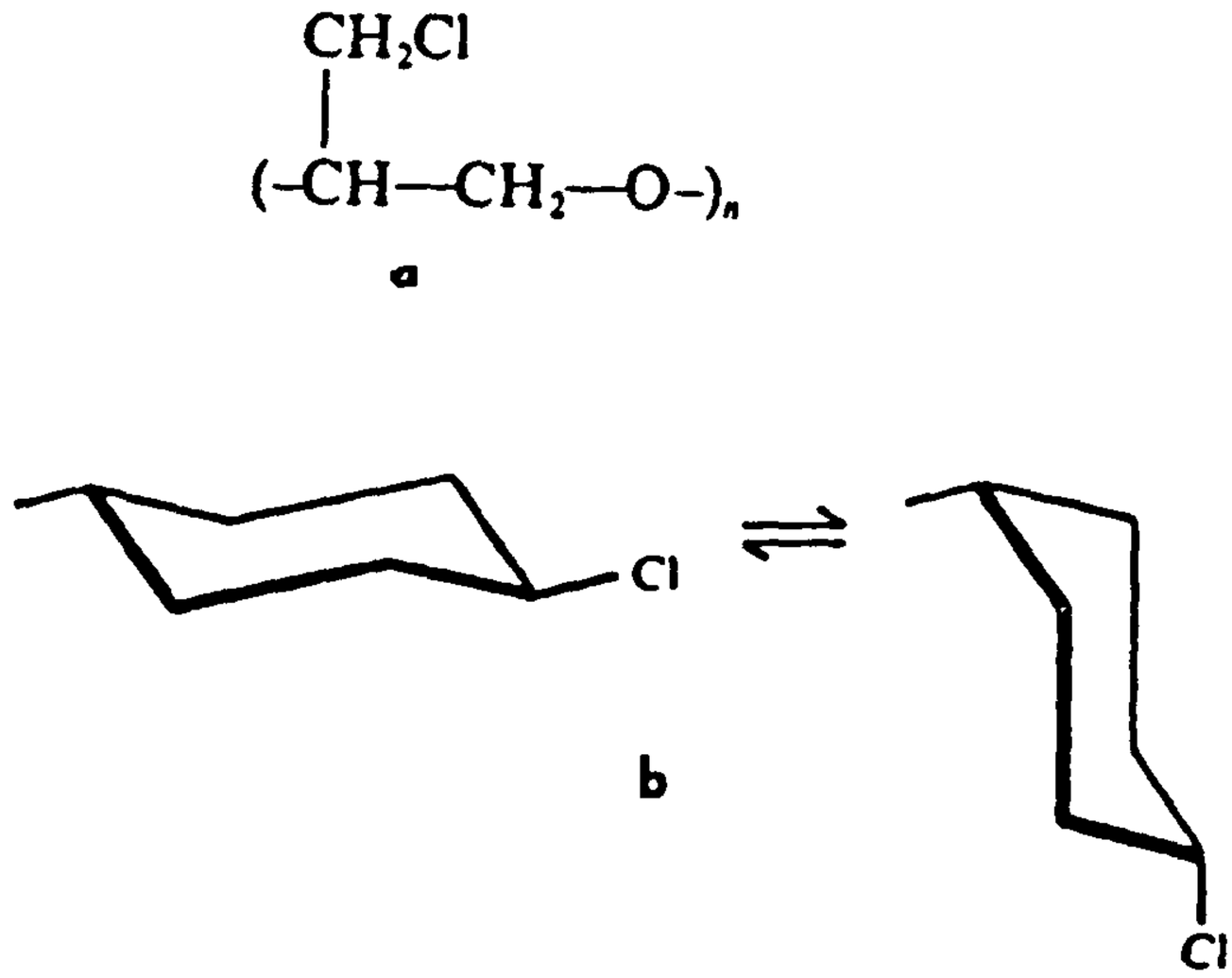


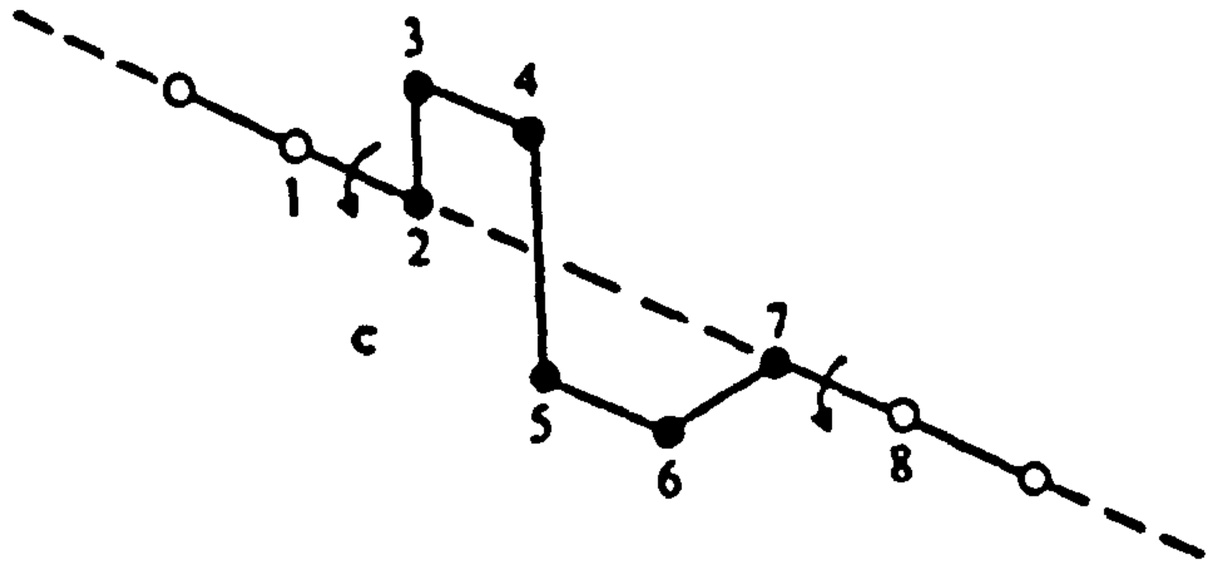


Fig. (4.17) Diagrams of molecular relaxation mechanisms a- rotation of a side group about a C-C bond, b- conformational flip of chlorohexane, c- crankshaft rotation in polyethylene. (ref. 23)

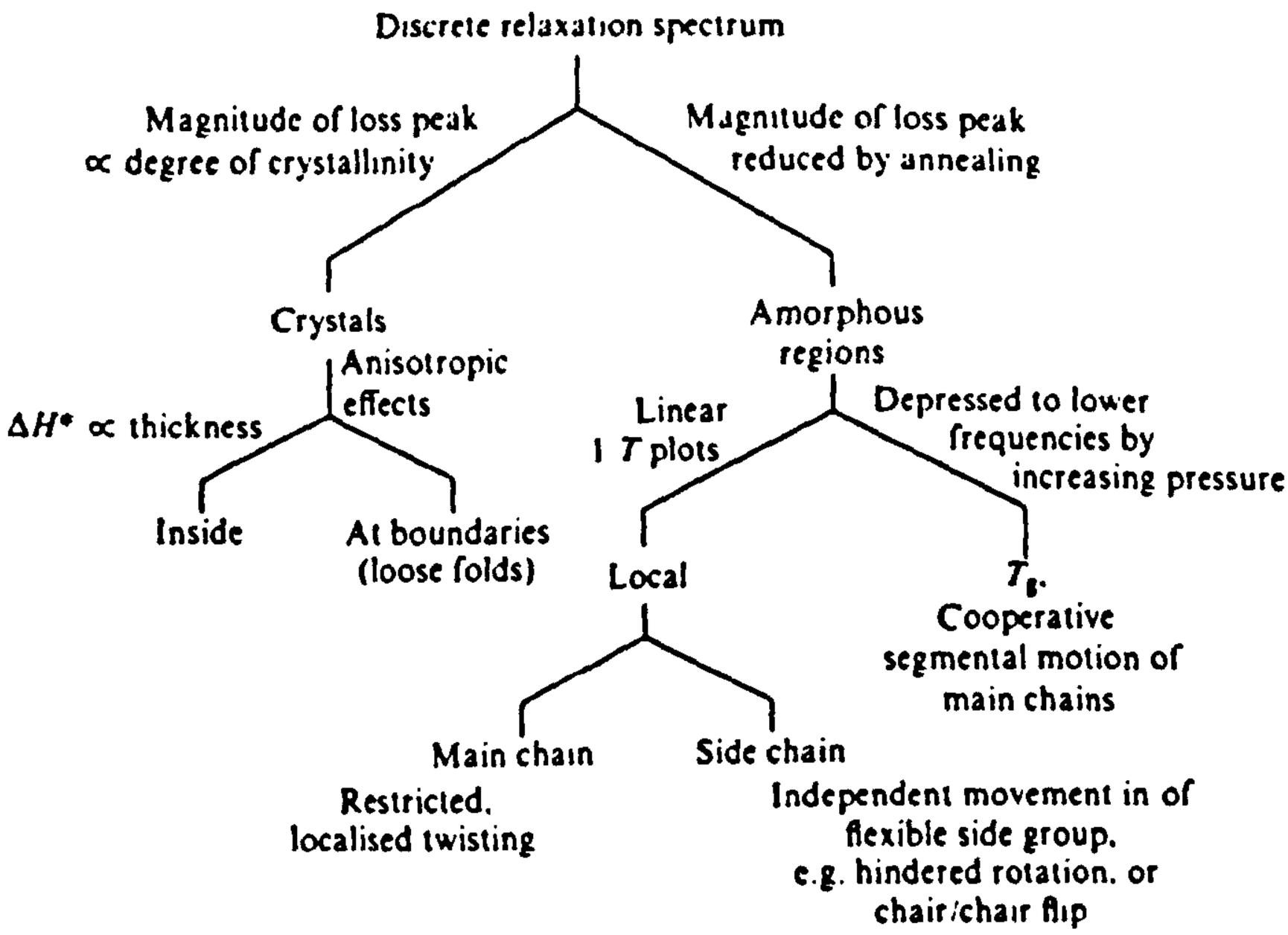


Fig. (4.18) Generalised pattern of dielectric relaxation processes in polymers. (ref. 23)

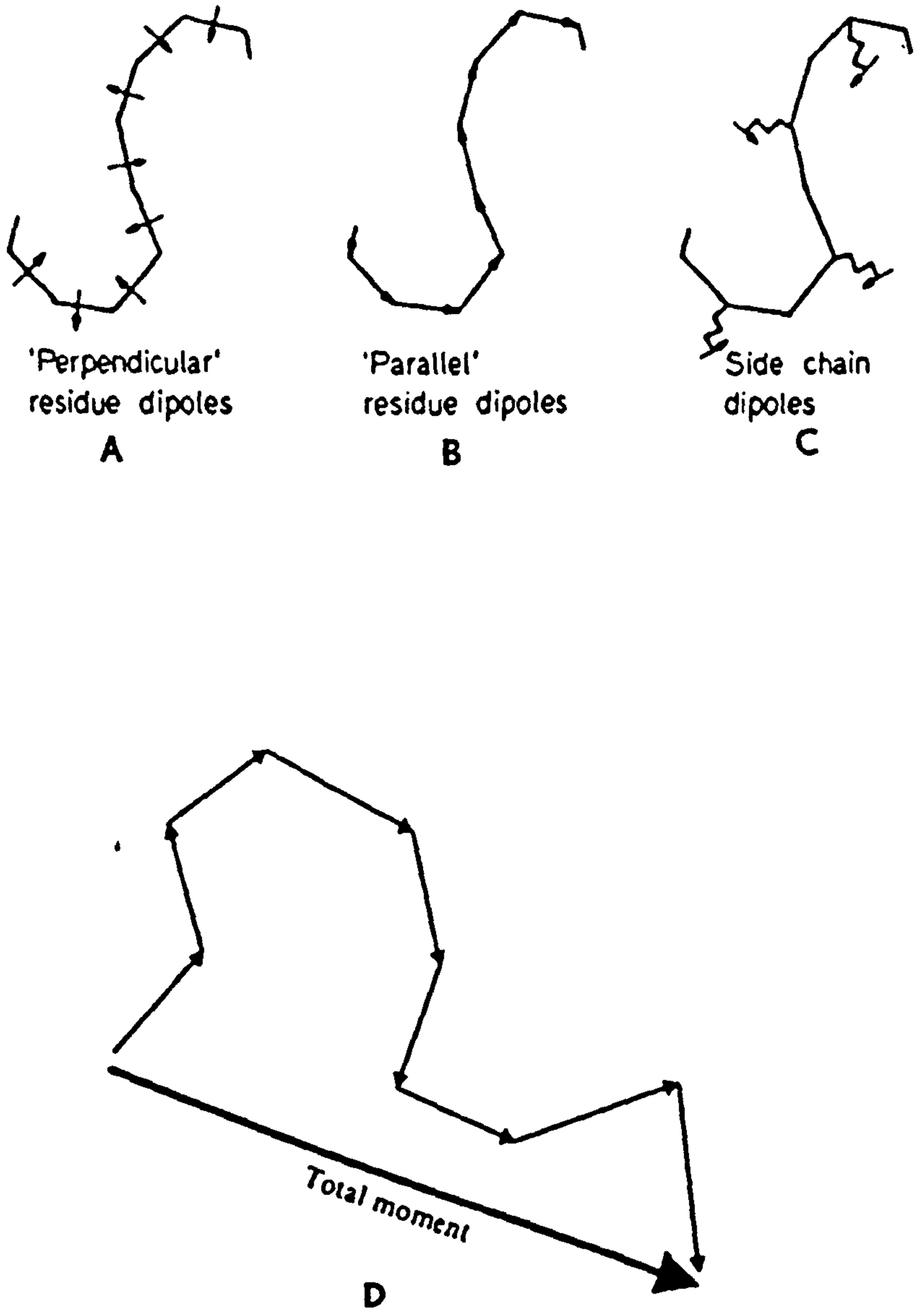


Fig. (4.19) Perpendicular (a), parallel (b) and side-chain residue (c) dipoles in a polymer chain. (d) Vectorial addition of unit dipoles along a polymer chain. (ref. 23)

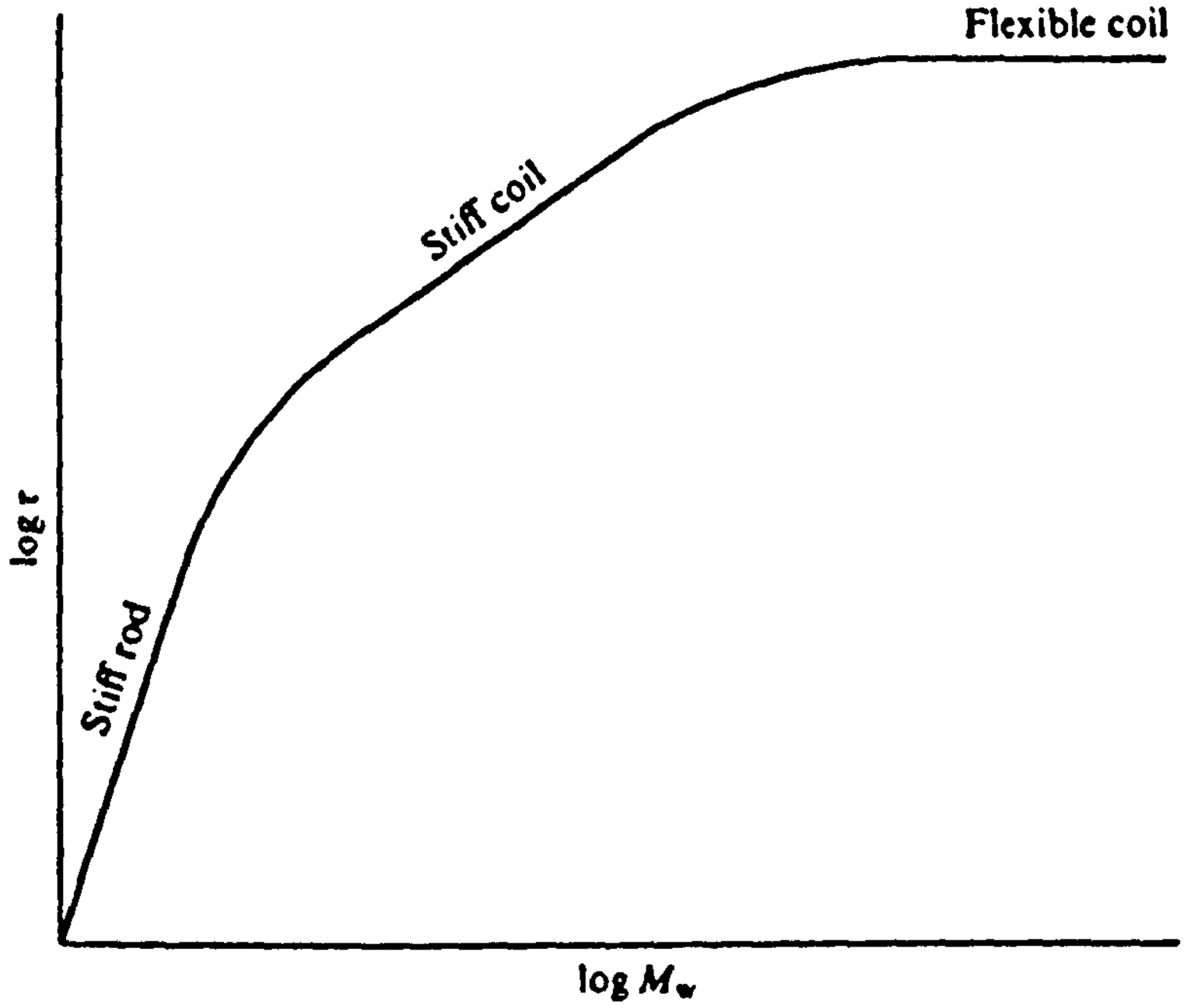


Fig. (4.20) Schematic molecular-weight dependence of the relaxation time for whole-molecule rotation. (ref. 23)

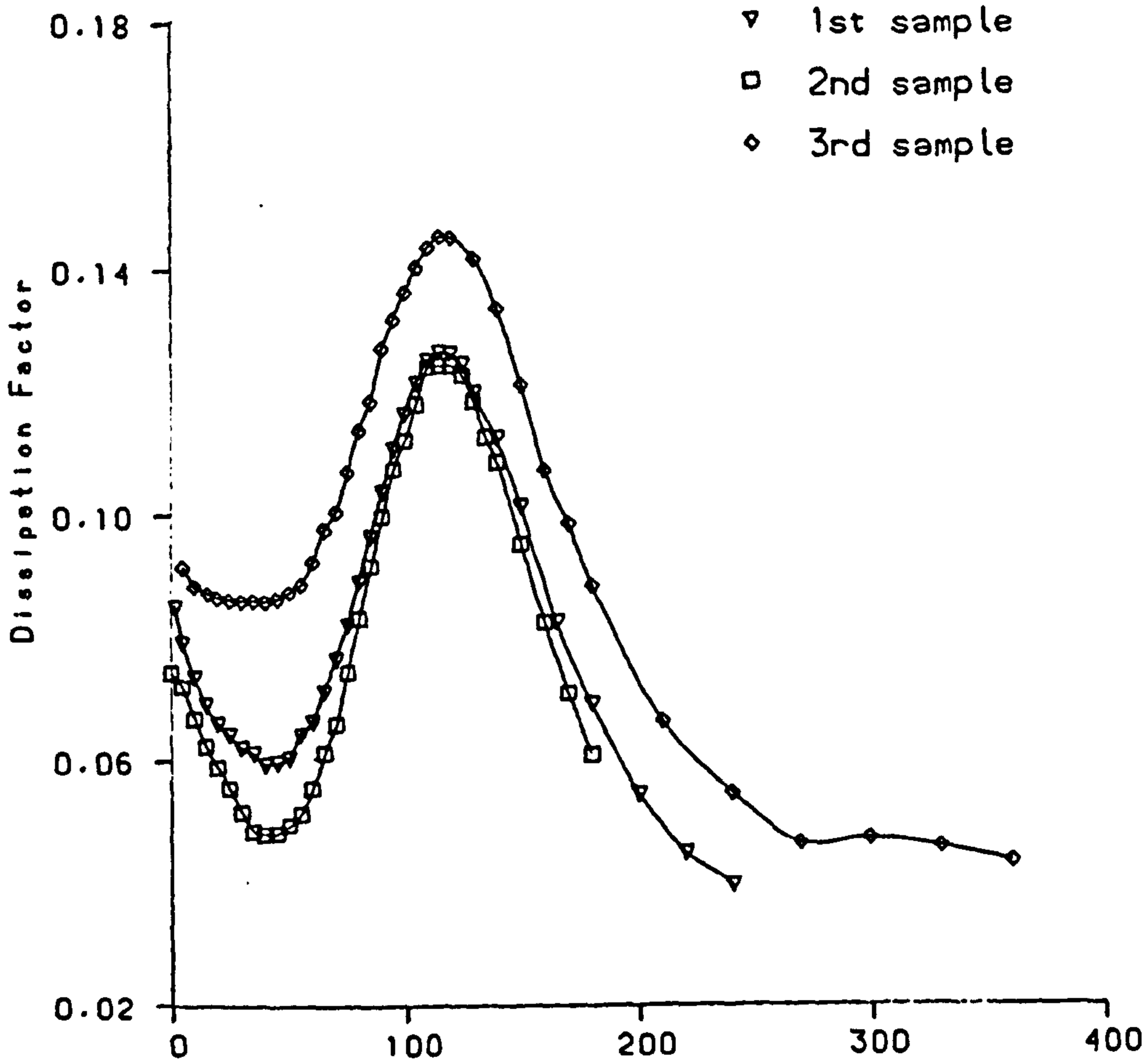


Fig. (4.21a) Dissipation factor versus reaction time for MY750/HY956 sample at room temperature.

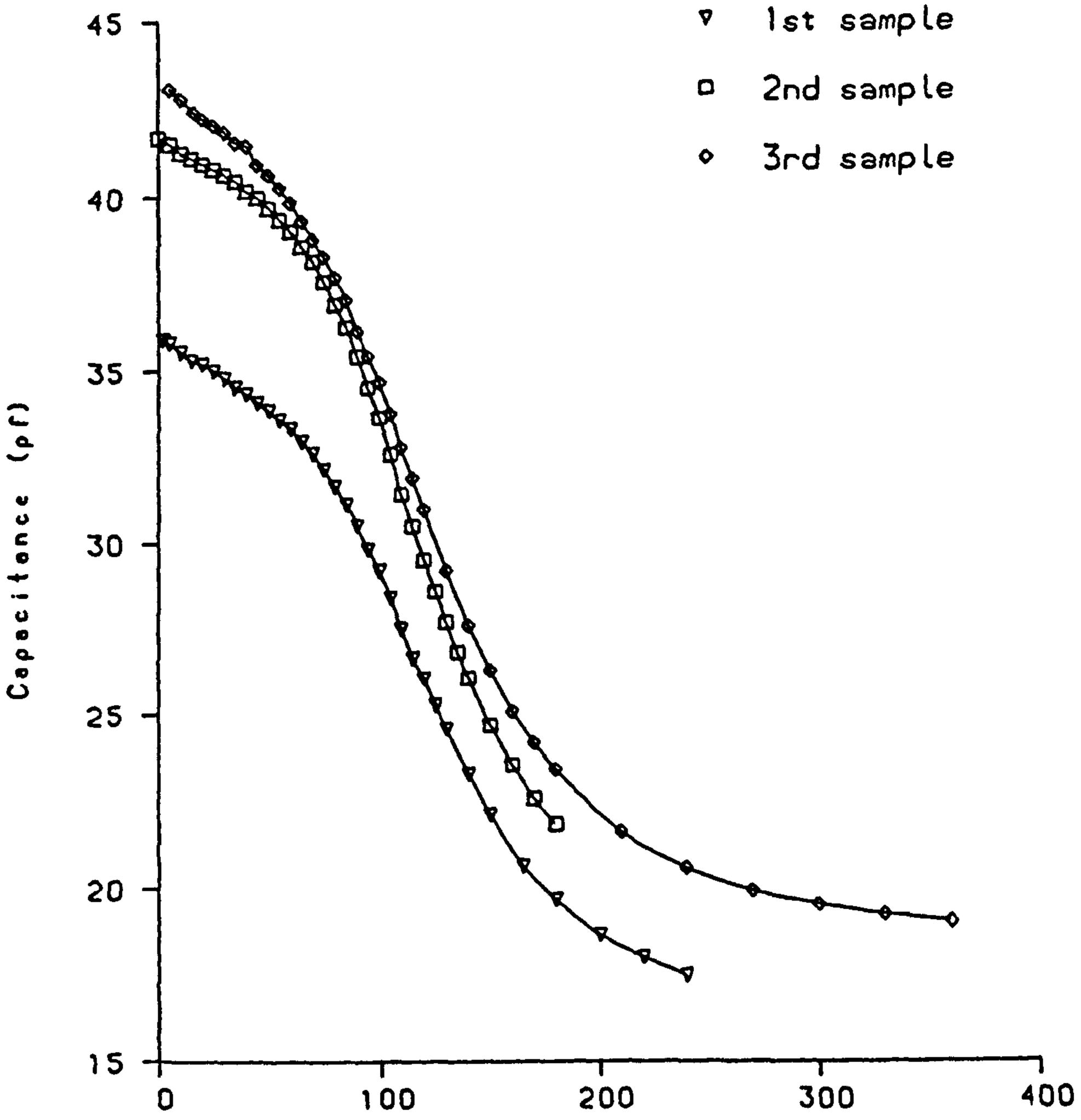


Fig. (4.21b) Capacitance versus reaction time for MY750/HY956 sample at room temperature.

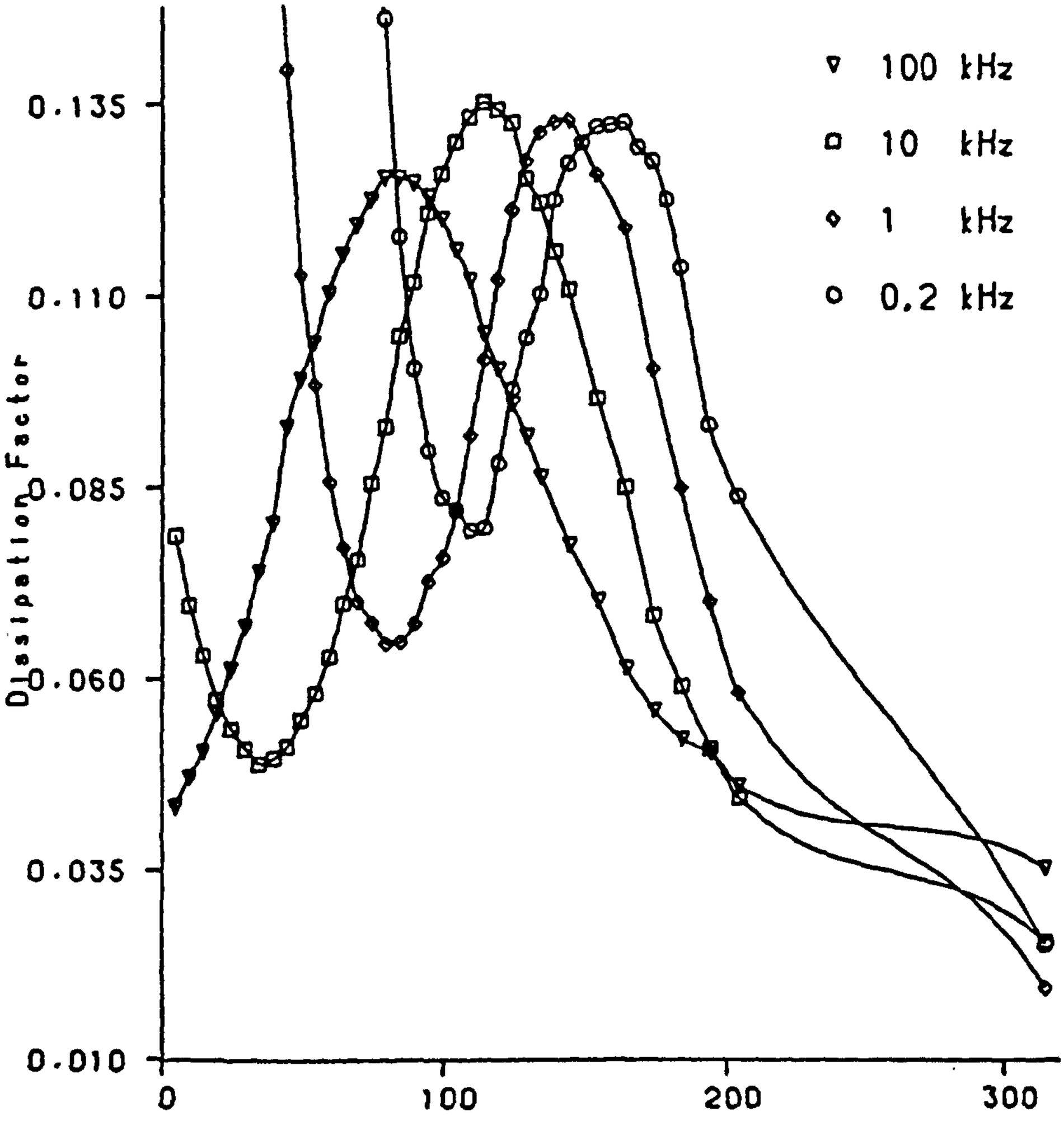


Fig. (4.22a) Dissipation factor versus reaction time for MY750/HY956 sample at different frequencies at 20 °C during curing.

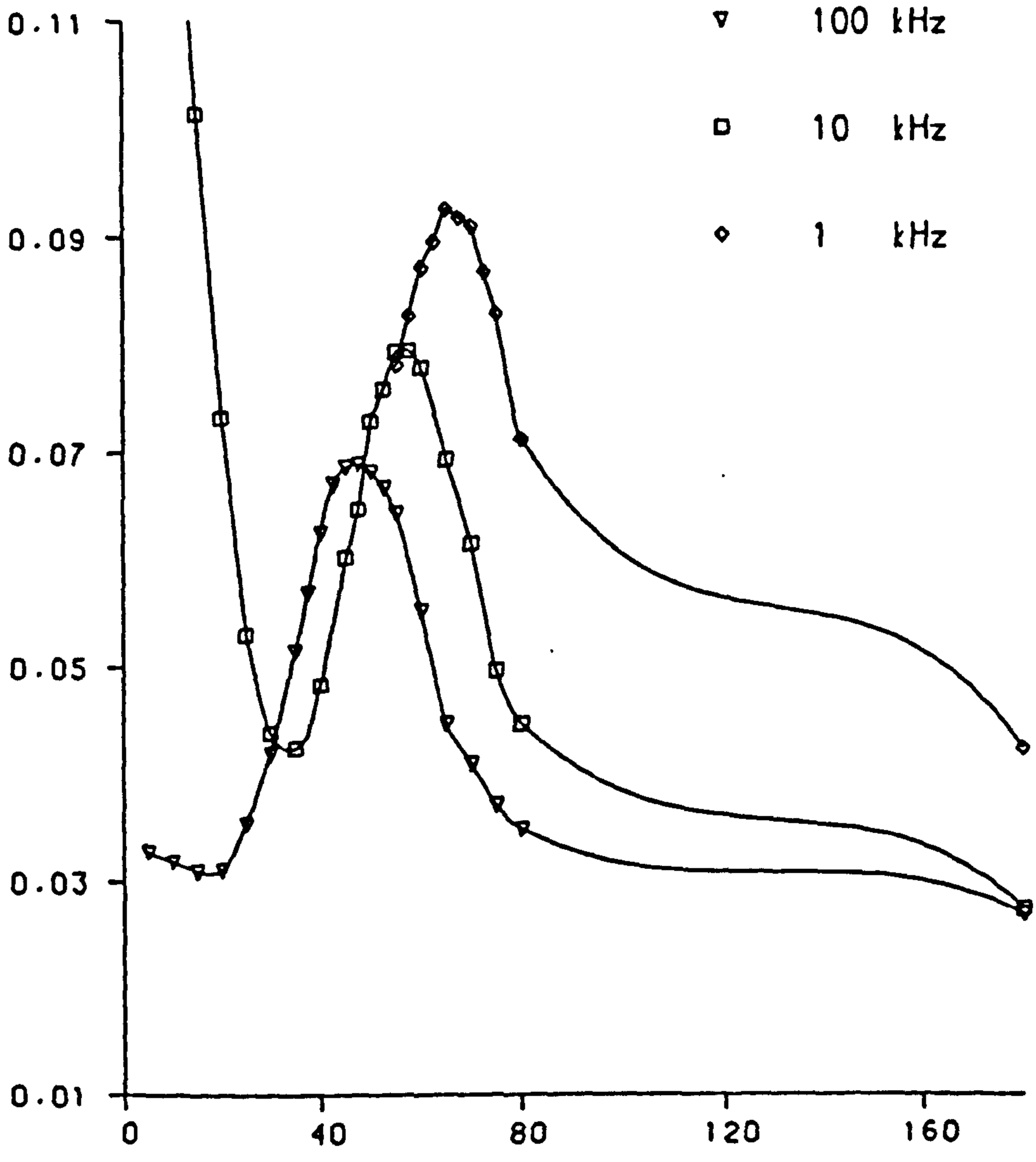


Fig. (4.22b) Dissipation factor versus reaction time for MY750/HY956 sample at different frequencies at 40 °C during curing.

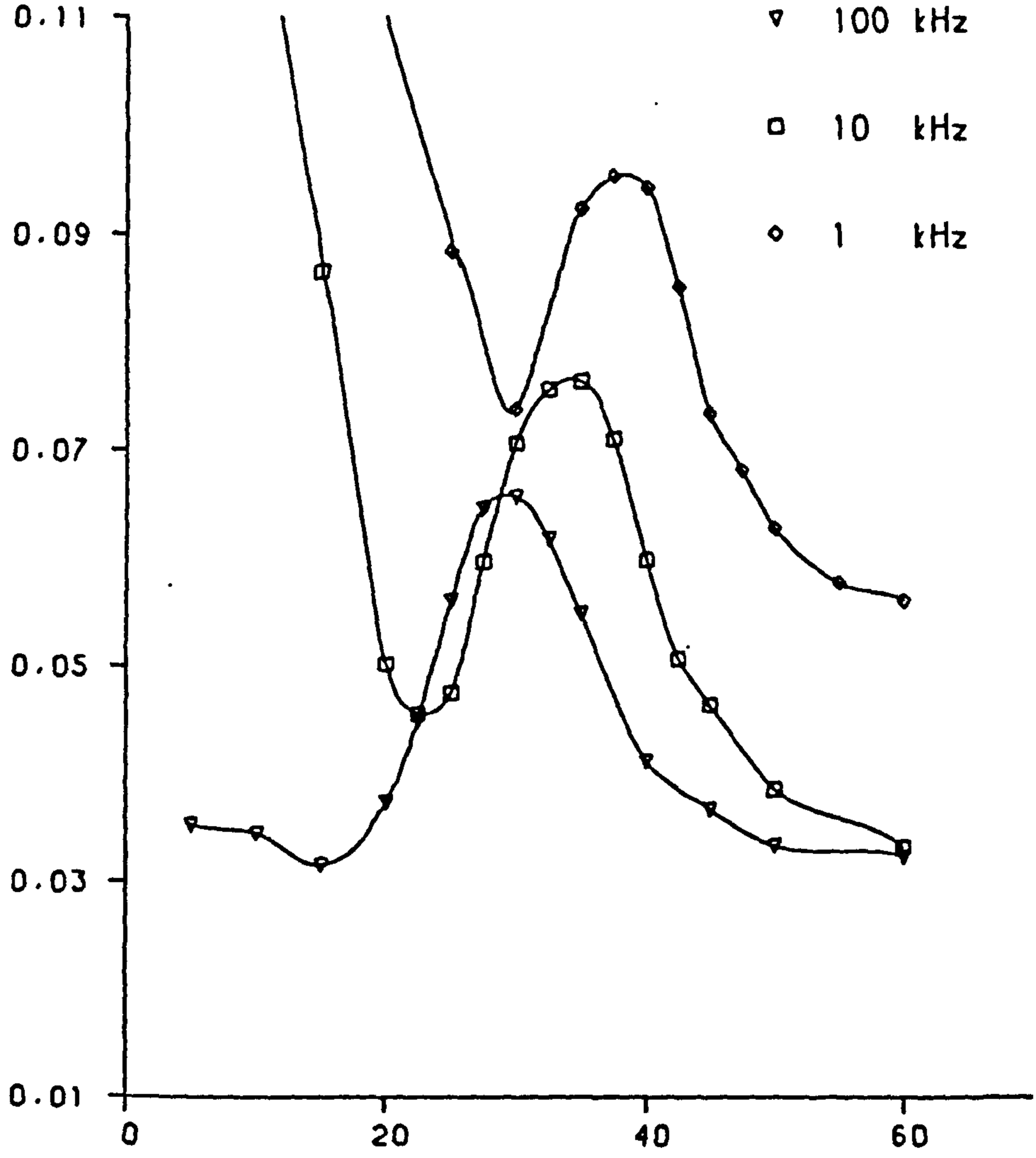


Fig. (4.22c) Dissipation factor versus reaction time for MY750/HY956 sample at different frequencies at 60 °C during curing.

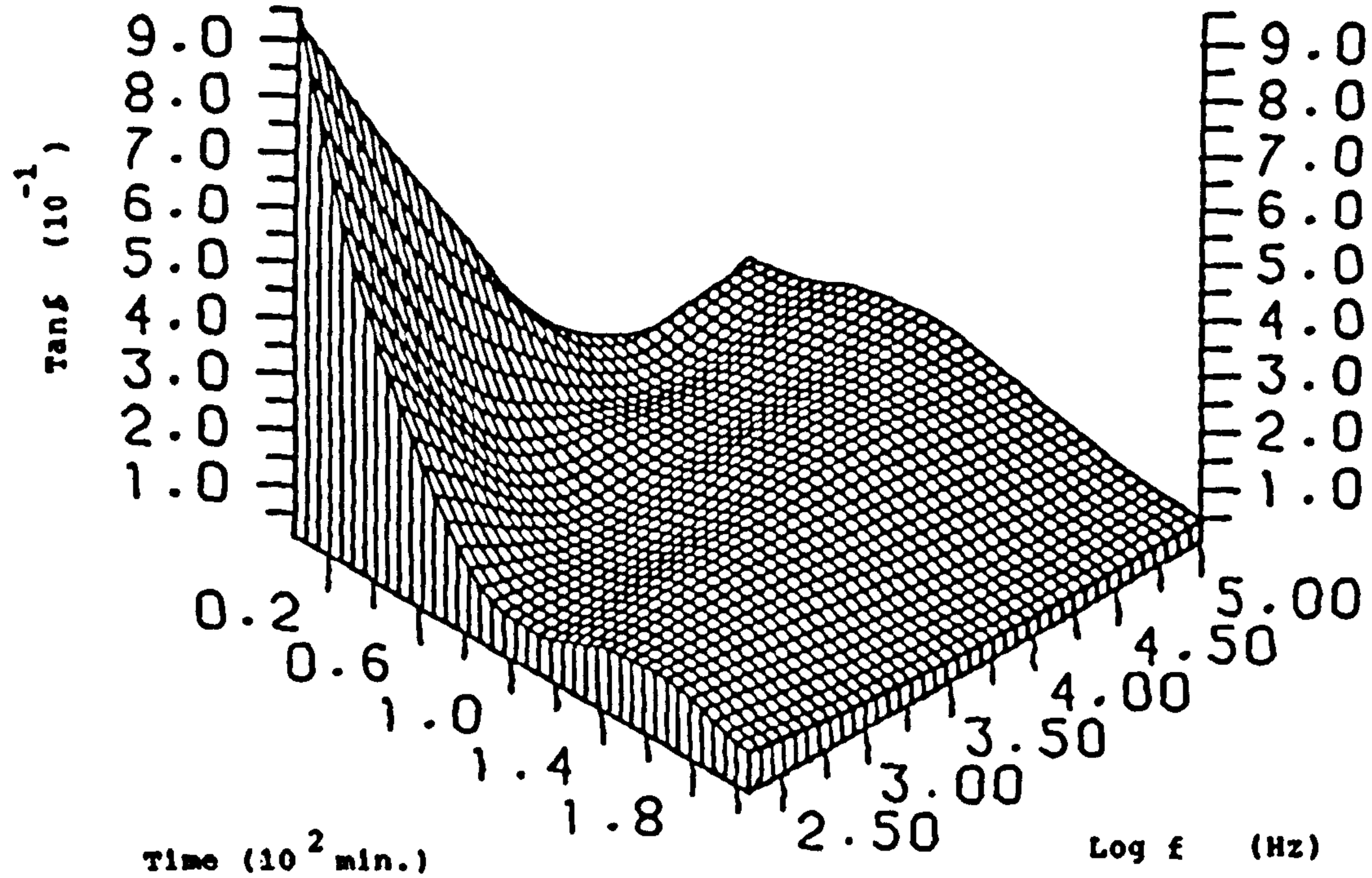


Fig. (4.22d) Dissipation factor versus reaction time for HY750/HY956 sample at different frequencies at 20 C in three dimension graphs during curing.

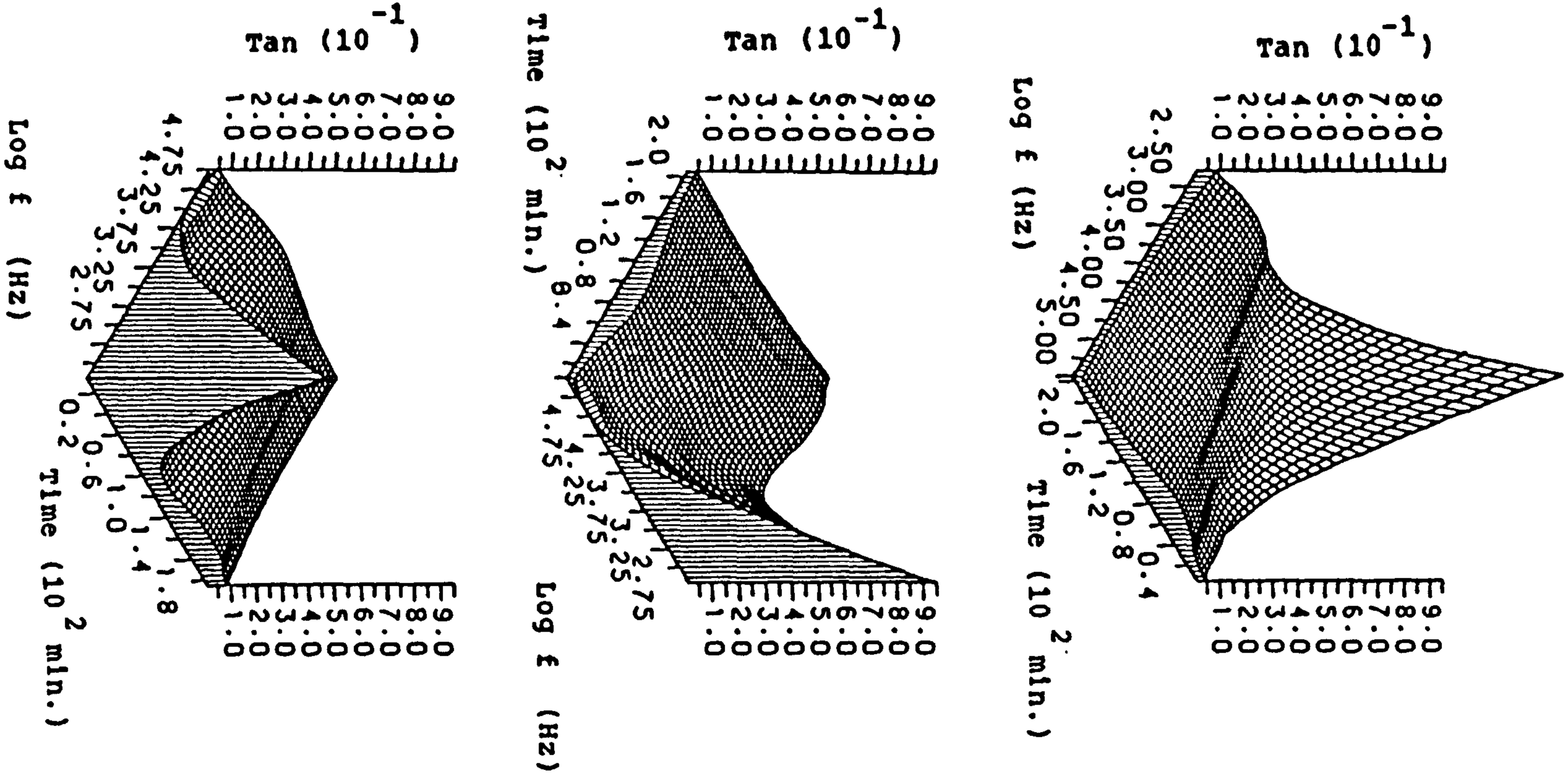


Fig. (4.22e) Dissipation factor versus reaction time for MY750/HY956 sample at different frequencies at 20 °C in three dimension graphs (in three different views) during curing.

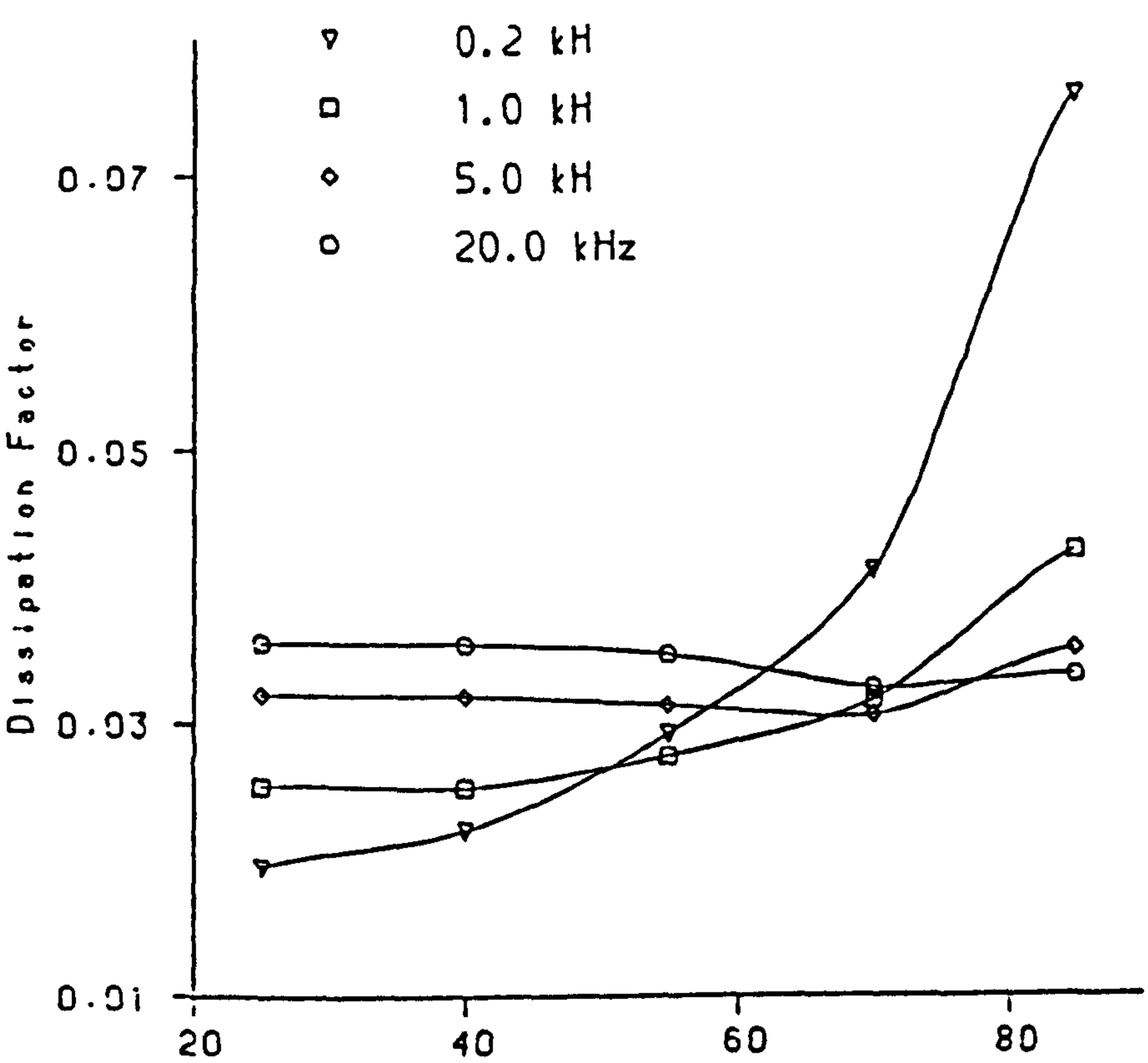


Fig. (4.23) Dissipation factor versus temperature for cured MY750/HY956 sample at different frequencies.

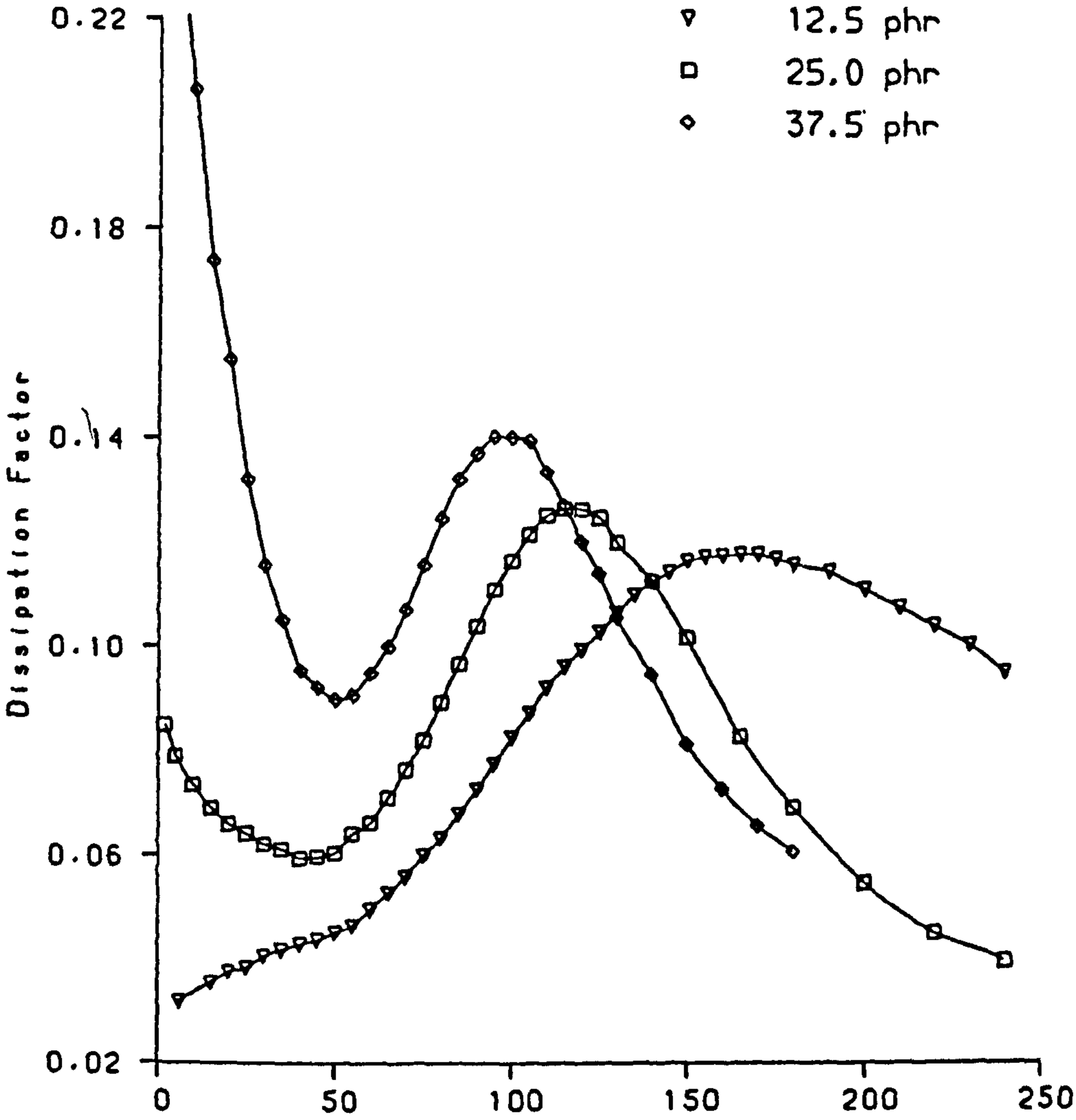


Fig. (4.24) Dissipation factor versus reaction time for MY750/HY956 sample for different concentration of hardener at room temperature.

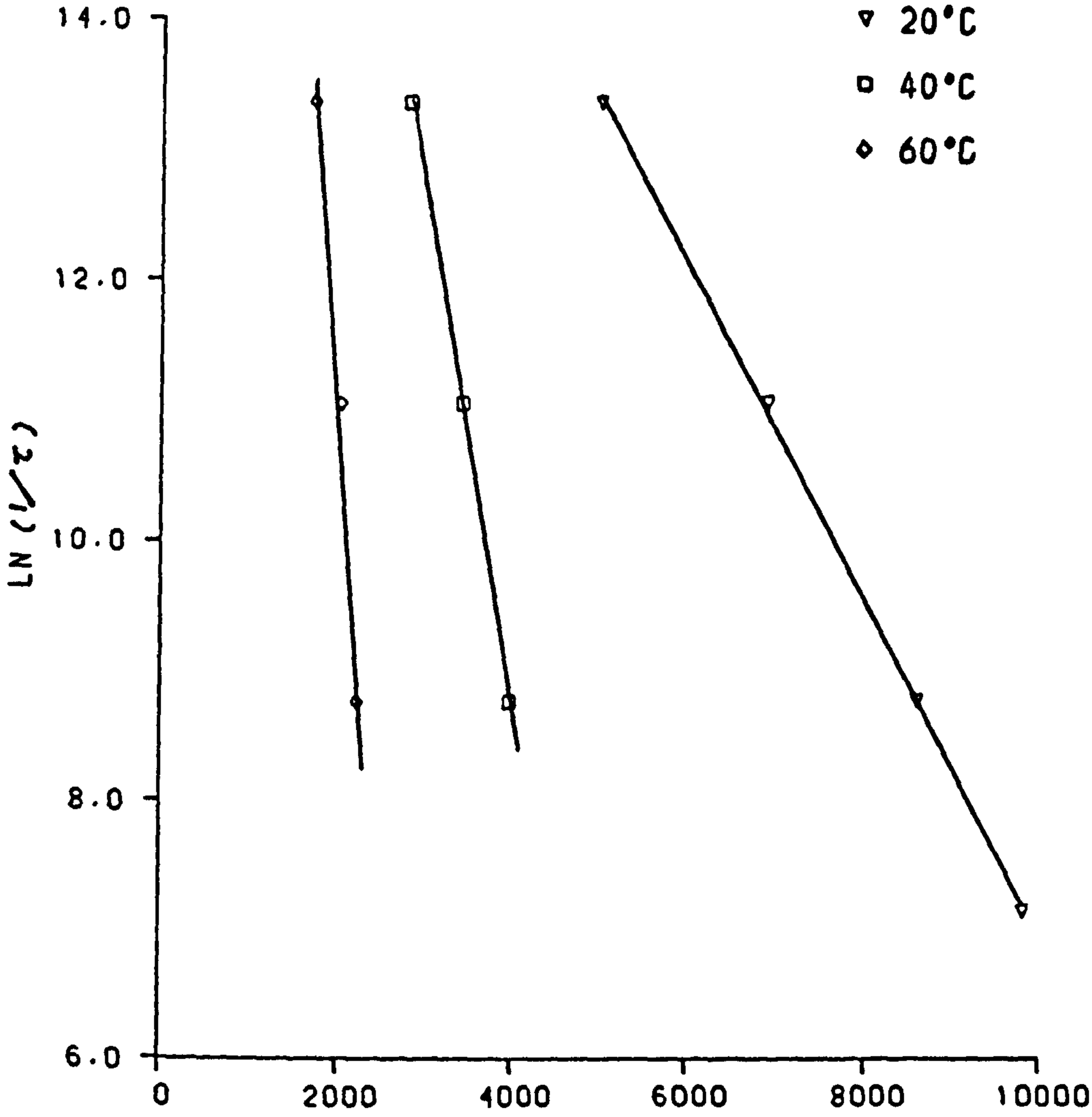


Fig. (4.25) Ln $1/t$ versus time for MY750/HY956 sample at different temperature.

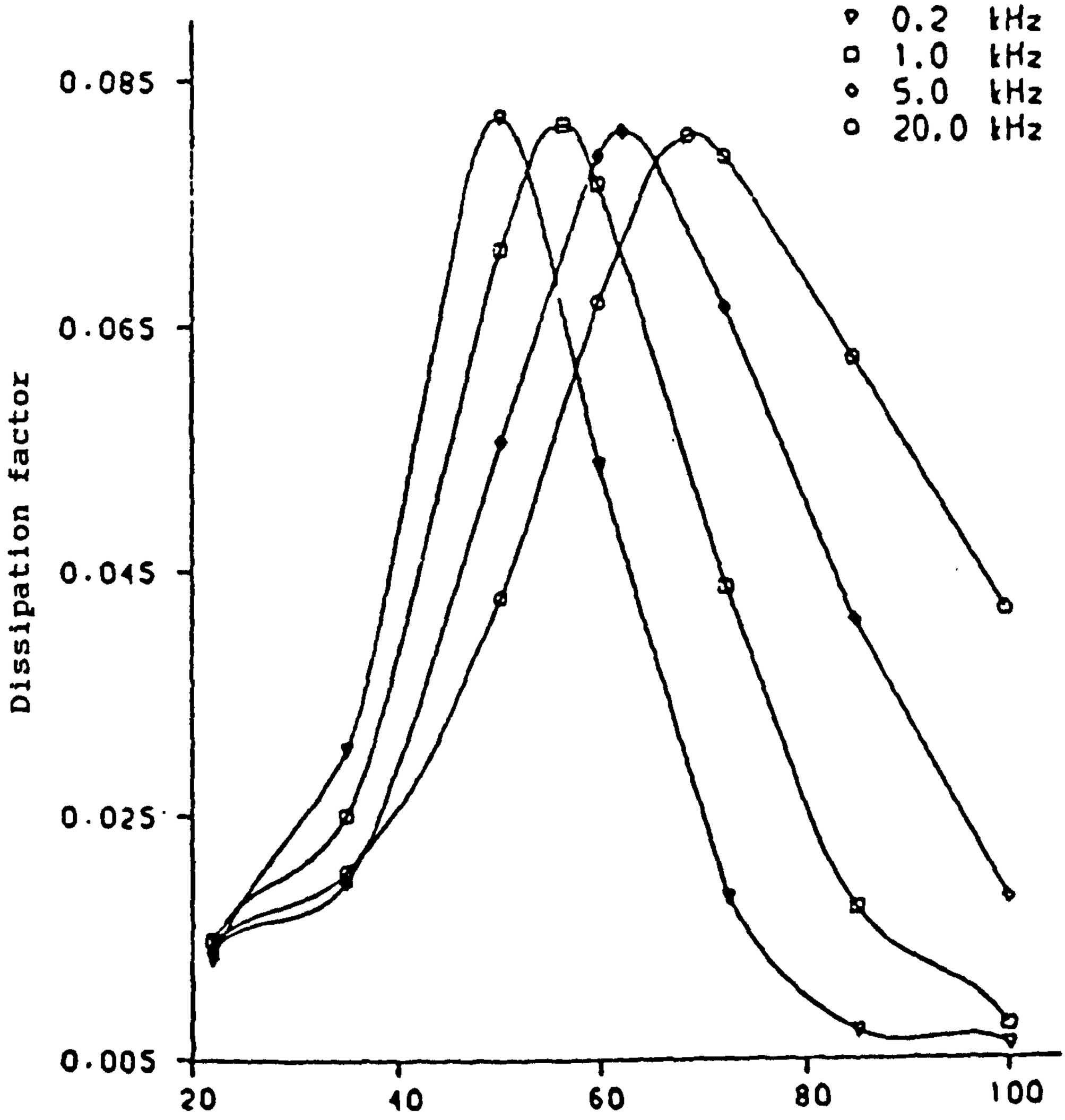


Fig. (4.26a) Dissipation factor versus temperature for cured MY750/DDSA sample.

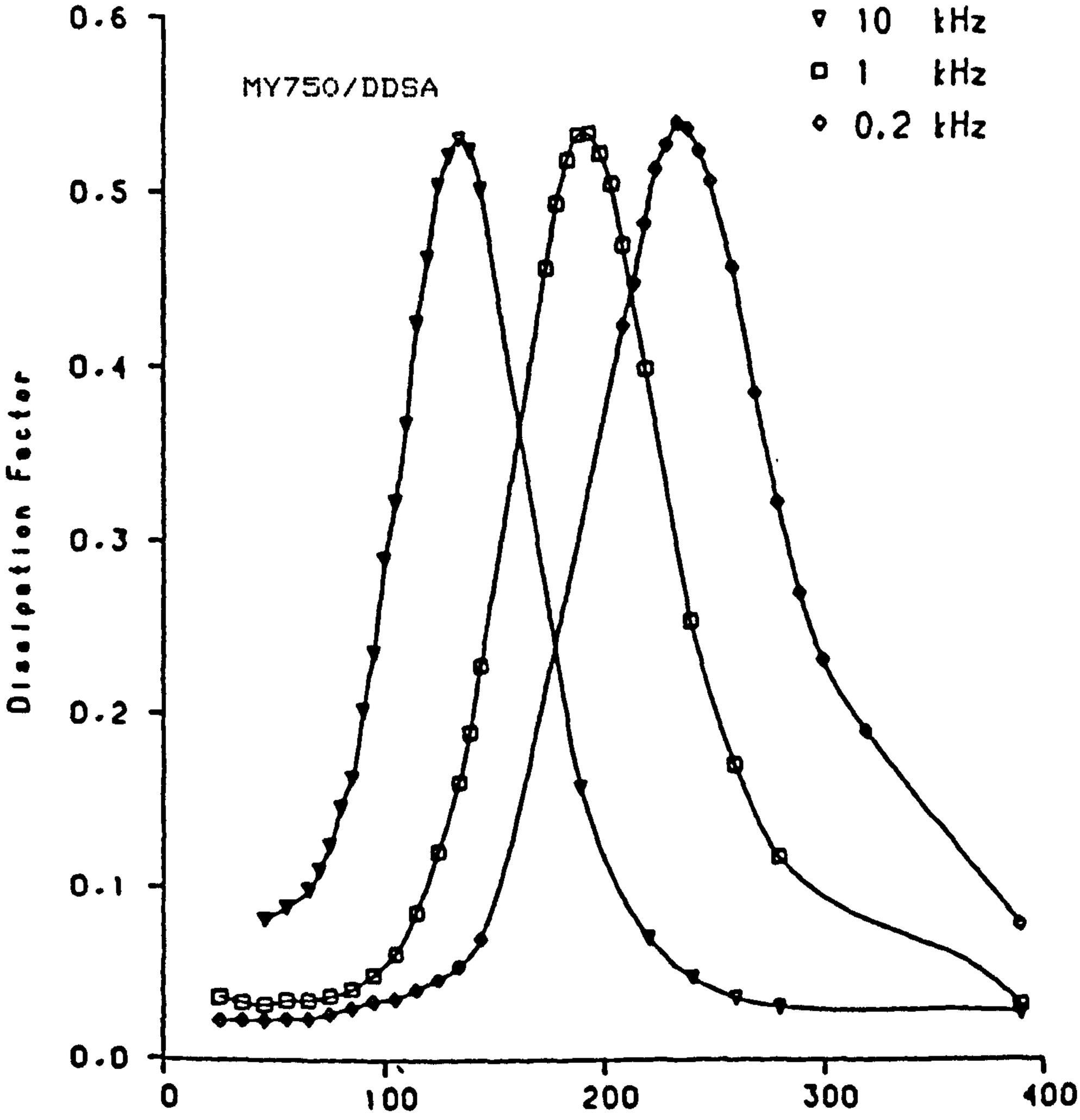


Fig. (4.26b) Dissipation factor versus reaction time During curing at 90°C.

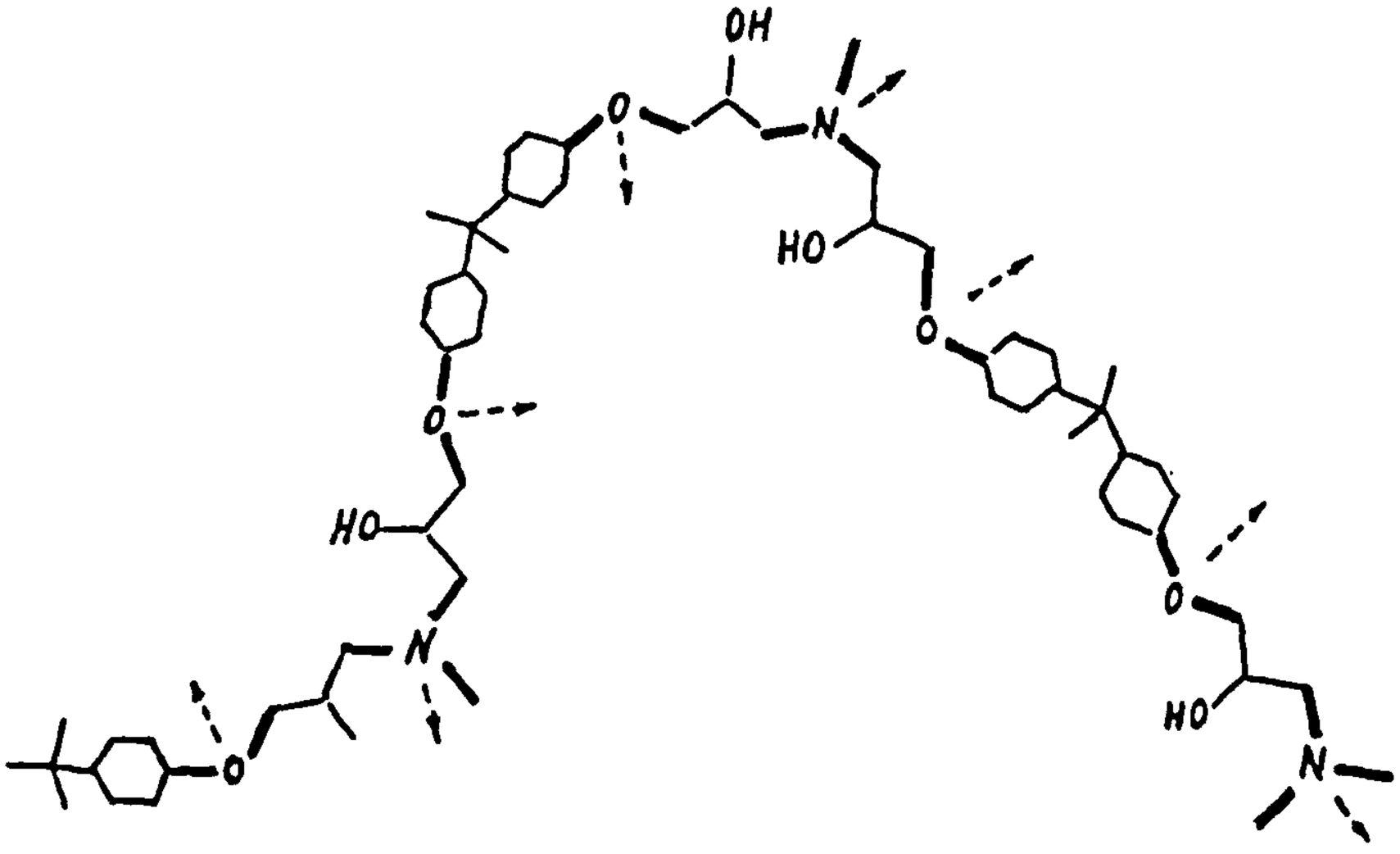


Fig. (4.27) The schematic diagram of polymer molecule of Epoxy/Amine system before gelation. (where "---" is the dipole of polar chemical bond attached to the backbone).

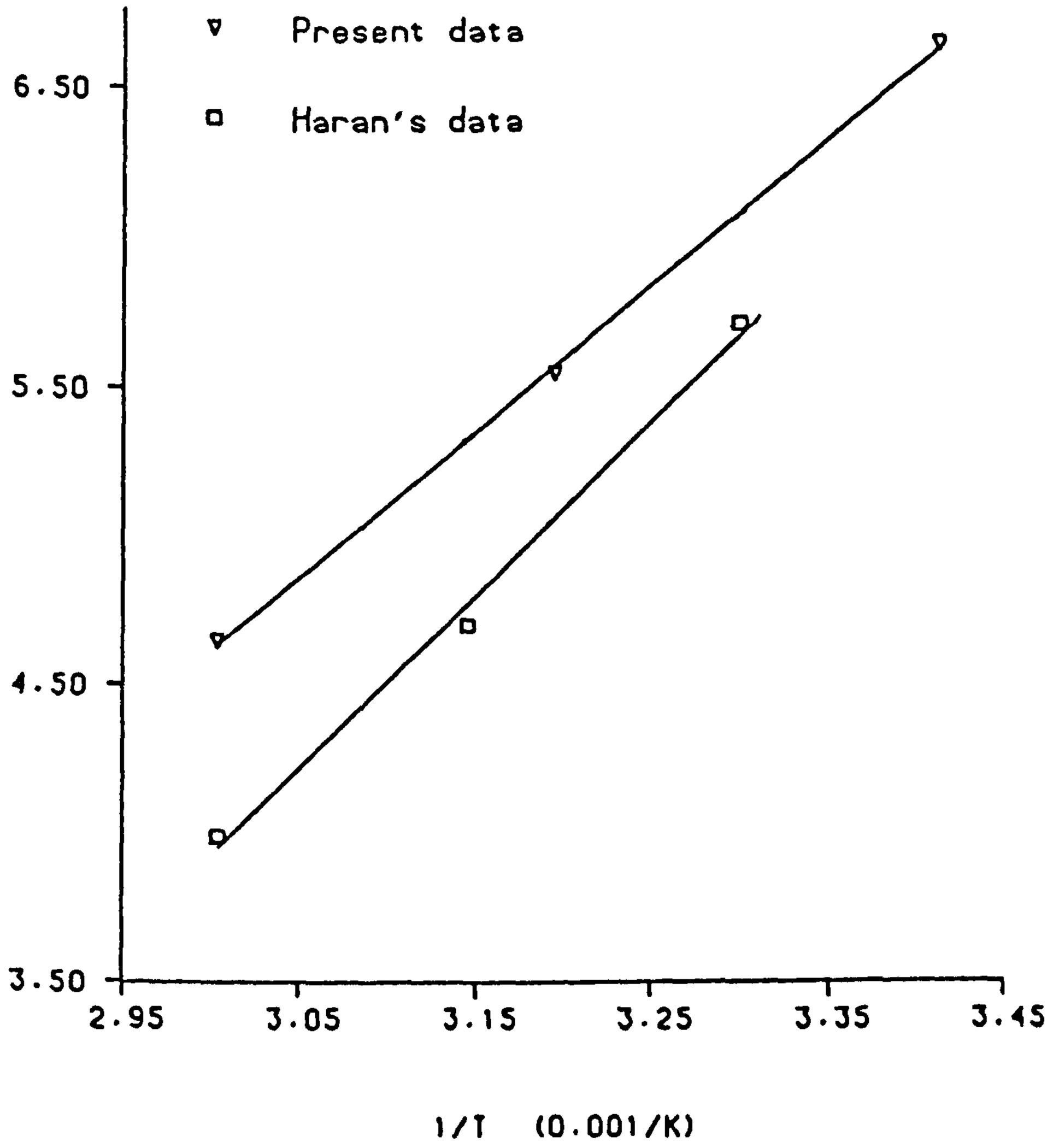


Fig. (4.28) Ln slope of fig. (4.25) versus 1/T for MY750/HY956 sample and for Haran's data.

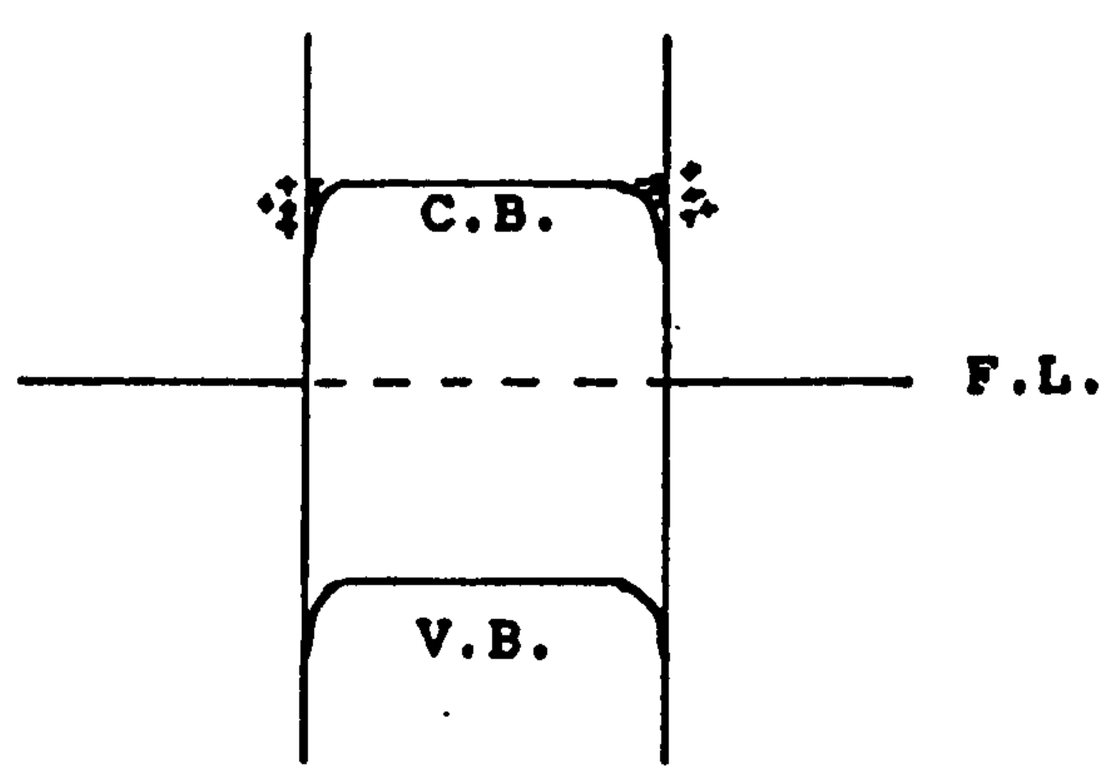


Fig. (5.1) Metal-Insulator-Metal contact.

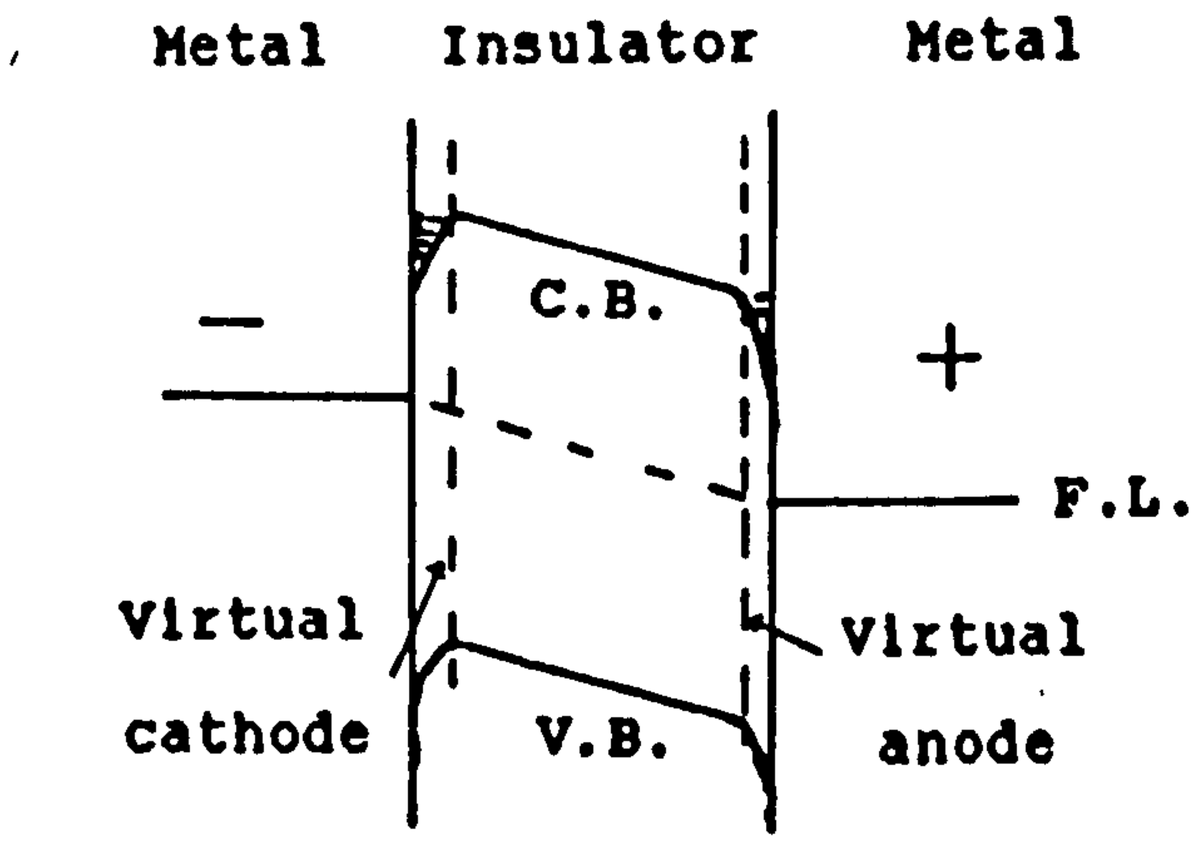


Fig. (5.2) Metal-Insulator-Metal contact with voltage bias.


Fig. (5.3) One-Carrier space charge limited current-voltge characteristic for an insulator with a single trap level.

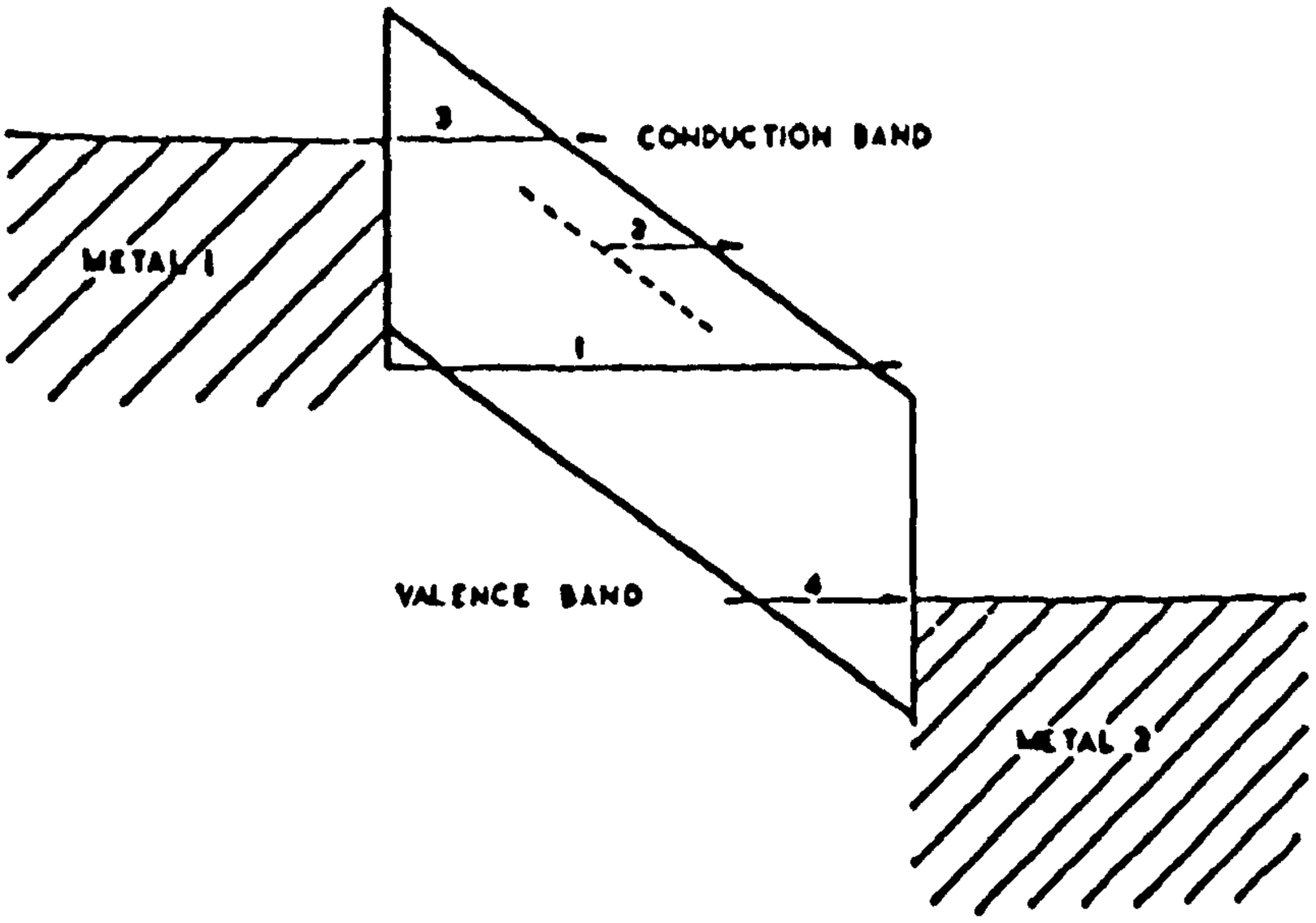


Fig. (5.4) Possible tunneling and internal field emission in metal-insulator-metal films.

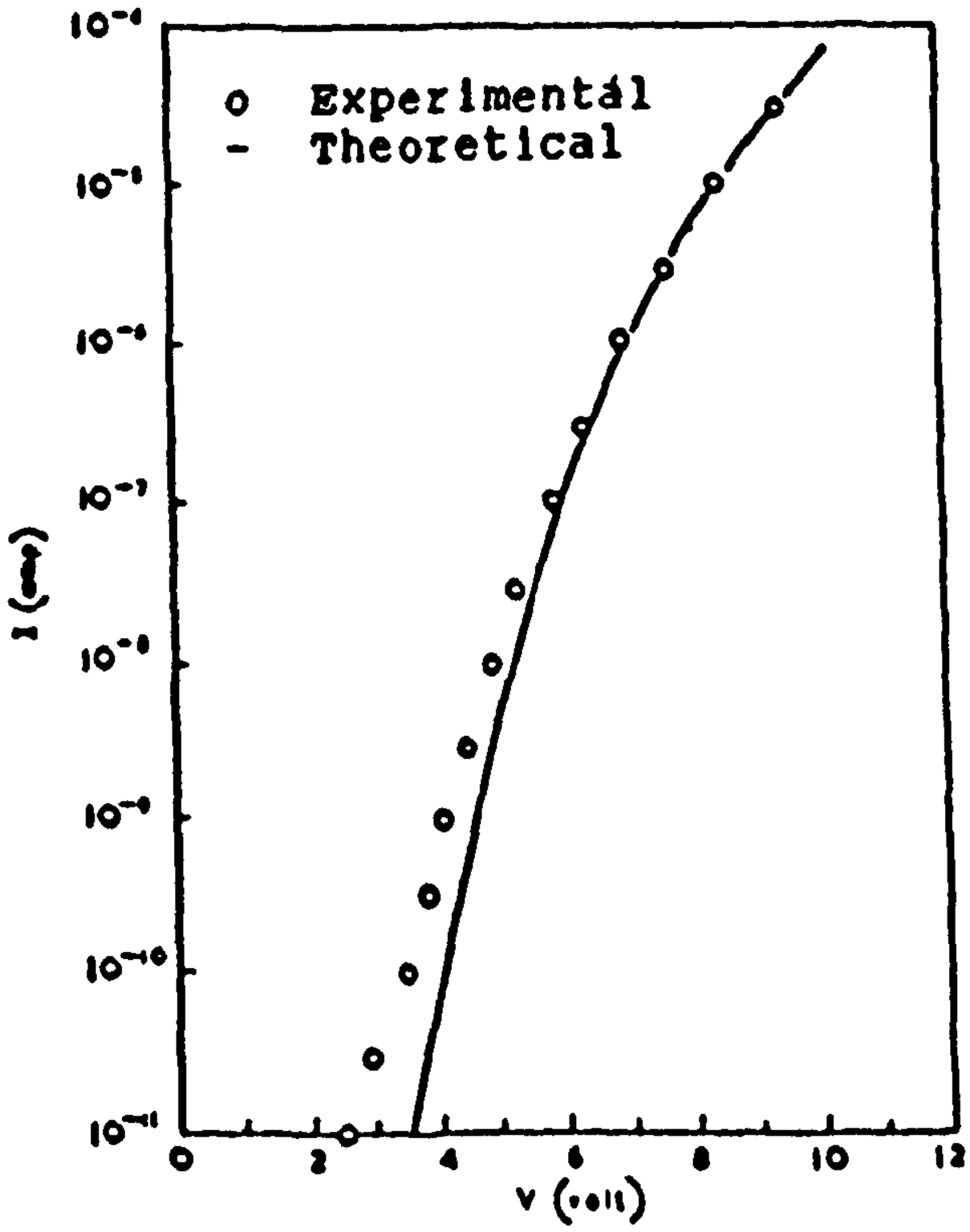


Fig. (5.5) Current-Voltage characteristic for tunneling into the conduction band of the insulator. (Ref. 102)

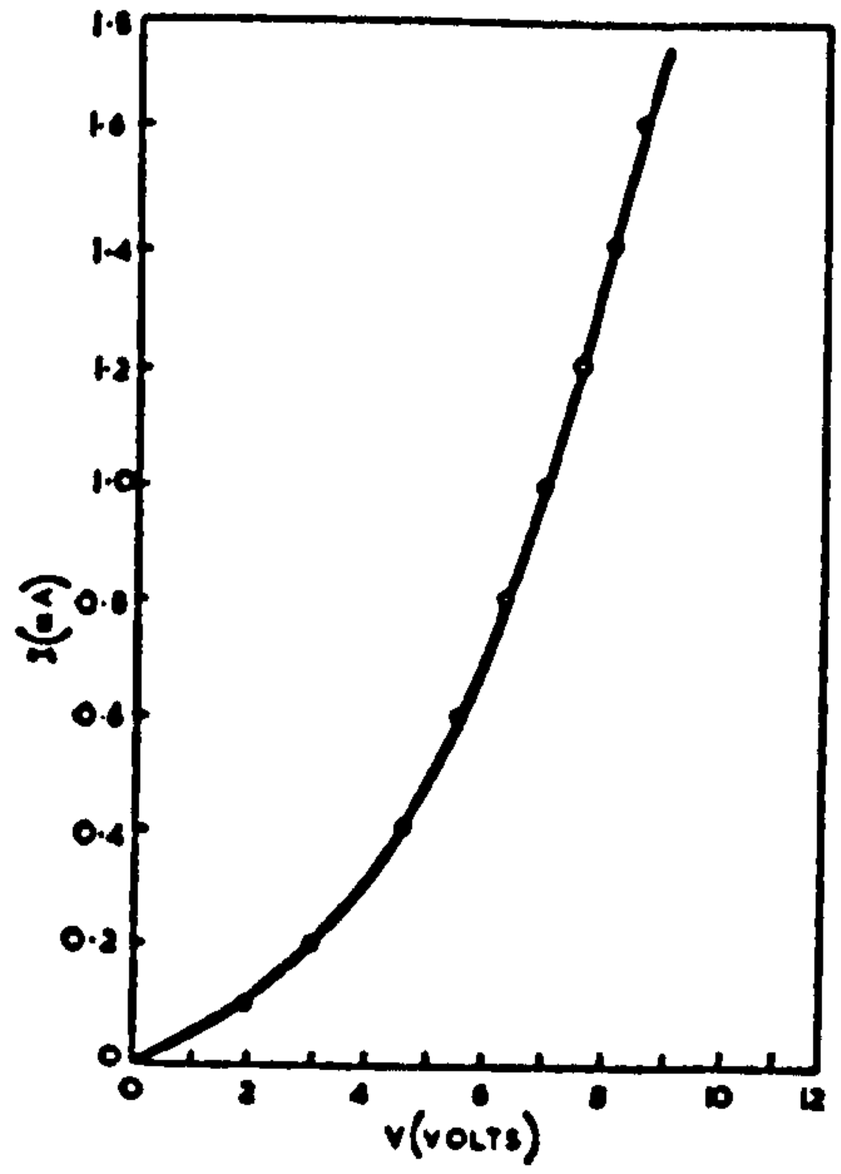


Fig. (5.6) Current-Voltage characteristic for Schottky emission. (Ref. 103)

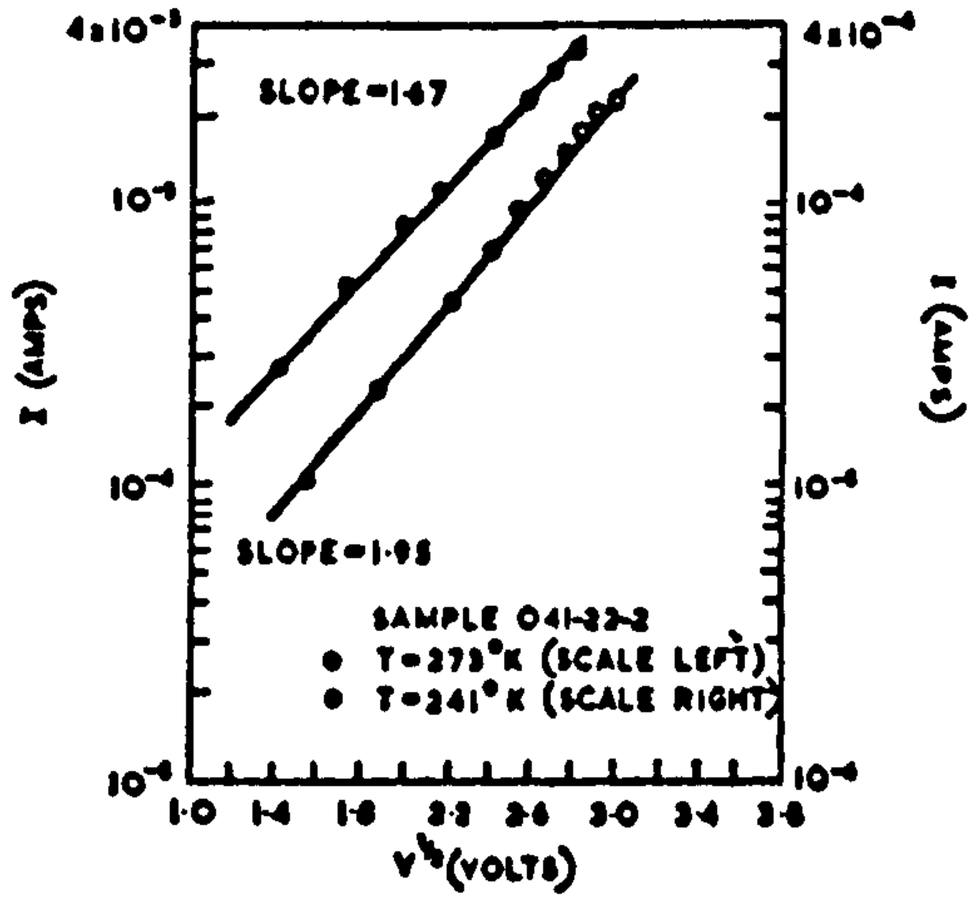


Fig. (5.7) Log I against $V^{1/2}$ for Schottky emission. (Ref. 103)

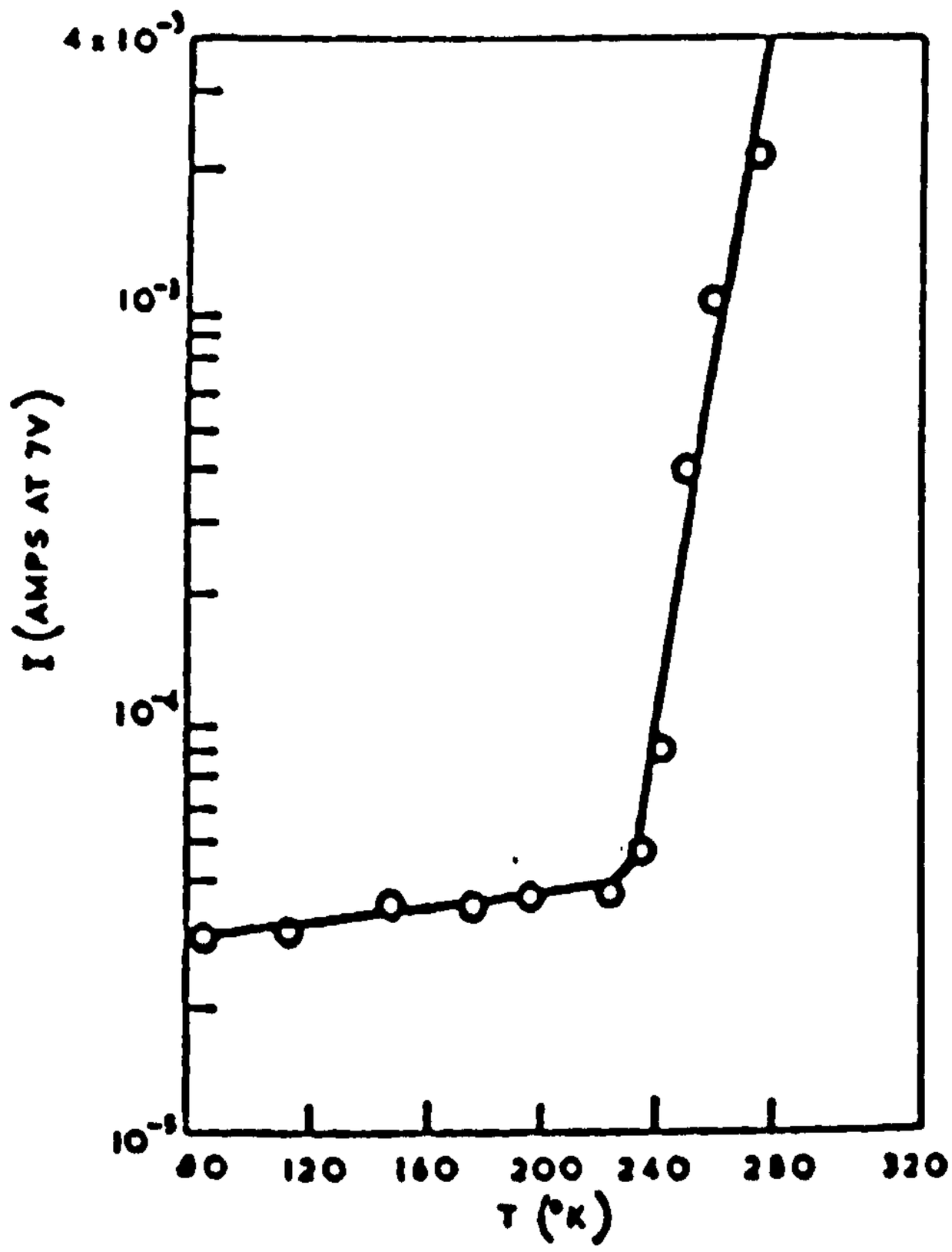


Fig. (5.8) Temperature variation of the current at constant voltage for Schottky emission. (Ref. 103)

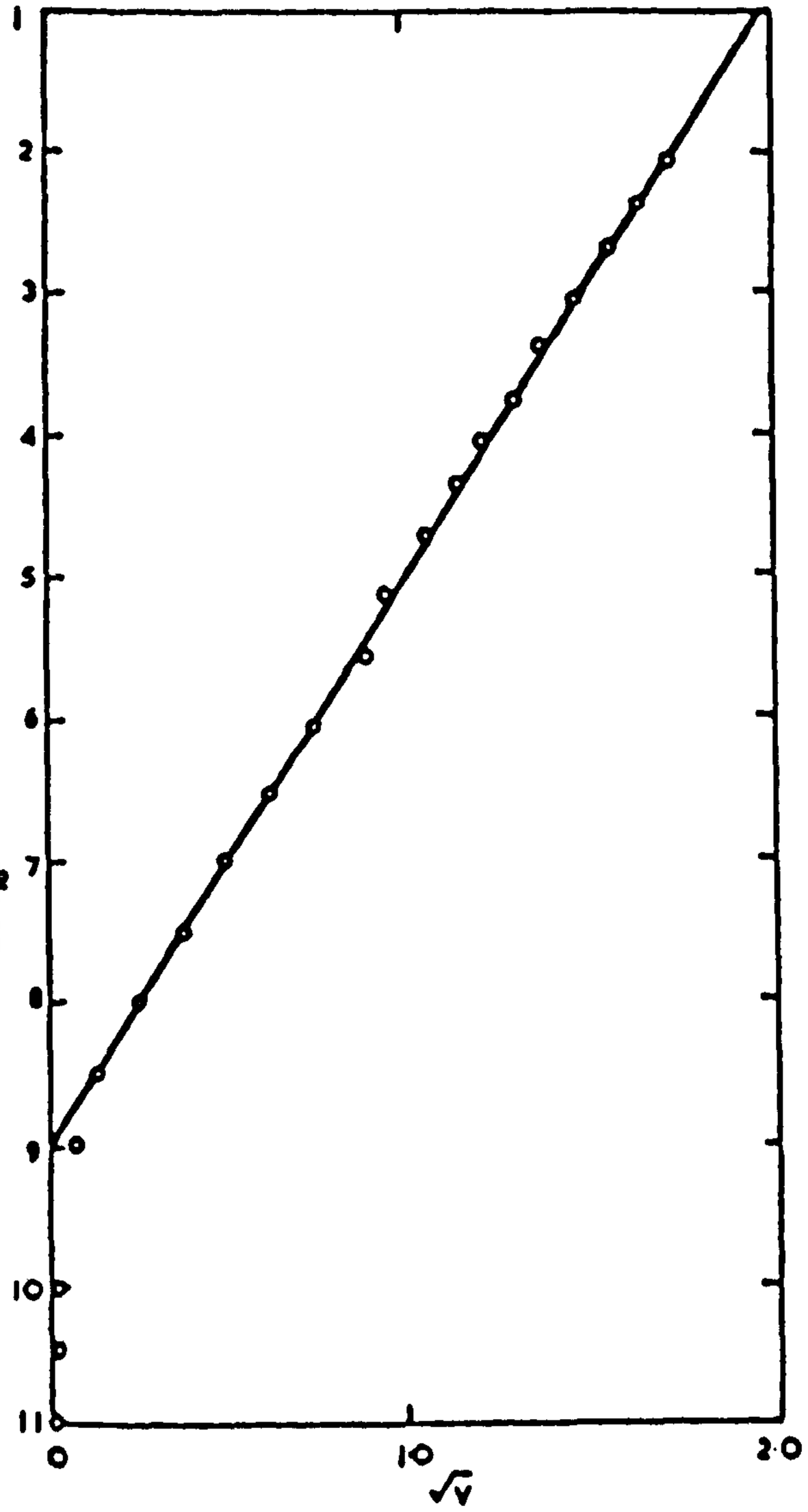


Fig. (5.9) Current-Voltage characteristic for Poole-Frenkel effect. (Ref. 105)

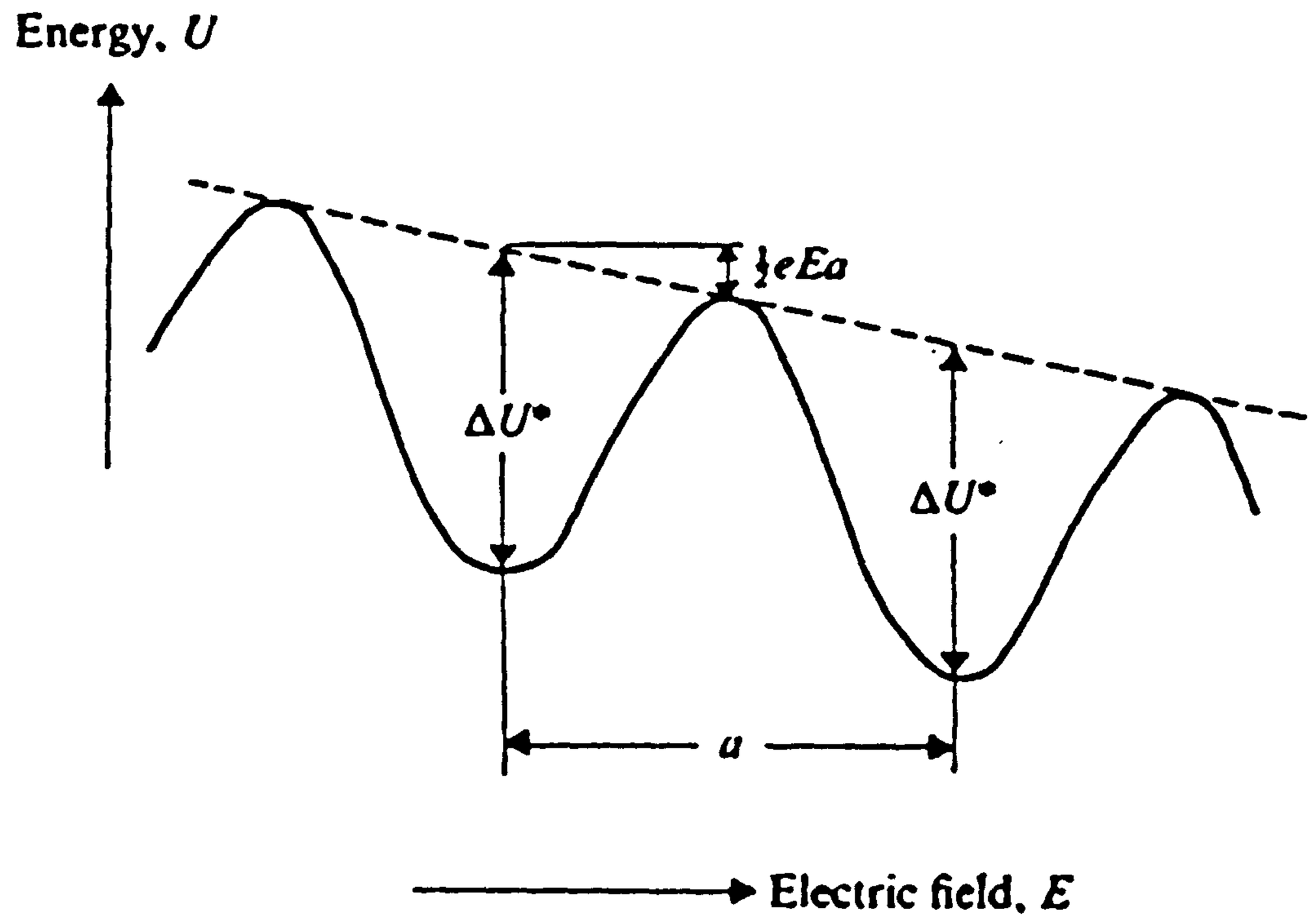


Fig. (5.10) Diagram showing the deformation of ionic potential-energy wells by an applied electric field.

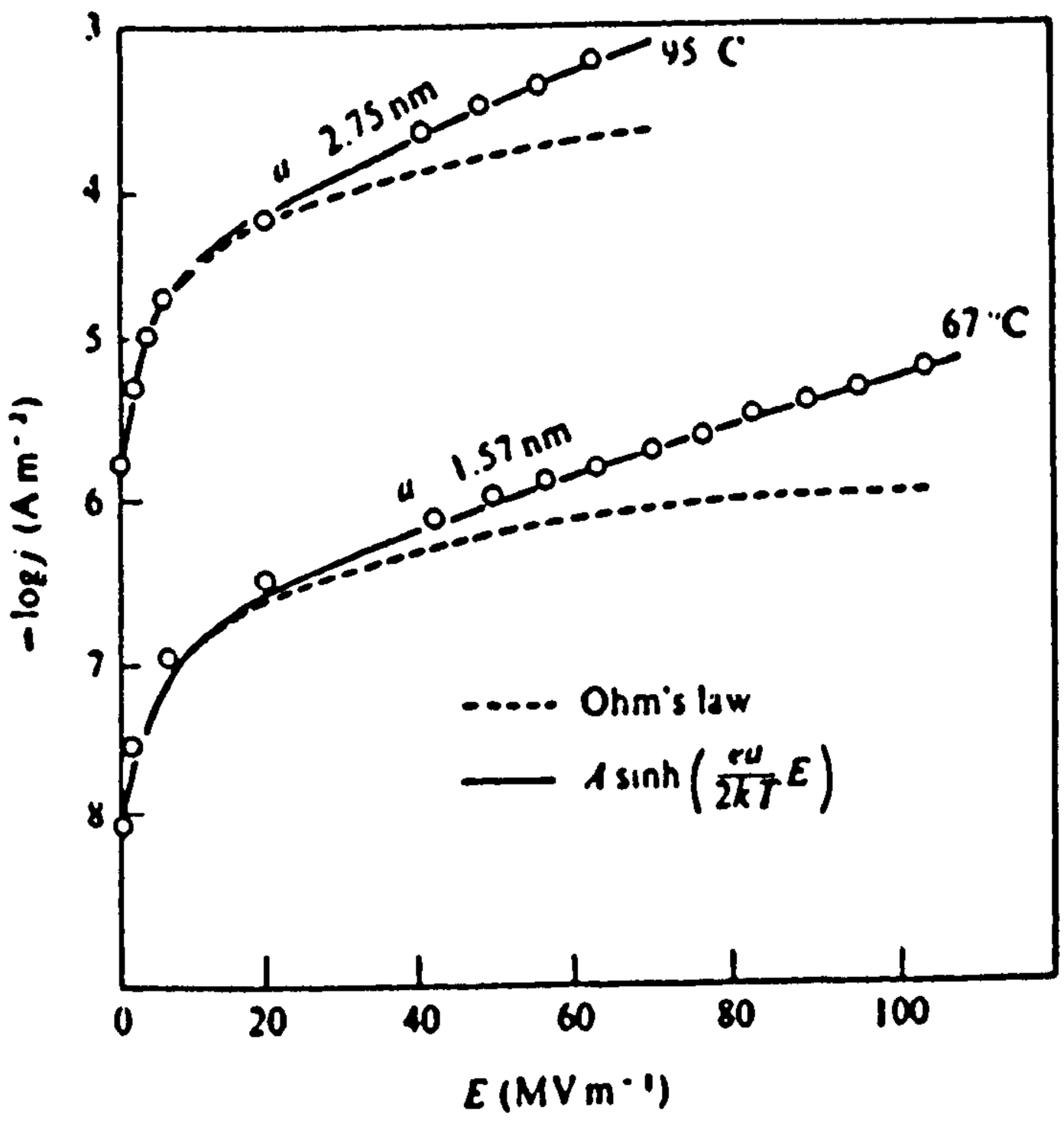


Fig. (5.11) The effect of electric field strength on conduction in poly(vinylchloride). (Ref. 113)

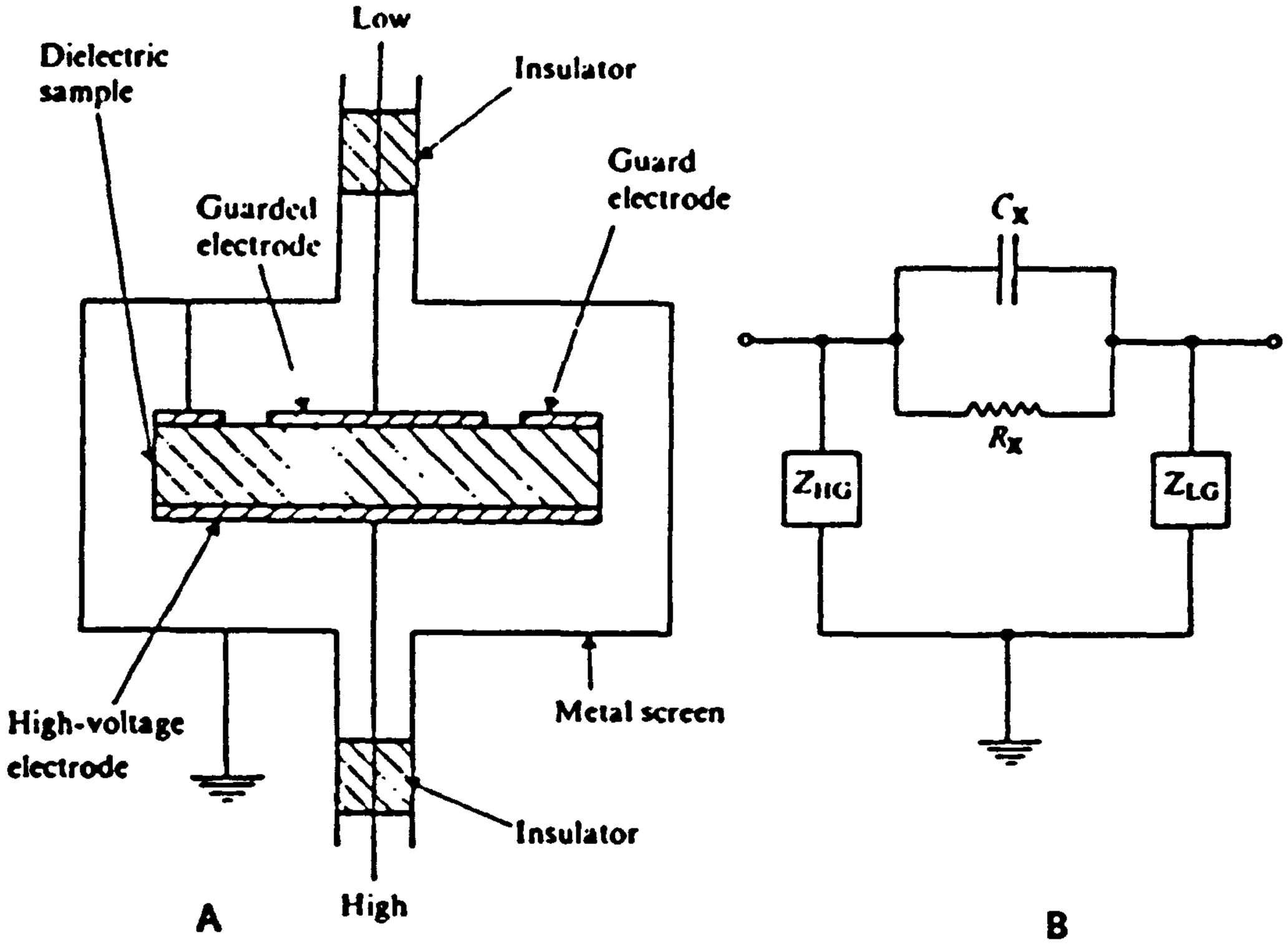


Fig. (5.12) A 3-Terminal specimen holder a- diagram of shielded electrode system with guard ring b- equivalent electrical circuit of the cell.

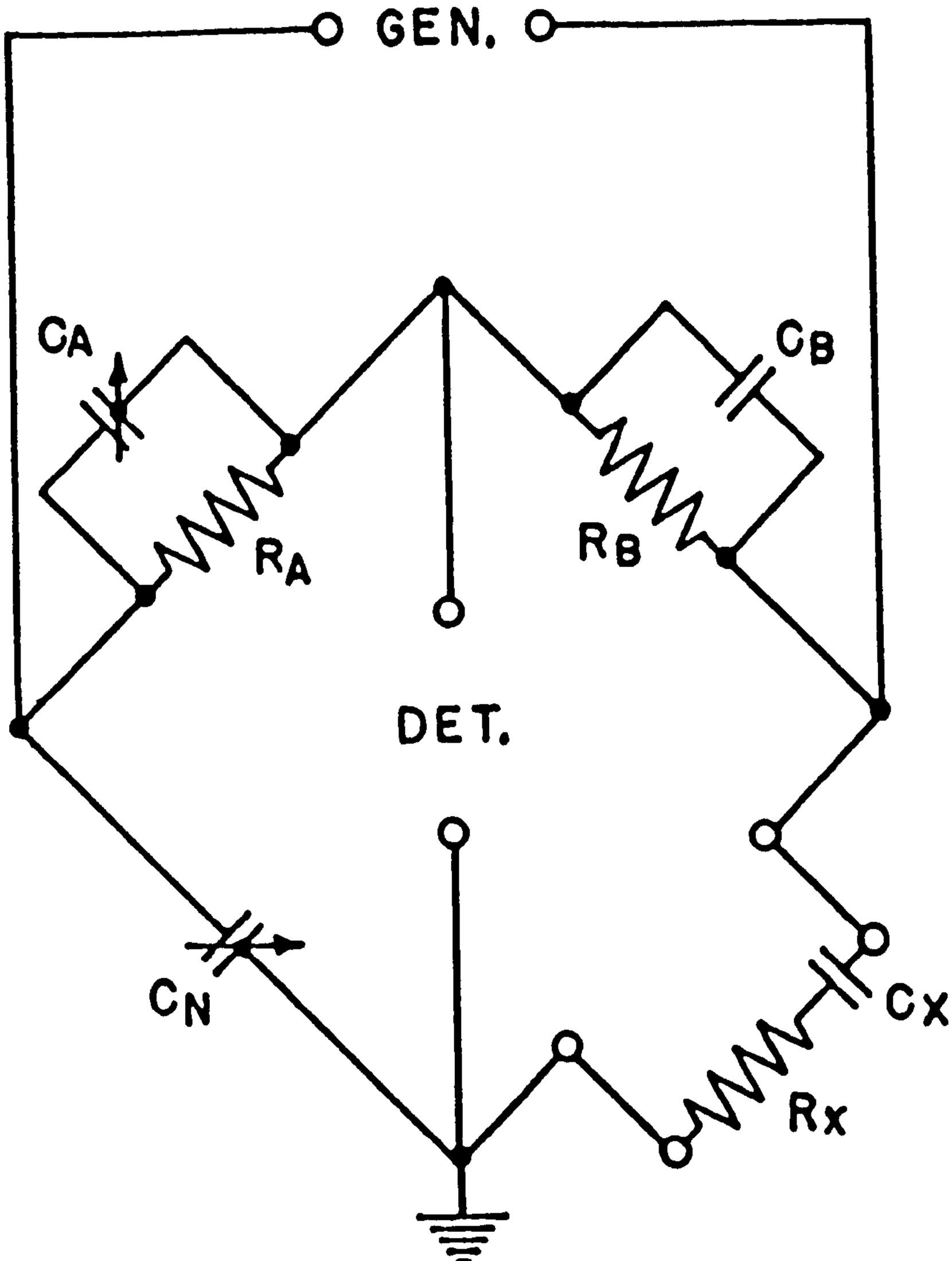


Fig. (5.13) Schering Bridge Circuit.

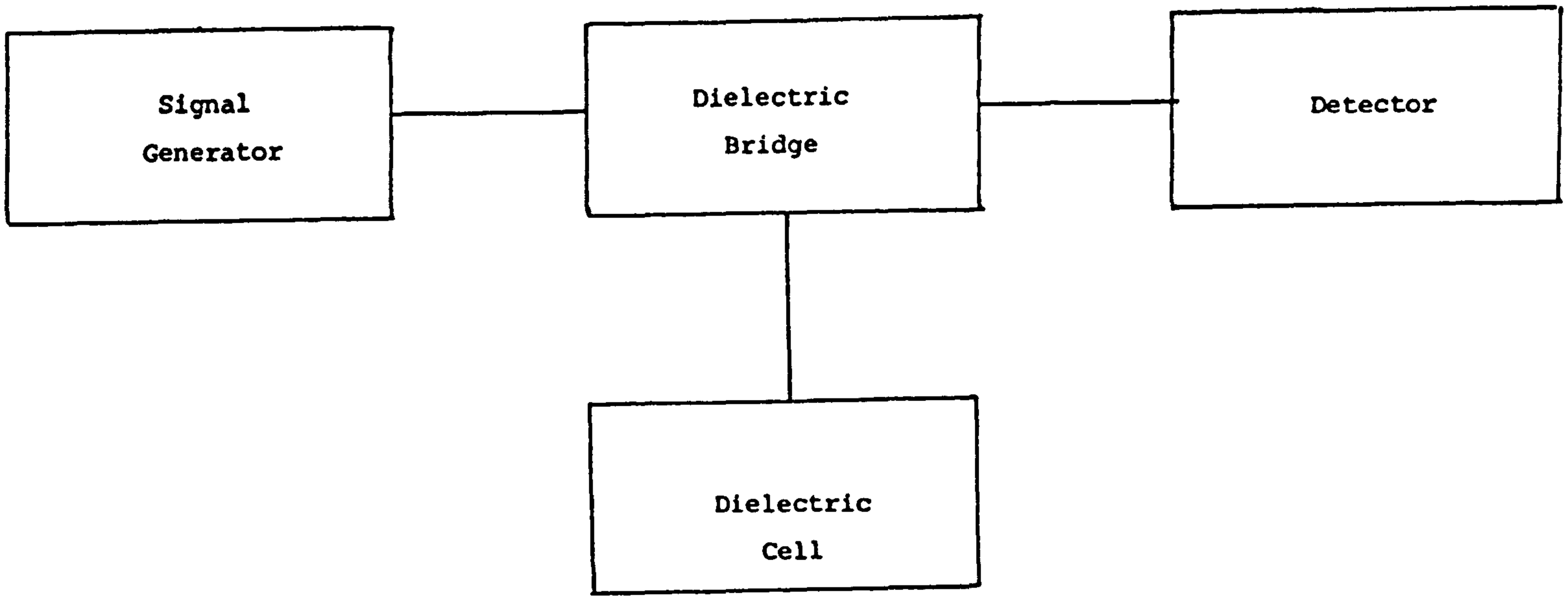


Fig. (5.14) Schematic representation of the dielectric measurement system.

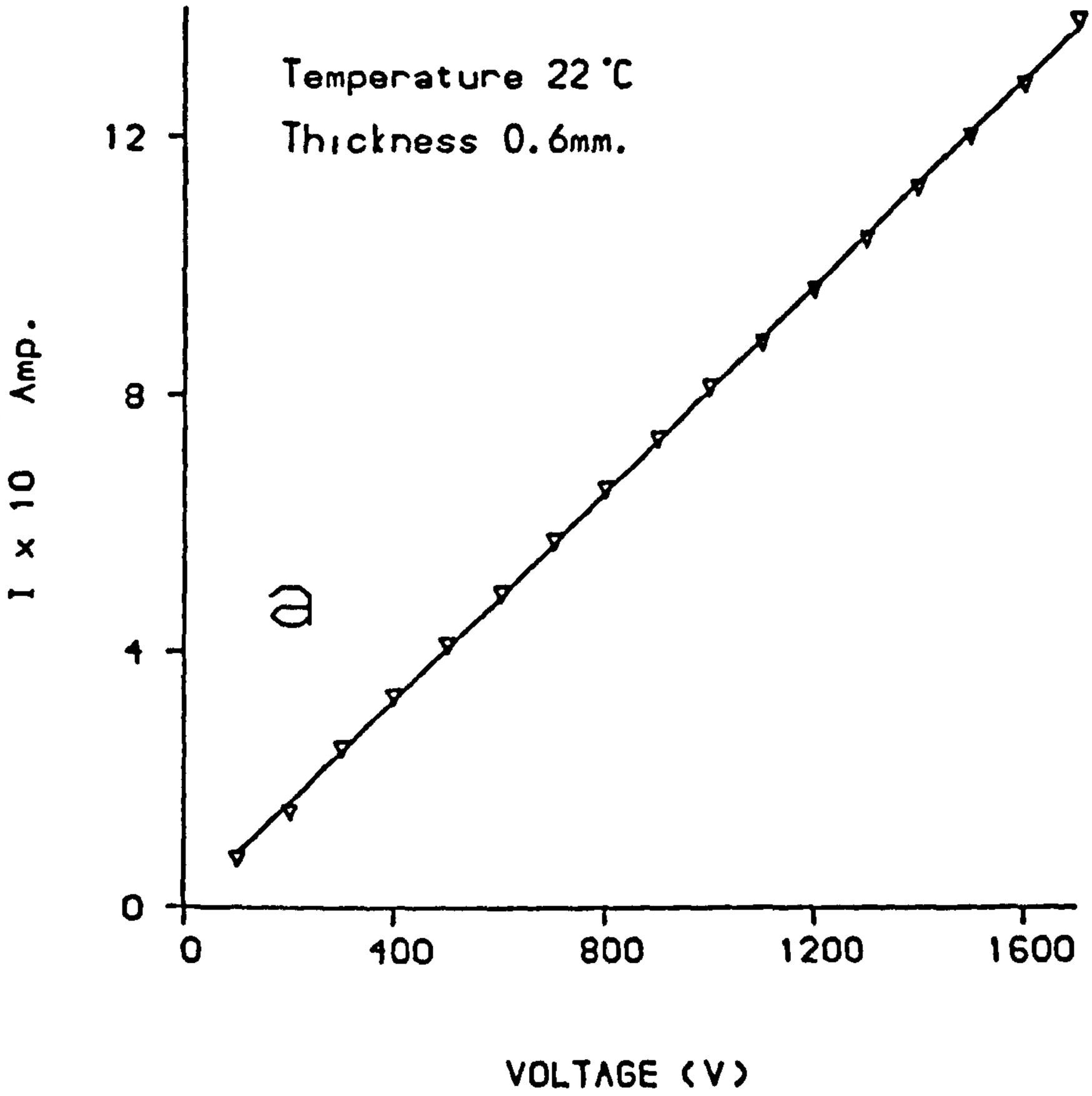


Fig. (5.15a) Current- Voltage characteristic for MY750/HY956 epoxy system of 0.6mm thickness at 22 °C.

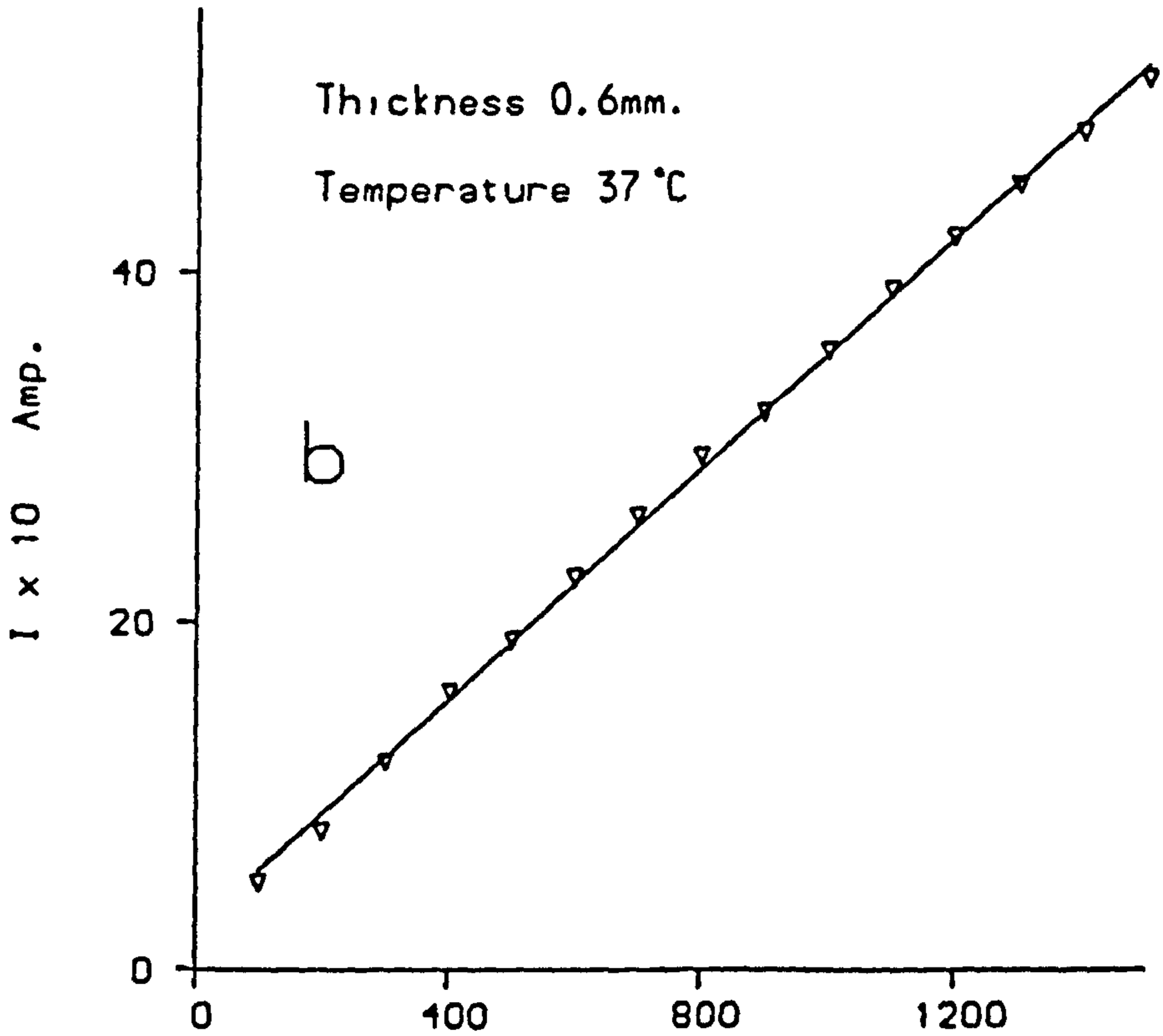


Fig. (5.15b) Current- Voltage characteristic for MY750/HY956 epoxy system of 0.6mm thickness at 37 °C.

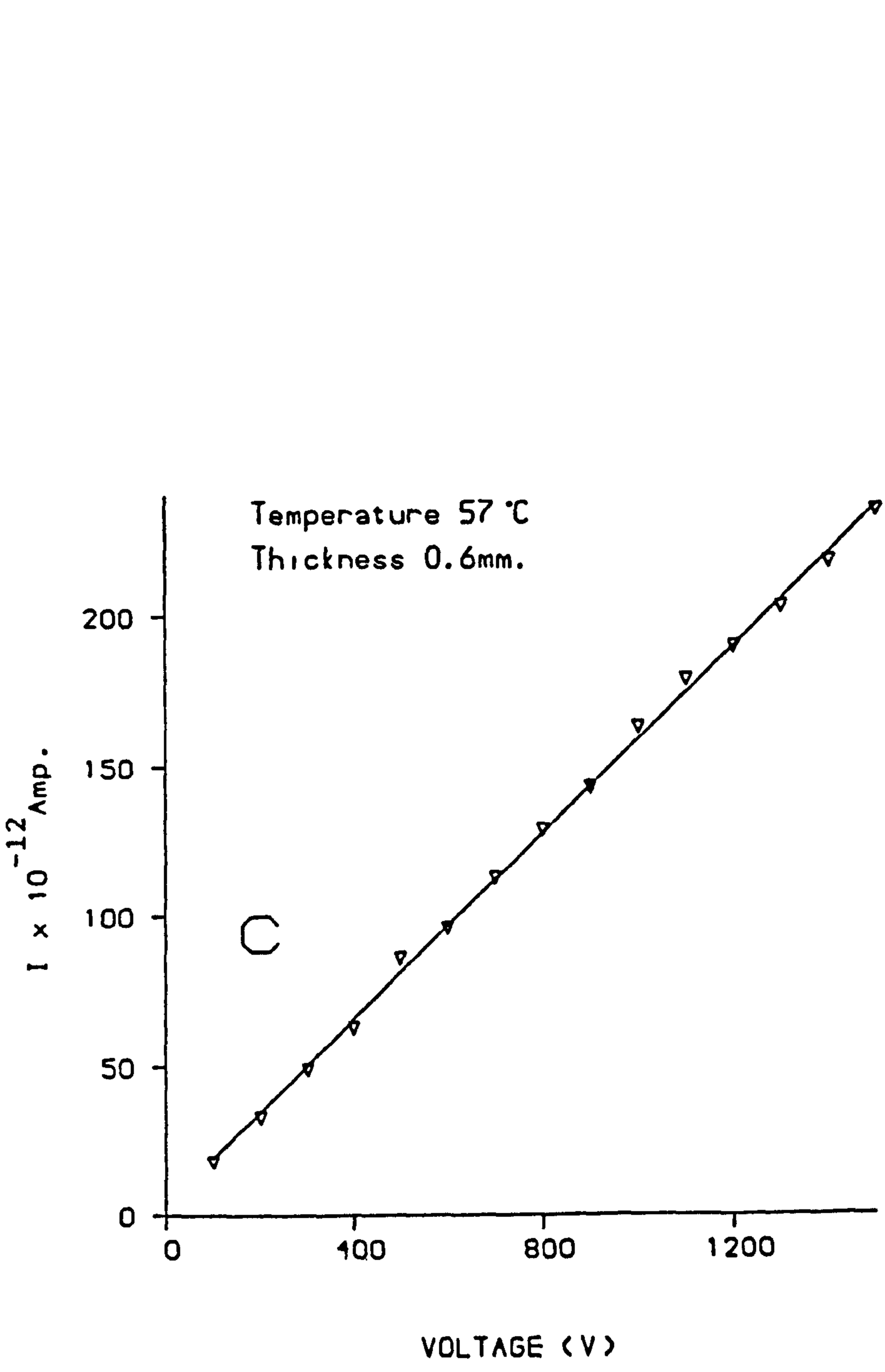


Fig. (5.15c) Current- Voltage characteristic for MY750/HY956 epoxy system of 0.6mm thickness at 57 °C.

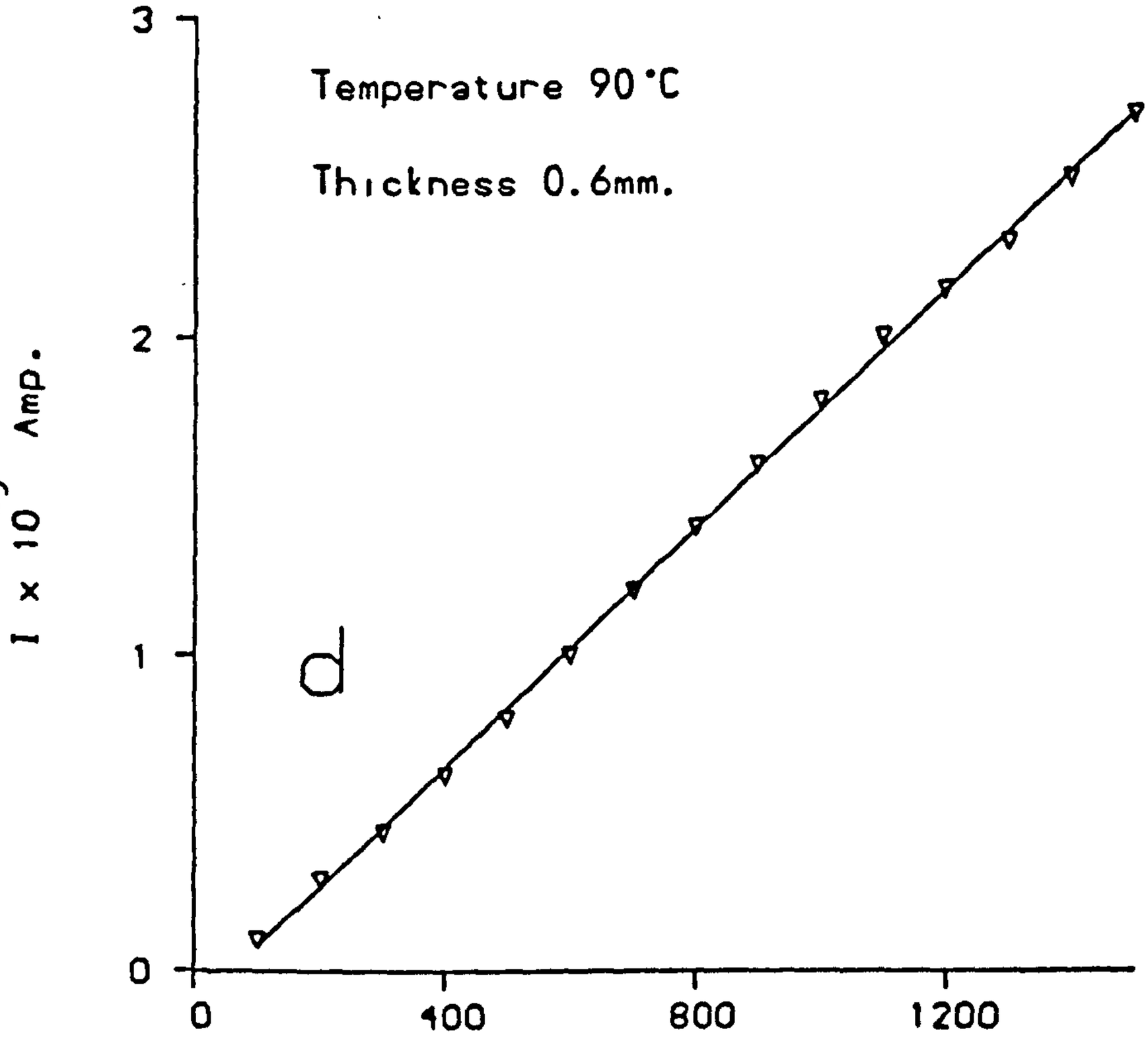


Fig. (5.15d) Current- Voltage characteristic for MY750/HY956 epoxy system of 0.6mm thickness at 90 °C.

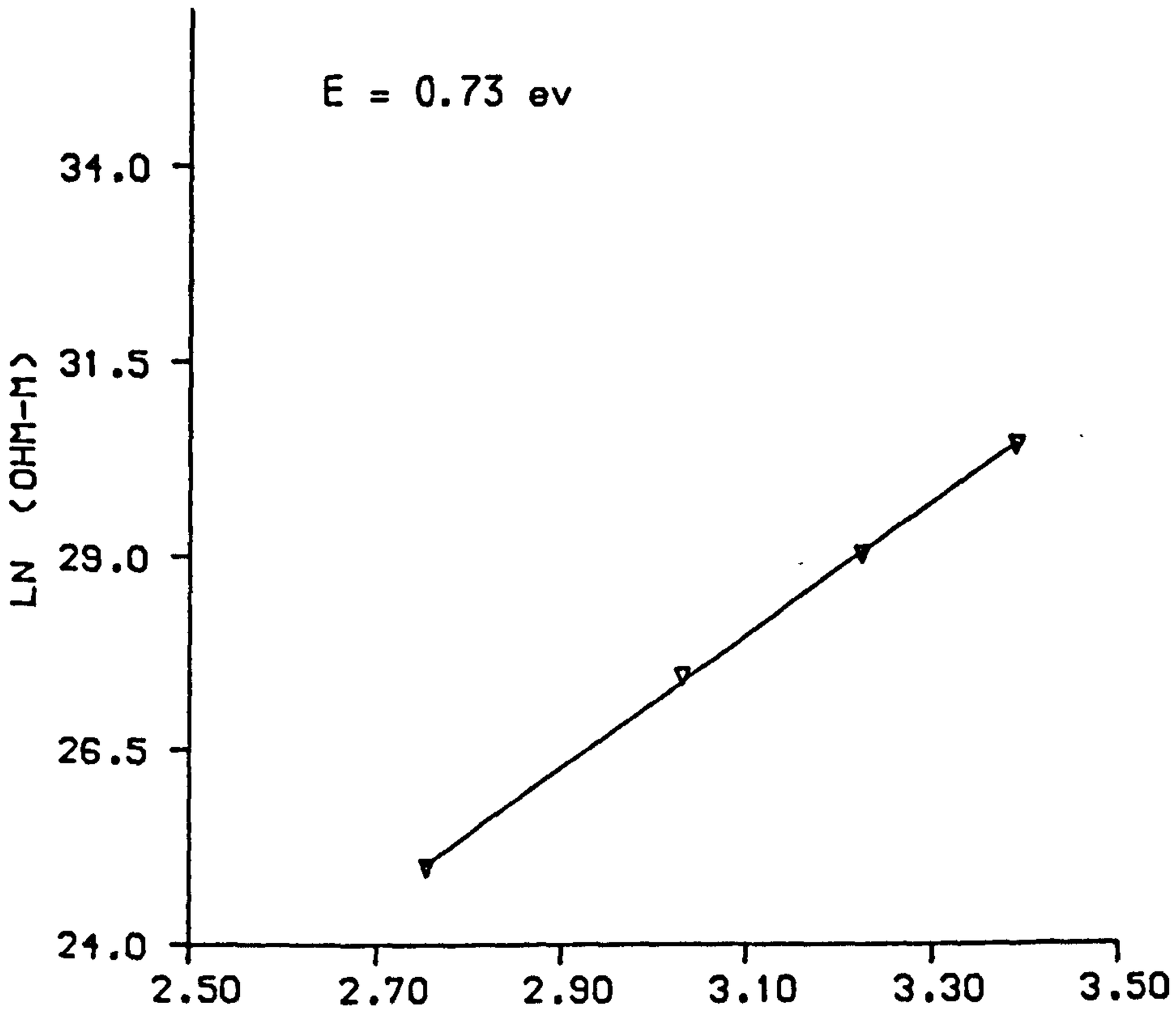


Fig. (5.16) Arrhenius plot of dc resistivity against 1/temperature for MY750/HY956 epoxy system of 0.6mm thickness.

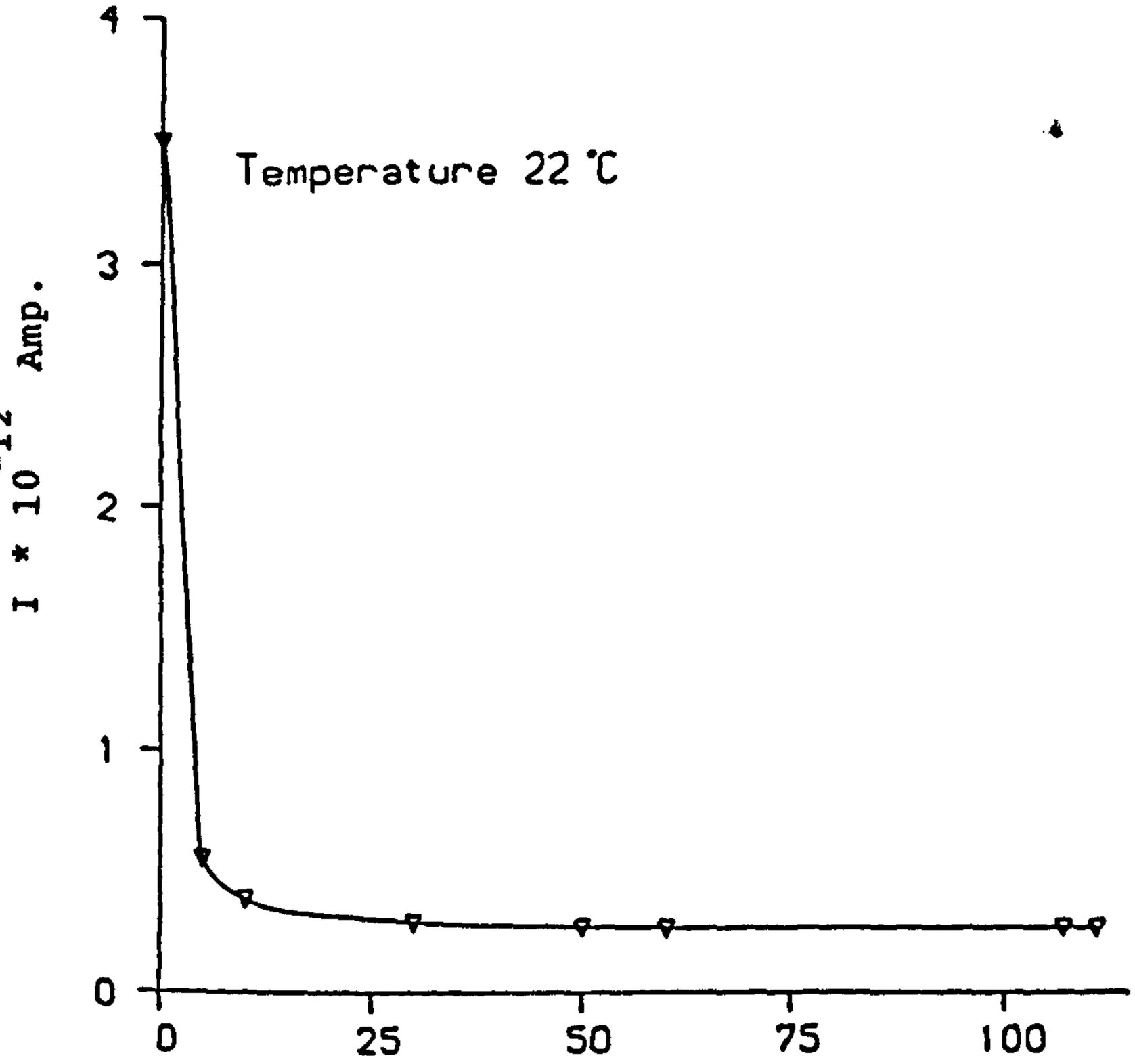


Fig. (5.17a) Current- Time characteristic for MY750/HY956 epoxy system of 0.6mm thickness at 22 °C.

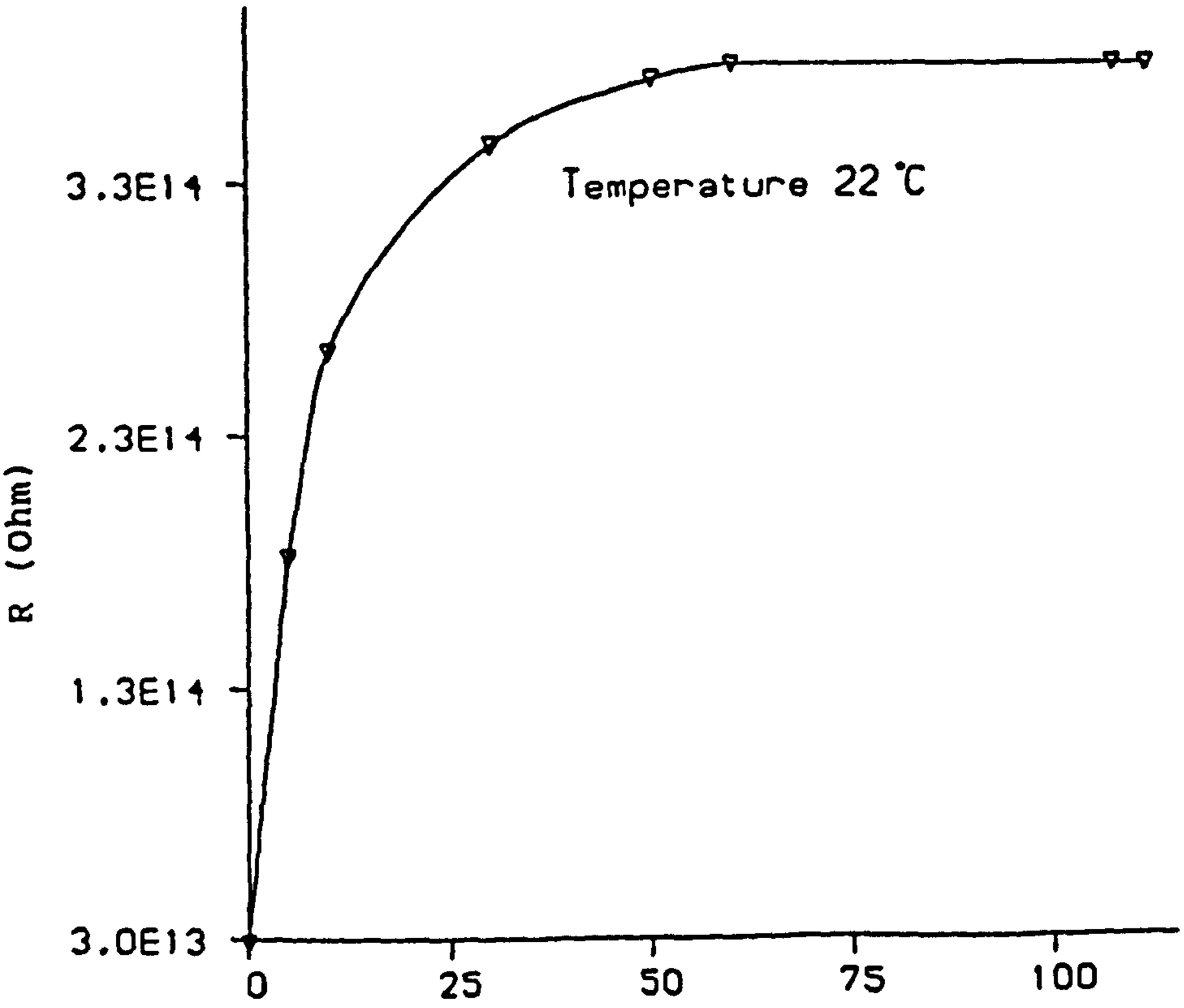


Fig. (5.17b) Resistance- Time characteristic for MY750/HY956 epoxy system of 0.6mm thickness at 22 °C.

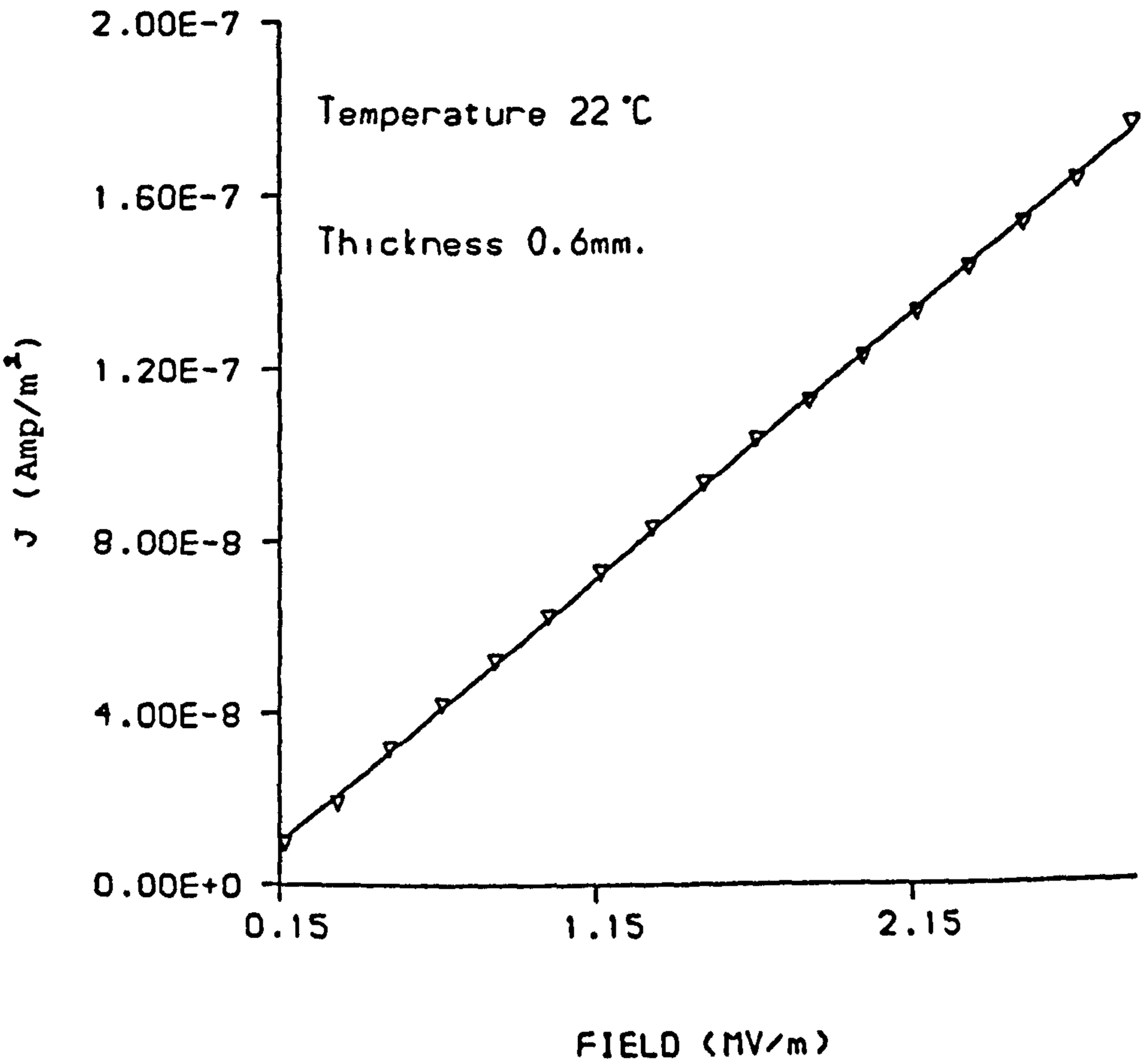


Fig. (5.18a) Current density- Field characteristic for MY750/HY956 epoxy system of 0.6mm thickness at 22 °C.

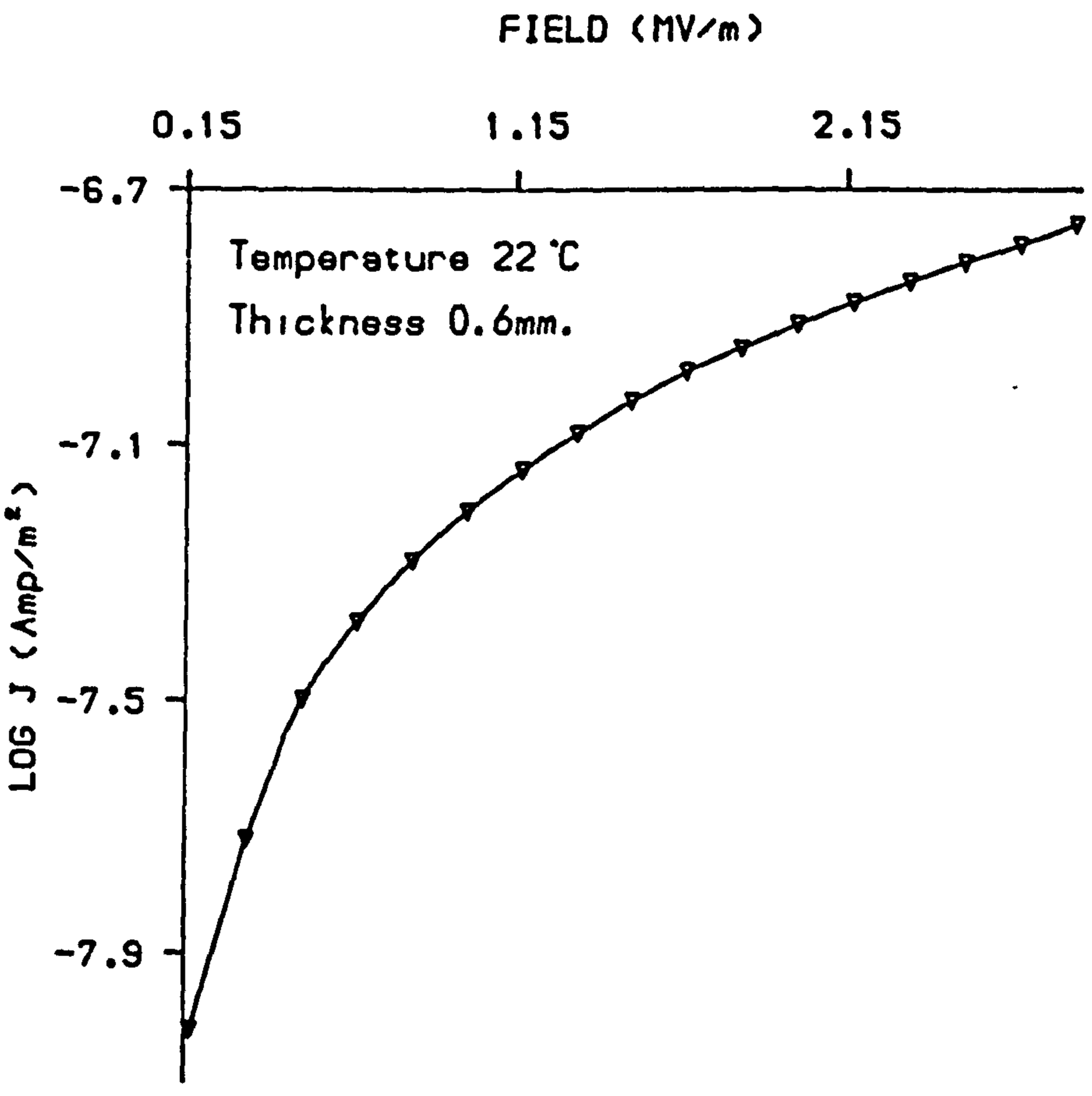


Fig. (5.18b) Log (Current density)- Field characteristic for MY750/HY956 epoxy system of 0.6mm thickness at 22 °C.

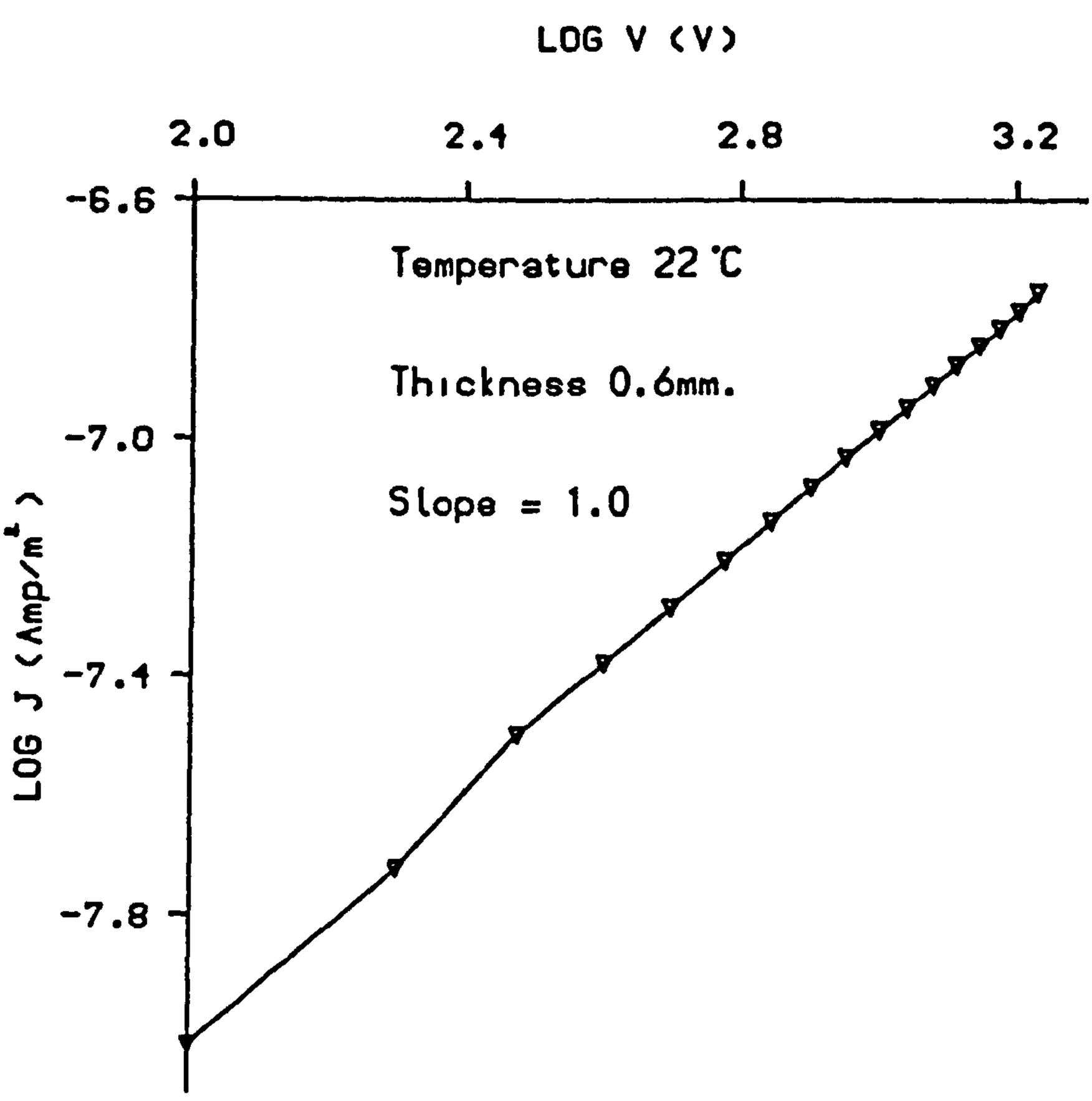


Fig. (5.18c) Log (Current density) - Log (Voltage) characteristic for MY750/HY956 epoxy system of 0.6mm thickness at 22 °C.

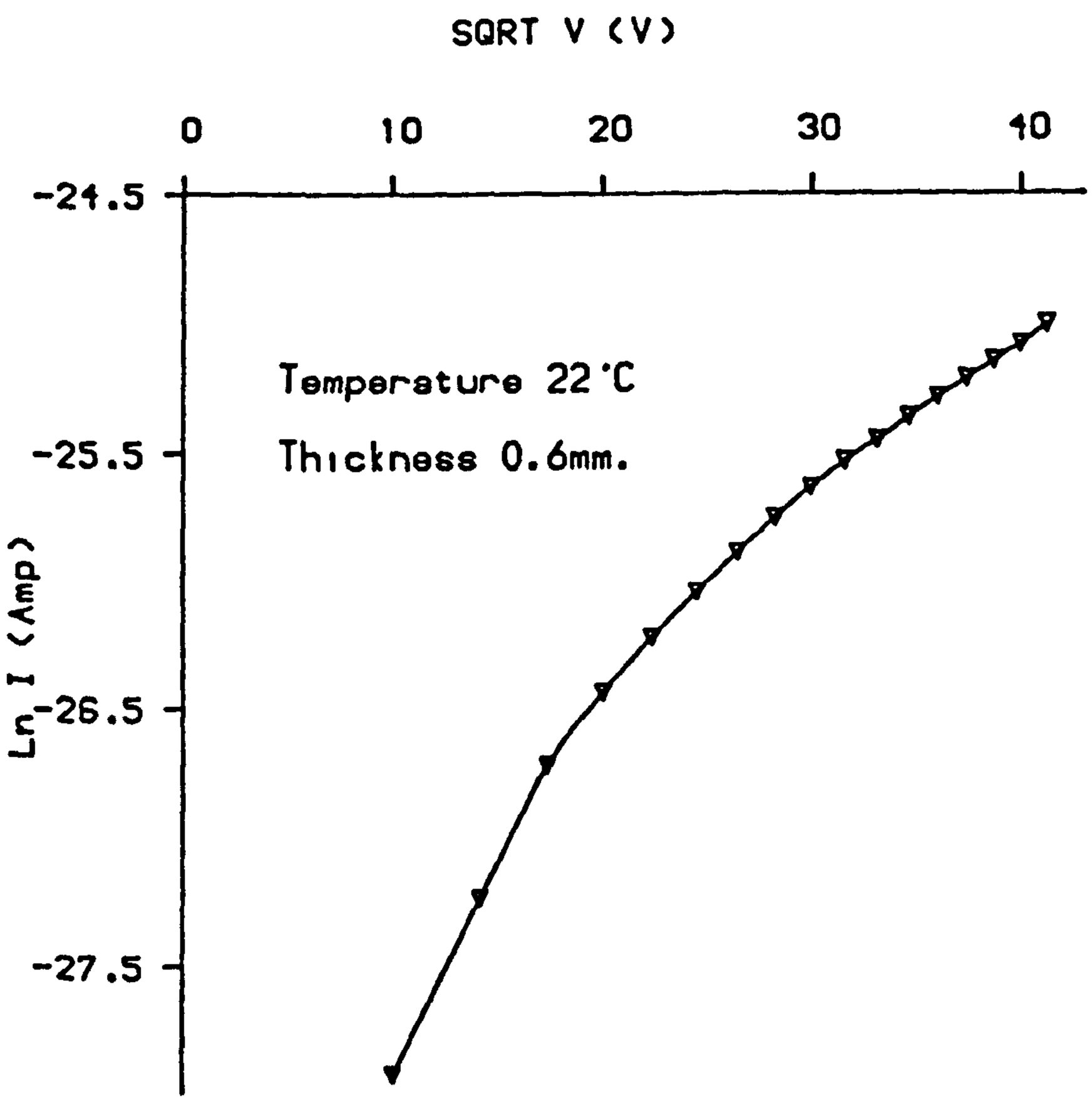


Fig. (5.18d) Ln (Current)- (Voltage)$^{1/2}$ characteristic for MY750/HY956 epoxy system of 0.6mm thickness at 22 °C.

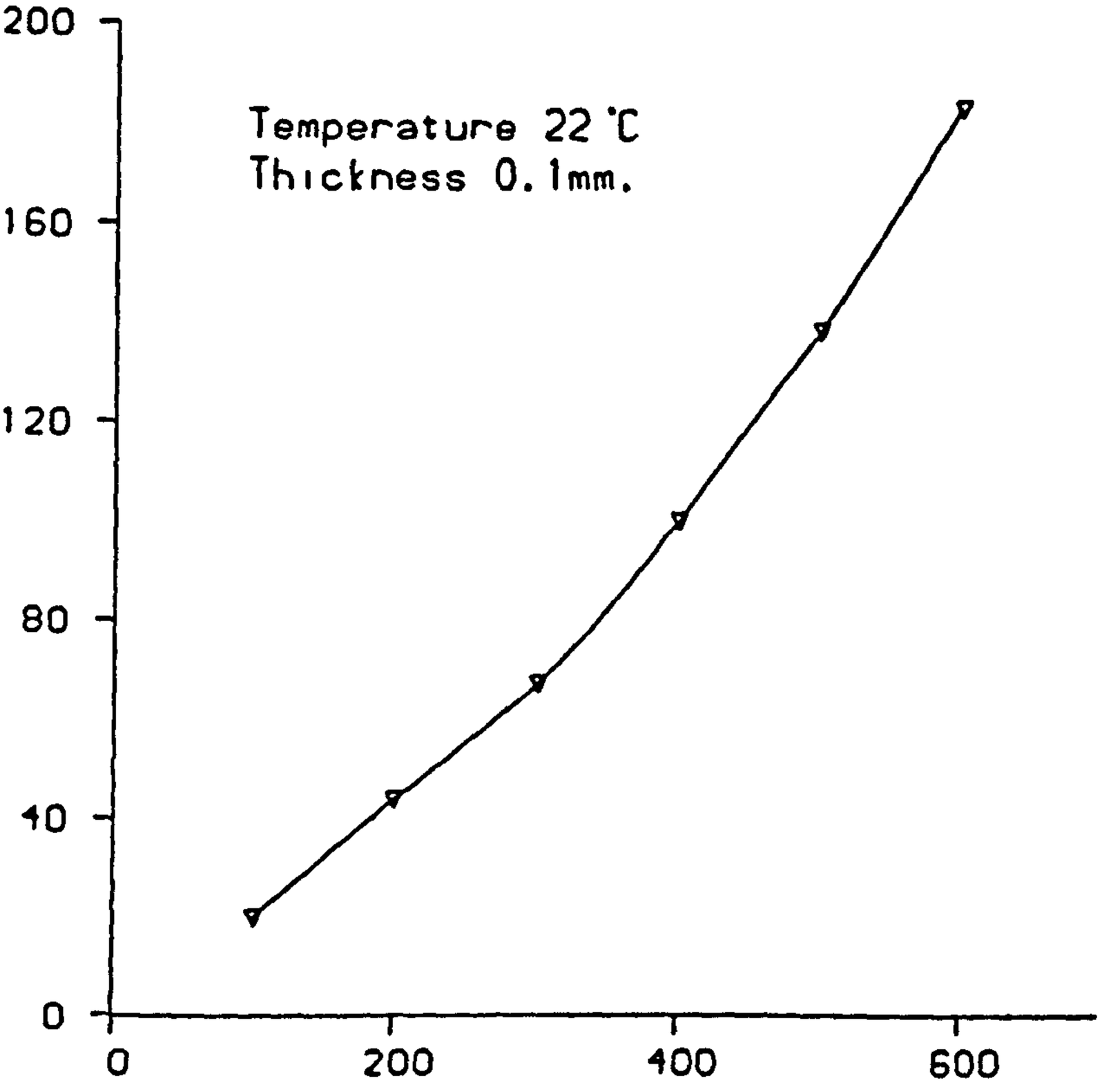


Fig. (5.19a) Current-Voltage characteristic for MY750/HY956 epoxy system of 0.1mm thickness at 22 °C.

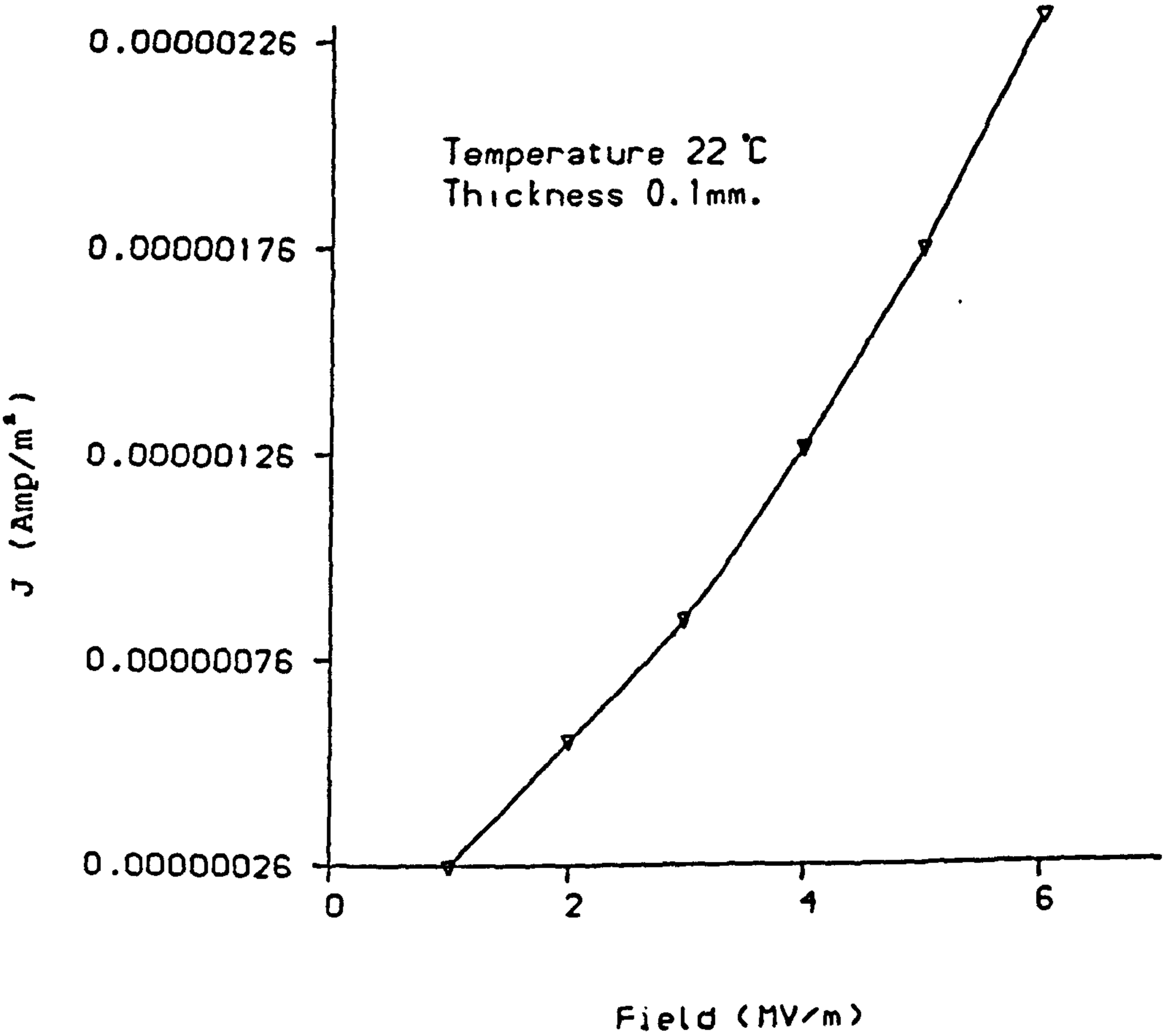


Fig. (5.19b) Current density- Field characteristic for MY750/HY956 epoxy system of 0.1mm thickness at 22 °C.

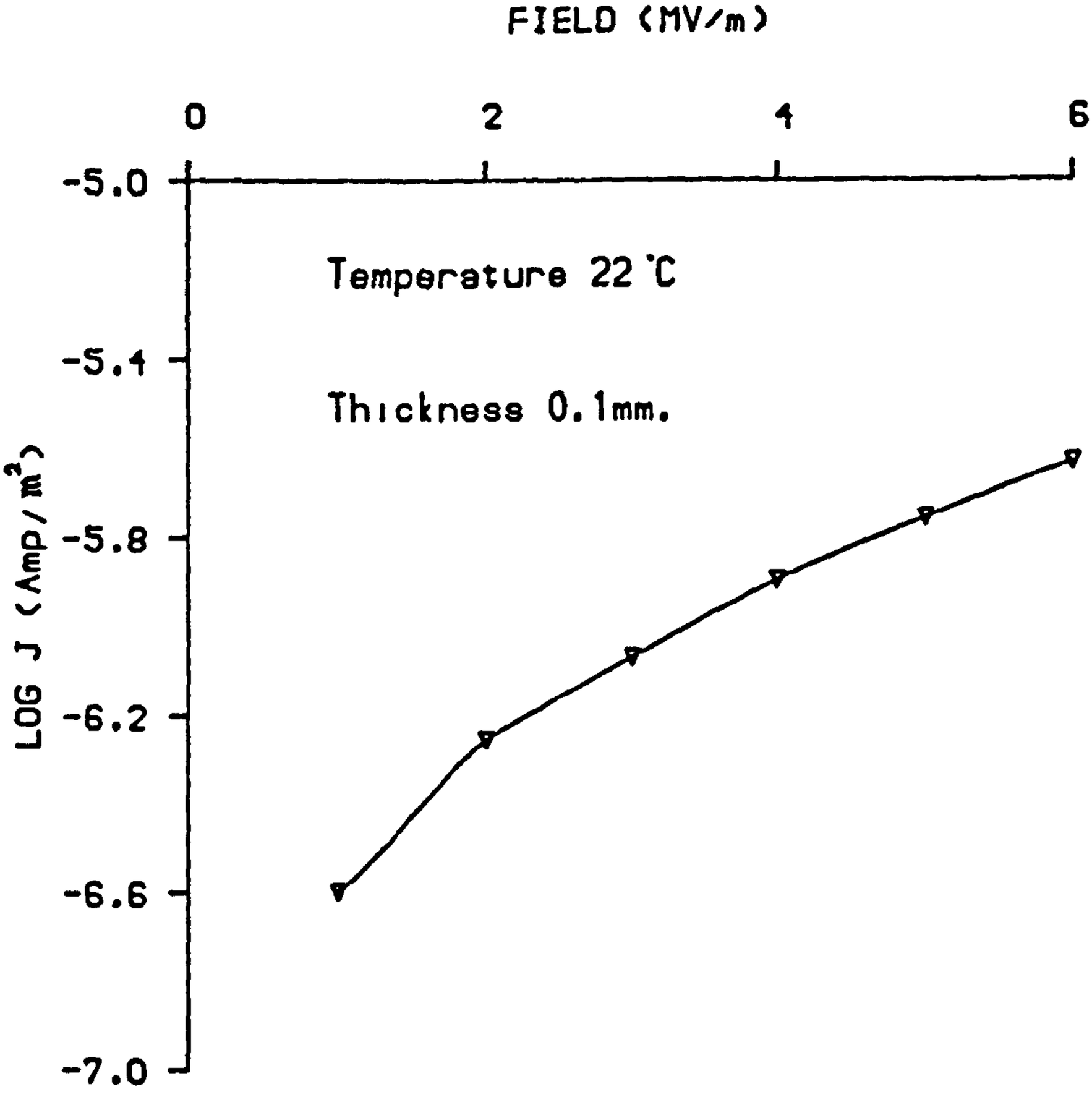


Fig. (5.19c) Log (Current density)- Field characteristic for MY750/HY956 epoxy system of 0.1mm thickness at 22 °C.

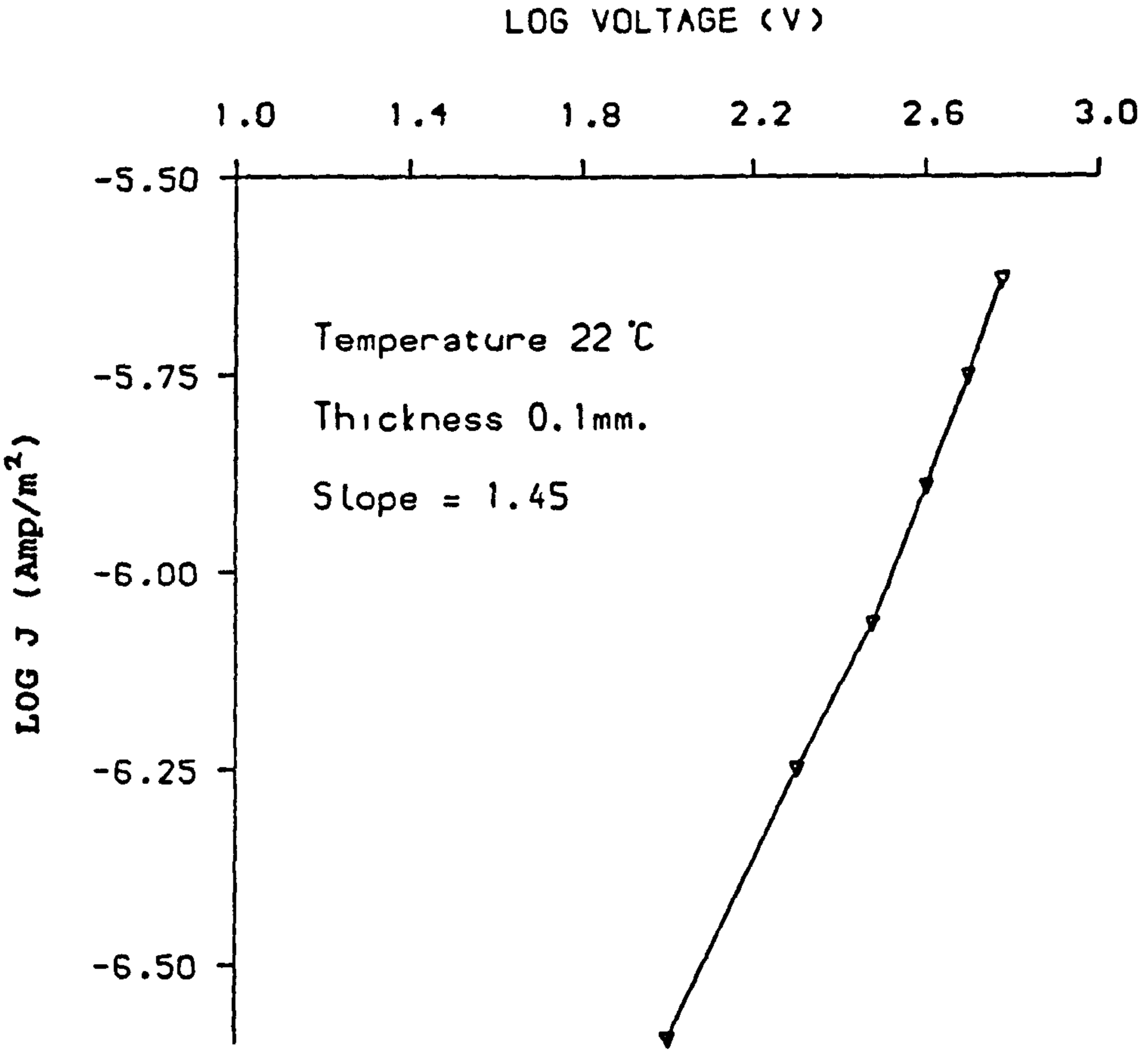


Fig. (5.19d) Log (Current density)- Log (Voltage) characteristic for MY750/HY956 epoxy system of 0.1mm thickness at 22 °C.

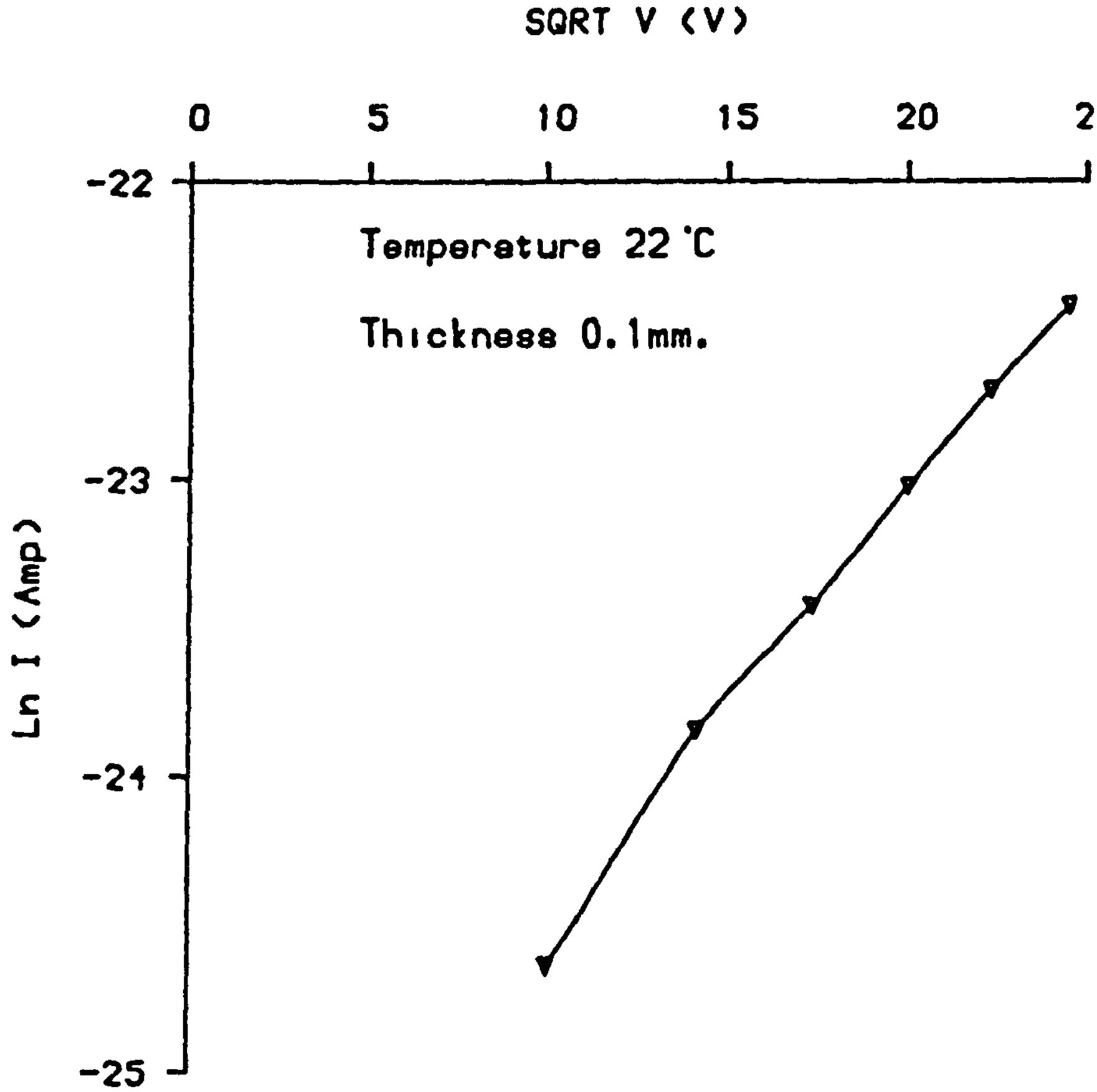


Fig. (5.19e) Ln (Current)- (Voltage)$^{1/2}$ characteristic for MY750/HY956 epoxy system of 0.1mm thickness at 22 °C.

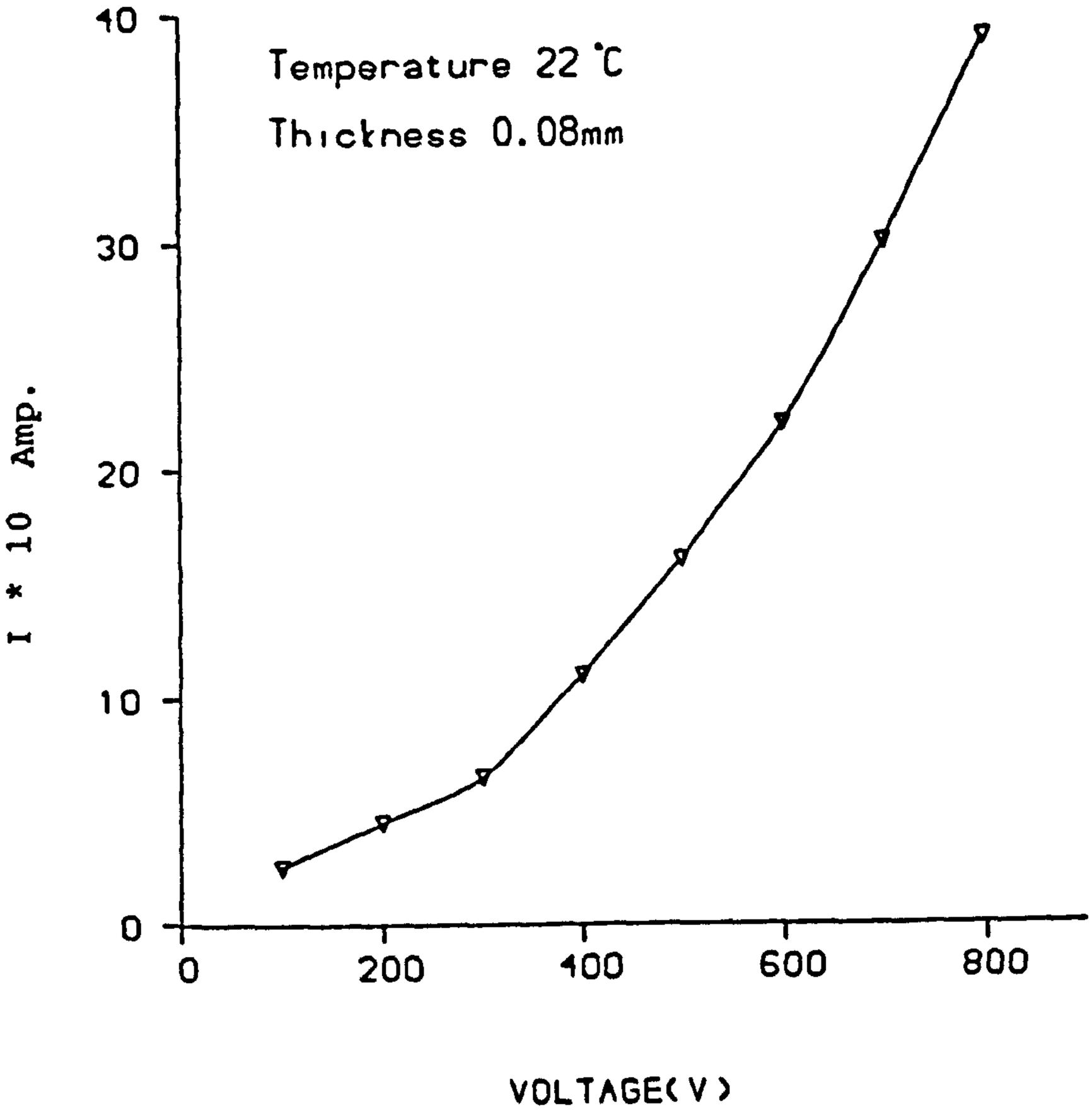


Fig. (5.20a) Current-Voltage characteristic for MY750/HY956 epoxy system of 0.08mm thickness at 22°C.

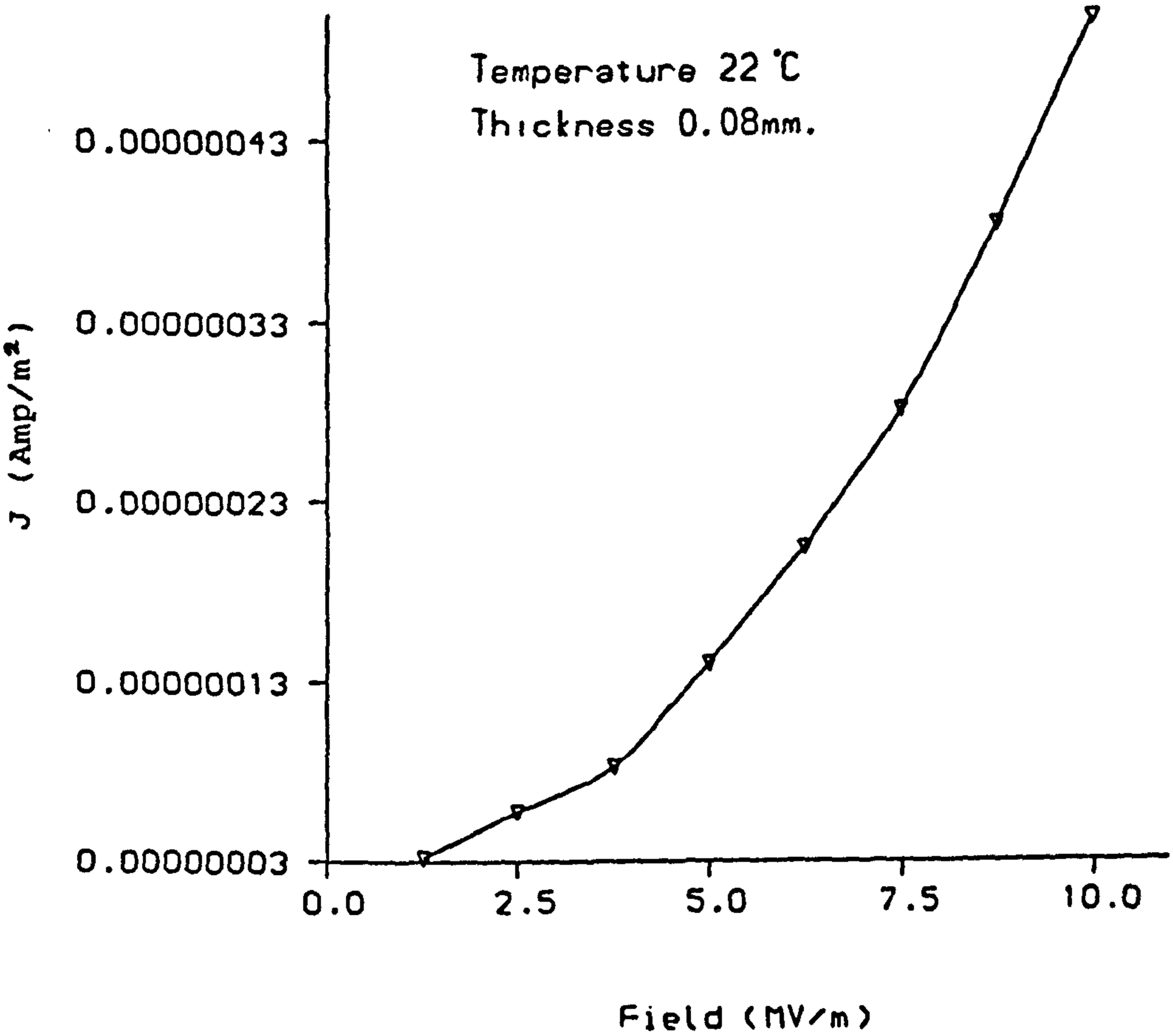


Fig. (5.20b) Current density- Field characteristic for MY750/HY956 epoxy system of 0.08mm thickness at 22 °C.

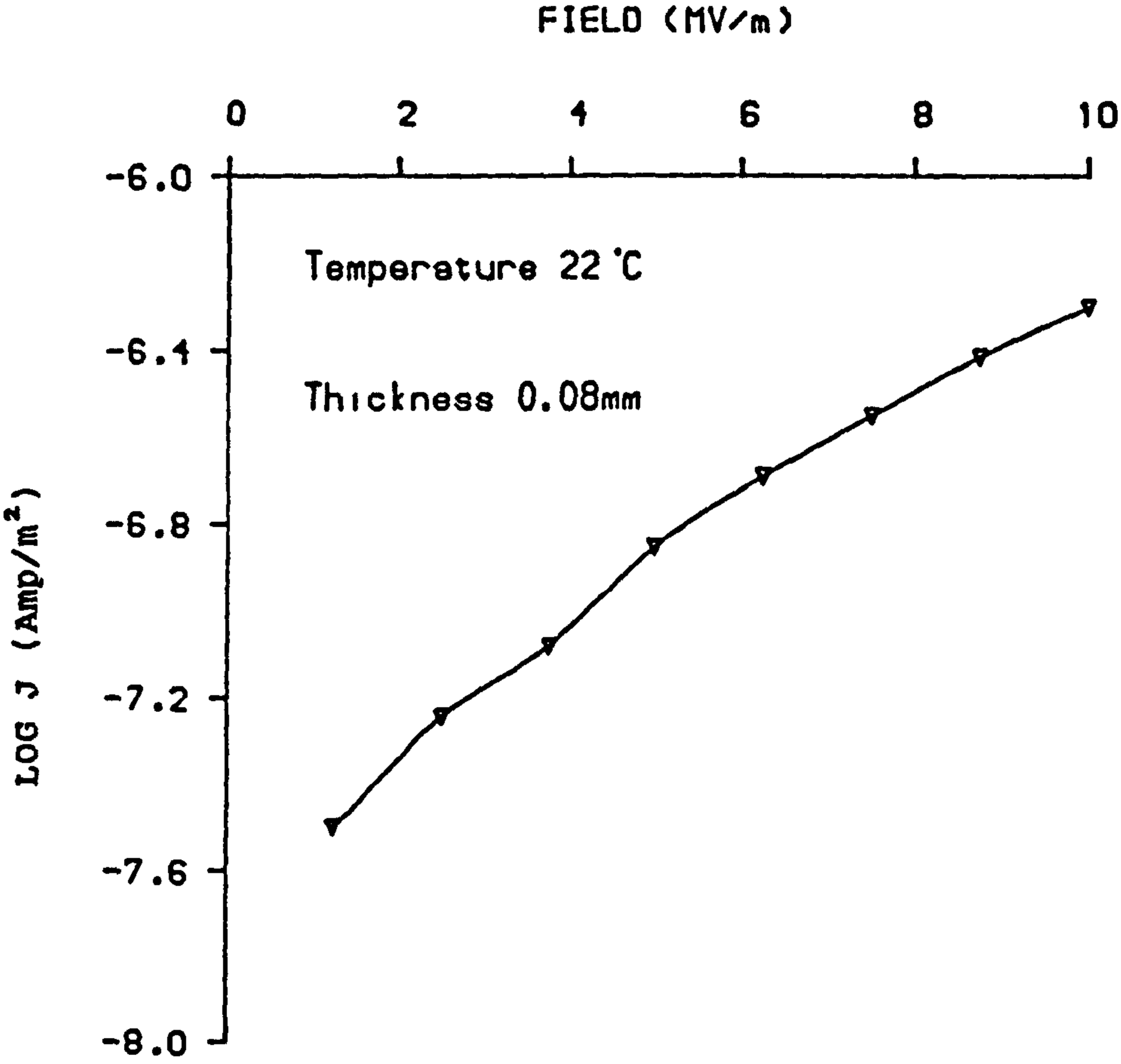


Fig. (5.20c) Log (Current density)- Field characteristic for MY750/HY956 epoxy system of 0.08mm thickness at 22 °C.

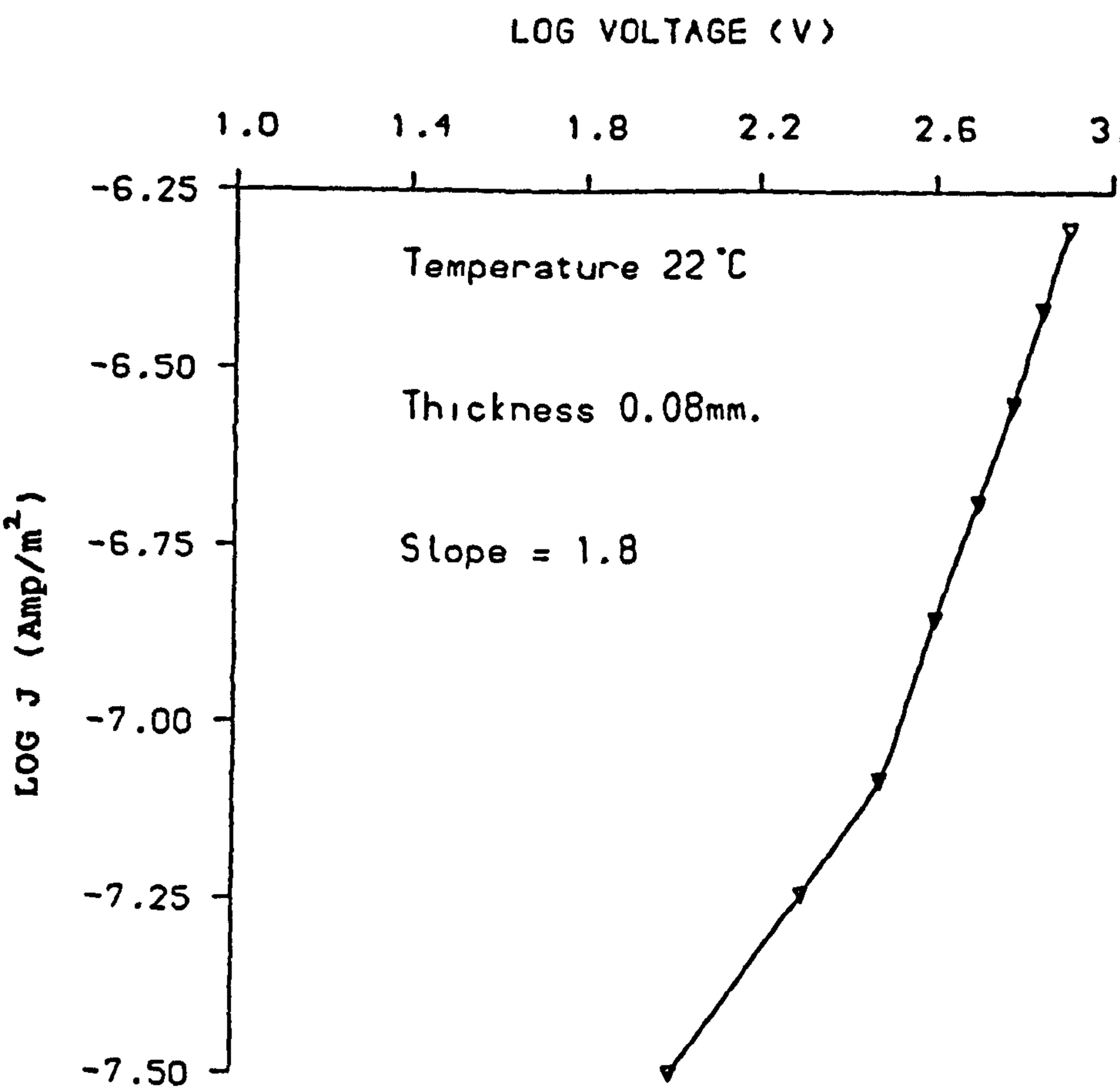


Fig. (5.20d) Log (Current density)- Log (Voltage) characteristic for MY750/HY956 epoxy system of 0.08mm thickness at 22°C.

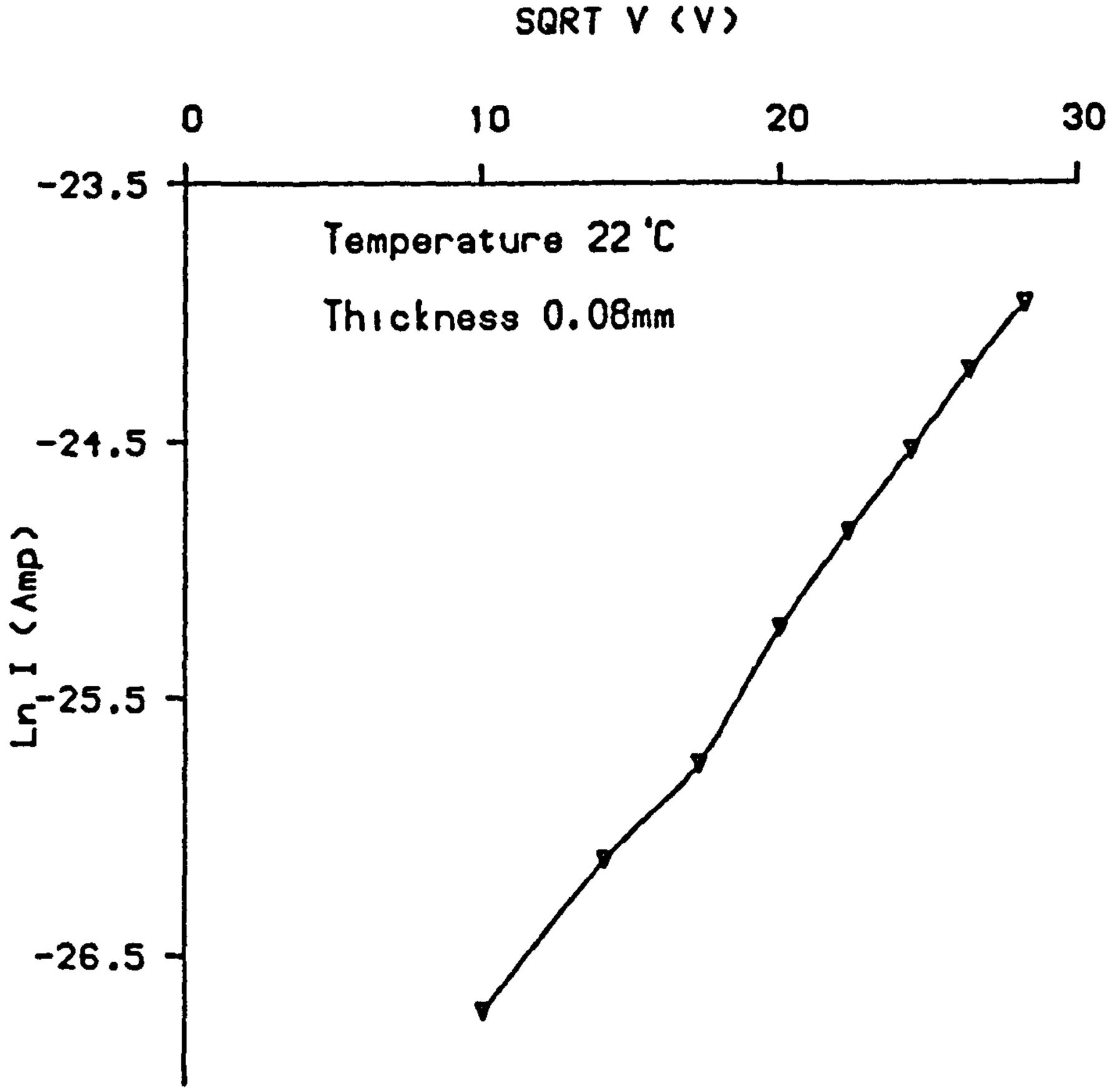


Fig. (5.20e) Ln (Current)- (Voltage)$^{1/2}$ characteristic for MY750/HY956 epoxy system of 0.08mm thickness at 22 'C.

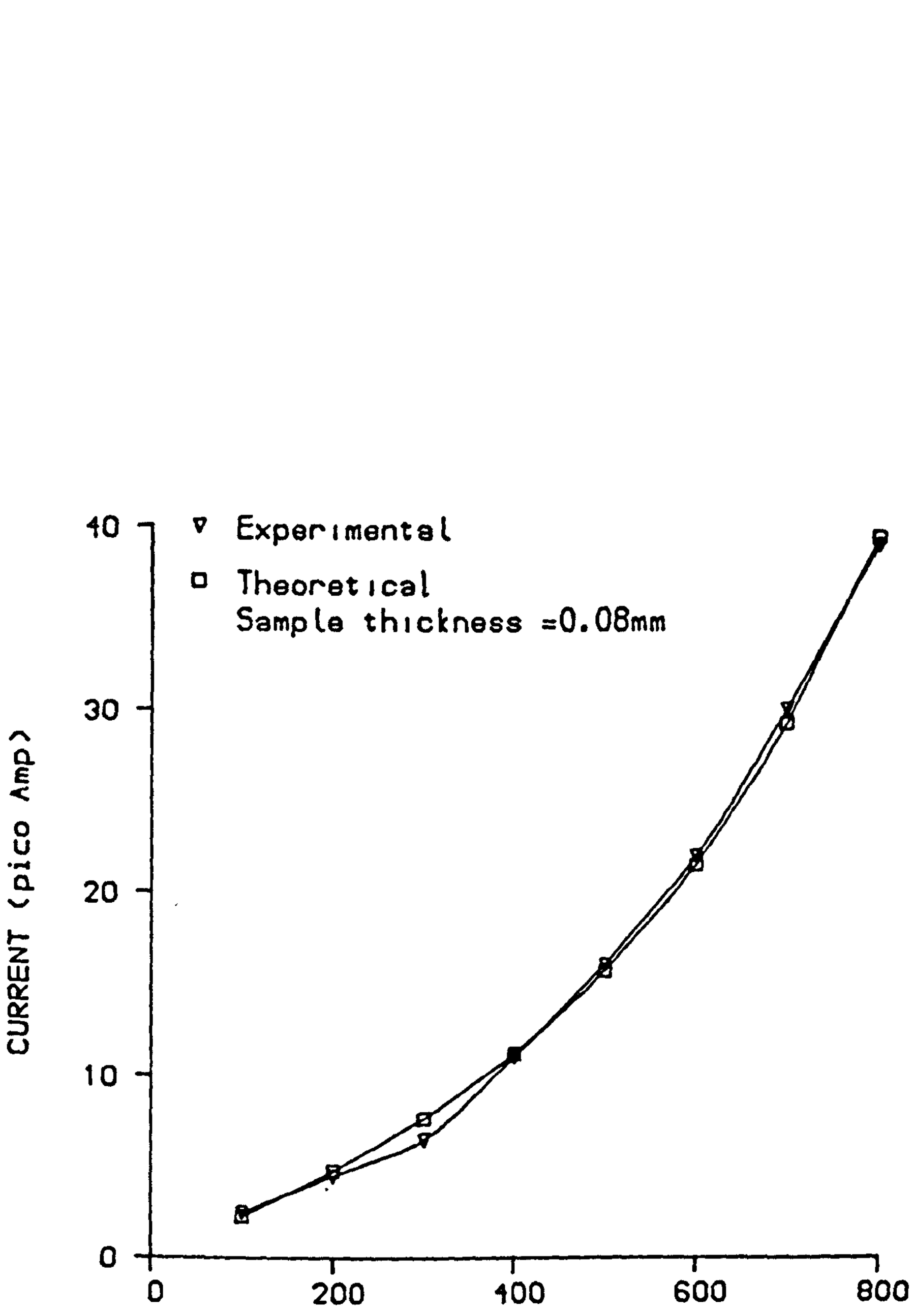


Fig. (5.21a) Current-Voltage characteristic (theoretical and experimental) for MY750/HY956 epoxy system of 0.08mm thickness at 22 °C.

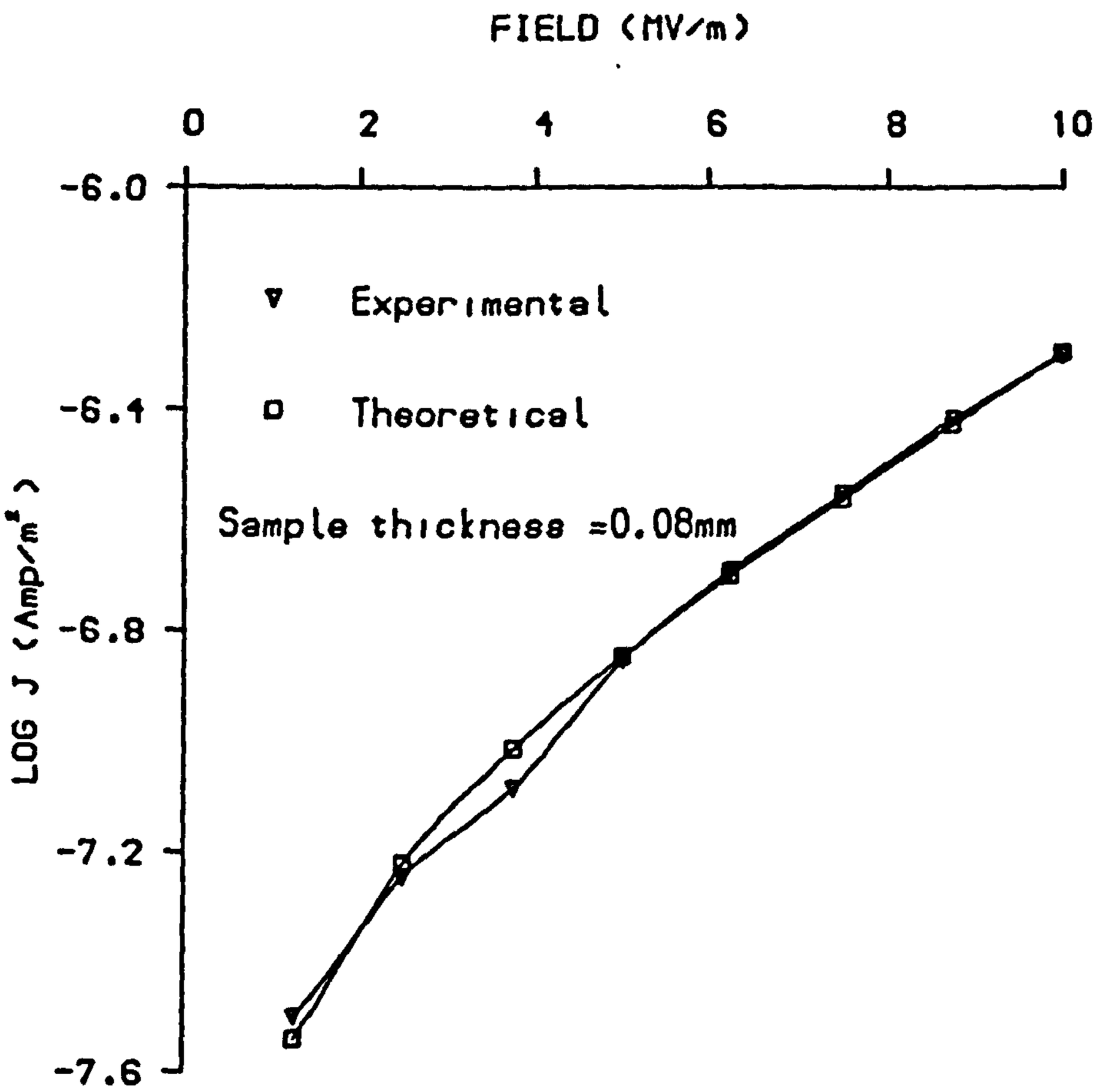


Fig. (5.21b) Log (Current density)- Field characteristic (theoretical and experimental) for MY750/HY956 epoxy system of 0.08mm thickness at 22 ℃.

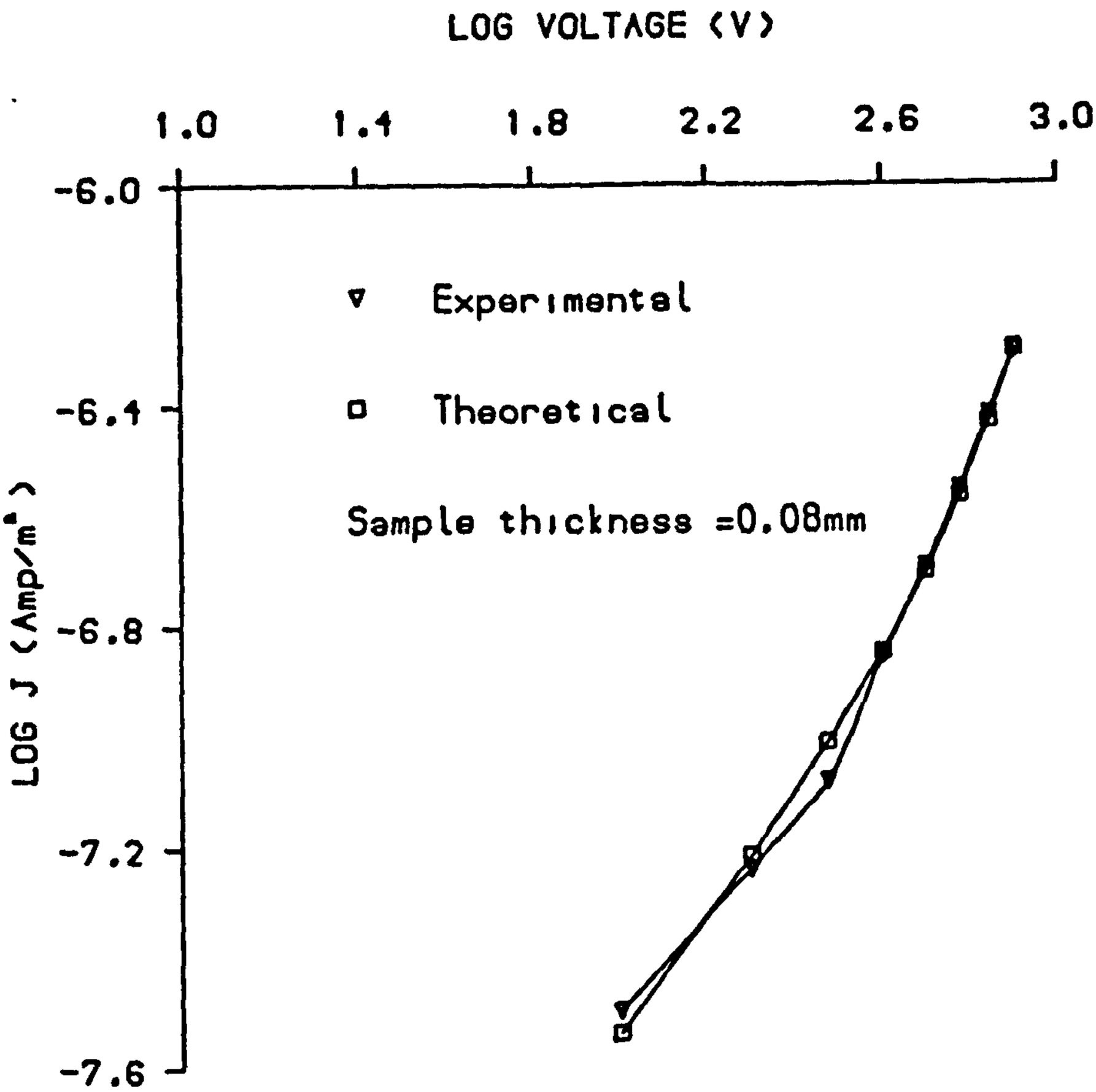


Fig. (5.21c) Log (Current density)- Log (Voltage) characteristic (theoretical and experimental) for MY750/HY956 epoxy system of 0.08mm thickness at 22 ℃.

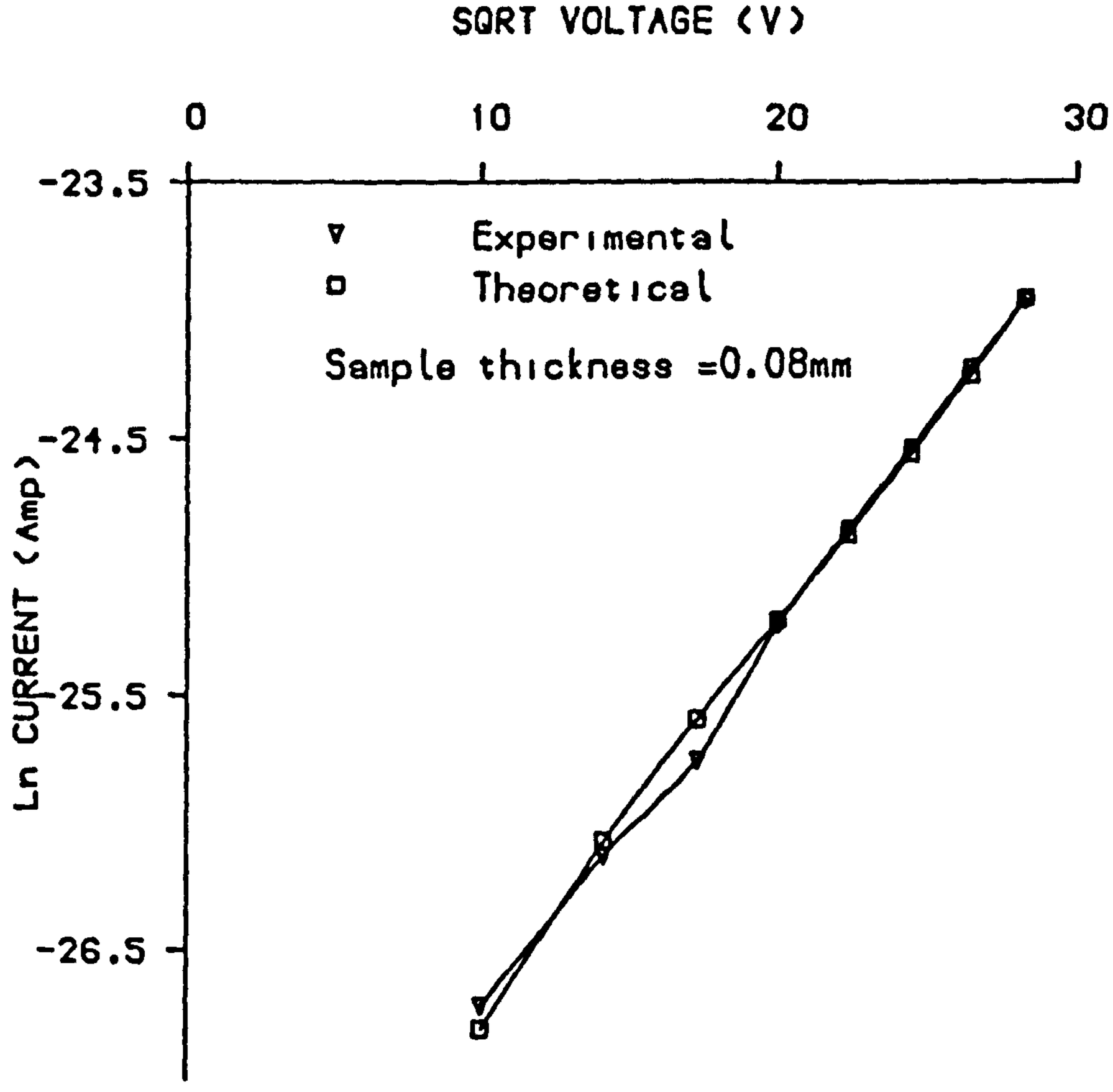


Fig. (5.21d) Ln (Current)- (Voltage)$^{1/2}$ characteristic (theoretical and experimental) for MY750/HY956 epoxy system of 0.08mm thickness at 22 °C.

| | | | | | | | | | |
|---|---|---|---|---|---|---|---|---|---|
| 0.038 | 0.021 | 0.008 | 0.001 | 0.003 | 0.015 | 0.042 | 0.086 | 0.153 | 0.249 |
| 0.036 | 0.019 | 0.007 | 0.001 | 0.003 | 0.017 | 0.046 | 0.092 | 0.163 | 0.262 |
| 0.034 | 0.017 | 0.006 | 0.000 | 0.004 | 0.020 | 0.050 | 0.099 | 0.172 | 0.275 |
| 0.032 | 0.016 | 0.005 | 0.000 | 0.005 | 0.022 | 0.054 | 0.106 | 0.182 | 0.289 |
| 0.030 | 0.014 | 0.004 | 0.000 | 0.007 | 0.025 | 0.059 | 0.113 | 0.192 | 0.303 |
| 0.028 | 0.013 | 0.003 | 0.001 | 0.008 | 0.028 | 0.064 | 0.120 | 0.202 | 0.317 |
| 0.026 | 0.012 | 0.002 | 0.001 | 0.009 | 0.031 | 0.069 | 0.128 | 0.213 | 0.332 |
| 0.025 | 0.010 | 0.002 | 0.001 | 0.011 | 0.034 | 0.074 | 0.136 | 0.224 | 0.347 |

Figure (5.22) Plot of the sum of squares function.

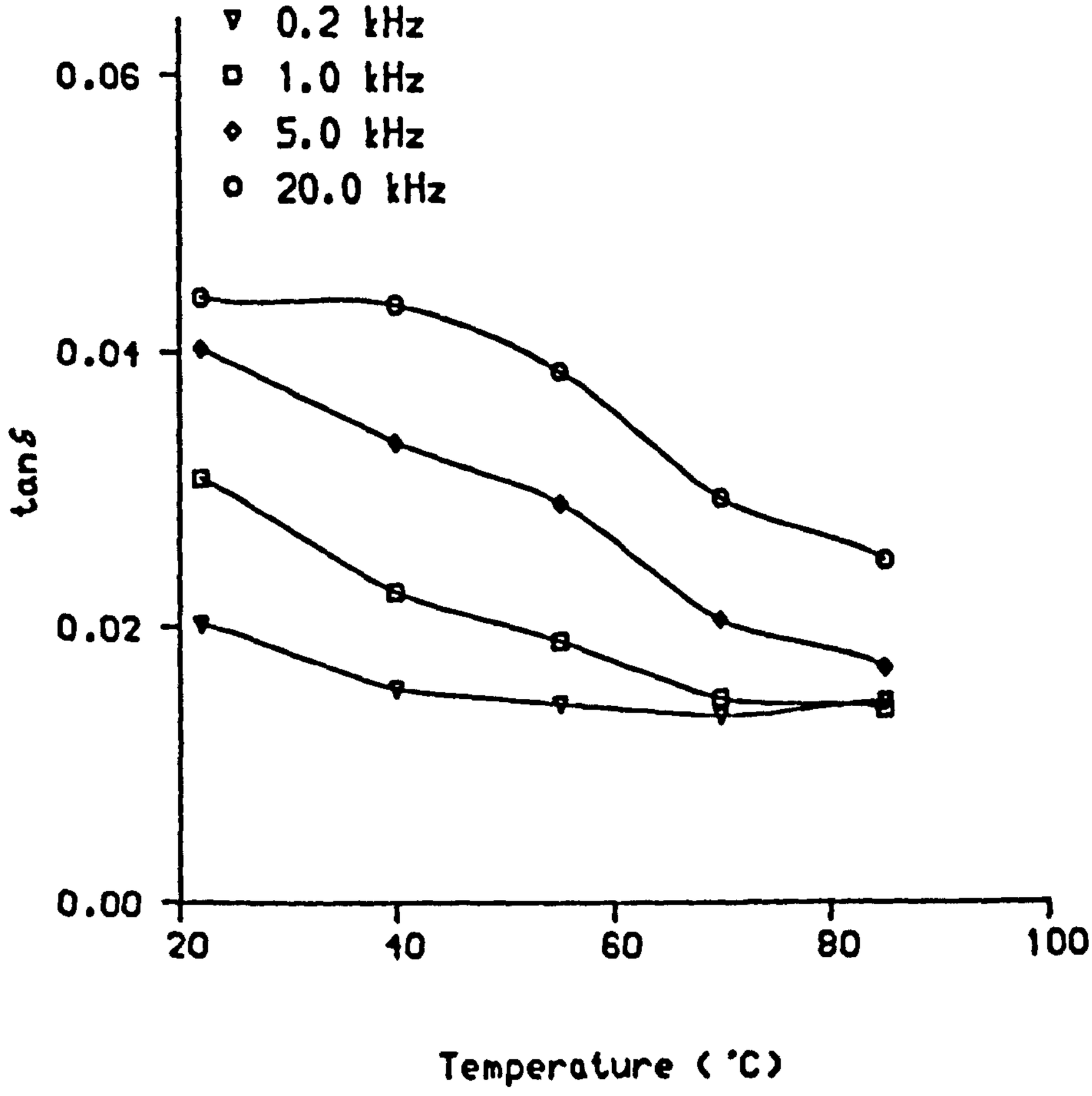


Fig. (5.23) Typical plots of tan δ against temperature for MY750/HY956 epoxy system at different frequencies.

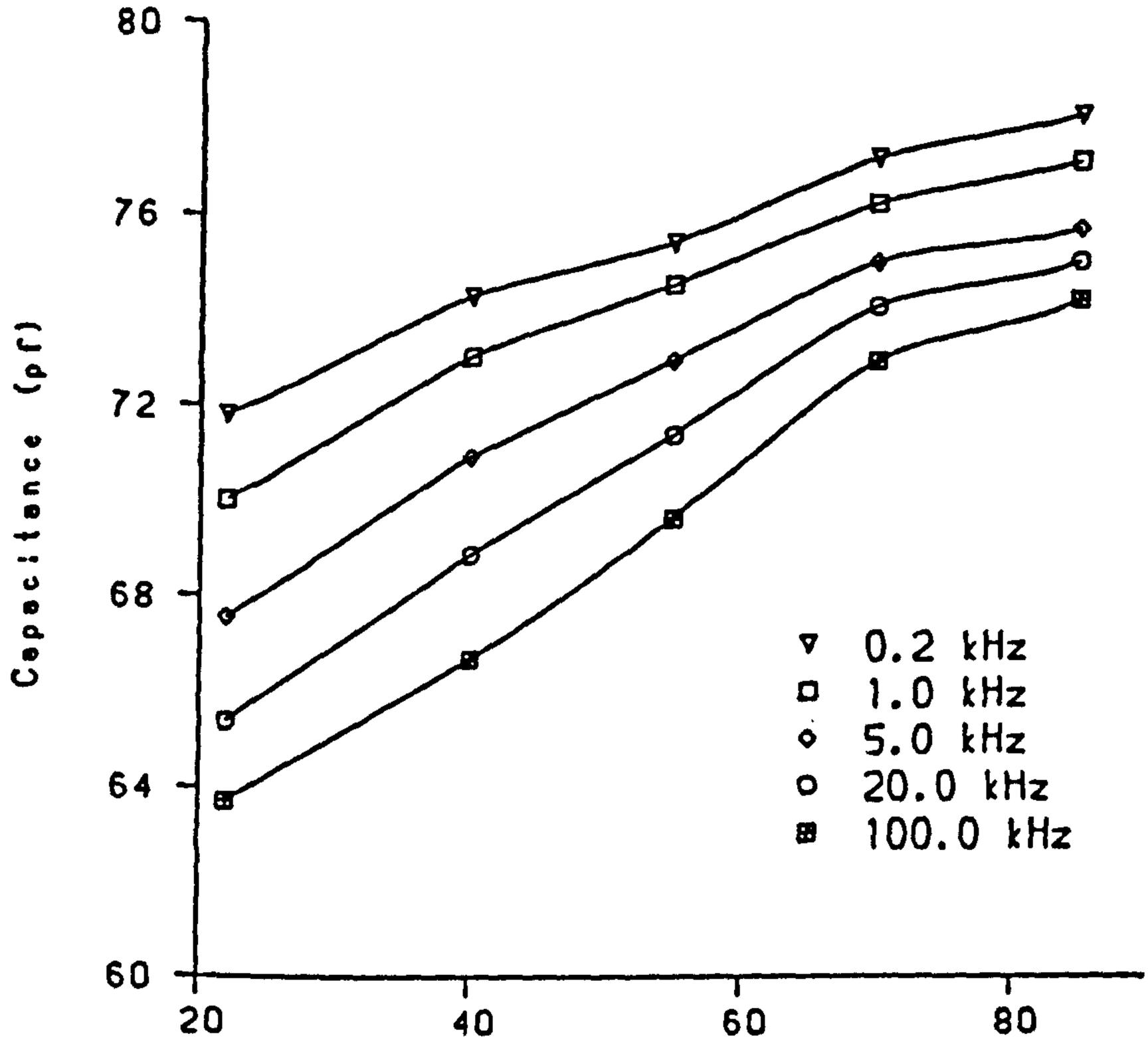


Fig. (5.24) Typical plots of capacitance against temperature for MY750/HY956 epoxy system at different frequencies.

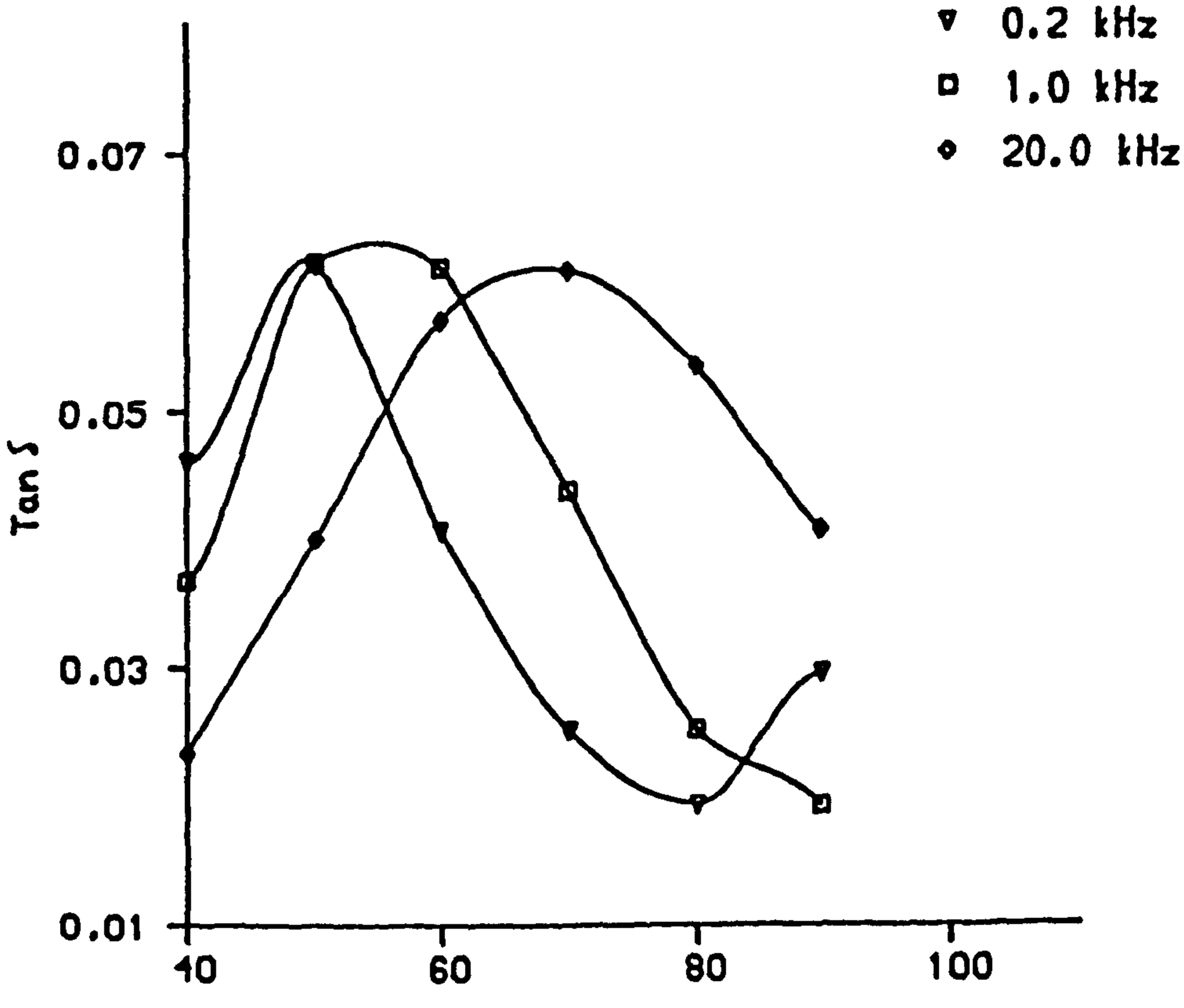


Fig. (5.25) Typical plots of tanδ against temperature for MY750/DDSA epoxy system at different frequencies.

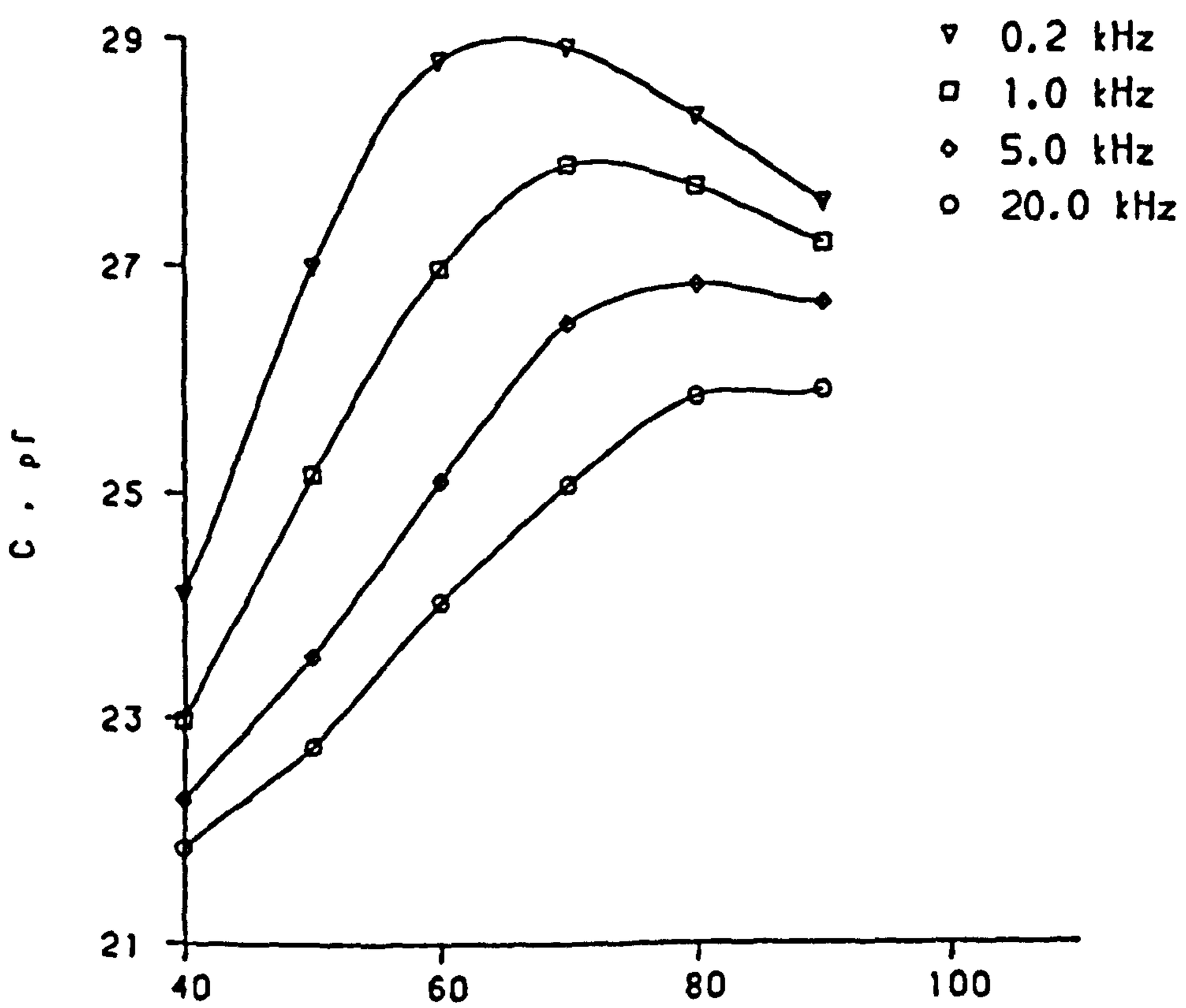


Fig. (5.26) Typical plots of capacitance against temperature for MY750/DDSA epoxy system at different frequencies.

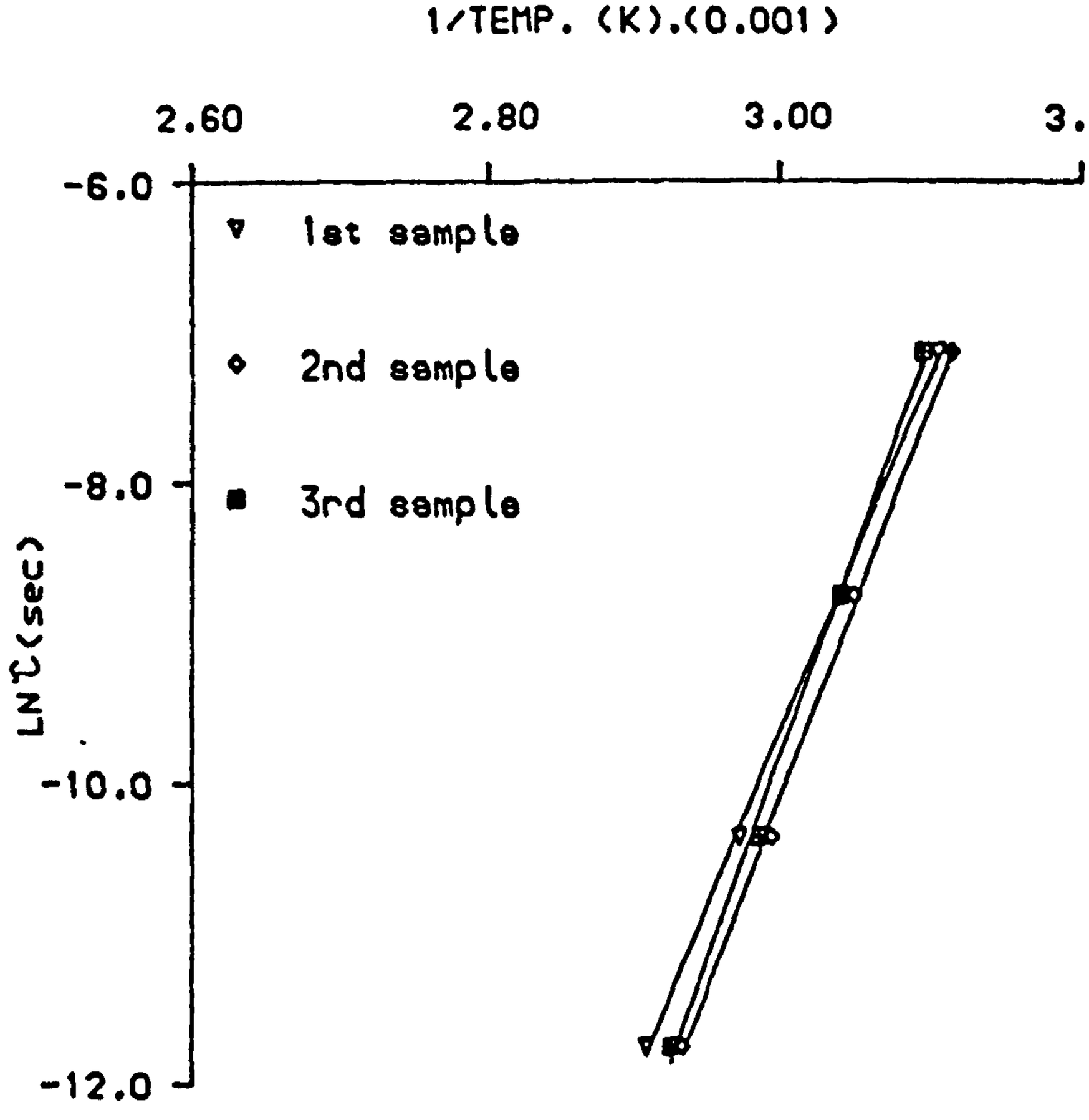


Fig. (5.27) Plots of logτ against 1/temperature for MY750/DDSA epoxy system.

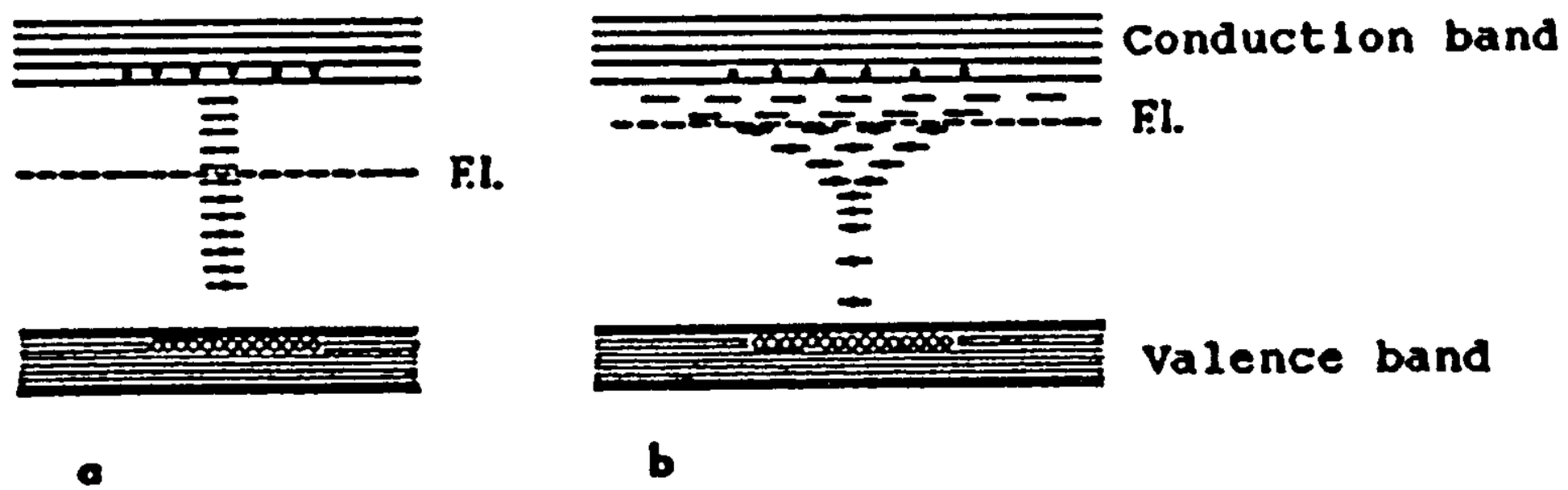


Fig. (6.1) Distribution of traps in depth a- uniform
b- exponential

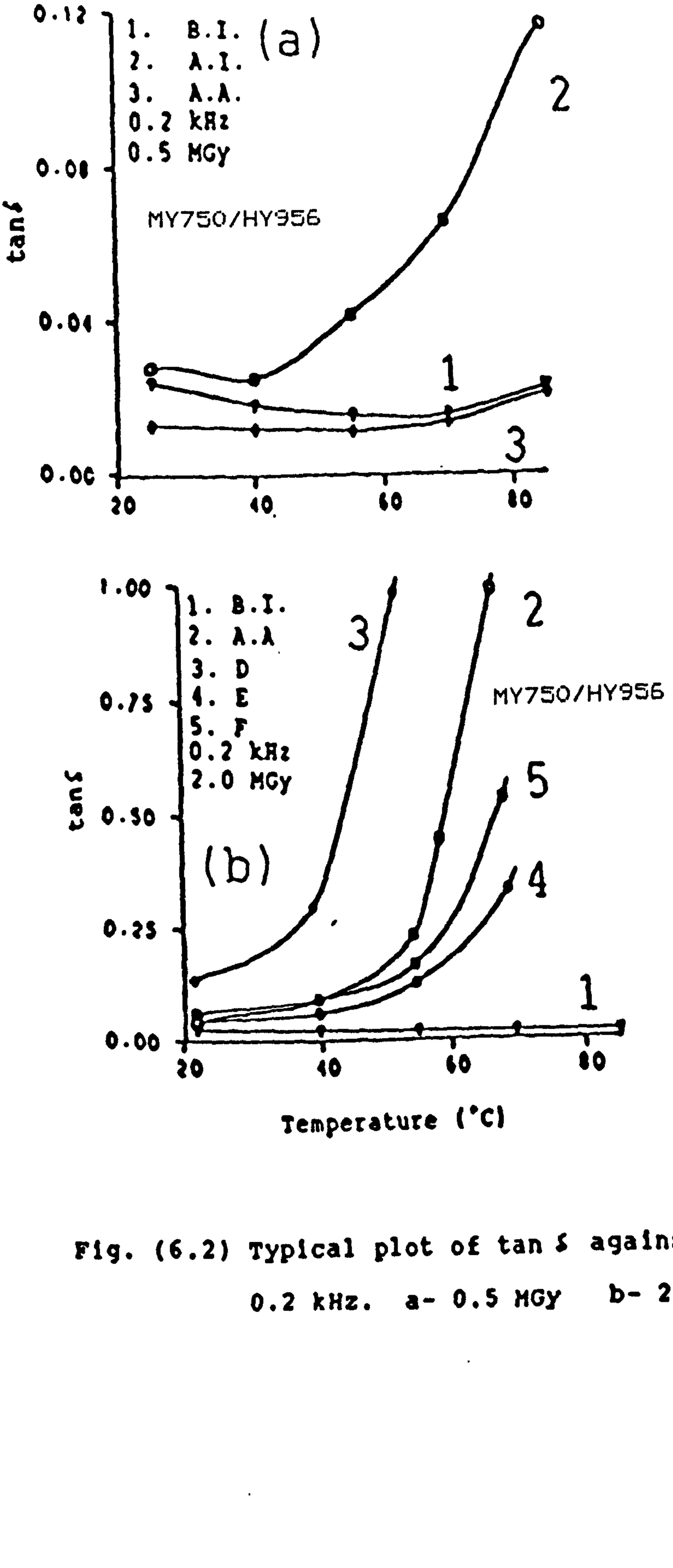


Fig. (6.2) Typical plot of tan δ against temperature at 0.2 kHz. a- 0.5 MGy b- 2.0 MGy.

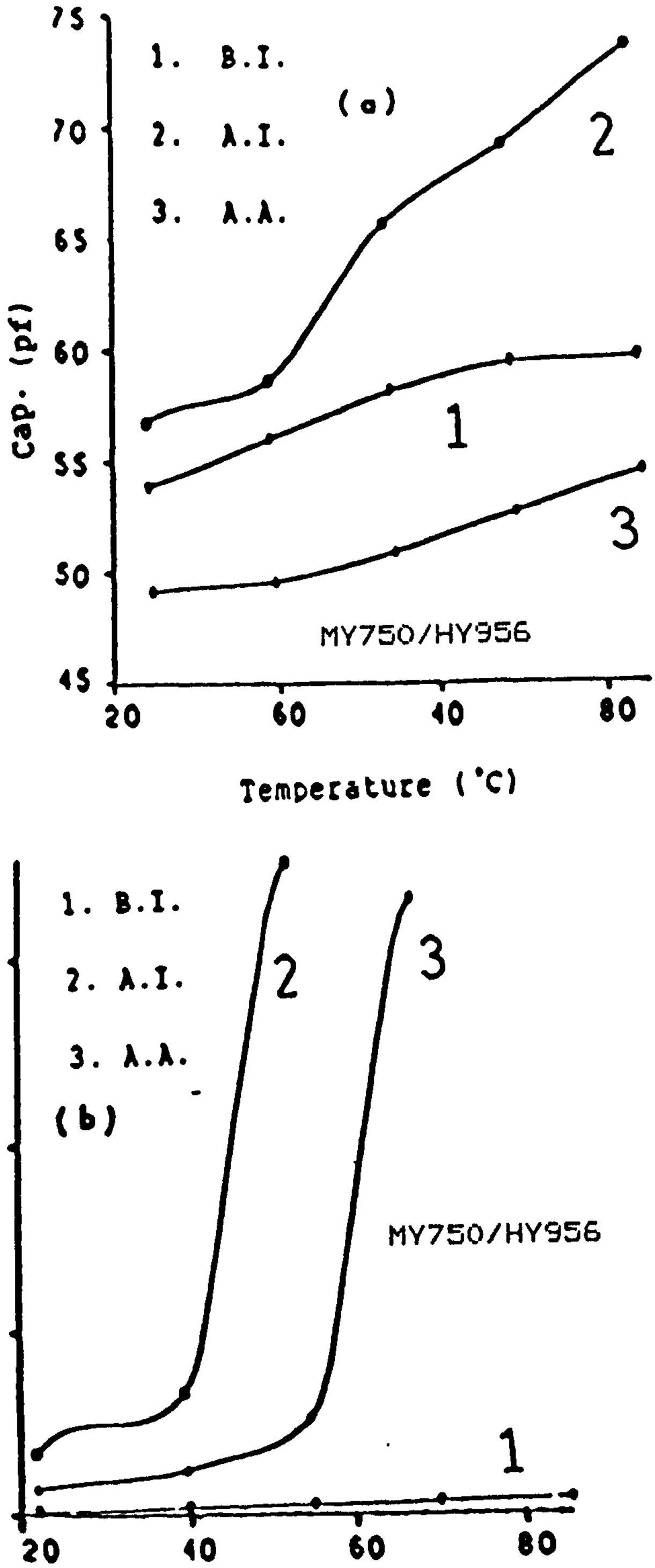


Fig. (6.3) Typical plot of capacitance against temperature at 0.2 kHz. a- 0.5 MGy b- 2.0 MGy.

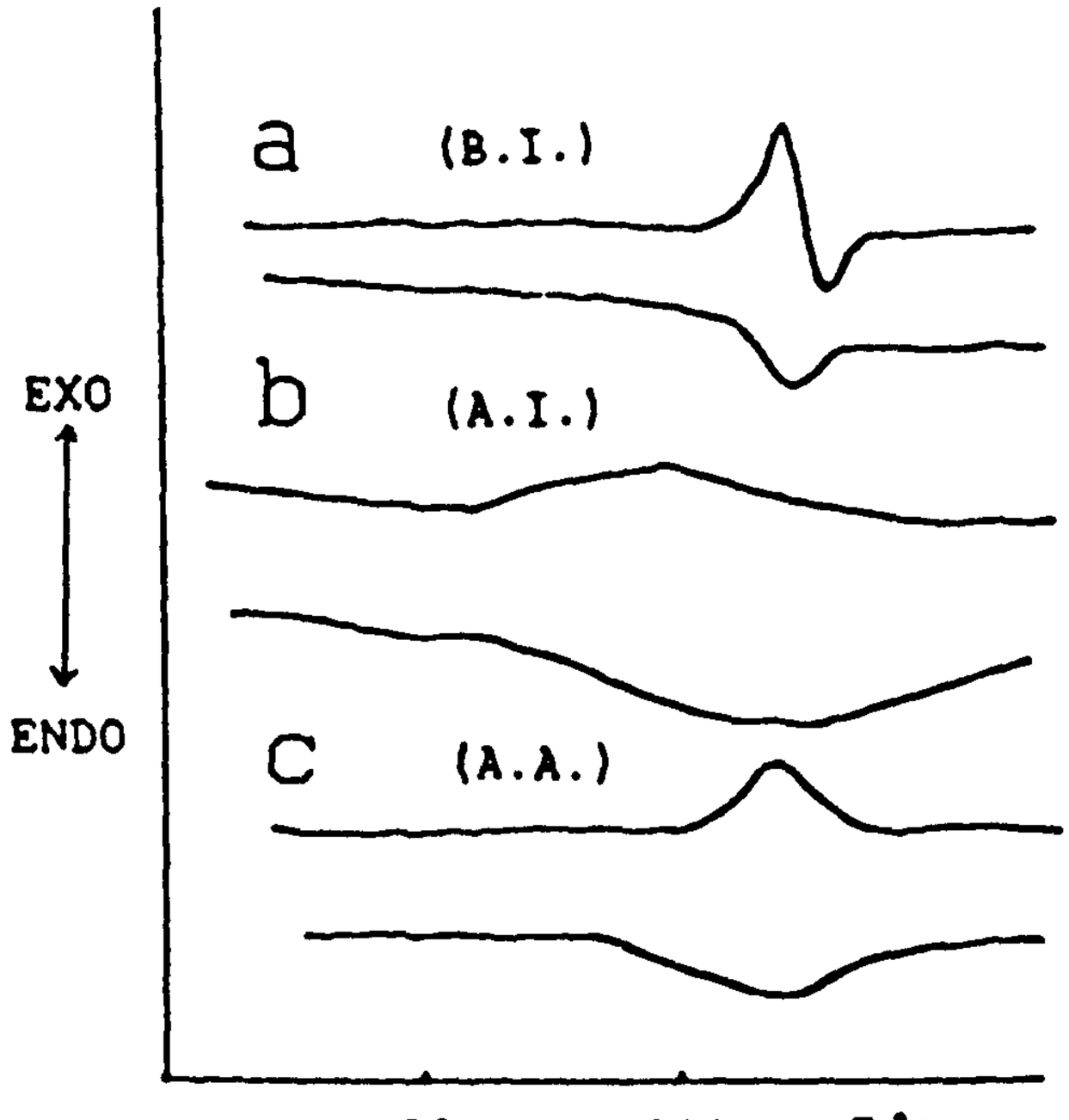


Fig. (6.4) DSC of MY750/HY956 epoxy system.

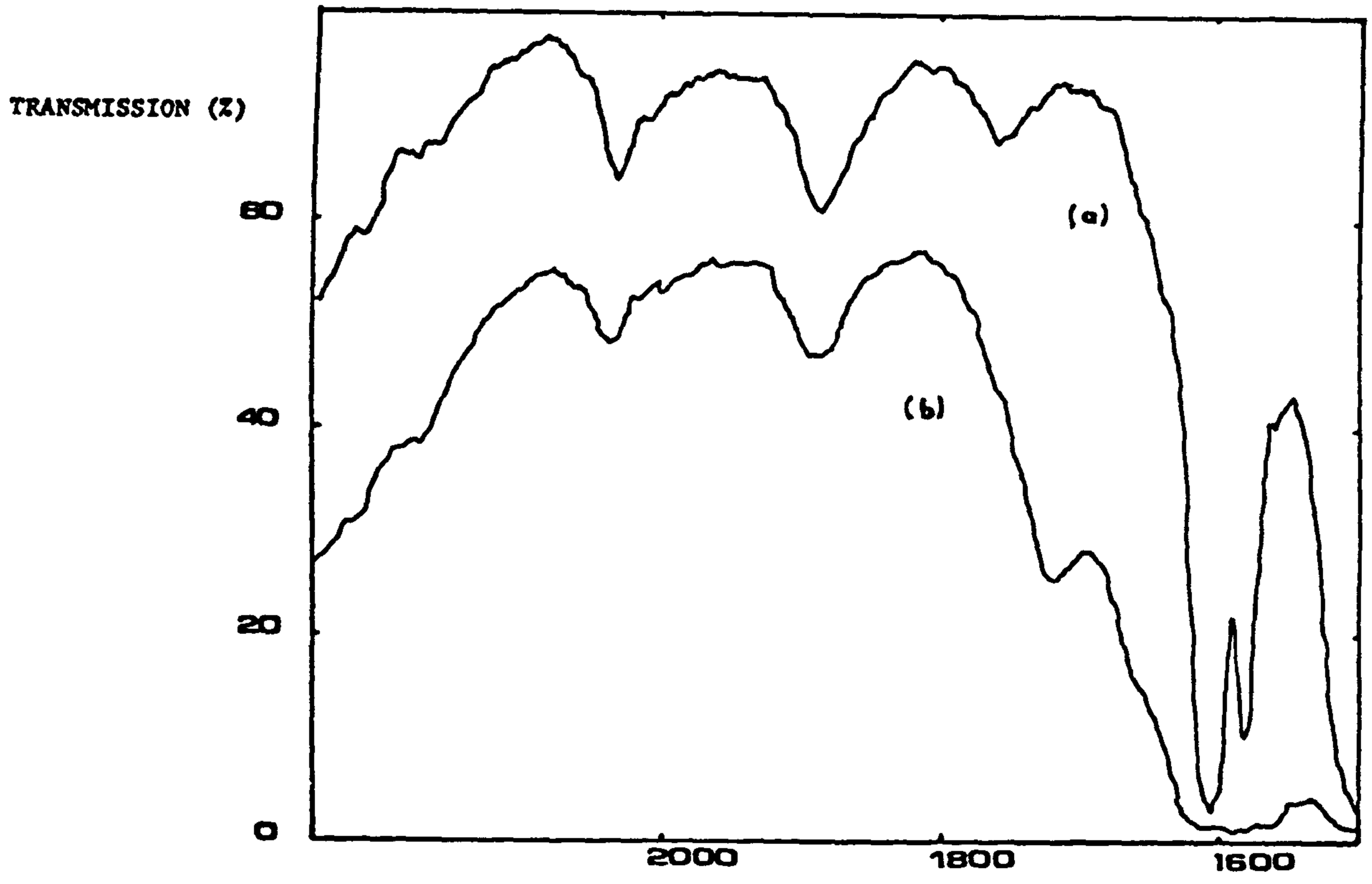


Fig. (6.5) infrared spectrum of a MY750/HY956 epoxy system a- unirradited b- after 2.3 MGy irradiation.

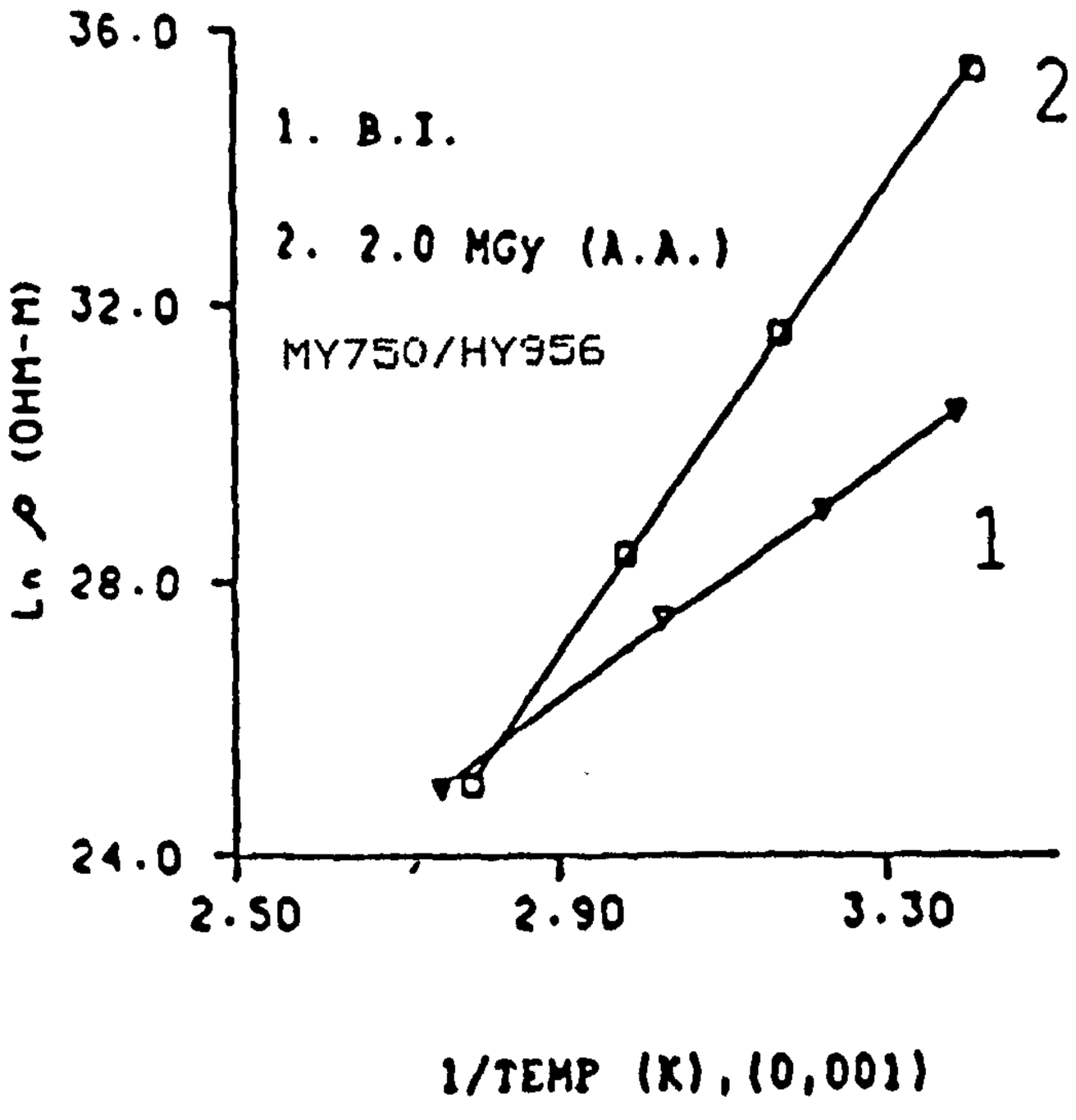


Fig. (6.6) Arrhenius plots of d.c. resistivity before irradiation and after annealing.

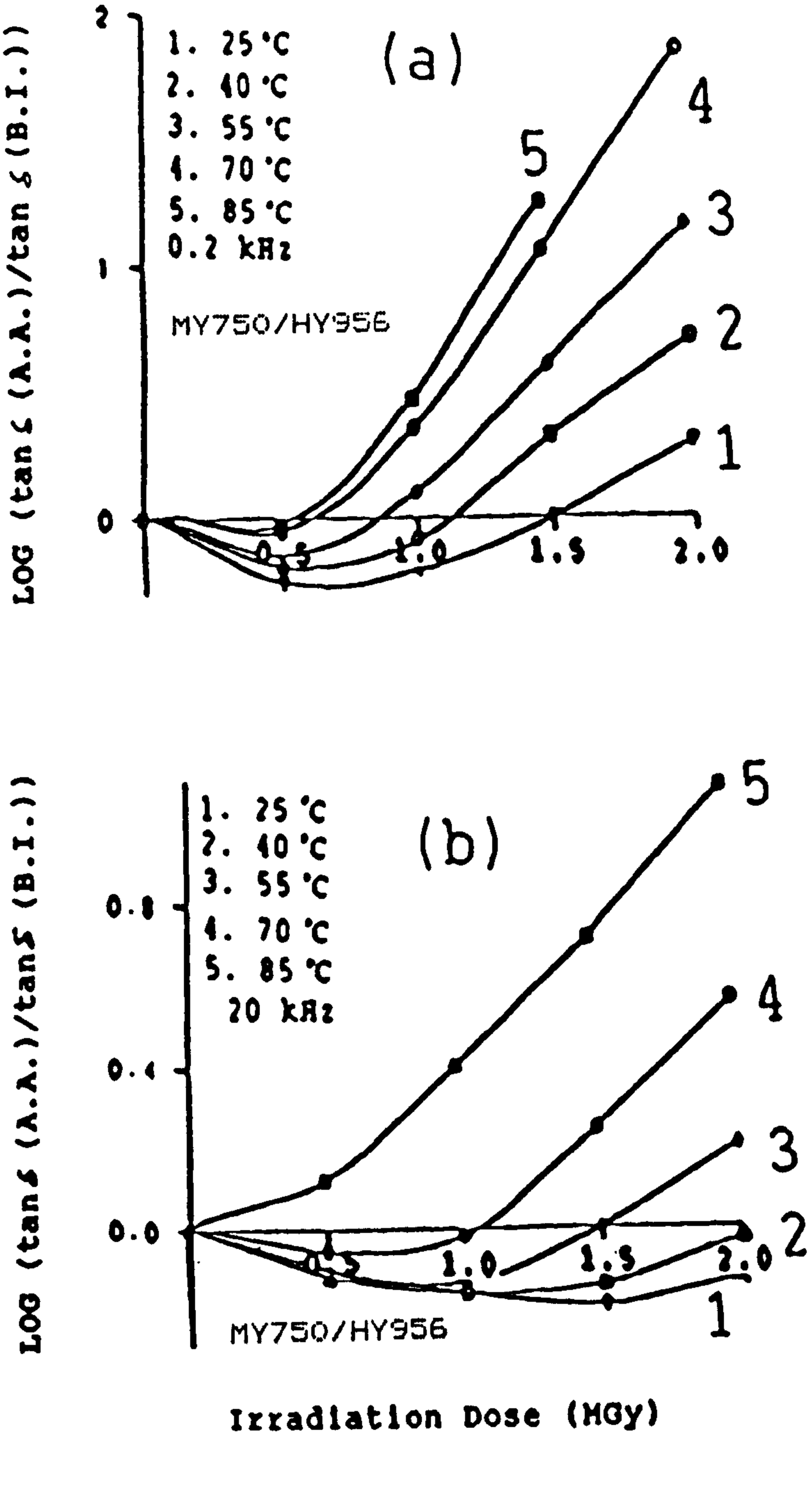


Fig. (6.7) Ratio of log tan δ after annealling irradiation as a function of irradiation dose a- 0.2 kHz b- 20 kHz measuring frequency.

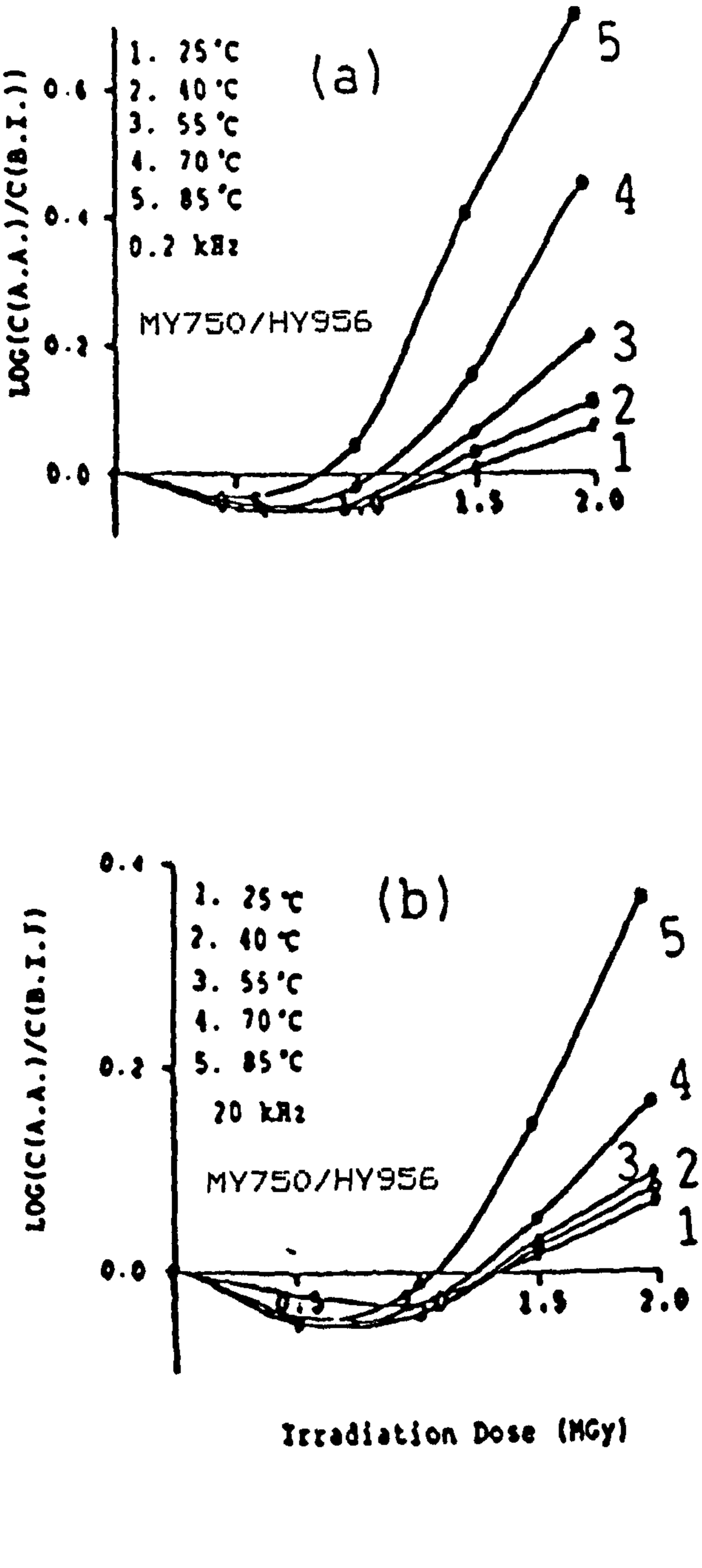


Fig. (6.8) Ratio of log capacitance after annealing to before irradiation as a function of irradiation dose at a- 0.2 kHz b- 20 kHz measuring frequency.

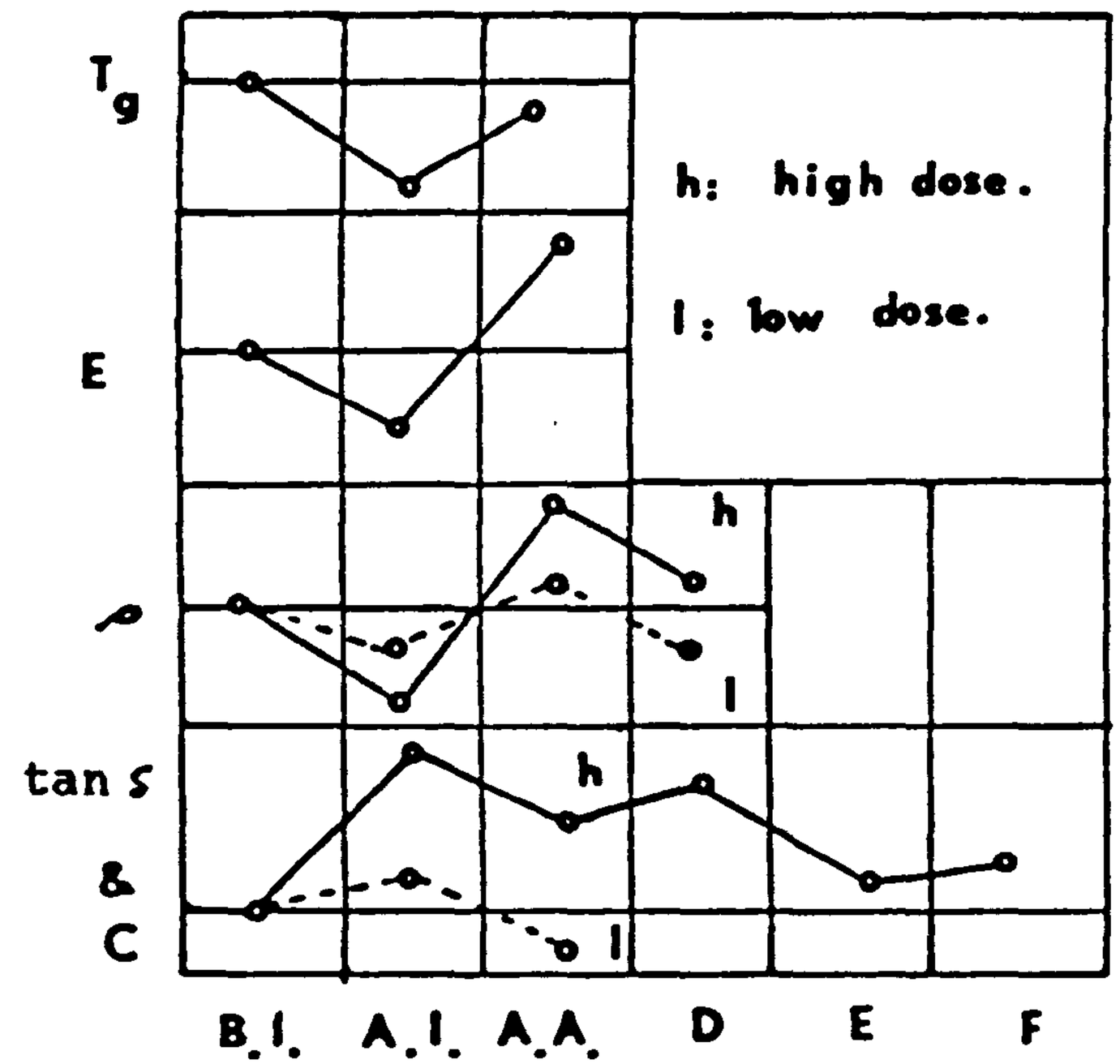


Fig. (6.9) Summary of the effect of the irradiation and annealing on some of the properties of MY750/HY956 epoxy system.

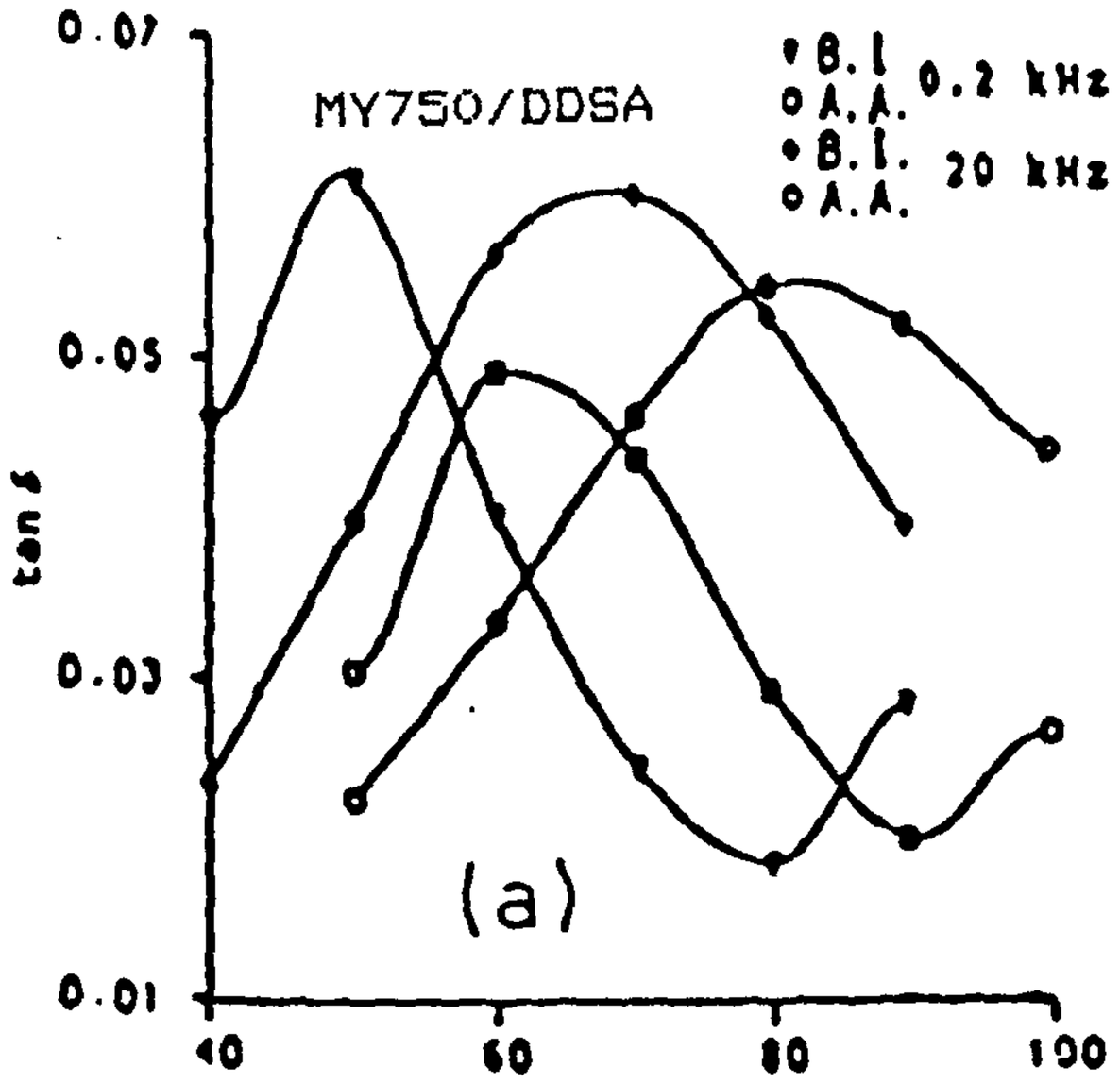


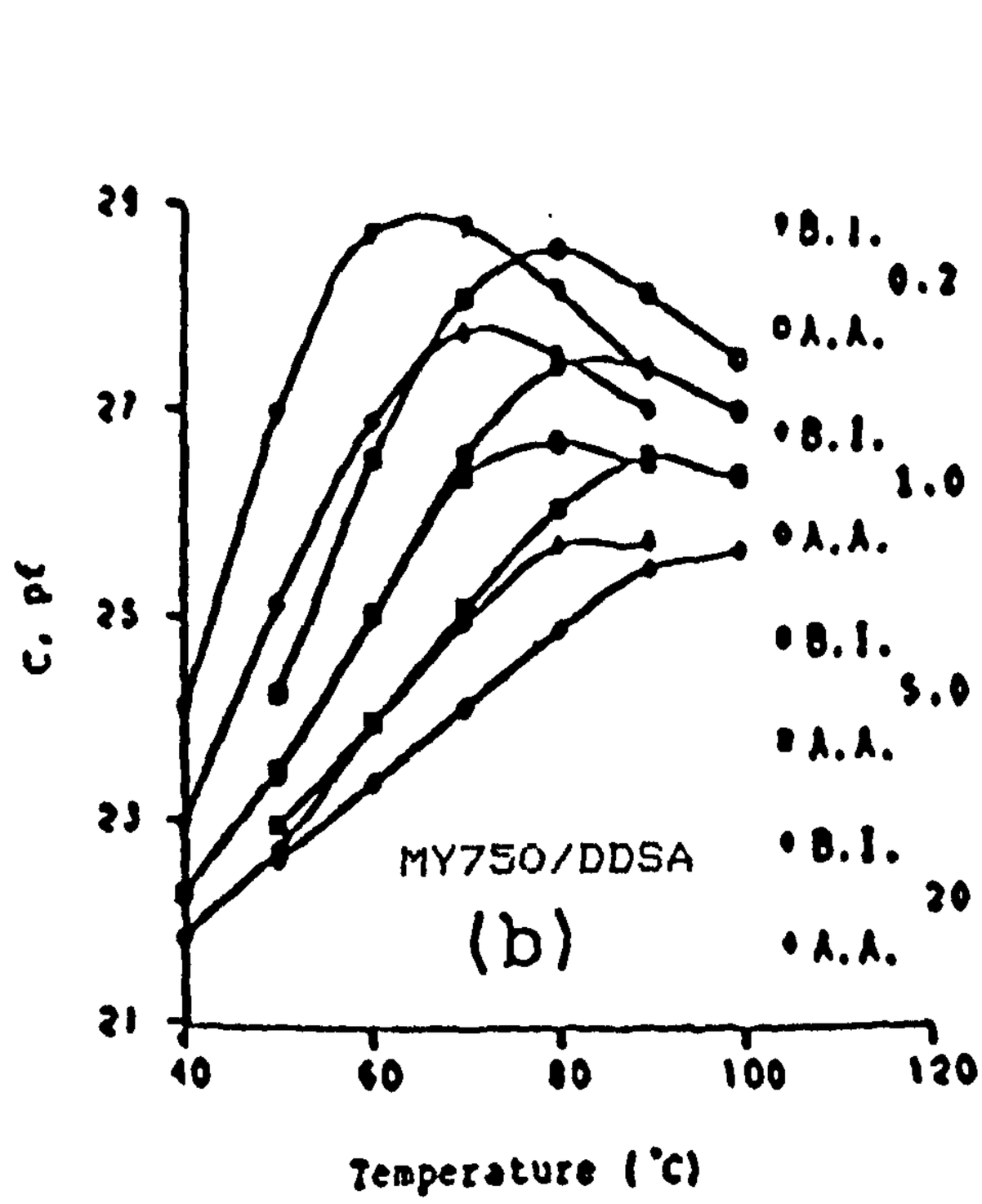


Fig. (6.10) Typical plots of tan δ (a) and C (b) against temperature at different frequencies before and after irradiation at 1MGy.

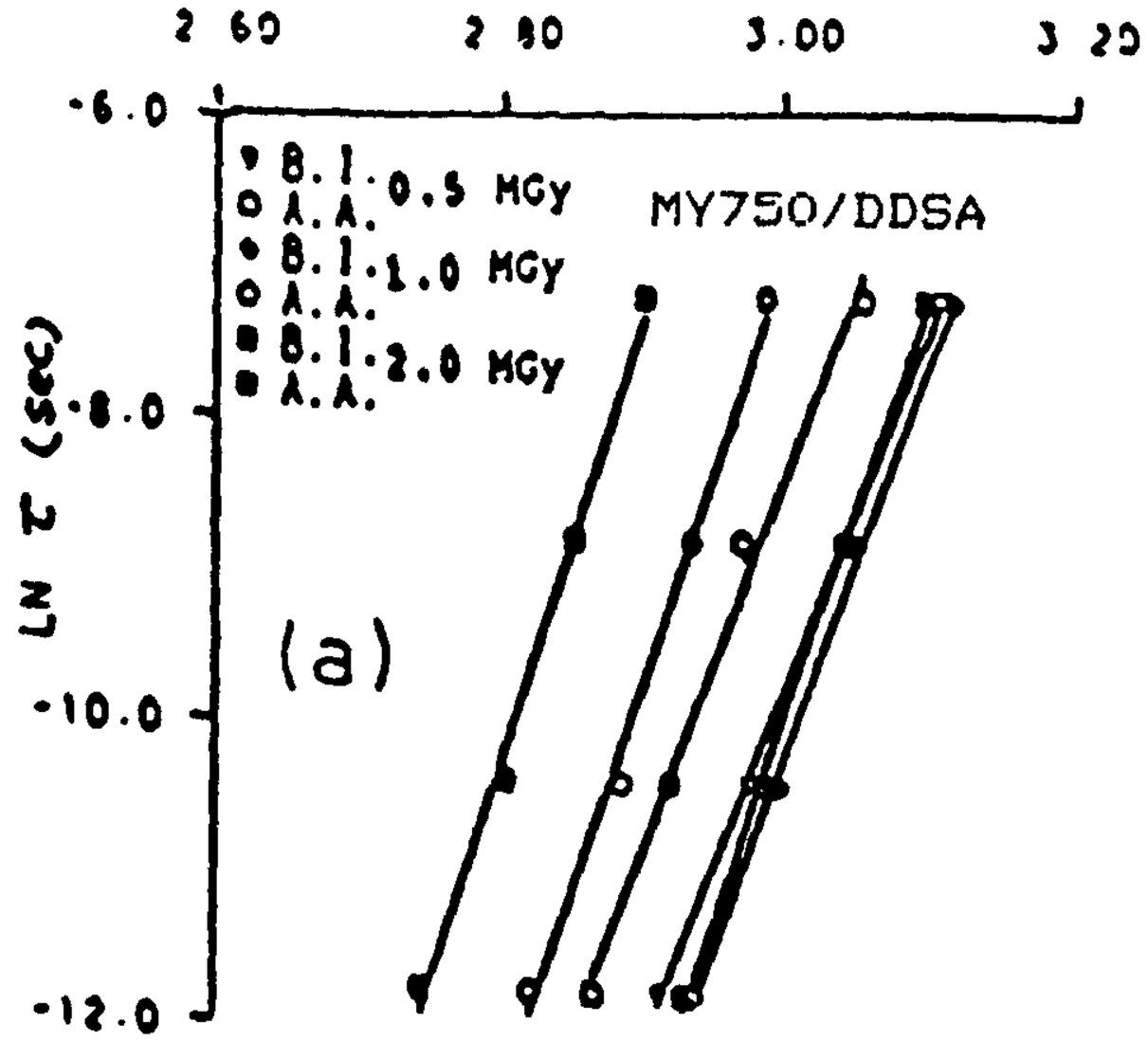


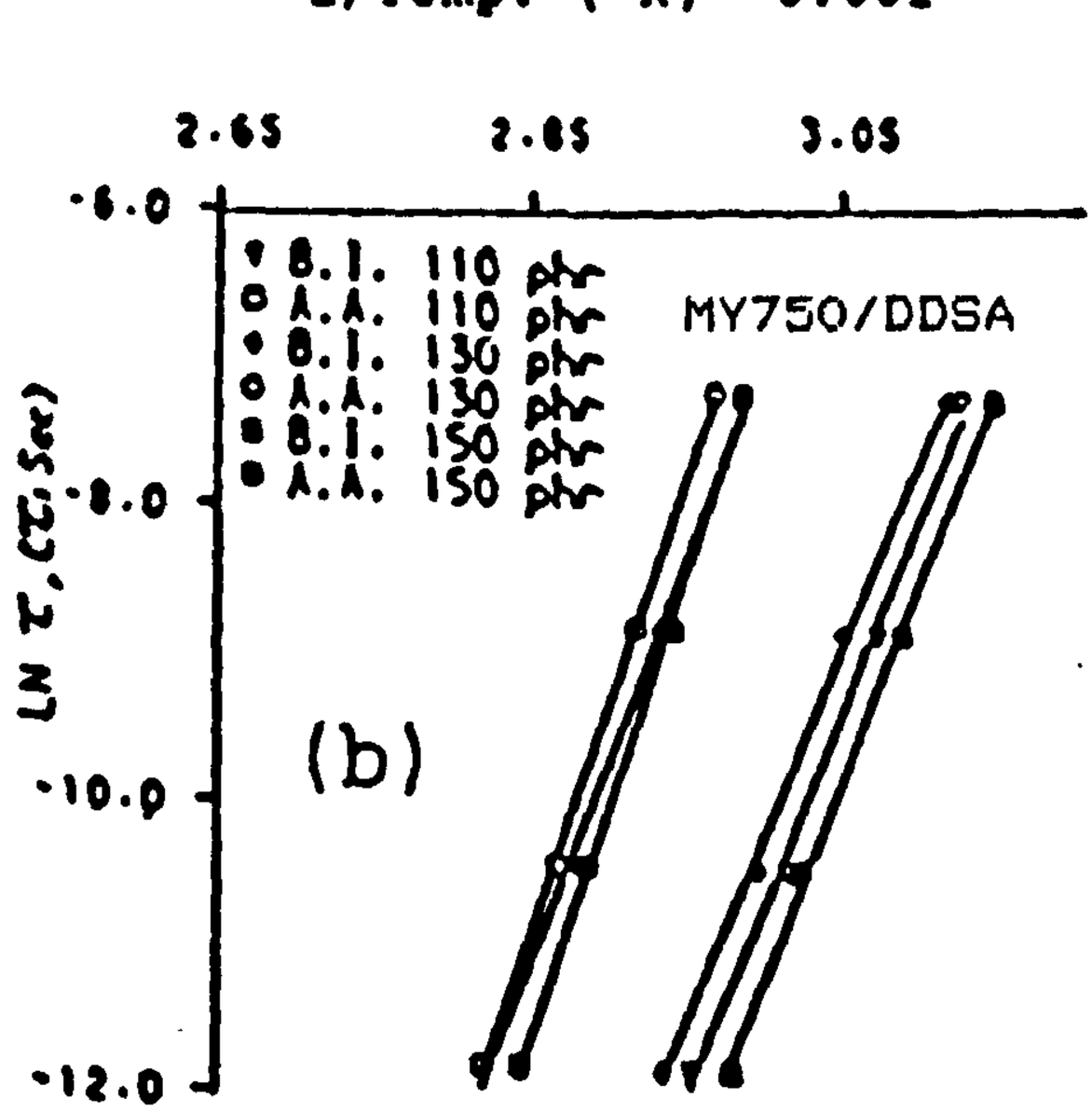


Fig. (6.11) Plots of log $\tau$ against 1/T; a- at different doses, b- at different concentration of DDSA hardener (phr).

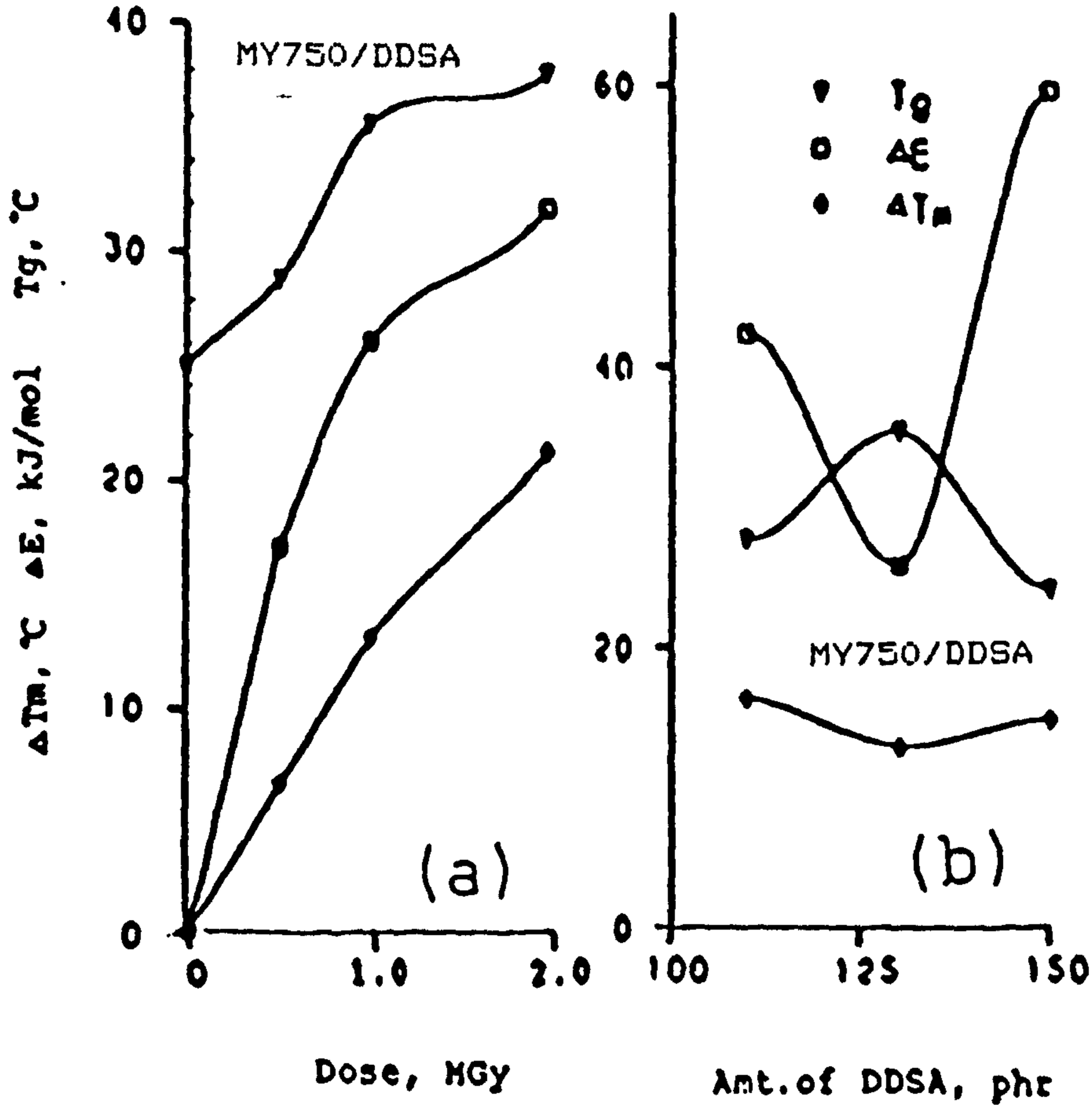


Fig. (6.12) plots of ΔTm, ΔE, Tg against a- Irradiation doses and b- concentration of hardener (phr).

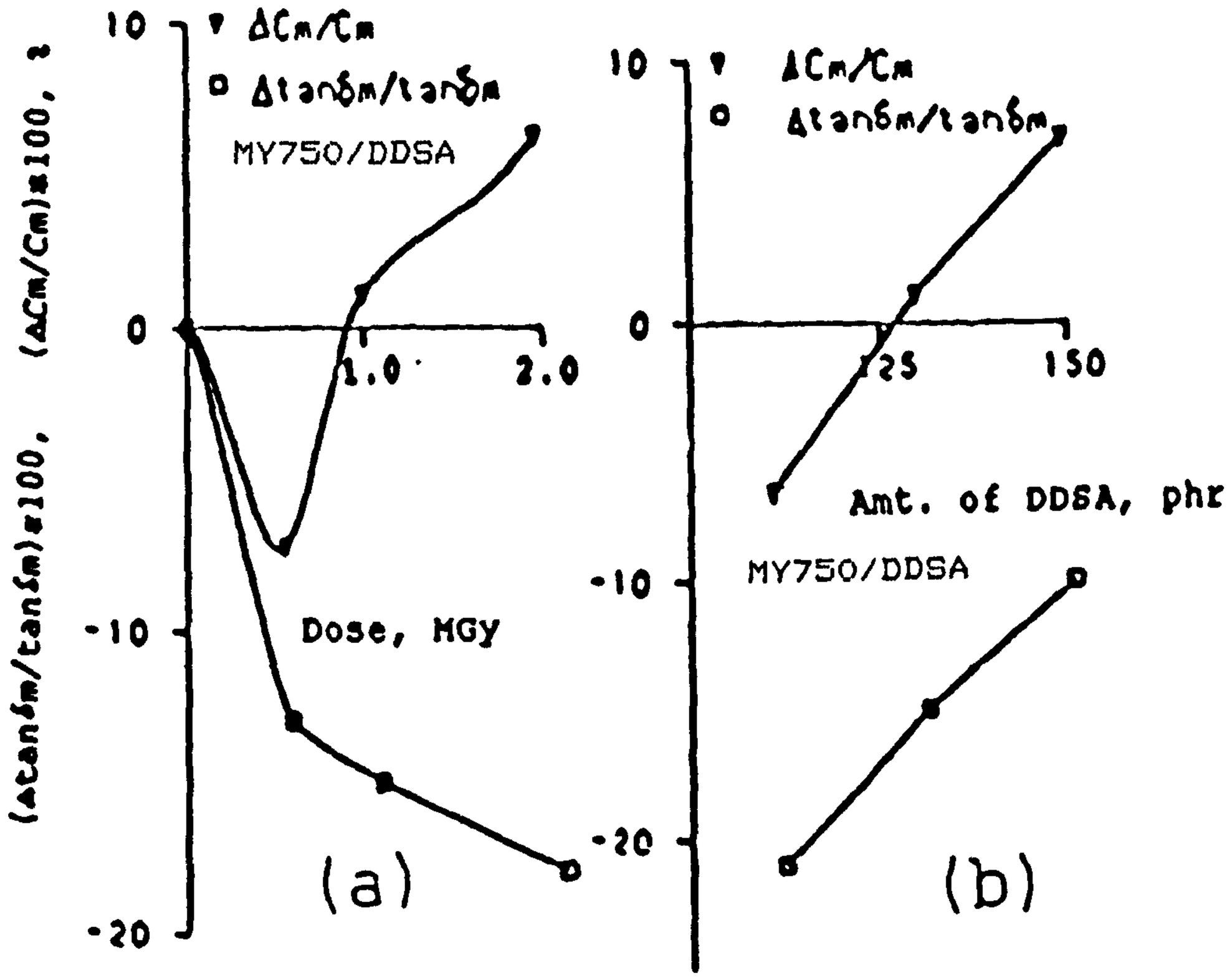


Fig. (6.13) Plots of $\Delta \tan\delta_m / \tan\delta_m$ and $\Delta C_m / C_m$ against a- irradiation doses and b- concentration of DDSA hardener (phr).

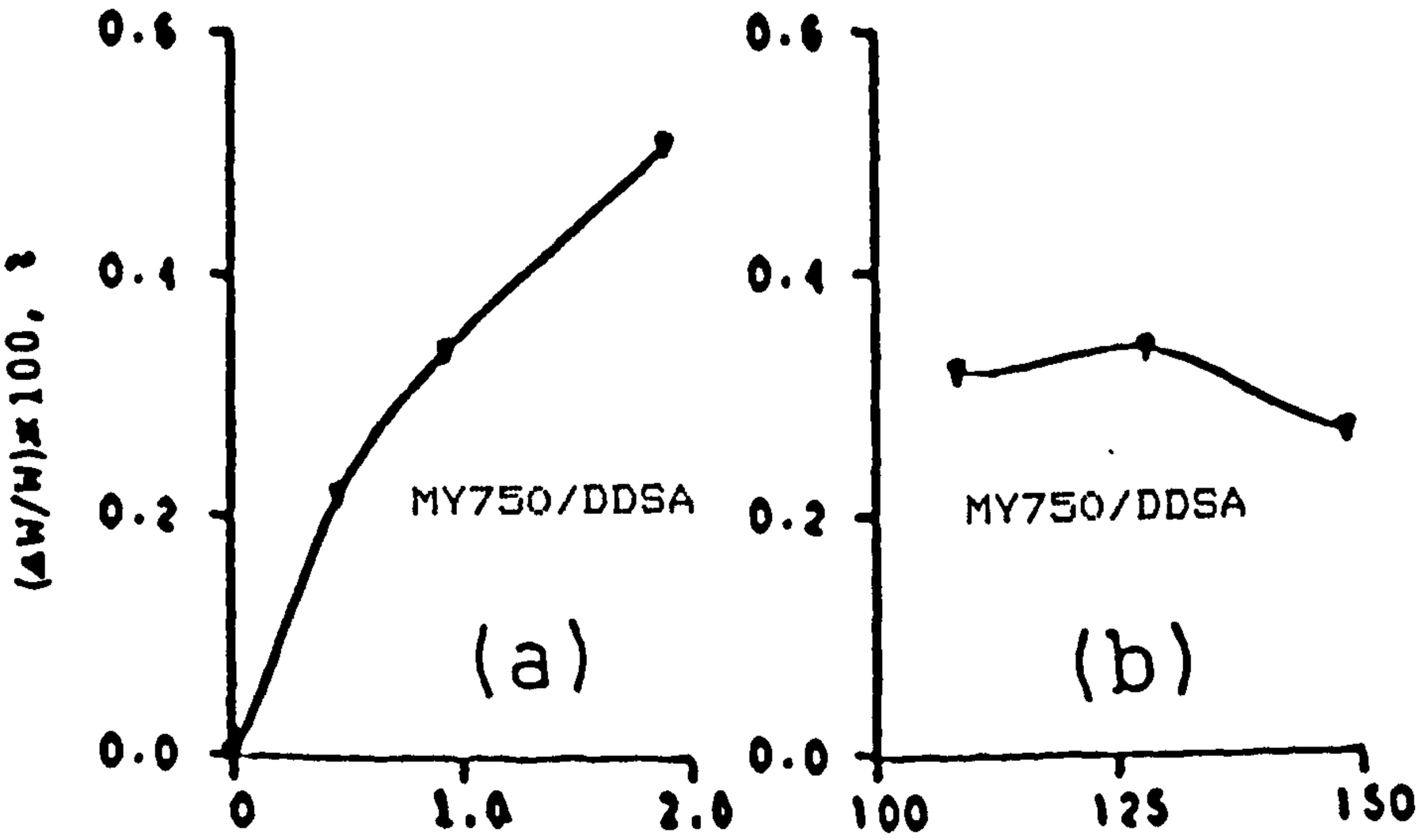


Fig. (6.14) Plots of ΔW / W against a- irradiation doses and b- concentration of DDSA hardener (phr).

A

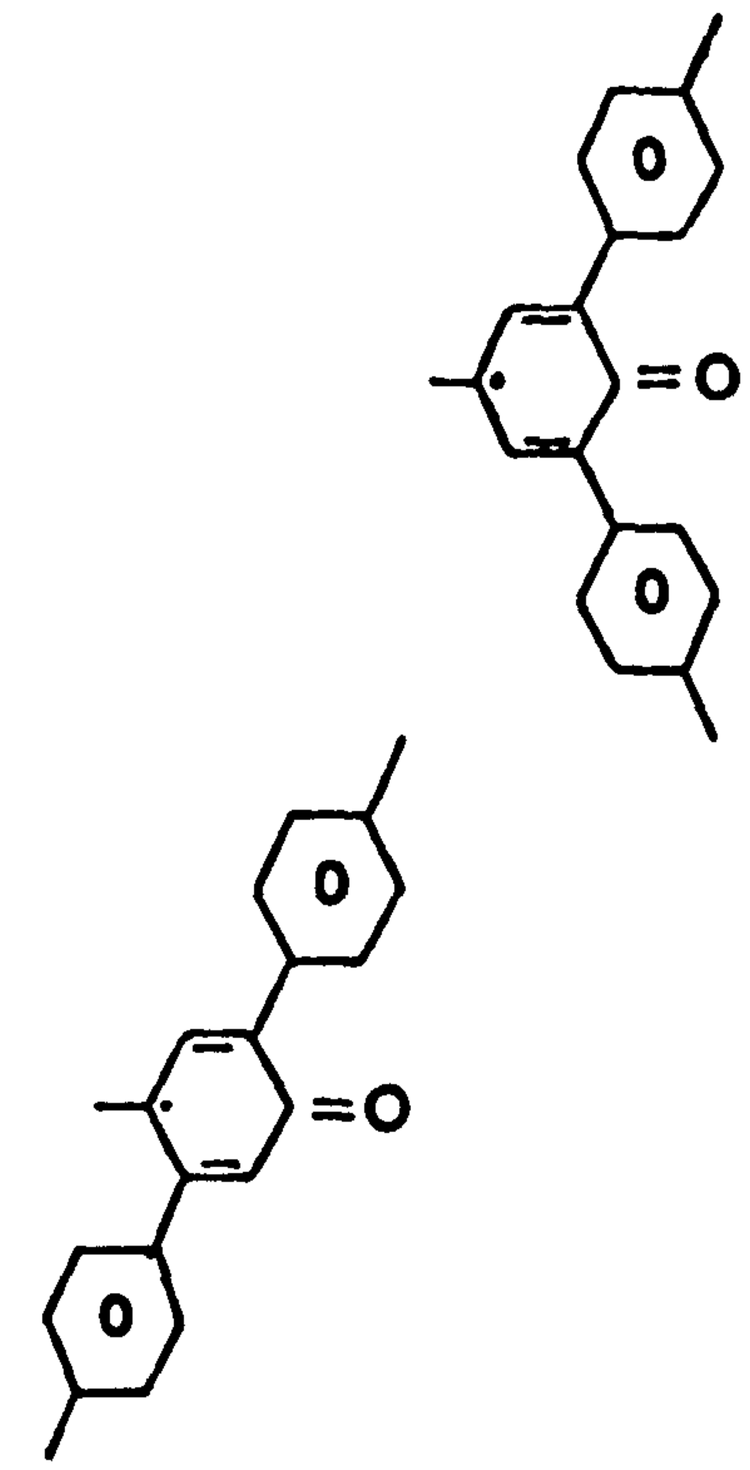

B

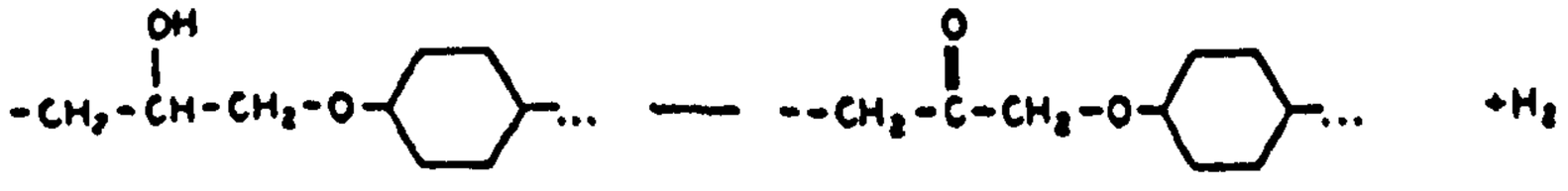

Fig. (6.15) Chemical formula for irradiation- produced a- colour change, b- carbonyl group.

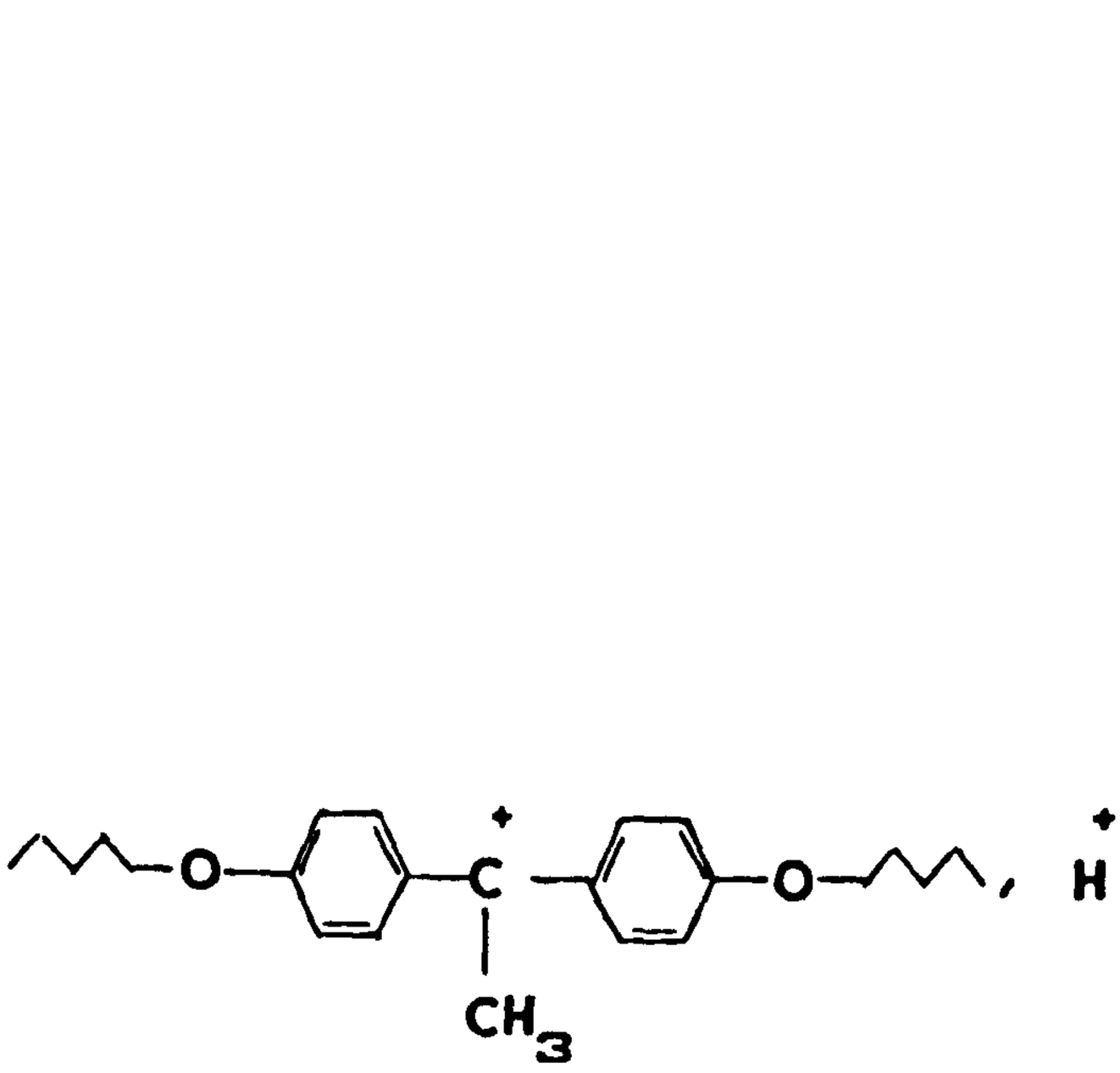


Fig. (6.16) chemical formula for irradiation- produced ions.

# PUBLICATIONS

APPENDIX NOT COPIED

ON INSTRUCTION FROM

UNIVERSITY